UTS UNIVERSITY OF TECHNOLOGY SYDNEY

ARSENIC REMOVAL FROM WATER BY NOVEL IRON-BASED ADSORBENTS

by Thi Hai Nguyen

Thesis submitted in fulfilment of the requirements for
the degree of

Doctor of Philosophy
under the supervision of
Principal supervisor: Dr. Tien Vinh Nguyen
Co-supervisor: Emeritus Prof. Saravanamuthu Vigneswaran

University of Technology Sydney
Faculty of Engineering and Information Technology
July, 2022

CERTIFICATE OF ORIGINAL AUTHORSHIP

I, Thi Hai Nguyen declare that this thesis, is submitted in fulfilment of the requirements for the award of Doctor of Philosophy, in the School of Civil and Environmental Engineering/Faculty of Engineering and Information Technology at the University of Technology Sydney.

This thesis is wholly my own work unless otherwise referenced or acknowledged. In addition, I certify that all information sources and literature used are indicated in the thesis.

This document has not been submitted for qualifications at any other academic institution.

This research is supported by the Australian Government Research Training Program.

Signature: Thi Hai Nguyen

Production Note:
Signature removed
prior to publication.

Date: 13/07/2022

ACKNOWLEDGEMENTS

First of all, I would like to take this occasion to express my heartfelt appreciation to my supervisors Dr. Tien Vinh Nguyen and Emeritus Prof. Saravanamuthu Vigneswaran for their committed supervision, and endless support. Working and studying under their supervision was a great honor and privilege. I am very appreciative for everything they have done for me, especially the time they have spent on helping me revise my manuscripts and thesis. I would also like to thank them for their patience, motivation enthusiasm, and immense knowledge, as well as their friendship and understanding, which have helped me overcome difficulties during my PhD.

I would like to express my sincere thanks to Prof. Paripurnanda Loganathan and Dr. Tran Nguyen Hai for their invaluable assistance and guidance throughout my studies, as well as their constructive comments, suggestions, and dedicating a considerable amount of time to each of my relevant research articles.

I would like to express my gratitude to the Australian Government Department of Foreign Affairs and Trade's (DFAT) innovationXchange (iXc) and Aus4Innovation programs and the University of Technology Sydney (UTS) for financial support for my research. I am thankful to Prof. Trinh Van Tuyen from the Institute of Environmental Technology (IET), Vietnam Academy of Science and Technology, Hanoi, Viet Nam; Assoc. Prof. Vu Duc Loi from the Institute of Chemistry, Vietnam Academy of Science and Technology, Hanoi, Viet Nam; and Assoc. Prof. Nguyen Thi Hoang Ha from the University of Science, Vietnam National University (VNU), Hanoi, Viet Nam for their supporting my PhD research during the period I conducted laboratory experiments and field trials in Vietnam.

The greatest thanks must be given to my family, whose love and support are constant sources of motivation for me. Last but not least, I would love to express my deepest

gratitude to my husband, my stepdaughter, and my son - Nguyen Huu Vu, Nguyen Phuong Linh, and Nguyen Thanh Vinh, who are always by my side, there to support me, and to give me love, power, and encouragement.

Finally, I would like to give special thanks to my friends at VNU, IET, and UTS, especially Ms. Van Le - School Academic Officer in the School of Civil and Environmental Engineering for their support to me during my PhD life.

JOURNAL PAPERS PUBLISHED

JOURNAL PUBLICATIONS

1**. Thi Hai Nguyen,** Hai Nguyen Tran, Hai Anh Vu, Minh Viet Trinh, Tien Vinh Nguyen, Paripurnanda Loganathan, Saravanamuthu Vigneswaran, Tuan Minh Nguyen, Van Tuyen Trinh, Duc Loi Vu, Thi Hoang Ha Nguyen (2020). Laterite as a low-cost adsorbent in a sustainable decentralized filtration system to remove arsenic from groundwater in Vietnam. *Science of The Total Environment*, **699**, 134267 (IF: **10.753**; SJR: **Q1**).

2**. Thi Hai Nguyen**, Anh Thao Nguyen, Paripurnanda Loganathan, Tien Vinh Nguyen, Saravanamuthu Vigneswaran, Thi Hoang Ha Nguyen, Hai Nguyen Tran (2021). Low-cost laterite-laden household filters for removing arsenic from groundwater in Vietnam and waste management. *Process Safety and Environmental Protection*, **152**, 154-163 (IF: **7.926**; SJR: **Q1**).

3. **Thi Hai Nguyen**, Hai Nguyen Tran, Tien Vinh Nguyen, Saravanamuthu Vigneswaran, Van Tuyen Trinh, Thanh Dong Nguyen, Thi Hoang Ha Nguyen, Trong Nhuan Mai, Huan-Ping Chao (2021). Single-step removal of arsenite ions from water through oxidation-coupled adsorption using Mn/Mg/Fe layered double hydroxide as oxidizing agent and adsorbent. *Chemosphere*, 133370 (IF: **8.943**; SJR: **Q1**).

4. **Thi Hai Nguyen,** Seongchul Ryu, Paripurnanda Loganathan, Jaya Kandasamy, Tien Vinh Nguyen, Saravanamuthu Vigneswaran (2022). Arsenic adsorption by low-cost laterite column: Long-term experiments and dynamic column modeling. *Process Safety and Environmental Protection*, **160**, 868-875 (IF: **7.926**; SJR: **Q1**).

5. **Thi Hai Nguyen**, Paripurnanda Loganathan, Tien Vinh Nguyen, Saravanamuthu Vigneswaran, Thi Hoang Ha Nguyen, Hai Nguyen Tran, Quoc Bien Nguyen (2022).

Arsenic removal by a pomelo peel biochar coated with iron. *Chemical Engineering Research and Design.* (*accepted*).

6. Tien Vinh Nguyen, Saravanamuthu Vigneswaran, **Thi Hai Nguyen**, Dai Quyet Truong, Van Tuyen Trinh, Duc Loi Vu, Nhat Thuy Vu, Manh Khai Nguyen, Hai Nguyen Tran (2022). Household water filters for arsenic and other pollutants removal in Vietnam. Water E-journal (*accepted*).

CONFERENCE PAPERS AND PRESENTATION

1. **Thi Hai Nguyen**, Minh Viet Trinh, Hai Anh Vu, Hai Nguyen Tran, Van Tuyen Trinh, Tuan Minh Nguyen, Thanh Dong Nguyen, Thi Hoang Ha Nguyen, Tien Vinh Nguyen, Saravanamuthu Vigneswaran. (2018). Arsenate removal from aqueous solution by a low-cost laterite based adsorbent. 8th International Forum on Green Technology and Management (IFGTM 2018), 4-5th September 2018, Hanoi, Vietnam.

2. **Thi Hai Nguyen**, Hai Anh Vu, Minh Viet Trinh, Hai Nguyen Tran, Tien Vinh Nguyen, Saravanamuthu Vigneswaran, Tien Minh Nguyen, Van Tuyen Trinh, Duc Loi Vu, Thi Hoang Ha Nguyen. A sustainable decentralised filtration system to remove arsenic from groundwater in the Red River Delta, Vietnam. The IWA Water and Development Congress & Exhibition 2019. 5th IWA Water and Development Congress & Exhibition 2019.

3. **Thi Hai Nguyen**, Hai Nguyen Tran, Quoc Bien Nguyen, Tien Vinh Nguyen, Saravanamuthu Vigneswaran, Van Tuyen Trinh, Thanh Dong Nguyen, Thi Hoang Ha Nguyen, Trong Nhuan Mai. (2020). Arsenic removal from water by Mn/Mg/Fe layered double hydroxides. 10th International Forum on Green Technology and Management (IFGTM 2020), 28th November 2020, Hanoi, Vietnam.

4. **Thi Hai Nguyen**, Hai Nguyen Tran, Quoc Bien Nguyen, Tien Vinh Nguyen, Saravanamuthu Vigneswaran, Thi Hoang Ha Nguyen. (2021). Removal of As(III) and As(V) from water using iron-coated pomelo peel (ICPP). 17th International Conference on Environmental Science and Technology (CEST2021), 1-4 September 2021, Athens, Greece.

5. **Thi Hai Nguyen**, Seongchul Ryu, Paripurnanda Loganathan, Saravanamuthu Vigneswaran, Tien Vinh Nguyen. (2021). Arsenic adsorption: Long term experiments and dynamic column modeling. 2nd International Conference on Waste, Energy and Environmental (ICWEE-2021) 23-24th Septermebr 2021, India.

6. **Thi Hai Nguyen**, Seongchul Ryu, Paripurnanda Loganathan, Jaya Kandasamy, Tien Vinh Nguyen, Saravanamuthu Vigneswaran. (2022). Theoretical adsorption modeling and simulation of toxic arsenic removal in continuous systems by Mn/Mg/Fe layered double hydroxide. International Online Conference on Sustainable Technologies in Water Treatment and Desalination (STWTD-2022) 28-29th January 2022, India.

7. **Thi Hai Nguyen**, Tran Nguyen Hai, Van Tuyen Trinh, Duc Loi Vu, Tuan Minh Nguyen, Anh Thao Nguyen, Paripurnanda Loganathan, Tien Vinh Nguyen, Saravanamuthu Vigneswaran, Thi Hoang Ha Nguyen. (2022). Arsenic removal from groundwater by low-cost laterite filtration systems. 2nd Vietnam Conference On Earth And Environmental Sciences (VCEES-2022) 7-11th August 2022, Vietnam.

AWARDS

Best Poster Award at the International Water Association Water and Development Congress 2019. A sustainable decentralised filtration system to remove arsenic from groundwater in the Red River Delta, Vietnam.

CONTENTS

LIST OF TABLES

LIST OF FIGURES

NOMENCLATURE

Al	: Aluminum
As	: Arsenic
As(III)	: Arsenite
As(V)	: Arsenate
C	: Cement
$C°$	: The selected standard state of As (C° = 1 mol/L)
C_d	: The total concentration of As (mg/L) in solution after desorption
C_e	: The total arsenic concentrations (mg/L) at equilibrium
C_o	: The total arsenic concentrations (mg/L) at beginning
C_t	: The total arsenic concentrations (mg/L) at time *t*
DI	: Deionized water
EBCT	: Empty bed contact time
EDS	: Energy-Dispersive X-ray Spectroscopy
Fe	: Iron
FTIR	: Fourier Transform Infrared Spectroscopy
g	: The exponent whose value must lie between 0 and 1 (dimensionless)
K	: The Khan equilibrium constant (L/mg)

k_1	: The rate constant of the pseudo-first-order equation (1/min)
k_2	: The pseudo-second-order rate constant [g/(mg×min)]
k_{AV}	: The Avrami kinetic constant (1/min)
$K_{Equilibrium}$	: The thermodynamic equilibrium constant (dimensionless)
K_F	: The Freundlich constant, which characterizes the strength of adsorption ((mg/g)(L/mg)n)
K_L	: The Langmuir constant related to the affinity between adsorbent and As (L/mg)
K_{LF}	: The Langmuir–Freundlich constant (L/mg)
K_{model}	: The Langmuir constant (KL)(L/mol)
K_{RP}	: The Redlich–Peterson constants (L/g)
k_{TH}	: The Thomas adsorption rate constant (L/h.mg)
L	: Lime
m_1	: The mas of adsorbent used (g)
m_2	: The mass of arsenic loaded adsorbent (g)
MCL	: The maximum contaminant limit
Mg	: Magnesium
Mn	: Manganese
Mn/Mg/Fe-LDH	: Mn/Mg/Fe-Layer Double Hydroxide
n_{AV}	: The fractional adsorption order corresponding to adsorption mechanism.

n_F	: The Freundlich intensity parameter, which indicates the magnitude of the adsorption driving force or surface heterogeneity(dimensionless; 0<n<1)
n_K	: The exponent of the Khan model (dimensionless)
n_{LF}	: An exponent of the Langmuir-Freundlich model(dimensionless; surface heterogeneity constant)
NLTT	: Natural laterite
nZVI	: Nanoscale zero-valent iron
PFO	: Pseudo-second-order
pH_{IEP}	: pH value at the isoelectric points
pH_{PZC}	: pH value at the point of zero charge
PPCI	: Pomelo peel biochar coated with iron
PSO	: Pseudo-first-order
Q	: The volumetric flow rate (L/h)
QCVN01:2009/BYT	: Vietnam Technical Regulation on Drinking Water Quality
q_d	: The mass of arsenic desorbed if the adsorption process is reversible (mg/g)
q_e	: The amount of arsenic adsorbed onto adsorbent at equilibrium (mg/g)
Q_K	: The Khan maximum adsorption capacity of adsorbent (mg/g)
Q_{LF}	: The Langmuir–Freundlich adsorption capacity of adsorbent (mg/g)

Q_{max}	: The Langmuir maximum adsorption capacity of adsorbent (mg/g)
q_r	: The mass of arsenic that remained adsorbed after desorption (mg/g)
q_t	: The amount of arsenic adsorbed onto adsorbent at time t (mg/g)
q_{TH}	: The maximum column As(V) adsorption capacity (mg/g)
R	: The gas constant [0.00831 kJ/(mol×K)]
R^2	: The determination coefficient values
S/S	: Solidification/stabilization
S_{BET}	: Brunauer-Emmett-Teller surface area
SEM	: Scanning Electron Microscope
T	: The absolute temperature (^{0}K)
TCLP	: Toxicity characteristic leaching procedure
TCVN 6355:2-2009	: Vietnam Technical Standard on Bricks Test Methods
TCVN 6477:2016	: Vietnam Technical Standard on Concrete Bricks
USEPA	: United States Environmental Protection Agency
V_1	: The volume of the arsenic solution (L)
V_2	: The volume of the desorbing agents (L)
V_{Total}	: Total Pore Volume
WHO	: World Health Organization

XPS	: X-ray photoelectron spectroscopy
XRD	: X-ray Diffraction
XRF	: X-ray Fluorescence
$\Delta G°$	: The standard Gibbs free energy change
$\Delta H°$	: The standard enthalpy change
$\Delta S°$	: The standard entropy change
$\chi 2$	: The Chi-Square values
a_{RP}	: The Redlich–Peterson constants (L/mg)g
α	: The initial rate constant of the Elovich equation [mg/(g×min)]
β	: The desorption constant during any one experiment (g/mg)
γ	: The activity coefficient of As in solution.

ABSTRACT

This thesis aims to develop novel iron-based adsorbents and investigate their performance in removing arsenic (As) from the water environment. Due to iron having a high affinity toward As ions, iron-containing adsorbents are deemed to be promising materials for removing As effectively from aquatic environments. In this study, 3 new iron-based adsorbents were successfully developed and investigated in detail in their ability to remove both arsenate (As(V)) and arsenite (As(III)) from synthetic and real contaminated groundwater. These were: (i) NLTT, a natural laterite obtained from natural iron–rich subsoil rock from Thach That district, Hanoi, Vietnam through the simple production process; (ii) PPCI, an iron-impregnated biochar derived from combination of iron coating and slow pyrolysis carbonization processes of an agricultural waste product - pomelo peel; and (iii) Mn/Mg/Fe-LDH, a Mn/Mg/Fe-layered double hydroxides adsorbent obtained through the simple co-precipitation method. Results of this study show that these three studied iron-based adsorbents can remove both As(III) and As(V) effectively from water environments. Mn/Mg/Fe-LDH exhibited the highest adsorption capacity toward both As ions and could be used for very high polluted water sources. The Langmuir maximum adsorption capacities of Mn/Mg/Fe-LDH toward As(III) and As(V) were 56.1 mg/g and 32.2 mg/g, respectively. The maximum adsorption capacities of PPCI were 11.77 mg/g for As(III) and 15.28 mg/g for As(V), respectively. PPCI could be a new solution of reusing pomelo peel, a widespread agricultural waste, for remediating As from contaminated water. Referring to immediate practical applications, NLTT is the most suitable candidate for As removal in Vietnam's rural areas due to its local availability, low cost (calculated commercial price of US$ 0.10/kg) and good As adsorption capacity (0.512 mg/g for As(III) and 0.580 mg/g for As(V)). NLTT has been successfully

implemented as a filter media in both household and community filters in the Red River Delta, Vietnam. The long-term monitoring results show that both household and community filtration systems packed with NLTT could produce safe drinking water with As levels below the WHO and Vietnam's drinking water limits after operating for 6–7 months. The exhausted NLTT adsorbent could be successfully managed by using solidification/stabilization method. The concrete bricks met the requirements of building materials as used in the construction industry. Although NLTT exhibited poorer adsorption capacities than PPCI and Mn/Mg/Fe-LDH, NLTT can quickly become a commercially viable As filter media. For PPCI and Mn/Mg/Fe-LDH, they have emerged as two practical promising adsorbents for removing As from water environments in the future.

Keywords: Arsenic removal; Adsorption; Laterite; Iron-impregnated biochar; Layer double hydroxides; Water treatment

CHAPTER 1. INTRODUCTION

1.1. Background of research

Water is necessary to life, and "everyone has the right to sufficient, continuous, safe, acceptable, physically accessible, and affordable water for personal and domestic use" (UN General Assembly, 2010). However, the lack of clean and safe drinking water is still a serious issue throughout the world and becoming worse. According to the World Health Organization (WHO), there were 785 million people suffering from the lack of even basic drinking water and most of them live in developing countries (WHO, 2017). Contaminated drinking water directly affects and endangers human health and is linked to the transmission of diseases.

Arsenic (As) is a highly toxic element and is ranked number 1 in the hazardous substances list recommended by the United States Agency for Toxic Substances and Disease Registry. As contamination in groundwater is a serious issue in many countries such as Bangladesh, Vietnam, India, China, USA, Mexico, etc. (Khan and Ho, 2011). Over 230 million people in nearly 108 countries worldwide are impacted by As contaminated groundwater (Shaji et al., 2020). There are 180 million people throughout South Asia (Bangladesh, India, Pakistan, and Nepal), China, and Southeast Asian countries (Vietnam, Thailand, and Cambodia) facing a high risk of As poisoning (Kim et al., 2011; Shaji et al., 2020). In natural water bodies, As is mainly found in two states: trivalent As (As(III), arsenite) and pentavalent As (As(V), arsenate). Both forms are highly toxic inorganic species (Smedley and Kinniburgh, 2002). The toxicity of As(III) is much greater than that of As(V). Consumption of As contaminated water over a long

period of time can seriously harm the lungs, liver, skin, and organs in the human body (Jain and Chandramani, 2018).

In Vietnam, the majority of its 97 million people live in two deltas, the Red River Delta located in the north and the Mekong River Delta located in the south, where the groundwater is highly contaminated by As (Berg et al., 2001; Agusa et al., 2006; Glodowska et al., 2021; Nguyen et al., 2020a). The total As concentration in groundwater in the Red River Delta and Mekong River Delta ranges from 0.001–3.05 mg/L (average 0.159 mg/L) and 0.001–0.845 mg/L (average 0.039 mg/L), respectively (Berg et al., 2007). The continuous use of As contaminated groundwater in daily activities threatens nearly ten million people in the Red River Delta and nearly one million people in the Mekong River Delta are at great risk of As poisoning. In the Red River Delta, Hanoi's suburb and Ha Nam province are considered to be the two areas most affected by As-contaminated groundwater (Berg et al., 2001; Agusa et al., 2006; Glodowska et al., 2021; Nguyen et al., 2020a).

Given the As contamination problem in water sources worldwide, a number of techniques have been developed and applied in removing As from drinking water. The treatment technologies include coagulation/flocculation, ion exchange, adsorption, oxidation, membrane, and phytoremediation (Ngo et al., 2002; Mohan and Pittman, 2007; Malik et al., 2009; Litter et al., 2019; Singh et al., 2021; Weerasundara et al., 2021). Notably, most people affected by As poisoning in water reside in rural areas in developing countries. Thus, simple and cost-effective As treatment technologies are needed. Of these technologies, adsorption is expected to be the most cost-effective method for removing As at the decentralized or local level (including households and small communities) because it is highly efficient, involves low capital cost, low energy consumption, simple

in design and operations, and generates minimal waste. Many commercial, synthetic, and natural materials have been studied as adsorbents in removing As from water environments. Iron-containing materials have been found to be the most suitable adsorbents because they possess high affinity to As (Pena et al., 2005; Giles et al., 2011). Iron-based adsorbents can also be magnetically collected, contributing to minimizing the secondary pollution or recycling laden adsorbents. Thus, in this thesis, three adsorbents containing iron (Fe) in their composition were devised from three different sources: a natural mineral (laterite), an agricultural waste (pomelo peel), and commercial chemicals and their performance was investigated in detail for both As(III) and As(V) removal in water environments.

Some popular commercial adsorbents (i.e., activated alumina and activated carbon) have been utilized to remove toxic As(III) and As(V) in drinking water treatment strategies (Kalaruban et al., 2019). However, their materials and regeneration costs are relatively high which limit their applications in most As contaminated areas, especially in developing countries' rural areas. Unlike commercial products, low-cost adsorbents based on natural mineral and waste industrial products (e.g., clay, goethite, zeolites, laterite, red mud, fly ash, etc.) possess certain favorable aspects, including local availability, inexpensiveness, and efficient As removal (Nguyen et al., 2009; Nguyen et al., 2020a). These factors have promoted the use of low-cost adsorbents as alternative adsorption media over the currently employed expensive adsorbents in removing As from contaminated water (Mohan and Pittman, 2007). Natural laterite is commonly formed in hot and wet tropical areas and is distributed widely in many areas throughout Vietnam (e.g., Thach That district, Hanoi; Ba Vi district, Hanoi, and Tam Duong district, Vinh Phuc) and other countries. This material is a potential medium for As removal because of

the natural presence of Fe and aluminium (Al) oxides/hydroxides in its constituents (Glocheux et al., 2013). *In the first part of this thesis, the new material, NLTT was developed from natural laterite collected from Thach That district (NLTT), Hanoi, Vietnam through the simple production process. The performance of NLTT on both As(III) and As(V) removal from the aqueous environment was investigated in detail through both batch and column studies with synthetic water in the laboratory*.

In addition to As removal by mineral-based adsorbents, there is increasing interest in combining iron with supporting media, including: (i) man-made materials such as cement (Kundu and Gupta, 2006), sand (Herbel and Fendorf, 2006; Chang et al., 2008), activated carbon (Chang et al., 2010), activated alumina (Kuriakose et al., 2004), and slag (Zhang and Itoh, 2005); (ii) natural-derived materials like cork granulates (Pintor et al., 2018), sugarcane bagasse (Pehlivan et al., 2013b), rice husk (Pehlivan et al., 2013b; Cope et al., 2014), and seaweeds (Vieira et al., 2017). The results from these studies demonstrate that iron-coated adsorbents achieved good As removal capacity. Many studies reveal that biochar can provide an excellent matrix to load iron because of its superior surface area and high porosity (Li et al., 2016a; He et al., 2018). Thus, some researchers tried to load iron on biochar in order to produce As adsorbents (Aredes et al., 2013; Zhang et al., 2013). Using biochar derived from agriculture industry residues could serve as a practical option for groundwater treatment in developing countries because of its abundant local availability, low-cost, simple preparation, and environmental friendliness. Pomelo (*Citrus maxima* or *Citrus grandis*) is the largest citrus fruit abundantly available in tropical countries, and Vietnam is no exception. With its high biomass, pomelo peel (30% by weight of the fruit) can cause environmental pollution when disposed of as waste (Liang et al., 2014; Wu et al., 2017).

Pomelo peel is a promising biomass-derived adsorbents because it contains many polysaccharides, including cellulose, pectin, and lignin (Zhang et al., 2019). Several studies reported that pomelo peels could be used to adsorb lead (Lim et al., 2019), cadmium (Saikaew et al., 2009), copper (Tasaso, 2014), and organic dye (Jayarajan et al., 2011; Zhang et al., 2019). However, their adsorption efficiency towards anionic species such as As(V) is poor because they possess negative surface charges which do not favor the adsorption of similarly charged anionic species. For this reason, they need to be modified in order to adsorb the anionic species. According to Cheng et al. (2020), an activated adsorbent produced from pomelo peel biochar provided a large specific surface area (up to 2457 m^2/g) and total pore volume (1.14 cm^3/g), which were responsible for the large adsorption capacity of the antibiotic tetracycline. The large surface area and high pore volume strongly associated with the presence of organic functional groups in the biochar can also facilitate the coating of iron compounds. Li et al. (2016b) successfully coated Fe_3O_4 on the porous surface of biochar derived from spongy pomelo pericarp. In other studies, iron oxide particles coated biochar obtained from the pomelo peel were successfully prepared and used for removing organic compounds such as Reactive Red 21 (Nguyen et al., 2020d), chrome, phenol (Dong et al., 2021), and rhodamine B (Liu et al., 2019a). Results of these studies indicate a good potential of using pomelo peel-derived biochar as an iron-coating adsorbent. Conversely, to the best of my knowledge, no study has yet been done or published on using this adsorbent to remove As from water. *Thus, in the second part of this study, an iron-coated biochar adsorbent derived from an agricultural waste, pomelo peel was developed and its performance regarding both As(III) and As(V) ions was investigated in detail.*

Recently, layered double hydroxides (LDHs) have garnered a lot of attention in removing both toxic cations and anions in aquatic environments due to their unique properties and simple synthesis processes (Asiabi et al., 2017; Wang et al., 2018; Tran et al., 2019). The LDHs belong to the synthetic clay group, one that possesses different ionic layer structures such as positively charged brucite-like layers and non-framework charge compensating anions in their galleries. With this in mind, the positive charge of the material's brucite layers can efficiently react with toxic anions via the electrostatic-attraction mechanism. Meanwhile, the host anions in the interlayer regions (i.e., CO_3^{2-} and NO_3^- anions) demonstrate a very high exchange with toxic anions in solution (Asiabi et al., 2017; Hudcová et al., 2017; Mubarak et al., 2018; Wang et al., 2018; Varga et al., 2021). Unlike As(V), As(III) exists as neutral molecular form (without any charge; $H_3AsO_3^o$ ions) with solution pH from 0 to 9.2 (Hudcová et al., 2017; Nguyen et al., 2020a), so the adsorption of As(III) using layered double hydroxides through their positively charged surface or host anions in their interlayer region might not be feasible. Some research has attempted to transform As(III) into As(V) by using oxidizing agents including peroxydisulfate, iron, chlorine, hypochlorite, manganese, and then remove As(V) from water (also known as a two-step removal process). For example, Neppolian et al. (2008) used peroxydisulfate ions to effectively oxidize As(III) into less toxic As(V) anions. However, after the oxidation process, a further removal stage (i.e., adsorption or coagulation) is required. To solve this problem, some researchers developed a material that exhibited advantageous properties (acting as oxidant and adsorbent) for removing both As(III) and As(V) from water. A one-step removal process of both As(III) and As(V) using Fe(II)/Mn(II) oxides was reported by Bai et al. (2016). Herein, As(III) ions in solution were firstly oxidized into As(V) anions when it contacted the Fe(II)/Mn(II)

oxides; subsequently, oxidized As(V) and As(III) in solution were adsorbed by this oxide material. This removal process involved a combination of mechanisms, namely oxidation-coupled adsorption. Most reseach done on As removal by LDH-based adsorbents focused on As(V) (Wang et al., 2009; Huang et al., 2015; Asiabi et al., 2017; Hudcová et al., 2017). This is due to the high anion-exchange capacity of such materials (Wang et al., 2018; Tran et al., 2019). Bagherifam et al. (2014) prepared Zn/Al-LDH and applied it in removing As(III) and As(V) from solution. Their findings revealed that Zn/Al-LDH has a higher removal capacity of As(V) than toxic As(III). This is due to the nature of metal salts (Zn and Al) employed during the synthesis of LDH. In other words, the removal of toxic As(III) by the LDH-based materials still needs to be better understood. *Thus, in the third part of this study, a new layered double hydroxide (Mn/Mg/Fe-LDH) was prepared from three metals (Mn, Mg, and Fe) through a one-step co-precipitation process. Consequently, the new Mn/Mg/Fe-LDH was investigated for its ability to remove both As(III) and As(V) ions from synthetic water.* Here, the Fe and Mn metals were selected because their oxides have been acknowledged as effective oxidants able to convert As(III) to As(V).

After finishing laboratory experiments for theoretical knowledge, it was critical to carry out an investigation on the application of adsorbents for removal of As in real contaminated groundwater. Based on the favorable results of NLTT in the laboratory and its low cost (calculated commercial price of US$ 0.10/kg), NLTT has beenemployed as a water filter media in several household and community water filter systems in Ha Nam province and Hanoi, Vietnam, where groundwater is seriously affected by As contamination. *In the fourth part of this thesis, the performance of NLTT in the field was evaluated through continuous monitoring of 4 representative household water filtration*

systems in Hoang Tay commune, Ha Nam province and Phuong Tu commune, Hanoi's suburb and 1 childcare water filtration system in Hoang Tay commune over 6-7 months. The management of exhausted NLTT by the solidification/stabilization method was also investigated.

1.2. Objectives and scope

The main goal of this thesis is to develop three novel iron-based adsorbents, namely (i) natural laterite from Thach That, Vietnam (NLTT), (ii) iron-coated biochar derived from pomelo peel (PPCI), and (iii) Mn/Mg/Fe layered double hydroxides (Mn/Mg/Fe-LDH) and evaluate their performance in removing As(III) and As(V) from aqueous environment. Moreover, the practical application of one new adsorbent - NLTT in removing As from real As-contaminated groundwater sources to an acceptable level in drinking water supplies - was also investigated through conducted field trials.

The specific objectives of this study are as follows:

1. Developing NLTT adsorbent and evaluating its performance on As(III) and As(V) removal in the laboratory and in the field (Chapters 3 and 6).
2. Developing PPCI adsorbent and evaluating its performance on As(III) and As(V) removal in the laboratory (Chapter 4).
3. Developing Mn/Mg/Fe-LDH adsorbent and evaluating its performance on As(III) and As(V) removal in the laboratory (Chapter 5).

In general, the following aspects of each adsorbent were investigated:

- ✓ Developing adsorbent;
- ✓ Evaluating the performance of adsorbent on As(III) and As(V) removal through batch and column studies with synthetic water;

- ✓ Determining adsorbent's characteristics before and after As adsorption;
- ✓ Investigating the mechanisms of As(III) and As(V) removal by adsorbent;
- ✓ Mathematical modeling, including kinetics, isotherms, and column models of As(III) and As(V) adsorption with each adsorbent.

In addition, more specific objectives were applied for NLTT:

- ✓ Evaluating the performance of the household and community water filters packed with NLTT in treating As-contaminated groundwater in Vietnam;
- ✓ Managing exhausted NLTT.

1.3. Research significance

This study successfully developed three novel iron-based adsorbents. Their performance in removing As from aqueous solution was investigated through detailed studies, including effects of contact time, initial As concentration, pH of the solution, temperature, presence of co-existing anions in batch study; and initial As concentration, column bed height and velocity in column study. The complex As removal mechanisms were identified through experimental results and detailed materials' characterization. As well, the study was carried out with both representative inorganic forms of arsenic (As(III) and As(V)) in water, which has not been investigated in detail yet. Last but not least, this study provided not only theoretical knowledge but also a practical application. One new adsorbent, NLTT, has been investigated successfully in many household and communities water filtration systems in As contaminated areas over a long period of time.

1.4. Thesis structure

This thesis is structured in to seven chapters and they are summarized here.

Chapter 1 (Introduction) introduces the key issue of As contamination in water, solutions and challenges in As treatment. It also highlights the advantages of adsorption technology in removing As ions. This chapter briefly presents the benefits of the iron-based adsorbents, including the new natural laterite NLTT, iron-coated biochar derived from pomelo peel PPCI, and Mn/Mg/Fe-LDH in As removal from water.

Chapter 2 (Literature review) presents a critical review of (i) sources, species, and toxicity of As in natural water; (ii) effects of As on human health and drinking water standards of As in drinking water; (iii) As treatment technologies; (iv) adsorption technology, including iron-based adsorbents, adsorption modeling, adsorption mechanism; and (v) management of exhausted adsorbents.

Chapter 3 presents the preparation and performance of low-cost NLTT adsorbent in removing As(III) and As(V) from synthetic water. The NLTT's characteristics before and after adsorption were determined using X-ray Fluorescence (XRF), X-ray Diffraction (XRD), scanning electron microscopy integrated energy dispersive X-ray spectroscopy (SEM-EDS), Fourier transform infrared spectroscopy (FTIR), surface area of adsorbent (S_{BET}), and the point of zero charge (pH_{PZC}). This chapter discusses the experimental results on the effects of pH solution, contact time, initial As concentration, coexisting anions, temperature on both As(III) and As(V) removal by NLTT as well as desorption process. In addition, the experimental results of As adsorption on NLTT columns at different experimental conditions were presented and discussed. Adsorption mechanisms

were identified through the experimental results and NLTT characterization. A mathematical modelling on the performance of fixed-bed columns is also discussed.

Chapter 4 presents the method of preparing iron-coated biochar derived from pomelo peel (PPCI) as well as the performance results (batch and column) of PPCI concerning As(III) and As(V) removal. The characterization of PPCI before and after adsorption as well as the As removal mechanism are also discussed in detail.

Chapter 5 presents a simple co-precipitation method of preparing a new layered double hydroxides material (Mn/Mg/Fe-LDH). The batch and column experiments of As(III) and As(V) adsorption on Mn/Mg/Fe-LDH were carried out and the results are discussed in detail. The characterization and adsorption mechanism of Mn/Mg/Fe-LDH toward As(III) and As(V) removal are also presented.

Chapter 6 presents the application of NLTT as a new filter media in household and community water filtration systems for treating of As contaminated groundwater in Ha Nam province and Hanoi' suburb, Vietnam. The performance results of long-term monitoring (6–7 months) of 4 household and 1 childcare water filtration systems, including the material's characterization are reported and explained. This chapter also presents an analysis of the management of exhausted NLTT using stabilization/solidification method.

Chapter 7 summarizes the main findings of this study and proposes recommendations for future work on these new adsorbents.

The flow diagram of the seven chapters is presented in **Figure 1.1**.

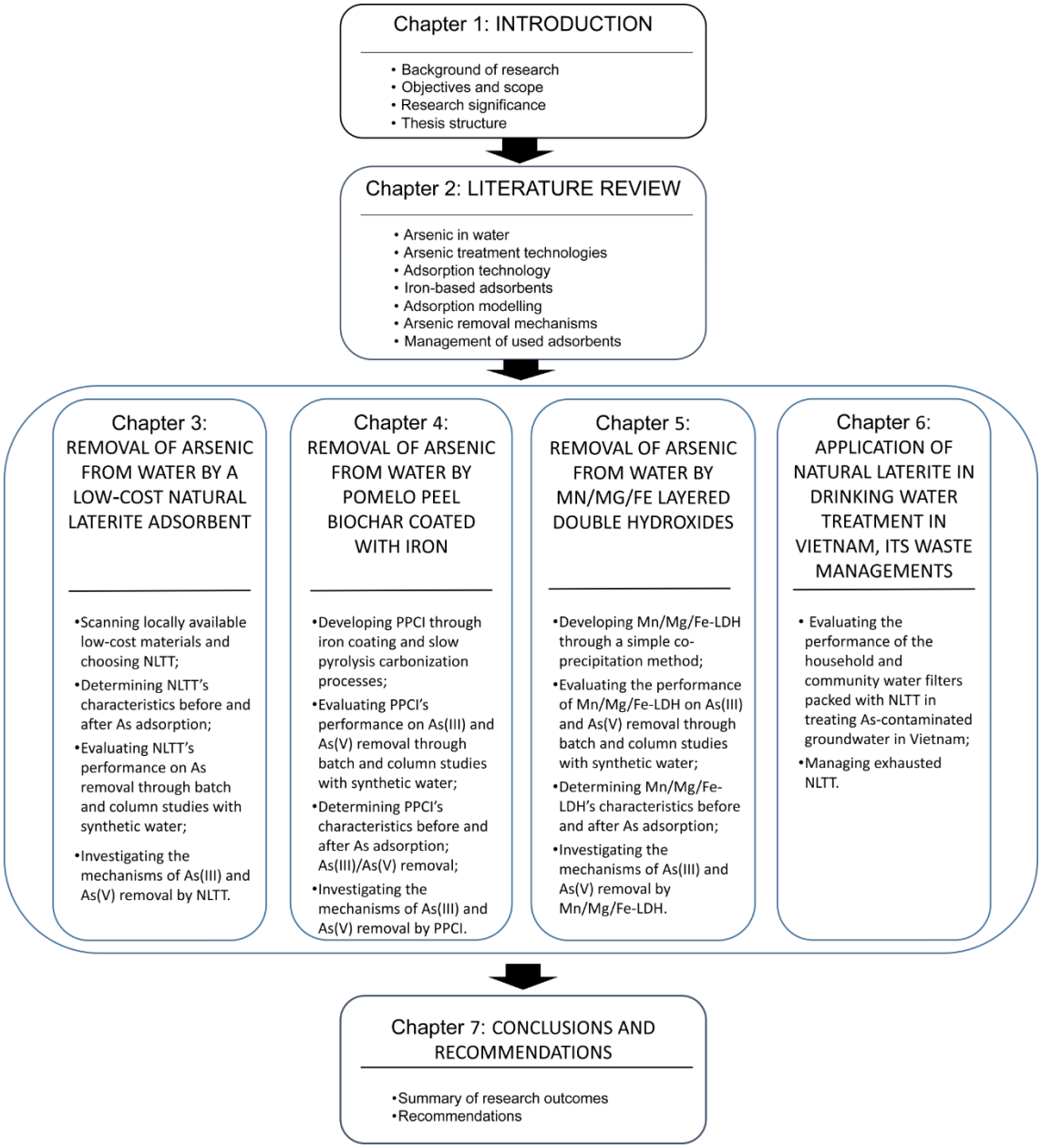

Figure 1.1. Flow diagram of the thesis

CHAPTER 2. LITERATURE REVIEW

2.1. Sources of arsenic

The main sources led to the presence of As in groundwater include natural activities and human activities (Smedley and Kinniburgh, 2002; Kim et al., 2011) (**Table 2.1**). In nature, As is a major constituent of more than 200 minerals. Arsenopyrite (FeAsS), pyrite ($Fe(SAs)_2$), realgar (AsS), orpiment (AS_2S_3), and lollingite ($FeAs_2$, $FeAs_3$, and $FeAs_5$) are the most common As-containing minerals (Smedley and Kinniburgh, 2002). The leaching of As from mineral sediment to groundwater is considered to be a major cause of As in groundwater in many areas and is controlled by a number of factors, including: reducing and oxidizing conditions; abundance of degradable organic material; and hydrogeological and morphological characteristics of the aquifer. The reducing and oxidation of As-rich soil and minerals, as well as the dissolution of As-rich Fe oxyhydroxide, are the reasons for As contamination in groundwater in many countries such as Bangladesh, Taiwan, India, Vietnam, Hungary, and Romania (Berg et al., 2007). In the Mekong and Red River Deltas in Vietnam, several hydrological features, including rapidly sedimentation of alluvial materials, delta topography characteristic, and decomposition of organic matter-rich sediments, have been identified as the primary reasons of natural occurring As in groundwater (Berg et al., 2007). As can also occur under oxidation conditions, and it can be found in the arid and semi-arid areas found in the United States, Mexico, and Argentina. In Latin America, the main As sources are linked to magmatic activities, including volcanic ash and sulfide deposits. Thus arsenic contamination has been detected in more than 100 aquifers throughout river basins in this area (Masuda, 2018; Bundschuh et al., 2021).

Table 2.1. Sources leading to of the presence of As in nature

Main sources	Sub-sources
1. Natural processes	Weathering activities of minerals (As rich minerals: pyrite (FeS_2), arsenopyrite (FeAsS), and other As sulphide minerals), rock (igneous, metamorphic, and sedimentary rocks), sediments (unconsolidated sediments: alluvial mud, clay, and sand), or soils. Volcanic activities: Dissolution of As from volcanic rocks, volcanic ash, and geothermal fluids into ground - and surface water and soils. Biological activities: relating to the depleting oxygen level in the alluvial's bottom lakes and rivers.
2. Anthropogenic processes	Industrial activities: mining and mining-related activities, smelting of non-ferrous metals, combustion products (wood, coal, and trash), medical waste, wood treatment agents, etc. Agricultural activities: pesticides, herbicides, insecticides, feed additive.

Mining and mining-related activities (Sn-mining, Au- mining, and Pb–Zn–Ag mining) are also believed to be a cause of As mobility in water in many parts of the United

States, Thailand, Ghana, and elsewhere (Kim et al., 2011). The formation of acid mine drainage contributes to the oxidation reactions, dissolves, and releases As from minerals into water. Smelting of non-ferrous metals and combustion products (wood, coal, and trash) are key industrial activities that contribute to As contamination of the environment (Bundschuh et al., 2021). Another anthropogenic As source derives from the widespread use of As-containing pesticides and herbicides.

2.2. Arsenic species

In the environment, As may occur in a variety of oxidation states, including -3, 0, +3, and +5. However, As is typically present in inorganic forms of trivalent arsenite [As(III)] or pentavalent arsenate [As(V)] in natural water (Siddiqui and Chaudhry, 2017; Smedley and Kinniburgh, 2002). As(III) is more toxic (approximately 5–10 times) than As(V) because of its high solubility and mobility (Wang and Mulligan, 2006; Jang et al., 2016; Gupta, 2018). Notably, the occurrence of differences of As speciation in aqueous environment is strongly dependent on pH. **Figure 2.1** shows the distributions of As species as a function of pH. **Figure 2.2** shows how redox potential and pH control the dominance of As species in natural water**.** Under the slightly reducing condition and low pH (pKa < 9.2), As(III) is found in stable form H_3AsO_3. In oxidizing conditions, the charged As(V) species ($H_2AsO_4^-$, $HAsO_4^{2-}$, AsO_4^{3-}) is dominant in the pH range of 2.3–11.6, while at the highly acidic and alkaline environment, $H_3AsO_4^o$ and AsO_4^{3-} can be presented as arsenate species. The deprotonation of As species in solution is listed in **Table 2.2.**

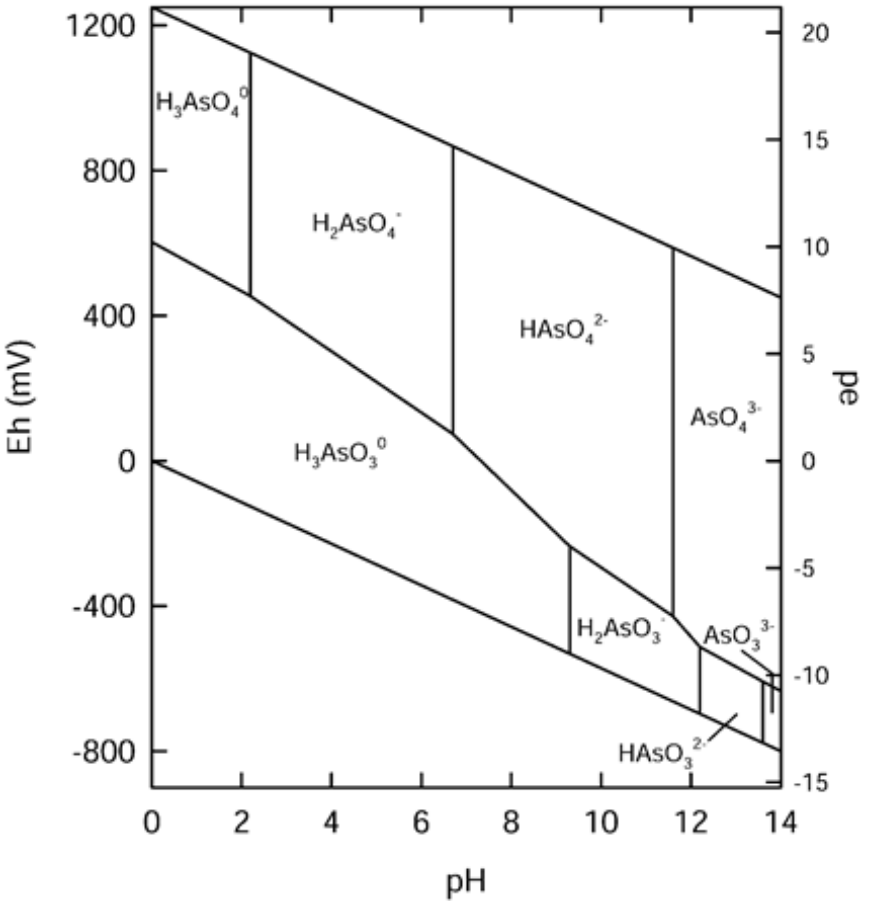

Figure 2.1. Eh–pH diagram of As species (Smedley and Kinniburgh, 2002)

Table 2.2. Deprotonation of As species in solution

Deprotonation of As(III) species	
$H_3AsO_3^o \rightleftharpoons H^+ + H_2AsO_3^-$	$Pka_1 = 9.2$
$H_2AsO_3^- \rightleftharpoons H^+ + HAsO_2^{2-}$	$Pka_2 = 12.1$
$HAsO_2^{2-} \rightleftharpoons H^+ + AsO_3^{3-}$	$Pka_3 = 12.7$
Deprotonation of As(V) species	
$H_3AsO_4^o \rightleftharpoons H^+ + H_2AsO_4^-$	$Pka_1 = 2.3$
$H_2AsO_4^- \rightleftharpoons H^+ + HAsO_4^{2-}$	$Pka_2 = 6.8$
$HAsO_4^{2-} \rightleftharpoons H^+ + AsO_4^{3-}$	$Pka_3 = 11.6$

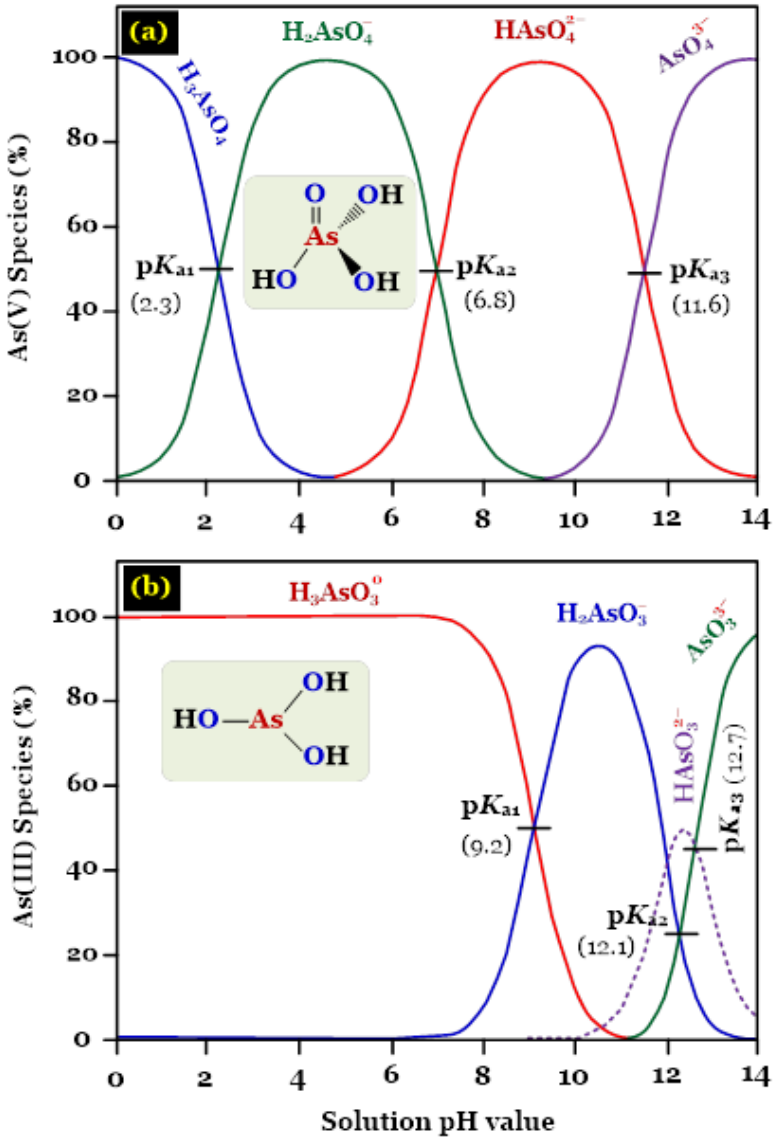

Figure 2.2. Distribution of (a) As(V) and (b) As(III) species as a function of pH

(The numbers in parentheses denote the pKa value). Data were adapted from the literature (Kumar and Jiang, 2017; Arencibia et al., 2020) with some revisions.

2.3. Effect of arsenic on human health

As is a highly toxic and carcinogenic substance that enters the human body by ingestion and/or inhalation. The toxicity of As to humans is primarily determined by the chemical form and physical state of the molecules involved. Moreover, the effects of As

on human health depend on the amount of As consumed and individual factors such as sex, age, health status, individual sensitivity to As, nutritional status, and lifestyle. As affects almost all organs and other functions of the human body, such as cardiovascular, integumentary, hematopoietic, nervous, respiratory, endocrine, immune, hepatic, and renal systems. Long-term exposure to As has been proven to cause carcinogenesis in the skin, lungs, liver, bladder, kidneys, and prostates in people.

Over 230 million people in over 108 countries are considered to be harmed by contaminated groundwater. More than 180 million people in South Asia (Bangladesh, India, Pakistan, and Nepal), China, and Southeast Asia (Vietnam, Thailand, and Cambodia) are in danger of being poisoned by As (Kim et al., 2011; Shaji et al., 2020). In Bangladesh, 85 million people are now exposed to As contaminated water and 27% of groundwater has been found to be contaminated with high As concentrations (> 0.05 mg/L) (Smedley and Kinniburgh, 2002). In some districts in Bangladesh, more than 90% of tube wells are contaminated by As. In India, the concentration of As in groundwaters from the affected areas is reported to be at a high level, up to 1.80 mg/L, and more than one million people suffer from chronic As poisoning. In Southeast Asia, million residents are at risk from consuming As contaminated groundwater. In Red River Delta, Vietnam, groundwater samples from private small-scale tube wells have As levels varying from 0.001–3.05 mg/L. The most affected areas of the country are mainly the rural ones (Berg et al., 2007; Kim et al., 2011).

2.4. Standards of arsenic in drinking water

The recommended value for a safe limit for As (0.01 mg/L) in drinking water is established by the World Health Organization (WHO). However, in many countries such

as Mexico and Bangladesh, the permissible limits for As in drinking water is higher, up to 0.05 mg/L (Mohan and Pittman Jr, 2007; Kim et al., 2011). **Table 2.3** shows the allowable value of As in drinking water in major nations affected by As contamination.

Table 2.3. Drinking water limits for As in different countries

Country	Drinking water limits (mg/L)
World Health Organization (WHO)	0.01
Germany, USA, Taiwan, Vietnam, China, Australia, India	0.01
Chile, Bangladesh, Argentina, Mexico, Nepal	0.05

2.5. Arsenic treatment technologies

Removing As from water has been proposed utilizing a range of advanced and conventional treatment methods, at both the laboratory and full-scale operating levels. The main As treatment technologies include oxidation, coagulation-flocculation, phytoremediation, ion exchange, membrane filtration, and adsorption (Ngo et al., 2002; Mohan and Pittman Jr, 2007; Malik et al., 2009; Litter et al., 2019; Singh et al., 2021; Weerasundara et al., 2021). A brief description of these techniques is presented in **Table 2.4**.

Table 2.4. Methods for treating arsenic in water

Technology	Description	Advantages	Disadvantages
Oxidation	Several oxidants are used to oxidize toxic As(III) into less hazardous compounds (As (V)). Chemical oxidation is used as a pre-treatment procedure to improve the removal efficiency of other techniques.	Easy to operate Has the ability to manage a large amount of water High efficient for the removal of As(III)	Requires additional treatment methods Generates toxic chemicals and carcinogens
Coagulation-flocculation	Chemical reagents are used to destabilize and increase the size of the particles. The large flocs are then physically separated from the liquid. In water treatment, filtration is commonly used to achieve this separation.	Works quite well across a wide pH range Hasthe ability to handle a large amount of water High efficient for the removal of As(V)	Requires additional separation step Highly affected by coagulant dose Dose not work well for As(III) extraction

Technology	Description	Advantages	Disadvantages
Phytoremediation	Plants serve to remove contaminants from contaminated soil and water. Pollutants from polluted soil and water are taken up by the root systems of the plants.	Environmentally friendly Economically feasible Prevents the risk of spreading contaminants	Requires a large space Depends on location, season, and plants Requires biomass management after treatment
Membrane Filtration	Water is passed through a semi-permeable barrier of the membrane and then contaminants separated from water. The membrane allows water and some components to pass through while others are prevented (including As).	High removal efficiencies Maximum efficiency of 99% for As(V) Low space requirement Can efficiently remove multiple contaminants	High capital cost High running and maintenance cost High rejection of water Requires pretreatment methods

Technology	Description	Advantages	Disadvantages
Ion Exchange	The reversible interchange of the same charged ions between one ion present on the surface of an insoluble solid with other ions in a solution.	Independent of pH solution and influent concentration Reduces toxic sludge production Maximum efficiency of 97.9% for As(V)	Dose not work well for As(III) extraction and require the pre-treatment Interference from SO_4^{2-}, TDS, Se, F^- and NO_3^- anions to As ions
Adsorption	This process is a surface phenomenon between adsorbent and adsorbate. Concentrated adsorbates onto the surface of adsorbent, leading to reducing their concentration in solution.	Simplicity in operation and maintenance Cost-effectiveness High removal efficiency Some adsorbents able to remove both As(III) and As(V)	Highly affected by competitive anions (PO_4^{3-}, CO_3^{2-} and SiO_3^{2-}) Requires management of the exhausted adsorbent to prevent As spreading back into the environment

Each treatment method possesses its own set of advantages and disadvantages. For example, the oxidation method has received positive attention due to its simplicity, inexpensive installation cost, ability to handle a large water volume, and effectiveness in removing As(III). However, the utilized oxidants can create poisonous and carcinogenic chemicals, which are disadvantages (Sorlini et al., 2010, Singh et al., 2021; Weerasundara et al., 2021). In ion exchange, the treatment process is independent of pH solution and influent concentration, and there is no need to adjust the pH solution. However, the presence of other anions such as SO_4^{2-}, F^-, and NO_3^- can reduce the capacity to remove As with this method. Moreover, suspended particles and iron precipitates can quickly block the system and reduce the effectiveness of As removal (Mohan and Pittman, 2007; Malik et al., 2009; Litter et al., 2019). Coagulation-flocculation can remove 90% of As(V) from a solution, and it is normally applied on a centralized water treatment scale. Its disadvantages include a large initial capital investment, and pre-treatment requirements (Hering et al., 1997; Mohan and Pittman, 2007) which are time- and cost-consuming. Of these, the application of membrane filtration has recently been widely applied due to its high efficiency, easy and minimum operation by human personnel, employed in both centralized and decentralized scales, and saving of space (Schmidt et al., 2016, Singh et al., 2021). However, this technology is still quite expensive, consumes a lot of power, and generates a significant amount of water rejection. Moreover, together with As and other pollutants, reverse osmosis membranes remove necessary trace ions in treated drinking water. Phytoremediation technology is an environmentally friendly method but its disadvantages are large space requirements and climate dependence (Ngo et al., 2002; Mohan and Pittman, 2007). Of the various methods of As removal, the adsorption process is generally considered to be an effective option for decentralized treatment systems

(communities and household levels) because of its simplicity and cost-effectiveness, simple design, easy operation, and maintenance (Mohan and Pittman, 2007; Nguyen et al., 2020a). Many adsorbents are only successful in removing As(V) and not really able to deal with As(III). For this reason, when a high As(III) level is found in water, the pre-treatment step (oxidation step to transform As(III) to As(V)) is required. In adsorption technology, many iron-containing adsorbents were reported to have a dual function, acting as oxidation agents as well as adsorbent.

2.6. Adsorption technology

2.6.1. Adsorbent and adsorption concept

Adsorption is a physical-chemical process that occurs when adsorbates are adsorbed to the surface of adsorbents. Numerous adsorbents are applied in the As removal, as natural adsorbents (laterite, zeolite, clay minerals, etc.); industrial by-products (red mud, iron mine waste sludge, etc.); agricultural by-products (biochar, activated carbon, etc.); and synthetic materials (layered double hydroxides nanomaterials, iron-oxide coated material, etc.). The factors that affect the adsorption process include adsorbent particle size, adsorbent dosage, pH, initial adsorbate concentration, temperature, and contact time.

2.6.2. Removal of As by iron-based adsorbents

Iron-based adsorbents have been extensively developed and applied to remove As species from the water environment due to their high affinity towards As. In the literature, popular iron-based adsorbents are classified into 6 groups (Hao et al., 2018) as follows:

- Iron oxides/hydroxides.
- Iron-coated natural mineral adsorbents.

- Iron-coated bio-adsorbents.
- Iron-coated activated carbon.
- Nanoscale zero-valent iron (nZVI) and nZVI coated adsorbents.
- Iron-based layered double hydroxides (LDH).

2.6.2.1. Iron oxides/hydroxides

Among iron-based adsorbents, iron oxides/hydroxides are the most extensively investigated due to their high affinity towards As and ease of accessibility. The most well-known iron oxides/hydroxides are magnetite (Fe_3O_4), hematite (Fe_2O_3), and FeOOH polymorphs (e.g., goethite (α-FeOOH), akaganèite (β-FeOOH), lepidocrocite (γ-FeOOH), ferrihydrites ($Fe_{10}O_{14}(OH)_2$), granular feric hydroxide (GFH)) (Chowdhury and Yanful, 2010; Hao, et al., 2018). Furthermore, the polymorphs of the FeOOH group are normally synthesized by chemical precipitation methods from Fe(III) or Fe(II) salts. Banerjee et al. (2008) reported that granular ferric hydroxide (GFH) with akaganèite (β-FeOOH) in their main composition was used as a commercial adsorbent on an industrial scale. GFH possessed a particle size of 0.32–2mm, a surface area of 240–300 m^2/g, pH_{PZC} of 7.6–7.8, and an adsorption capacity of 1.1 mg/g towards As(V) at pH = 6.5.

Many studies also investigated the As(III) removal capacity of iron oxides nanoparticle adsorbents. Magnetite (Fe_3O_4) and hematite (Fe_2O_3) were reported to be able to remove both As(III) and As(V) (Chowdhury and Yanful, 2010; Bujňáková et al., 2013). Fe(III) ions in these minerals were employed to oxidize the stable As(III) to As(V). During the As(III) oxidation process, Fe(III) ions were also reduced to Fe(II) ions.

Table 2.5. The Langmuir maximum adsorption capacity *(Q_{max})* of As by some iron oxides/hydroxides

Adsorbents	S_{BET} (m^2/g)	Co As (mg/L)	m/V (g/L)	pH	Q_{max} (mg/g)		References
					As(III)	As(V)	
Granular ferric hydroxide (GFH)	240–300	-		6.5	-	1.1	Banerjee et al. (2008)
Nanocrystalline-Fe_3O_4	11.9	1–100	8	7.9	-	4	Bujňáková et al. (2013)
Mixed magnetite–maghemite nanoparticles	49	0.5–4	0.4	2	3.69	3.71	Chowdhury and Yanful, (2010)
Geothite (from USA)	13	0.1–3	1.25	7	-	1.31	Ramirez-Muñiz et al. (2018)
Geothite (from China)	9.015	-	1	7	-	1.183	Dai et al. (2016)
Hematite (from India)	14.40	0–0.5	4.2	2	-	0.20	Singh et al. (1996)
Hemantite (from Sinopharm chemical reagent company, China)	4.159	-	1	7	-	0.845	Dai et al. (2016)
Natural laterite (from India)	18.05	1–3	20	7.2	0.17	-	Maiti et al. (2007)
Laterite soil (from India)	15.36	-	20	7.2	-	0.18	Maji et al. (2008)
Natural siderite (from Germany)	-	0.25–2		2	1.04	0.52	Guo et al. (2007)

With this mind, some natural iron-rich minerals such as laterite, laterite soil, and siderite are considered as promising and cost-effective materials for As adsorption (Guo

et al., 2007; Maiti et al., 2007; Maji et al., 2008). Laterite adsorbents exhibit a large specific surface area and possess a high amount of Fe (18.05–182 m^2/g and 45.64–52.05%, respectively) (Maiti et al., 2007; Maji et al., 2008). As a result, it was shown to be more successful at removing As from water than goethite (α-FeOOH), magnetite (Fe_3O_4), and hematite (Fe_2O_3) for As removal from water environment. Natural siderite has also been investigated extensively for its ability to remove As(III) and As(V) species from water. However, the adsorption capacity of siderite was relatively poor (Guo et al., 2007). **Table 2.5** shows the Langmuir adsorption capacity of iron oxides/hydroxides towards As reported in the literature.

2.6.2.2. Iron-coated natural mineral adsorbents

The most common natural minerals adsorbents include minerals in clay group (such as kaolinite, montmorillonite, bentonite, etc.), rocks in zeolite group (chabazite-phillipsite, clinoptilolite, and volcanic glass), sand, and rock. These materials are very popular in many parts of the world, but they exhibit low As adsorption capacity due to the presence of negative charges in their surface structure. Thus, the development and investigation of iron-coated natural mineral adsorbents on As removal has become more attractive recently due to their abundant local availability, simplicity, and environmental friendlessness. Fe(III)-modified montmorillonite was synthesized from sodium-exchanged montmorillonite (Na-M) with Fe(III) salt. The adsorbent characterization showed that polymeric Fe(III) species were in fact well distributed on the external surface of the resulting adsorbent. The maximum adsorption capacity of the Fe-M toward As(V) was 3.9 mg/g at the pH solution of 6 (Luengo et al., 2011). Foroutan et al. (2019) examined the As removal ability of natural clay and clay/Fe-Mn composite. Their results indicated that the Langmuir maximum adsorption capacity of a composite of clay/Fe-Mn

towards As(V) was 120.70 mg/g, which is much greater than that of natural clay (86.86 mg/g). An iron modified clinoptilolite (Fe1-GC) was also synthesized for As(V) removal from a water environment. The adsorption rate of As(V) on Fe1–GC increased quickly in the first 5 minutes of contact and became constant after 60 minutes (Bilici and Pala, 2011). A number of papers employed iron-coated sands (Thirunavukkarasu et al., 2003; Gupta et al., 2005) and their reclaimed form (Hsu et al., 2008) as adsorbents to remove As from an aqueous solution. These iron-coated sands were considered to be effective media for As remediation from contaminated groundwater in rural and remote areas in developing countries. According to Gupta et al. (2005), iron-coated sand was prepared by mixing dried river sand and ferric nitrate solution at pH 11, and the Langmuir maximum adsorption of As(III) by iron-coated sand was 0.028 mg/g. This is significantly higher than uncoated sand (0.0056 mg/g) at pH 7.5.

2.6.2.3. Iron-coated bio-adsorbents

Iron-coated natural bio-adsorbents and iron-coated biochars are reported to be cost-effective, environmentally friendly, and sustainable sorbents that have a remarkable potential to efficiently remove As from water. The most common bio-adsorbents are agricultural waste (rice husks, sawdust, corn straw, corn stem, maize cobs, orange peel, pomelo peel, etc.).

The adsorption of As from water onto iron-coated natural bio-adsorbents has been reported widely (Khaskheli et al., 2011; Tian et al., 2011; Pehlivan et al., 2013b; Sheng et al., 2014; Dorraji et al., 2014). Most of the natural bio-adsorbents were normally pretreated by NaOH solution to increase the specific surface area and number of hydroxyl groups on the adsorbent's surface. Tian et al. (2011) synthesized magnetic wheat straw

by using co-precipitation method for As removal. They found that magnetic wheat straw (MWS) containing Fe_3O_4 could be recycled and reused for As adsorption at least ten times. Pehlivan et al. (2013b) evaluated the removal of As(V) by iron-impregnated rice husks. Their findings revealed that iron-coated rice husk is considered as a low-cost material for As(V) removal. **Table 2.6** shows the Langmuir adsorption capacity of reported iron-coated bio-adsorbents for removing As from water.

Biochar is a stable carbonaceous product and derived from agricultural or food-industry biomass, which is normally obtained by the pyrolysis process at a temperature ranging from 300 to 1000 °C. Due to its abundance, inexpensiveness, and widesprear availability, biochar has been proposed as a potential adsorbent for wastewater treatment. Iron-loaded biochar or biochar derived from iron-loaded bio-adsorbent could be an effective adsorbent in removing As from water. Rice husk is considered to be a potential adsorbent due to its hydrophilic, porous, and large surface area features, as well as its high resistance. Studies on using iron-coated rice husk as adsorbent for As removal were developed several years ago (Samsuri et al., 2013; Cope et al., 2014). Samsuri et al. (2013) showed that iron-coated rice husk biochars could be used in removing both As(V) and As(III). Their result revealed that the maximum adsorption capacity of iron-loaded biochar for As(V) and As(III) were 16.0 mg/g and 30.7 mg/g, respectively, which is much higher than rice husk biochar (Q_{max} As(V) = 7.1 mg/g and Q_{max} As(III) = 19.3 mg/g). Kim et al. (2019) conducted a study to investigate As(III) removal by Fe-modified biochar powder and beads. Their results indicated that the maximum As(III) adsorption capacity of iron-modified biochar powder and beads were 13.5 and 11.29 mg/g, respectively. The values were greater than that of a previous report for unmodified biochar (Kim et al., 2019).

Table 2.6. The Langmuir maximum adsorption capacity (Q_{max}) of As by some iron-coated bio-adsorbents

Adsorbents	S_{BET} (m^2/g)	T (^oC)	m/V (g/L)	pH	Co As (mg/ L)	Q_{max} (mg/g)		Ref.
						As(III)	As(V)	
Iron-coated honeycomb briquette cinder	-	50	0.26	7.5	0.10–0.50	-	0.961	Sheng et al. (2014)
Fe(III)-coated rice husk.	-	80	4	4	1–75	-	2.5	Pehlivan et al. (2013b)
Fe (III)-loaded chitosan hollow fibers	-	60	-	3.5	0.2–0.3	-	3.703	Dorraji et al. (2014)
Iron-loaded orange peel	-	60	10	7	0.01–50	-	37.5	Khaskheli et al. (2011)
Fe_3O_4 coated wheat straw	4.73	70	0.5	6–8	1–28	3.898	4.018	Tian et al. (2011)
Iron oxide amended rice husk char	77.3	550	1	6.8	0–2.5	-	0.6	Cope et al. (2014)
Fe-modified corn straws	208	620	1	7	0.2–50	-	8.25	Lin et al. (2017)
Fe-coated cork granulates	-	60	2.5		1–40	4.9	4.3	Pintor et al. (2018)
Fe-modified biochar powder	123.8	500	2.0	7.2	1–30	13.5	-	Kim et al. (2019)
Fe-modified biochar beads	123.8	500	2.4	7.0	1–30	11.29	-	
HA/Fe-Mn oxides-loaded biocha	82.877	70	0.5	7	10–70	-	35.59	Guo et al. (2019)

2.6.2.4. Iron-coated activated carbon

Granular activated carbon (GAC) has been applied as an adsorbent for removing various contaminants from water environment because of its high specific surface area property. It is also reported to be the most common commercial adsorbent applied at both centralized and decentralized contexts. However, GAC exhibits a low adsorption capacity toward As species because of its negatively charged surface. In the past few decades, many studies tried to load iron oxide onto activated carbons (hybrid adsorbents) in order to enhance As adsorption capacity and mechanical properties. In these composite adsorbents, iron oxide particles play a key role as an active component for As removal because of their high affinity towards As species. Meanwhile the advantage of using GAC is due to its high surface area. Thus, mixing between iron oxide and GAC was shown to be a feasible strategy for combining the outstanding features of two materials for As adsorption. There are various methods that have been developed and applied for coating iron onto GAC. The most common procedure was to employ an iron salt solution as a precursor, then precipitate ferric onto GAC at an appropriate pH. **Table 2.7** presents the maximum adsorption capacities of some iron-coated activated carbon adsorbents toward both As ions as documented in the literature.

The improvement of As adsorption capacity of iron-coated activated carbon has been reported (Chen et al., 2007; Tuna et al., 2013; Vitela-Rodriguez and Rangel-Mendez, 2013). Vitela-Rodriguez and Rangel-Mendez (2013) investigated the As removal capacity of activated carbons coated with iron hydro(oxide) nanoparticles at different ratios. Their results showed that modified activated carbon adsorbents exhibited high surface areas, ranging from 632 m^2/g to 1101 m^2/g. Their Langmuir maximum As adsorption capacity ranged from 0.370 mg/g to 1.250 mg/g. A few years later, Ryu et al.

(2017) successfully developed Fe–Mn binary oxide-impregnated GAC (IMIGAC) to remove both As(V) and As(III) from groundwater. Their results showed that IMIGAC effectively removed both As(III) and As(V) without pre-oxidation. The Langmuir adsorption capacities of As(III) and As(V) by IMIGAC were 18.4 mg/g and 16.0 mg/g at 20 ^{o}C, respectively.

Table 2.7. The Langmuir maximum adsorption capacity (Q_{max}) of As by some iron-coated activated carbon

Adsorbents	S_{BET} (m^2/g)	m/V (g/L)	Co As (mg/L)	Q_{max}		Ref.
				As(III)	As(V)	
AC modified with iron hydro(oxide) nanoparticles	632–1101	0.75	0.050	-	0.370–1.25	Vitela-Rodriguez and Rangel-Mendez (2013)
Iron-impregnated GAC	-	2.8	0.5–10	-	1.95	Chang et al. (2010)
Fe(II)-loaded IAC	987–	0.4	0.5–8.5	-	2.823	Tuna et al. (2013)
Fe(III)-loaded IAC	1231	0.4	0.5–8.5	-	4.663	
GAC-Fe	876	0.1–0.8	0.1	-	1.430	Kalaruban et al. (2019)
Iron-modified AC	-	0.1–20	20–22	38.8	51.3	Chen et al. (2007)
Iron hydroxide/manganese dioxide doped straw AC	507.5	1	0–350	75.82	-	Xiong et al. (2017)
IMIGAC	420.12	3.3	1–600	18.43	15.95	Ryu et al. (2017)

2.6.2.5. Nanoscale zero-valent iron (nZVI) and nZVI coated adsorbents

Nanoscale zero-valent iron (nZVI) has attracted a great deal of attention as an effective adsorbent in removing many common contaminants in aqueous environment. nZVI has been widely used to remove As from contaminated water because of its large surface area, remarkably small particle size, and high in-situ reactivity. The As was mostly removed through co-precipitation of As with iron oxides/hydroxides which was formed during nZVI corrosion (oxidation). In natural water, dissolved oxygen plays an essential role in corrosion reactions. In the presence of dissolved oxygen, a considerable amount of ferric hydroxide precipitate was produced rapidly fast from nZVI, as described by **Equations (2.1)** and **(2.2)**:

$$2Fe^0 + 4H^+ + O_2 \rightarrow 2Fe^{2+} + 2H_2O \quad \textbf{(2.1)}$$

$$2Fe^0 + 2H_2O \rightarrow 2Fe^{2+} + H_2 + 2OH^- \quad \textbf{(2.2)}$$

Fe(II) is a principal product, and now it can undergo further oxidative transformation depending upon redox conditions and pH, as described by **Equations (2.3)** and **(2.4)**:

$$2Fe^{2+} + 2H^+ + ½O^2 \rightarrow 2Fe^{3+} + H_2O \quad \textbf{(2.3)}$$

$$2Fe^{2+} + 2H_2O \rightarrow 2Fe^{3+} + H_2 + 2OH^- \quad \textbf{(2.4)}$$

Although nZVI was reported as a promising material for As removal, its direct application in water treatment systems could result in loss of material (because of its nanosize) and lead to enriched iron content in drinking water (Kanel et al., 2005; Kanel et al., 2006). Hence, some researchers proposed to load nZVI onto supporting adsorbents

for removal of As from water. Biochar itself is not an efficient adsorbent for As. However, Wang et al. (2017) demonstrated that biochar integrated with the nZVI could effectively remove As(V) from water environment. The adsorbed As(V) onto biochar-nZVI composite adsorbent could then be readily separated from the solution due to the magnetic property of the biochar-nZVI. A study of loading nZVI onto activated carbon (nZVI/AC) was investigated in removing As from drinking water through batch adsorption experiments (Zhu et al., 2009). The Langmuir adsorption capacities of nZVI/AC for As(V) and As(III) were 12.0 and 18.2 mg/g at pH 6.5, respectively. Kinetics data showed that the adsorption rate of nZVI/AC increased rapidly in the first 12 h and achieved equilibrium in approximately 72 h.

2.6.2.6. Iron-based layered double hydroxides (LDHs)

Recently, layered double hydroxides have attracted interest for removing As from water because of their simple synthesis process, unique properties, and high affinity towards As ions. The majority of previous iron-based LDHs were synthesized by incorporating Fe^{3+} ions with one or two other divalent cations such as Mg, Mn, Ni, Zn, Cu, and Co in the brucite-like layers. The most common method for the iron-based LDH synthesis process was synthesized by a common co-precipitation method at different mass ratios of cations. The adsorption of As by Mg/Fe-LDH adsorbents from aqueous environment has been investigated in numerous studies (Caporale et al., 2011; Kang et al., 2013). Caporale et al. (2011) reported that Mg/Fe-LDH possessed a surface area of 205 m^2/g and was an potential adsorbent for removal of both As(III) and As(V) from contaminated water. Otgonjargal et al. (2012) discovered that Mn–Fe–CO_3 layered double hydroxides (LDHs) were synthesized through the co-precipitation method, and exhibited a high adsorption capacity towards both As(V) and As(III). The incorporation

of Fe with two or three other metal ions into LDHs was attempted to improve the uptake efficiency of As(V) by Guo et al. (2012). Their findings showed that Cu/Mg/Fe/La-LDHs were effective in adsorbing As(V) from aqueous solution. Cu/Mg/Fe/La exhibited a Langmuir maximum adsorption capacity of As(V) of 43.5 mg/g. **Table 2.8** presents the Langmuir maximum adsorption capacity of As by reported iron-based LDHs in the literature.

Table 2.8. The Langmuir maximum adsorption capacity (Q_{max}) of As by some iron-based LDHs

Iron-based LDHs	Interlayer anion	S_{BET} (m^2/g)	Atomic ratio	m/V (g/L)	Co As (mg/L)	Q_{max} (mg/g)		Ref.
						As (III)	As (V)	
Mg/Fe-CLDH	CO_3^{2-}	145.3	Mg:Fe=5	1	50	-	50.24	Kang et al. (2013)
Fe/Al-LDH	Cl^-	87.42	Fe:Al=1	-	0.2–250	37.6	40.6	Hong et al. (2010)
ZnFe-LDH	SO_4^{2-}	11.9	Zn:Fe=1:1	0.2	2–100	-	96.91	Lu et al. (2015)
Fe-Mg-LDH	Cl^-	273	Mg:Fe=2	5	30–750	-	194.5	Caporale et al. (2011)
Cu/Mg/Fe/La-LDH	CO_3^{2-}	134	Cu:Mg:Fe:La =6:24:5:5	0.2	1–15	-	43.5	Guo et al. (2012)

2.6.3. Adsorption modeling

2.6.3.1. Kinetic adsorption models

The adsorption kinetic models are commonly used to describe the adsorption behaviors of adsorbents including the pseudo-first-order (Lagergren, 1898), pseudo-second-order (Blanchard et al., 1984), Elovich models (McLintock, 1967), and Avrami model (Putnis, 1992), which are provided under the nonlinear forms in **Equations 2.5, 2.6, 2.7,** and **2.8,** respectively.

$$q_t = q_e\left[1 - \exp(-k_1 t)\right] \quad \textbf{(2.5)}$$

$$q_t = \frac{q_e^2 k_2 t}{1 + q_e k_2 t} \quad \textbf{(2.6)}$$

$$q_t = \frac{1}{\beta}\ln(1 + \alpha\beta t) \quad \textbf{(2.7)}$$

$$q_t = q_e\left[1 - \exp\left(-\left(k_{AV} t\right)^{n_{AV}}\right)\right] \quad \textbf{(2.8)}$$

where: q_t (mg/g) denotes the amount of adsorbate adsorbed onto adsorbent at any t; C_t (mg/L) stands for the adsorbate concentration at any t; k_1 (1/min), k_2 [g/(mg×min)], α [mg/(g×min)], and k_{AV} (1/min) are the rate constant of the pseudo-first-order equation, pseudo-second-order, Elovich equation, and Avrami kinetic constant, respectively; β (g/mg) and n_{AV} represent the desorption constant during any one test and a fractional adsorption order corresponding to adsorption mechanism, respectively.

2.6.3.2. Isotherm adsorption models

Several adsorption isotherm models are applied to describe the equilibrium adsorption including the Langmuir model (**Equation 2.9**) (Langmuir, 1918), Freundlich

model (**Equation 2.10)** (Freundlich, 1907), Redlich–Peterson model (**Equation 2.11)** (Redlich and Peterson, 1959), Langmuir–Freundlich model **(Equation 2.12)** (Koble and Corrigan, 1952), and Khan model (**Equation 2.13)** (Al-Ghouti and Da'ana, 2020; Khan et al., 1997). The nonlinear forms of these models were defined by the equations below.

$$q_e = \frac{Q^{o}{}_{\max} K_L C_e}{1 + K_L C_e} \tag{2.9}$$

$$q_e = K_F C_e^{n_F} \tag{2.10}$$

$$q_e = \frac{K_{RP} C_e}{1 + a_{RP} C_e^{g}} \tag{2.11}$$

$$q_e = \frac{Q_{LF} (K_{LF} C_e)^{n_{LF}}}{1 + (K_{LF} C_e)^{n_{LF}}} \tag{2.12}$$

$$q_e = \frac{Q_{\mathrm{K}} K_{\mathrm{K}} C_{\mathrm{e}}}{(1 + K_{\mathrm{K}} C_{\mathrm{e}})^{n_{\mathrm{K}}}} \tag{2.13}$$

where: $Q_{\max}$ (mg/g) is the Langmuir maximum adsorption capacity of adsorbent; Q_{LF} (mg/g) is the Langmuir–Freundlich adsorption capacity of adsorbent; Q_{K} (mg/g) denotes the Khan maximum adsorption capacity of adsorbent. K_{L} (L/mg), K_{F} ((mg/g)(L/mg)$^{\mathrm{n}}$), K_{RP} (L/g), K_{LF} (L/mg) and K (L/mg) stand for the Langmuir constant, Freundlich constant, Redlich–Peterson constant, Langmuir–Freundlich constant, and Khan equilibrium constant, respectively. n_{F} and g are dimensionless and present for Freundlich intensity parameter and an exponent, respectively, whose value must lie between 0 and 1. a_{RP} (L/mg)^{g} is also the Redlich–Peterson constant; lastly, n_{LF} and n_{K} present the exponents of the Langmuir-Freundlich model and Khan model, respectively.

2.6.3.3. Column adsorption model

The Thomas model (Thomas, 1944) was used to describe the breakthrough curves. This model is the most popular and widely applied in column adsorption studies, with its

nonlinear and linear forms given in **Equations (2.14)** and (**2.15)**, respectively. Furthermore, it accurately describes the column adsorption capacity unlike many others.

$$\frac{C_t}{C_0} = \frac{1}{1 + \exp(k_{TH} q_{TH} \frac{m}{Q} - k_{TH} C_0 t)} \quad \textbf{(2.14)}$$

$$\ln\left(\frac{C_0}{C_t} - 1\right) = K_{TH} q_{TH} \frac{m}{Q} - k_{TH} C_0 t \quad \textbf{(2.15)}$$

where: k_{TH} (L/h.mg) presents the Thomas adsorption rate constant; q_{TH} (mg/g) denotes the Thomas maximum column adsorption capacity toward adsorbate, C_o (mg/L) and C_t (mg/L) stand for the inlet adsorbate concentration and the outlet adsorbate concentration at time *t*, respectively. *m* (g) presents the dried mass of adsorbent packed into column adsorption, *Q* (L/h) is the volumetric flow rate, and *t* (h) is the filtration time. The values of k_{TH} and q_{TH} are calculated from the linear plot of $\ln\left(\frac{C_0}{C_t} - 1\right)$ against t.

2.6.4. Main adsorption mechanisms

2.6.4.1. Oxidation of As(III) to As(V)

Generally, the behaviors of As(III) are different to that of As(V) in aqueous solution. As noted in **Section 2.2** about the distribution of As in water, As(III) species is found as charge anions only above pH 9.0–10, whereas, As(V) species exists as charge anions ($H_2AsO_4^-$ or $HAsO_4^{2-}$) in the environment with pH ranging from 2.2 to 11.5. In natural water of pH 6.0–8.0, As(III) species have been observed in a neutral state in the form of H_3AsO_3, which is not readily adsorbed onto adsorbents, and easily desorbed from adsorbents. Thus, no electrostatic attraction between H_3AsO_3 and surface of adsorbent occurs. The pre-oxidation stage of As(III) species to As(V) in forms of $H_2AsO_4^-$ (pH 2.2–7.08) and $HAsO_4^{2-}$ (pH 7.08–11.5) is essential to remove As(III) from water by adsorbents (Shen et al., 2017). According to the research, some oxidants have been used

for converting soluble As(III) to As(V), including iron, hydrogen peroxide, chlorine, hypochlorite, manganese, and titanium (Mishra and Mahato, 2016; Siddiqui and Chaudhry, 2017).

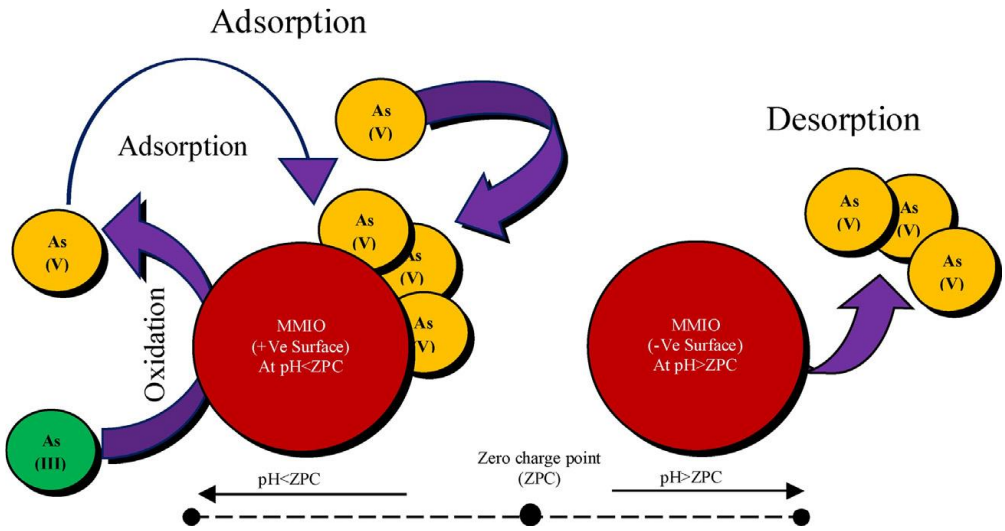

Figure 2.3. Representation of the As adsorption/desorption process by modified magnetic iron oxide (MMIO) (Siddiqui and Chaudhry, 2017)

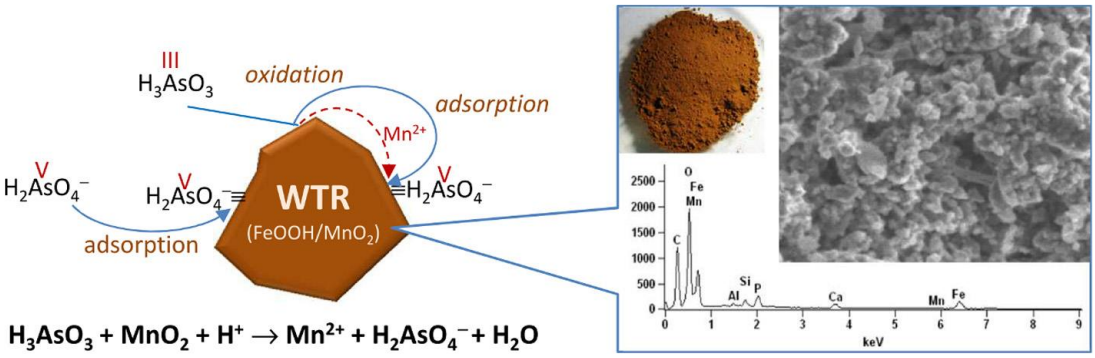

Figure 2.4. Oxidation process of As(III) to As(V) by water treatment residuals containing iron and manganese oxides (Ociński et al., 2016)

Figure 2.3 and **Figure 2.4** illustrate the oxidation mechanism of As(III) to As(V) by iron oxide, Mn(IV), and Mn(V). In addition, the incorporation other metals or even oxidants into metal oxides has been examined in other studies. Particularly, manganese oxide (MnO_2), manganese (Mn^{2+}) incorporating with iron oxide were found to be able to simultaneously oxidize As(III) to As(V) and then adsorb As(V) species. Ociński et al. (2016) claimed that when doing this, the effectiveness in removal As was higher.

2.6.4.2. Outer-sphere complexation

Outer sphere complexation (also known as weak electrostatic interactions) between As species in solution and the positively charged adsorbent surface has been reported as the predominant adsorption mechanism in many studies. Several analyses (Pehlivan et al., 2013a; Asmel et al., 2017; Pintor et al., 2018; Zhu et al., 2018) demonstrated that the Fe-As relationship between iron oxides/hydroxides and As(V) anions was controlled by electrostatic attraction. As(III) and As(V) speciation in natural water bodies are described in **Section 2.2**. The pH solution plays an important role when explaining the As adsorption mechanism by electrostatic phenomena. Adsorption process of As(V) occurs effectively at low pH than at high pH due to the positive surface charge of adsorbent attracts negative of two As(V) forms $H_2AsO_4^-$ and $HAsO_4^{2-}$ions. For As(III), no electrostatic force occurs because As(III) presents as neutral arsenious acid (H_3AsO_3) at most pH ranges (Zhu et al., 2018).

2.6.4.3. Inner-sphere complexation

Many studies have proven that As(III) was removed by iron oxides/hydroxides adsorbents by inner-sphere complexation mechanisms (Pehlivan et al., 2013a; Vieira et al., 2017). The formation of ligand exchanges (monodentate and bidentate surface

complexes) between hydroxyl groups and As(III) was found to be the dominant mechanism. **Figure 2.5** is an illustrative example of As adsorption on the calcined layered double hydroxides/reduced graphene oxide composites (ZnFe-CLDH/RGO) through complex mechanisms. Additionally, As(V) adsorption on the adsorbent could happen through ligand exchange on the inner-sphere adsorption. Basic adsorption reactions between the positively charged surface of hydroxyl groups with negatively charged As(V) ions can be described by the following **Equations (2.16)** and **(2.17)**:

$$2{\equiv}FeOH_2^+ + H_2AsO_4^- \leftrightarrows [({\equiv}FeO)_2\text{-}AsO(OH)]^- + H_3O^+ + H_2O \quad \textbf{(2.16)}$$

$${\equiv}FeOH_2^+ + H_2AsO_4^- \leftrightarrows [{\equiv}Fe\text{-}(O)_2\text{-}AsO(OH)]^- + H_3O^+ \quad \textbf{(2.17)}$$

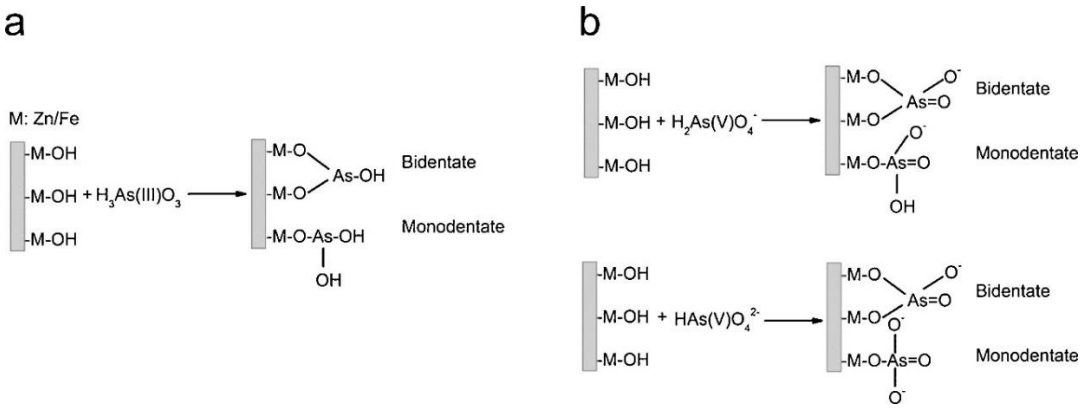

Figure 2.5. Inner-sphere complexation of As(III) (a) and As(V) (b) by ZnFe-CLDH/RGO (Zhu et al., 2018)

2.6.4.4. Anion exchange

Many studies strongly suggest that anion exchange is one of the key mechanisms in removing As by adsorbents (Caporale et al., 2011; McCann et al., 2018; Shen et al., 2017). For example, LDHs adsorbent has been reported as effective for removing As(V) via anion exchange. McCann et al. (2018) and Shen et al. (2017) demonstrated that there

was not only electrostatic attraction between As anions and the positive charge site in the LDH's external surface but also anion exchange between the interlayer region of LDH and As anions. **Figure 2.6** shows the main mechanisms of As(III) adsorption by LDHs nanomaterials, including ion exchange. Anirudhan and Unnithan (2007) successfully developed a novel anion exchanger made of coconut coir pith (CP-AE) in removing As(V). Furthermore the anion exchange mechanism plays a vital role for As removal via the interaction between $–NH^{+}(CH_3)_2Cl$ groups on the CP–AE surface and As(V) ions.

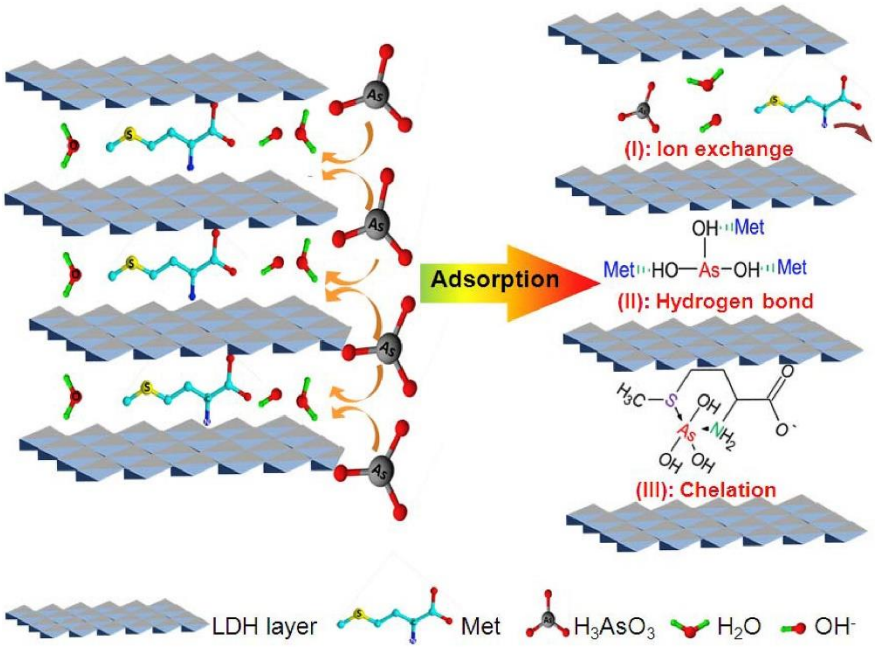

Figure 2.6. The mechanisms of As(III) adsorption by Zn_2Al-Met-LDHs (Shen et al., 2017)

2.7. Arsenic analysis in solution and adsorbent

After the As(V) adsorption process, both solution and surface of laden-As adsorbent normally contain only As(V). However, after the As(III) adsorption process, both solution and laden-As adsorbent can contain two As species, As(III) and As(V). The

presence of both As species is due to the possibility of oxidation from As(III) to As(V) occurring during the adsorption process through various interactions. **Figure 2.7** illustrates a summary of different analysis methods to identify total As and As species in both liquid and solid phases.

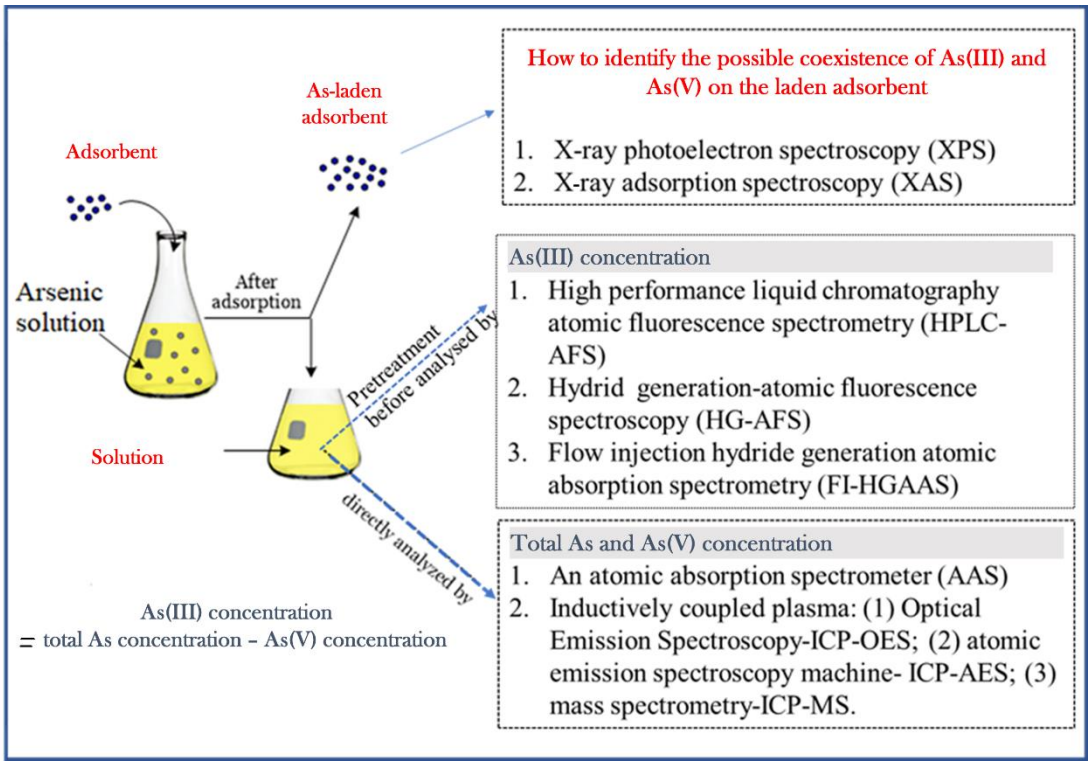

Figure 2.7. Analysis As in solid and liquid samples (Chang et al., 2010; Kong et al., 2014; Samad et al., 2016; Sun et al., 2017)

Some advanced techniques have been used to determine the oxidation state of As on the surface of the loaded adsorbent including X-ray absorption spectroscopy (XAS), X-ray Absorption Near Edge Spectroscopy (XANES), and X-ray photoelectron spectroscopy (XPS) (Samad et al., 2016; Sun et al., 2017).

In general, total As (As(III) and As(V)) in solution is widely analyzed using two techniques: firstly, an atomic absorption spectrometer (AAS); and secondly, inductively coupled plasma (ICP). ICP further includes optical emission spectroscopy (ICP-OES); inductively coupled plasma atomic emission spectroscopy machine (ICP-AES); and inductively coupled plasma mass spectrometry (ICP-MS) (Chang et al., 2010; Kong et al., 2014). The hydride generation-atomic fluorescence spectroscopy (HG-AFS), high-performance liquid chromatography atomic fluorescence spectrometry (HPLC-AFS), and flow injection hydride generation atomic absorption spectrometry (FI-HGAAS) are not only employed to detect the total As concentration but also used to determine the As(III) concentration (Kong et al., 2014).

2.8. Management of used adsorbents

Management of As exhausted adsorbents is a big challenge and requires appropriate methods because As is highly mobile and has the ability to seep back into the soil and water environments. There are three options often used to manage As exhausted adsorbents, including: (i) recovery and reuse, (ii) dilution and dispersion, and (iii) encapsulation of the material through solidification/stabilization techniques. A successful recovery process is defined when an As exhausted adsorbent can be restored its initial properties for effective reuse. However, recovery/reuse of As is not economical because As has limited markets. Meanwhile, dilution and dispersion methods exhibit disadvantages relating to cost and safety. For example, As oxides are highly volatile and can easily escape into the air environment during the incineration process. Thus, As can neither be destroyed directly nor completely incinerated. Encapsulation of As through solidification/stabilization techniques is the most attractive solution to deal with As waste

streams. Stabilization/solidification (S/S) is also a common and effective technique used to treat industrial wastes containing As.

Stabilization/solidification is the general term for a process that converts potentially hazardous liquid or solid wastes into less hazardous or non-hazardous forms and increases their solidity and structural integrity. Thus, although stabilization/solidification technology cannot remove contaminants, it can effectively wastes being transported into the environment by eliminating or significantly hindering the contaminant's mobility. Cement/lime is commonly used to mix with As waste to form insoluble compounds and a stabilized solid material to restrict contaminant migration. The integration between cement/lime ($Ca(OH)_2$) and As exhausted adsorbent leads to chemical reactions that reduce the leachability of a waste. The Ca-As compounds have been reported widely in several studies which used cement as a binder material. In As(III)-containing wastes, $CaHAsO_3$ was discovered to be the primary process for As fixation (Dutre and Vandecasteele, 1998). Calcium arsenate ($Ca_3(AsO_4)_2{\cdot}4H_2O$ $Ca_3(AsO_4)_2$, $Ca_5(AsO_4)_3(OH)$, $NaCaAsO_4{\cdot}7.5H_2O$, and $CaHAsO_4{\cdot}H_2O$) are also formed when As(V) in bearing samples reacts with hydrated lime ($Ca(OH)_2$) (Mollah et al., 1998; Vandecasteele et al., 2002; Jing et al., 2003;).

Numerous researches has been investigated the combination between Portland cement and other solidifying materials such as lime, iron, fly ash, silicate, ferrous sulfate, and sand for the immobilization of As (Akhter et al., 1990; Taylor and Fuessle, 1994; Palfy et al., 1999).

By encapsulating the exhausted adsorbent with concrete produced from cement, gravels and sand, Nguyen et al. (2020b) explored the solidification/stabilization method

of disposing of the As(V) waste in the As-laden modified manganese oxide ore. Their results revealed that solidified materials possessed adequate compressive strength and rapid chloride penetrability test, as well as volume of permeable voids. Consequenlty, they may serve as a construction material. Moreover, the amount of As(V) leaching from concretes preparation has been proven to have no environmental impact.

Kundu and Gupta (2008) conducted a study on solidification/stabilization (S/S) of exhausted iron oxide-coated cement (IOCC) after As adsorption process. They created five different solidified waste matrices by varying the ratios of binder elements (cement and lime) to toxic As sludge. The formation of calcite and precipitation, as well as conversion into non-soluble forms, were shown to be responsible for the decrease of As leaching from the solidified/stabilized samples. Elsewhere, Singh and Pant (2006) employed binder materials (Portland cement, calcium hydroxide, fly ash, and other polymeric materials) to stabilize/solidify an exhausted activated alumina waste. The production of calcite caused the smallest amount of As to leach from the matrix of activated alumina, fly ash, cement, and calcium hydroxide. Similarly, Kundu and Gupta (2008) reported that the formations of calcite led to sealing the pores the solidified sample and prevented As leaching from the stabilized/solidified samples.

2.9. Conclusions

This chapter reported that As is one of the most toxic elements found in water resources and a high As concentration in drinking water causes severe health problems. The removal of As from groundwater has attracted great interest from scientists, authorities, and communities. Numerous water treatment technologies have been devised to remove As from aquatic environments and of the current existing technologies,

adsorption is considered the most suitable method at a decentralized scale due to its high removal efficiency, simplicity in design, cost-effectiveness, and minimal generation of secondary waste. For filter media, iron-based adsorbents are the most suitable media for efficient removal of As from water due to the high affinity of iron towards As. However, most previous research on As removal by iron-based adsorbents focused only on As(V). Only a few studies on removing both As(III) and As(V) ions have been published. As(III) possesses unique properties so the removal of toxic As(III) is still a big problem for iron-based adsorbents. In addition, the application of iron-based adsorbents with real contaminated As water during a long period (in pilot-scale and full-scale contexts) is very limited. The management of exhausted adsorbents continues to be a difficult task and requires much more investigation. Thus, this study was conducted to develop and evaluate the As(III) and As(V) removal capacity of three novel adsorbents including NLTT (originated from natural mineral), PPCI (originated from agricultural waste), and Mn/Mg/Fe-LDH (synthesized from commercial chemicals). In the other words, the study was investigated with both representative inorganic As species (As(III) and As(V) in water. For practical application, one of three investigated adsorbents namely NLTT were packed in many household and communities water filtration systems as a filter media to remove As in As contaminated groundwater areas in Vietnam. Last but not least, the As-laden NLTT after adsorption process was managed by solidification/stabilization method.

CHAPTER 3. REMOVAL OF ARSENIC FROM WATER BY A LOW-COST NATURAL LATERITE ADSORBENT

This chapter focuses on As removal utilizing NLTT, an adsorbent produced from natural mineral. The results of the batch study, including the material characterization and adsorption mechanism of NLTT on As(III) and As(V) were published as part of the following paper in the journal Science of the Total Environment.

1. Nguyen, T. H., Tran, H. N., Vu, H. A., Trinh, M. V., Nguyen, T. V., Loganathan, P., Vigneswarana S., Nguyen, T.M., Trinh, V.T., Vu, D.L., Nguyen, T. H. H. (2020). Laterite as a low-cost adsorbent in a sustainable decentralized filtration system to remove arsenic from groundwater in Vietnam. Science of the Total Environment, 699, 134267 (IF: 10.753; SJR: Q1)

The column study that is described in this chapter was published in the journal Process Safety and Environmental Protection.

2. Nguyen, T. H., Nguyen, A. T., Loganathan, P., Nguyen, T. V., Vigneswaran, S., Nguyen, T. H. H., & Tran, H. N. (2021). Low-cost laterite-laden household filters for removing arsenic from groundwater in Vietnam and waste management. Process Safety and Environmental Protection, 152, 154-163 (IF: 7.926; SJQ:Q1)

3.1. Introduction

Iron and aluminum-containing materials are considered to be suitable adsorbents for removing As from water because they possess a high affinity to As (Pena et al., 2005; Giles et al., 2011). Nanomaterials (i.e., nano iron oxides/hydroxides, nano TiO_2, nano zero-valent iron, nano CuO, nano ZnO, and layered double hydroxides) have also been identified as highly-effective adsorbents for removing As(III) and As(V) from water media (Pena et al., 2005; Goh et al., 2008; Lata and Samadder, 2016; Siddiqui and Chaudhry, 2017). However, such nanomaterials exist in fine powder form and it is difficult to separate them from water after adsorption. In column-based filters they cause hydraulic problems by clogging the filters. Other popular commercial adsorbents such as activated carbon and activated alumina can also effectively remove As from water (Kalaruban et al., 2019). However, relatively high cost might prevent them from being considered for practical applications in village communities. As well, these materials need to be regenerated for reuse option (Mohan and Pittman, 2007). Low-cost natural adsorbents (goethite, zeolites, laterite, clay, red mud, fly ash, etc.) have been investigated as a replacement for current expensive adsorbents in treating As from contaminated water and wastewater. This is due to their local availability, low-cost and efficiency (Mohan and Pittman, 2007).

Goethite is considered as one of the most common forms of iron oxides found in soils and rocks. Wu et al. (2014) investigated a novel goethite which was synthesized by using sodium dodecyl sulfate assisted solution method. The Langmuir adsorption capacity of synthesized goethite toward As(V) was 60.6 mg/g at pH 7.0, which is much higher than those of compared adsorbents in the literature. Hematite and magnetite are

the most abundant iron oxide minerals existed in natural systems. Magnetite has chemical formular Fe_3O_4, which is common known narual magnetic mineral because of its structure containing divalent iron Fe^{2+} and trivalent iron Fe^{3+}. Aredes et al. (2013) conducted a study on using natural iron oxide minerals (hematite, magnetite, goethite, and laterite soil) for the removal of As from water. Their results showed that all of the natural iron oxide minerals were effective in removing As from solution. More detail information about As removal from aqueous solution by iron oxides and hydroxides minerals was presented in **Section 2.6.2.1.** According to Maiti et al. (2007) and Maji et al. (2008), natural laterite and laterite soil collected from India had been investigated for their performance in removing As. The results shows that they exhibited a good performance than that of goethite, magnetite, and hematite. However, to the best of my knowledge, no study has yet been published on using laterite collected from Vietnam to remove As from water environment.

Laterite is formed commonly in hot and wet tropical areas and is distributed widely throughout Vietnam (Thach That, Ba Vi, and Tam Duong). This material can be used as a potential adsorbent for As removal due to the natural presence of Fe and Al oxides/hydroxides in its composition (Glocheux et al., 2013). In this study, the natural laterite from Thach That (NLTT) together with six other local low-cost minerals and waste materials were first tested in the laboratory with synthetic water spiked with As for their ability to remove As. Based on the initial laboratory results, the NLTT material was selected and evaluated in detailed batch and column study for its performance in As removal. The sorption mechanisms of NLTT with As ion were further explored through

the characterization (morphological, textural, surface functionality properties, and the charge of adsorbent surface) of NLTT before and after adsorption.

3.2. Materials and methods

3.2.1. Preparation of adsorbent materials

Natural laterite (NLTT) used in this study was collected at Thach That district, Hanoi city, Vietnam. The collected NLTT was firstly washed with water three times to eliminate any adhering dirt and soluble compound on its surface and then placed in an oven at 105 °C for 48 h to remove excess water and moisture. The dried NLTT was ground and sieved into relatively homogeneous particle sizes ranging from 0.5 to 1 mm. These NLTT particles were washed with distilled water, dried at 85 °C for 24 h, and stored in tightly closed bags.

In this study, six other low-cost and waste materials (abundant in Vietnam) were also selected to explore their adsorption capacity of As in aqueous solution. They include the laterite (collected from Tam Duong, Vinh Phuc province), bentonite (Tay Ninh, Thanh Hoa province), feralite soil (Thai Nguyen province), red mud (the Bao Loc's mine, Lam Dong province), iron ore mining waste (the Trai Cau's iron ore mine, Thai Nguyen province), and iron ore mining waste (the Ban Cuon's iron ore mine, Bac Kan province). Such collected materials were ground to a particle-size range similar to NLTT (0.5–1.0 mm), washed, dried, and then stored in sealed bags.

3.2.2. Characterisation of adsorbent materials

The morphology and element composition of pristine and As-loaded NLTT were examined using scanning electron microscopy (SEM; Quanta-650) and energy dispersive

X-ray spectroscopy (EDS) techniques. The mineral and chemical composition of NLTT were determined using X-ray Diffraction (XRD; Empyrean-PANalytical) and X-ray Fluorescence (XRF; Pioneer-S4), respectively. The surface area of adsorbent was determined using N_2 adsorption isotherm with a Micromeritics sorptometer (Accu Pyr II 1340. V1.02) at 77 K. The presence of main function groups on the NLTT' surface was measured by Fourier transform infrared spectroscopy (FTIR; Nicolet iS5). Finally, using the common drift method (Partey et al., 2009; Maiti et al., 2013; Tran et al., 2017a) the pH value of NLTT at the point of zero charge (pH_{PZC}) was determined. According to this method, solutions of 0.01 mol/L NaCl in 100 mL test tubes were adjusted to pH values ranging from 2 to 9 (pH initial) using 0.1 mol/L NaOH and 0.1 mol/L HCl. Then, 2.5 g of NLTT were added to test tubes and shaken at 150 rpm at 25°C. After 24 h the final pH (pH final) of samples were measured. (pH final – pH initial) values were plotted on Y-axis against initial pH in X-axis. The intersection points of the resulting curve with the X-axis ((pH final – pH initial) = 0) was taken as the pH_{PZC}.

The NLTT's elemental composition was also determined by chemical analysis using strong acid digestion. In this method, 0.1 g NLTT sample was digested in a solution of 5 mL concentrated HNO_3 and 5 mL concentrated HCl in a microwave digester for 3 hours. The digested solution was diluted and analysed for metal concentrations using ICP-OES (Perkin Elmer 7300).

3.2.3. Batch adsorption experiment

Stock solutions of As(III) and As(V) (1000 mg/L) were prepared by dissolving $NaAsO_2$ (ACE chemicals company) and $Na_2AsO_4.7H_2O$ (BDH chemical Ltd.) in distilled water, respectively. Both $NaAsO_2$ and $Na_2AsO_4.7H_2O$ had been dried at 105 °C for 4 h

and kept in the desiccator before they were used to prepare the stock solutions. All chemicals and reagents used in this work were of analytical grade.

Initially, an adsorption experiment was conducted to identify the potential of laterite and the other six materials for removing As from water. Briefly, 0.25 g of each material was added into Erlenmeyer flasks containing 100 mL As(V) solution of 0.25 mg/L. The flasks were sealed, placed on a mechanical shaker, and shaken at 160 rpm for 24 h at 30 °C. Subsequently, the liquid samples were strained through a 0.45 μm filter before the As(V) residual concentration was examined. The result (presented in more detail in **Section 3.3.1**) demonstrated that the natural laterite material from Thach That (NLTT) was the most suitable adsorbent. For this reason, it was selected for the subsequent studies such as characterization, adsorption, and application.

Detailed batch adsorption experiments were conducted to study the effect of the several operating parameters (i.e., solution pH values, contact times, initial As concentrations, coexisting anions, temperatures, and desorbing agents) on using NLTT to remove As. Briefly, the effect of solution pH on the adsorption capacity of NLTT was determined by mixing 0.75 g material with 100 mL of 0.5 mg As/L solution in Erlenmeyer flasks at different pH values. The pH of the As solutions was adjusted from 2.0 to 10 ± 0.2 by adding either 1M NaOH or 1M HNO_3. To evaluate the effect of coexisting anions on As adsorption capacity of NLTT, similar experiments were carried out with the addition of different anions (such as Cl^-, CO_3^{2-}, HPO_4^{2-}, SO_4^{2-}, SiO_3^{2-}), with the concentration of each anion being 10 mM. Studies on adsorption kinetics were conducted at time intervals of 1, 5, 10, 20, 30, 60, 120, 180, 240, 300, 360, 420, 480, and 960 min at initial concentration of As(III) or As(V) of 0.5 mg/L and 0.25 mg/L, respectively.

Equilibrium adsorption experiments were conducted using As(III)/As(V) concentrations ranging from 0.10 to 25 mg/L at temperatures of 10 °C, 30 °C, and 50 °C. In these experiments the suspensions were shaken for 24 h to ensure equilibrium has reached. In all the above experiments the flasks containing the respective suspensions were placed in a shaker and shaken at 160 rpm. After predetermined shaking time, the solid was separated from solution by glass fiber filters. The liquid was then filtered through a 0.45μm syringe filter before analysing for As. Meanwhile, the above solid samples were dehydrated at 80 °C for 12 h and then stored in tightly closed bags for further analysis (i.e., FTIR, the textural, morphological properties and desorption). The total As concentration in the filtered samples was determined by an Inductively coupled plasma mass spectrometry (ICPMS-NexION 2000, US).

The amount of As adsorbed onto adsorbent at equilibrium, q_e (μg/g) and the amount of As uptake at time t, q_t (mg/g) were calculated using **Equations 3.1** and **3.2,** respectively. All experiments were conducted in duplicate and the average value was reported. Whole batch experiments were carried out at the constant ratio of NLTT amount/solution of 7.5-g NLTT/1.0 L of As solution.

$$q_e = \frac{C_o - C_e}{m_1} V_1 \quad \textbf{(3.1)}$$

$$q_t = \frac{C_o - C_t}{m_1} V_1 \quad \textbf{(3.2)}$$

where C_o, C_e, and C_t, are the concentrations (mg/L) of As in solution at beginning (denoted as the blank sample), equilibrium, and any time t (min), respectively; V_1 (L) is the volume of As solution applied, and m_1 (g) is the dried mass of adsorbent used.

Desorption experiments were carried out to determine the reversibility of the adsorption. In this study, the flasks containing 0.1 L of different desorbing agents (V_2) and predetermined amount (approximately 0.75 g) of As loaded NLTT (m_2) were placed in a shaker and shaken at 160 rpm for 24 h. The tested desorbing agents include deionized (DI) water at pH 12, 0.5M HCl, 0.5M NaOH, 0.5M NaCl and ethylenediaminetetraacetic acid (EDTA; 5%). The amount of As remained on adsorbent and the percentage of desorption were determined using **Equations 3.3** and **3.4,** respectively.

$$q_r = q_e - q_d = q_e - (\frac{C_d}{m_2} V_2) \quad \textbf{(3.3)}$$

$$\%Desorption = (\frac{q_e - q_r}{q_e - q_d}) \quad \textbf{(3.4)}$$

where C_d (mg/L) is the concentration of As in solution after desorption; q_r (mg/g) is the mass of As that remained adsorbed after desorption; and q_d (mg/g) is the mass of As desorbed if the adsorption process is reversible; V_2 (L) is the volume of desorbing agents applied, and m_2 (g) is the mass of As loaded adsorbent.

3.2.4. Column adsorption experiment

Four glass columns (0.03 m inner diameter and 0.50 m height) were set up to evaluate the removal efficiency of As(V) by NLTT at two initial As(V) concentrations and at two bed heights. Two columns were packed with 440 g NLTT which were corresponding to 0.41 m bed-height, and two other columns were packed with 160 g NLTT which were corresponding to 0.15 m bed height. Two different feed solutions of As(V) concentrations of 0.1 and 0.5 mg/L were pumped at fixed flow rates of 10 mL/min (corresponding to 0.85 m/h) using dosing pumps (Master flex L/S) through the 4 columns

in an up-flow mode. The empty bed contact time (EBCT) of two columns packed with 440 g and 160 g were 29 min and 11 min, respectively. NLTT During the first 3 weeks, when the ratios of As(V) concentration in the effluent to that in the influent (C_t/C_o) were below 0.80, samples were collected daily. After that, samples were collected every 2–4 days until the C_t/C_o reached 1. The samples were filtered using 0.45 µm syringe filters and the As concentration in the filtered solutions was identified using the method described in the **Section 3.2.3**. The schematic diagram of laboratory column study was presented in **Figure 3.1.**

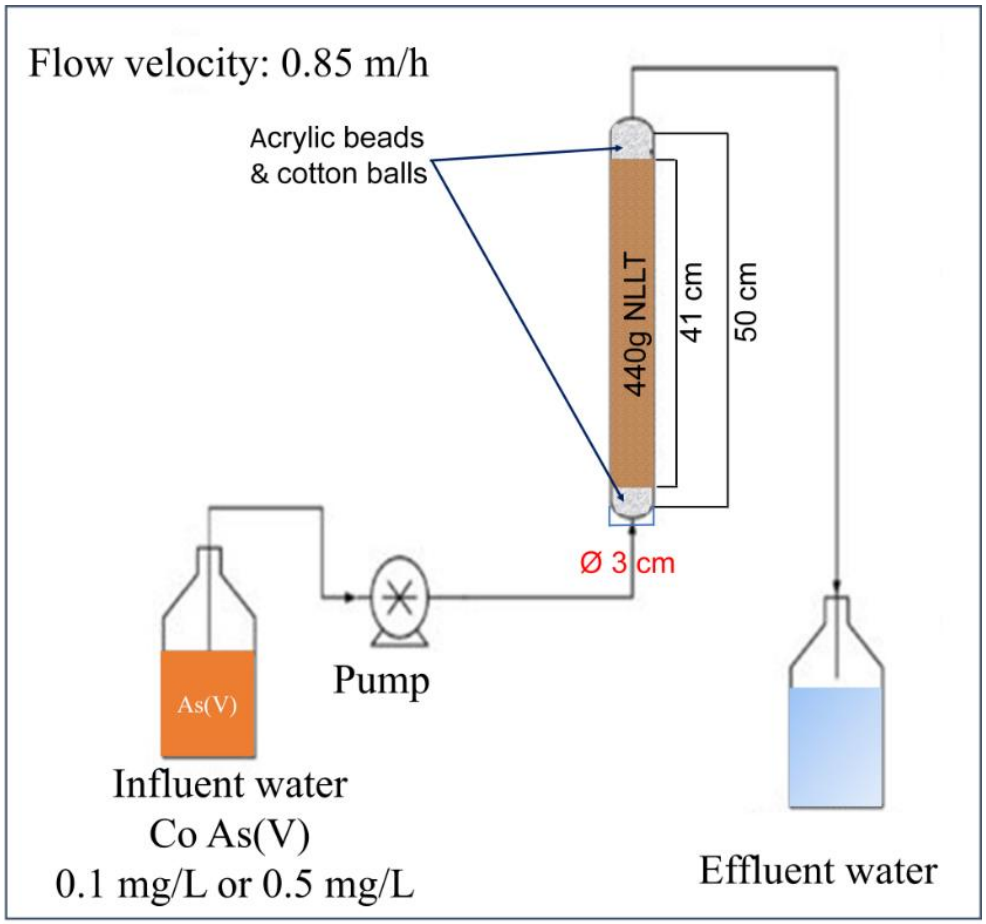

Figure 3.1. Schematic diagram of laboratory column study

3.3. Results and discussion

3.3.1. Comparison of the adsorption capacity of selected adsorbents

The removal of As(V) by the seven low-cost adsorbents used is presented in **Figure 3.2.**

Results show that the removal efficiency of As(V) declined in the following order: BTN (78,6%) > NLTT (76.0%) > IMWBC (72.4%) > IMWTC (71.0%) > NLTD (70.0%) > FTN (67.2%) > RMBL (62.4%). Although BTN had the highest removal percentage of As(V), after the adsorption process, the medium swelled inside the flask due to the presence of bentonite in this material. This phenomenon can be explained as bentonite is a phyllosilicate clay with 2:1-layer silicate structure and contains mainly smectite which has high swell index (Bhattacharyya and Gupta, 2008). The iron mining wastes (IMWBC and IMWTC) also exhibited good adsorptive removal due to their high iron content, which facilitate As removal (Altundoğan et al., 2000; Nguyen et al., 2009). However, using industrial waste as adsorbent dose pose the high risk of generating toxic heavy metals in the treated water.

Considering the following aspects—removal efficiency, availability, stability/potential risk, and cost (including exploration, transportation from the source to workshops, processing/grinding), of the adsorbents tested, NLTT from Thach That, Hanoi was found to be the most suitable media for As removal. The total cost including transport and processing is only US$ 0.20 /kg. Transport from the mine site and processing cost can be cut drastically when many communities around the childcare centre start using the

filtration technique and a large quantity of NLTT is transported in a single trip. In this case, the cost of the material can be reduced to US$ 0.10/kg. Thus, NLTT from Thach That, Hanoi was chosen for subsequent tests and pilot trial.

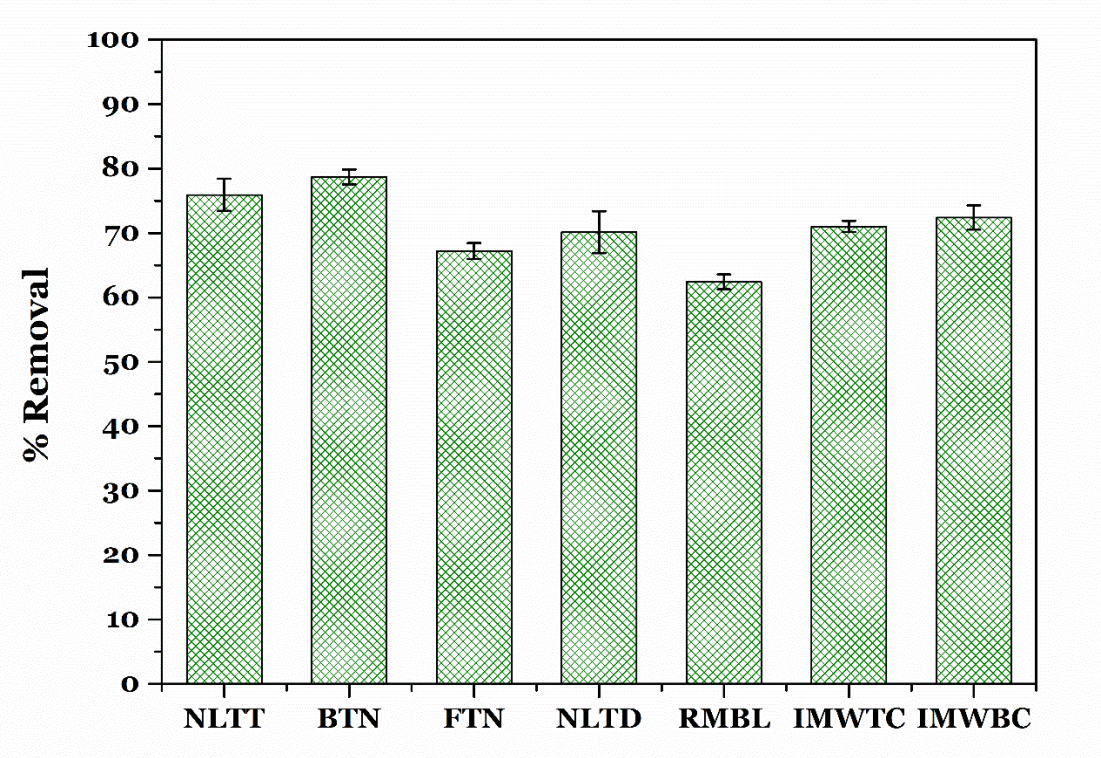

Figure 3.2. As(V) removal by different local low-cost materials

(adsorbent dose 2.5 g/L, initial As(V) concentration 0.25 mg/L). Note: laterite Thach That (NLTT), bentonite (BTN), feralite soil (FTN), laterite Tam Duong, red mud (RMBL), iron ore mining waste from the Trai Cau's iron ore mine (IMWTC), and iron ore mining waste from the Ban Cuon's iron ore mine (IMWBC)

3.3.2. Basic characteristics of the NLTT

The physisorption isotherm of the NLTT's nitrogen gas is illustrated in **Figure 3.3a**. According to the IUPAC technical report (Thommes et al., 2015), the physisorption

isotherm can been classified as the reversible Type II. In addition, the hysteresis loop (Type H3) appeared in the isotherm at the relative pressure ($p/p°$) higher than 4.0. The results suggest that the collected NLTT was a typical nonporous adsorbent. This conclusion was further confirmed by its textural parameters that were calculated from the nitrogen adsorption/desorption isotherm in **Figure 3.3a**. The calculation performance showed that the NLTT was a non-porous material, with its low BET specific surface area (S_{BET}; 155 m^2/g) and total pore volume (V_{Total}; 0.549 cm^3/g). Similarly, the relatively low S_{BET} (m^2/g) and V_{Total} (cm^3/g) values of other kinds of laterite derived from different geographical regions were reported in the literature, such as 17.5–18.5 m^2/g and 0.02–0.05 cm^3/g (Maiti et al., 2012) and 71–182 m^2/g and 0.07–0.35 cm^3/g (Maiti et al., 2013). Because the natural adsorbent is a non-porous material, the adsorption mechanism of As ions in solution involved in pore filling might less important than some surface interactions (i.e., complexation) (Cheng et al., 2019).

Figure 3.3b provides the FTIR spectrum of the NLTT. The presence of main function groups on the NLTT's surface was observed at several corresponding bands at approximately 1100 cm^{-1} (Si–O–Fe), 1030 cm^{-1} (Si–O), 910 cm^{-1} (Al–OH), 798 cm^{-1} (Fe–OH), and 530 and 460 cm^{-1} (Fe–O). In addition, the bands at in the region between 3730 cm^{-1} and 3100 cm^{-1} can be assigned to the OH stretching vibration in Si–OH, Al–OH, and even water. Lastly, the bands located at around 1630 cm^{-1} might belong to the mica group or water. The results were well consistent with studies done on other natural laterites (Maiti et al., 2013; Mitra et al., 2016). With As being intensively reported in the literature, the abundant presence of the hydroxyl groups on the adsorbent's surface was

expected to form the complexation reaction with As ions in aqueous solution (Siddiqui and Chaudhry, 2017; Zhao et al., 2018; Cheng et al., 2019).

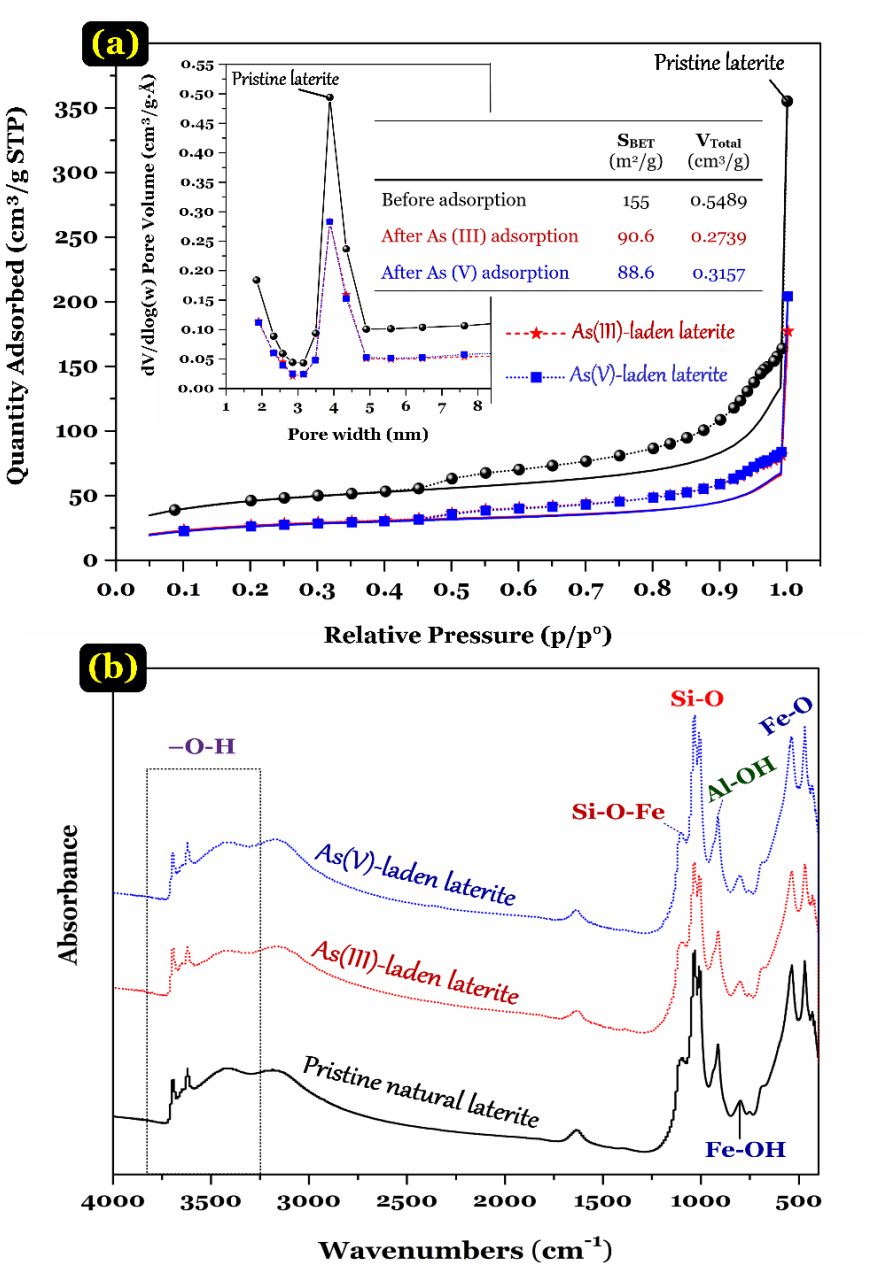

Figure 3.3. (a) Nitrogen adsorption/desorption isotherm of NLTT before and after As adsorption; and their pore size distribution (inset); and (b) FTIR spectrum of NLTT before and after As adsorption

According to the literature, the manganese and titanium oxides has been known as oxidants that convert As(III) to As(V) (Partey et al., 2008; Cheng et al., 2019). In their study, Zhao et al. (2018) found that the iron (hydro)oxides (i.e., ferrihydrite, hematite, and magnetite) can act as a promising catalyst in simulating the oxidation of As(III) onto As(V). Moreover, some clay minerals (i.e., nacrite, kaolinite, and illite) were expected to effectively adsorb As ions [As(III) and As(V)] and possibly oxidise As(III) to As(V) (Manning and Goldberg, 1997). The results of XRD analysis (**Figure 3.4a**) demonstrated that NLTT was composed of goethite, hematite, nacrite, quartz, and anatase. Furthermore, the XRF analysis **(Figure 3.4b)** indicated that the principal components of NLTT were Fe_2O_3 (48.7%), Al_2O_3 (18.2%), and SiO_2 (14.0%), while the minor ones were TiO_2 (2.89%), P_2O_5 (0.49%), and MnO (0.37%). Such available compounds make the NLTT a unique material that can act as a potential catalyst and promising adsorbent able to remove As contaminant from solution.

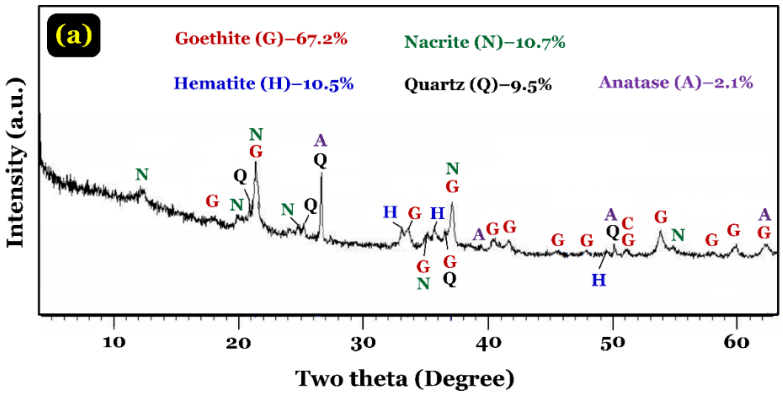

(b)

Components (%)	Fe_2O_3	Al_2O_3	SiO_2	TiO_2	P_2O_5	CaO	MnO
	48.7	18.2	14.0	2.89	0.49	0.42	0.37
	K_2O	MgO	Cr_2O_3	ZrO_2	CuO	BaO	ZnO
	0.30	0.12	0.11	0.05	0.03	0.03	0.01

Figure 3.4. (a) XRD spectrum and (b) XRF analysis result of the NLTT

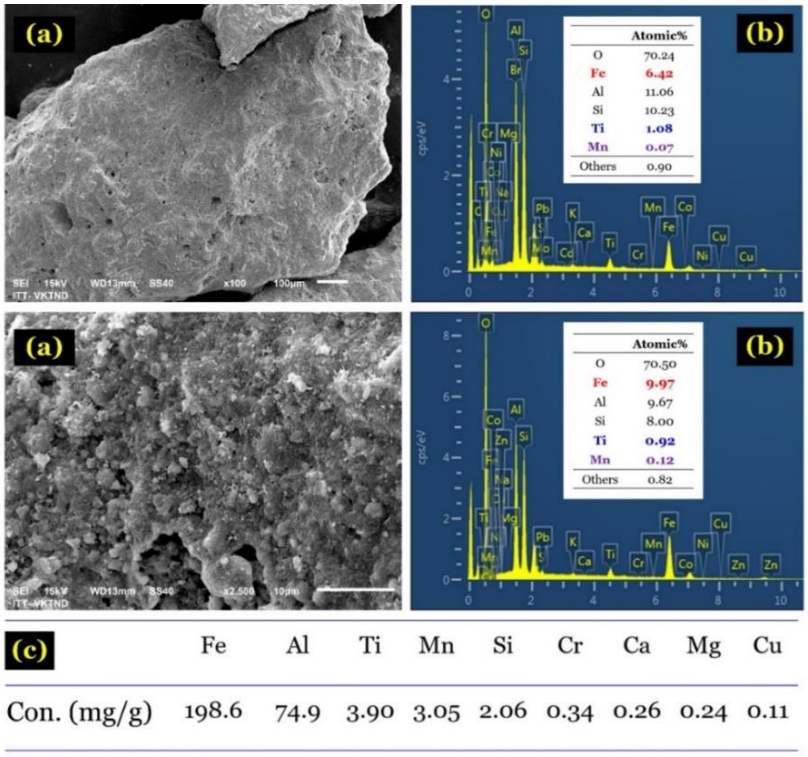

(c)	Fe	Al	Ti	Mn	Si	Cr	Ca	Mg	Cu
Con. (mg/g)	198.6	74.9	3.90	3.05	2.06	0.34	0.26	0.24	0.11

Figure 3.5. (a) SEM image and (b) EDS spectrum of the NLTT; and (c) concentration of metals in the NLTT

(determined by the acid digestion method)

The surface morphology of NLTT (determined by SEM) is provided in **Figure 3.5a.** The image indicates that the NLTT possessed a relatively irregular and heterogeneous surface morphology. In addition, the surface element analysis (obtained by EDS; **Figure 3.5b**) indicate the presence of dominant elements (i.e., O, Fe, Al, Si, Ti, and Mn) that possibly play an important role in the removal of As ions from water media. However, some heavy metals were observed in the EDS data, such as Zn (0.16% atomic), Cu (0.06%), Cr (0.02%), and Pb (0.01%). Therefore, further study was conducted by the acid digestion method to analysis the concentration of such elements in the NLTT. Results

(**Figure 3.5c**) show that the NLTT exhibited a high concentration of Fe (199 mg/g), Al (74.9 mg/g), Ti (3.90 mg/g), Mn (3.05 mg/g), and Si (2.06 mg/g). Notably, some heavy metals (i.e., Cr and Cu) was still detected in the structure of NLTT (**Figure 3.5c**). Therefore, when this material was applied in the real water treatment system (**Chapter 4**), it is necessary to evaluate the concentrations of potential heavy metals after passing the system.

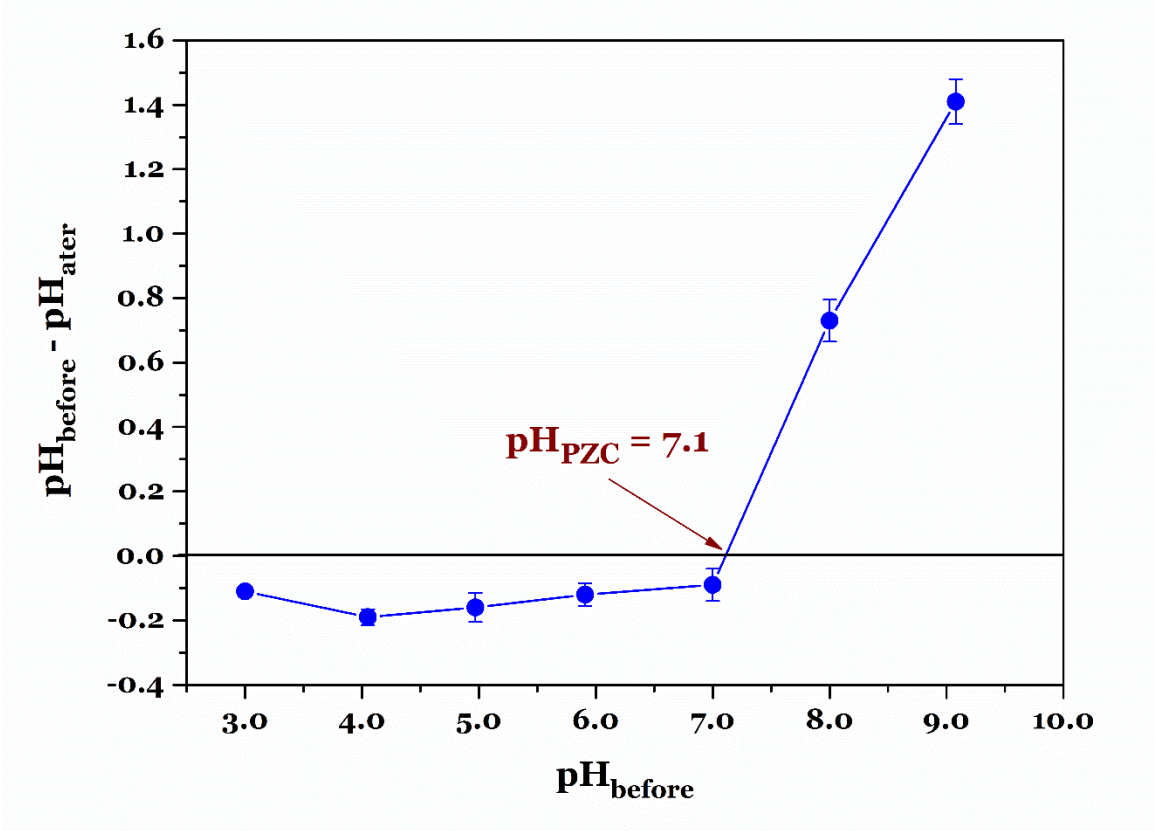

Figure 3.6. pHPZC of the NLTT determined by the "drift" method

(Experimental conditions: 2.5 g/L, 0.01 mol/L NaCl, 25 °C, and 24 h)

In general, adsorbent often exhibits an amphoteric nature in solution. In this study, the electrical state of the laterite' surface in solution was determined by the point of zero

charge (PZC). The pH_{PZC} of NLTT is 7.1 as determined by the drift method (**Figure 3.6**). Similarly, researchers found that the pH_{PZC} of other natural laterites collected from different geographical locations ranged from 7.4 to 8.3 (Partey et al., 2009; Maiti et al., 2013). Therefore, electrostatic attraction between the positively charged surface of laterite and target anionic pollutants in the solution was expected to simultaneously occur when the pH value of solution ($pH_{solution}$) was lower than the pH_{PZC} value.

3.3.3. Effect of initial solution pH values

In essence, the pH value exerts a strong effect on the surface charge of NLTT (**Figure 3.7**) and the stability of As species in solutions (**Figure. 2.2**). **Figure 3.7a** shows that the process of As(III) and As(V) adsorption onto NLTT was less dependent on the solution pH values from 2.0 to 10. A similar finding was reported elsewhere for the study of As(III) and As(V) adsorption onto: synthesized goethite (Lenoble et al., 2002), amorphous Fe oxide (Goldberg, 2002), laterite iron concretions (Partey et al., 2009), Fe(III)-impregnated activated carbon (Mondal et al., 2007), and acid-activated laterite (Maiti et al., 2010).

According to the As species stability diagram as a function of pH (**Figure 2.2),** pentavalent As is a triprotic acid (H_3AsO_4), and its pK_a values (**Table 2.1**) were determined to be approximately 2.3 (pK_{a1}), 6.8 (pK_{a2}), and 11.5 (pK_{a3}) (Kartinen and Martin, 1995; Lenoble et al., 2002; Smedley and Kinniburgh, 2002; Sharma and Sohn, 2009). In other words, As(V) species often exist as anion forms when $pH_{solution}$ was higher than 2.3 (the pK_{a1} of pentavalent As). They included monovalent $H_2AsO_4^-$ (within the pH range from approximately 3.0 to 6.0), divalent $HAsO_4^{2-}$ (pH = 7.0–11), and trivalent AsO_4^{3-} (pH = 12–14) (Mondal et al., 2007). Therefore, the electrostatic attraction might

play a dominant role in adsorbing As(V) anions in the solution when NLTT has net positive surface charge (pH below the pH_{PZC} of 7.1), and other contributors (i.e., pore filling and complexation) might be dominant when pH solution > 7.1.

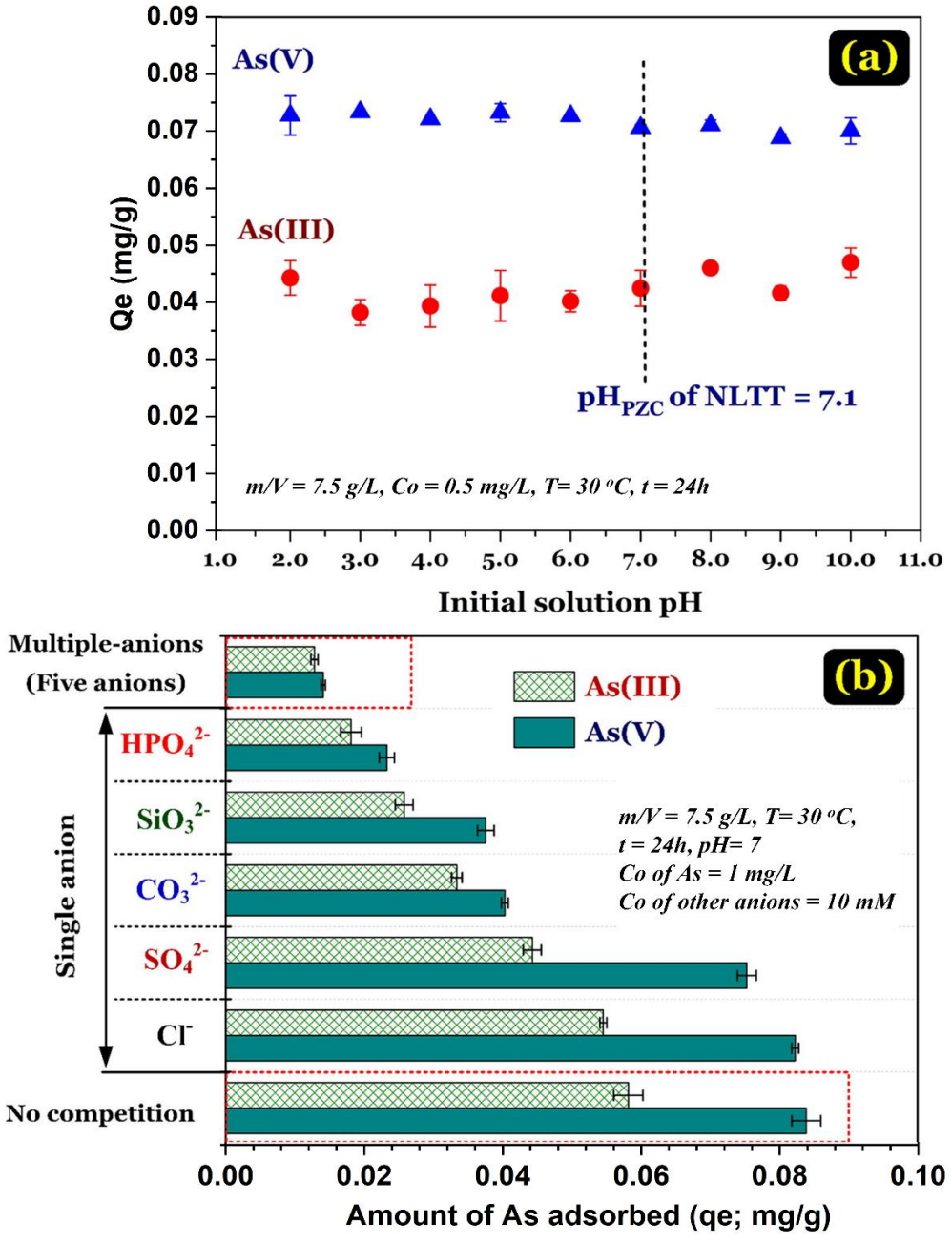

Figure 3.7. Effect of (a) initial solution pH values and (b) coexisting anions on the adsorption capacity of the NLTT towards As(III) and As(V)

In contrast, arsenous acid (H_3AsO_3) is weak acid, and the pK_a values of As(III) are approximately 9.2 (pK_{a1}), 12.1 (pK_{a2}), and 12.7 (pK_{a3}) as showed in **Table 2.1** (Kartinen and Martin, 1995; Lenoble et al., 2002; Smedley and Kinniburgh, 2002; Sharma and Sohn, 2009). Because of a high value pK_{a1}, As(III) exists the form of no charge ($H_3AsO_3^0$) within pH of the solution from 1.0 to 9.0 (Mondal et al., 2007; Partey et al., 2008). Thus, the adsorption of uncharged $H_3AsO_3^0$ through electrostatic attraction was not favourable. In this case, NLTT can remove As(III) from the solution through other potential mechanisms, such as pore filling (Mondal et al., 2007), oxidation-coupled adsorption (Muthu Prabhu et al., 2019), surface complexation (Siddiqui and Chaudhry, 2017).

3.3.4. Effect of coexisting single and mixed anions on As(III)/As(V) adsorption

The effect of coexisting anions (denoted as guest anions) on the As adsorption capacity of NLTT is provided in **Figure 3.7b**. Five anions, including chloride (Cl^-), sulphate (SO_4^{2-}), carbonate (CO_3^{2-}), silicate (SiO_3^{2-}), and monohydrogen phosphate (HPO_4^{2-}) were used to investigate their effects on As(III) and As(V) adsorption capacity by NLTT. These anions were chosen due to their common existence in the ground and surface water. In addition, previous studies (Hong et al., 2014; Lu et al., 2018) showed that their anions could affect the performance of adsorbents on As removal. Results indicate that the presence of other ions in solution caused a significant reduction in the removal efficiency of As, with the increasing order being: anion absence < chloride < sulphate < carbonate < silicate < monohydrogen phosphate < mixed anions (Cl^-, SO_4^{2-}, CO_3^{2-}, SiO_3^{2-}, and HPO_4^{2-}). An identical order of adsorption has been reported in the literature (Maji et al., 2007; Maiti et al., 2010; Sun et al., 2017; Wen et al., 2018). The decline in adsorption capacity might result from the competition between the guest anions

(acting as competitors) and As(V) anions for the absorbing sites on the surface of NLTT. Among investigated anions, the adsorption capacity of NLTT towards both As ions was strongest affected by the present of HPO_4^{2-}. This is caused by the similar tetrahedral structure of both HPO_4^{2-} and As, which lead to compete for the adsorption site. In contrast, the present of Cl^- in the solution had no noticeable effect on the As removal efficiency by NLTT adsorbent. This is because that Cl^- is a monovalent anion and possesses poorer ionic potential. It also lacks a tetrahedral structure for competition with As. For CO_3^{2-} and SiO_3^{2-} anions, they decreased the adsorption capacity of As onto NLTT because CO_3^{2-} could form monodentate inner-sphere complexes with iron oxide of NLTT and SiO_3^{2-} inhibits coagulation and crystalline growth of iron hydroxides of adsorbent (SunBaek and XiaoGuang, 2004). This means that the presence of these anions interferes the As adsorption process.

Notably, although As(III) exists as the uncharged $H_3AsO_3^0$ form (**Figure 2.2**), the adsorption capacity of NLTT was still affected by guest anions's presence. This result confirms the existence of the competition. In fact, As(III) was possibly partly oxidized into As(V) ions in solution through some particular oxidants (i.e., FeOOH, Fe_2O_3, MnO_2, and TiO_2) (Lenoble et al., 2004; Guan et al., 2012; Simeonidis et al., 2016; Siddiqui and Chaudhry, 2017; Zhao et al., 2018; Cheng et al., 2019;) that are available in the structure of the NLTT (**see Section 3.3.2**).

The experimental results show that adsorption capacity of NLTT towards As(V) was higher than that of As(III) at anion absence. The influence by the presence of multi-anions on NLTT's adsorption capacity for As(V) was found to be higher than that for As(III). For As(V), the presence of these anions decreased the adsorption capacity of

NLTT by 5.35 times, compared to only 4.26 times for that with As(III). The negative charge of As(V) and uncharge form of As(III) in the solution could be the reason for stronger effect on As(V) than that on As(III).

3.3.5. Adsorption kinetics

Figure 3.8a–b presents the influence of contact time on removing As with NLTT. The rate of As(V) and As(III) adsorption by NLTT increased quickly during the first 1 h of contact. Subsequently, the adsorption rate gradually decreased until the plateau was reached at around 120–360 min. In this study, three adsorption kinetic models – the pseudo-first-order (PFO) (Lagergren, 1898), pseudo-second-order (PSO) (Blanchard et al., 1984), and Elovich models (McLintock, 1967) – were used to model the experimental data. The essential information for these models may be found in **Section 2.6.3.1**.

To minimize the error functions, the parameters of such models were calculated from the non-line technique. The best fitting model was obtained with high R^2 and low χ^2 values. **Table 3.1** lists the relevant kinetic parameters for the As adsorption onto the NLTT. In general, the adsorption process was better descried by the PSO (R^2 = 0.934–0.993 and χ^2 < 18.4*10^-6) and Elovich (0.951–0.991 and χ^2 < 22.5*10^-6) models than the PFO model (0.829–0.988 and χ^2 58.5*10^-6–82.1*10^-6). According to the PSO adsorption rate constant k_2, it can be concluded that the adsorption process of As(V) onto the NLTT reached a faster equilibrium than that of As(III). Similarly, a higher value of the initial rate constant α for the As(V) adsorption suggest that the adsorption process of As(V) onto the NLTT occurred more quickly than that of As(III). These results demonstrate that As(V) had a higher affinity to the NLTT than As(III) in solution. Notably, the k_2 value decreased remarkably when the initial concentration of As(III) and

As(V) increased, thus confirming the negligible contribution of driving force during the As adsorption process.

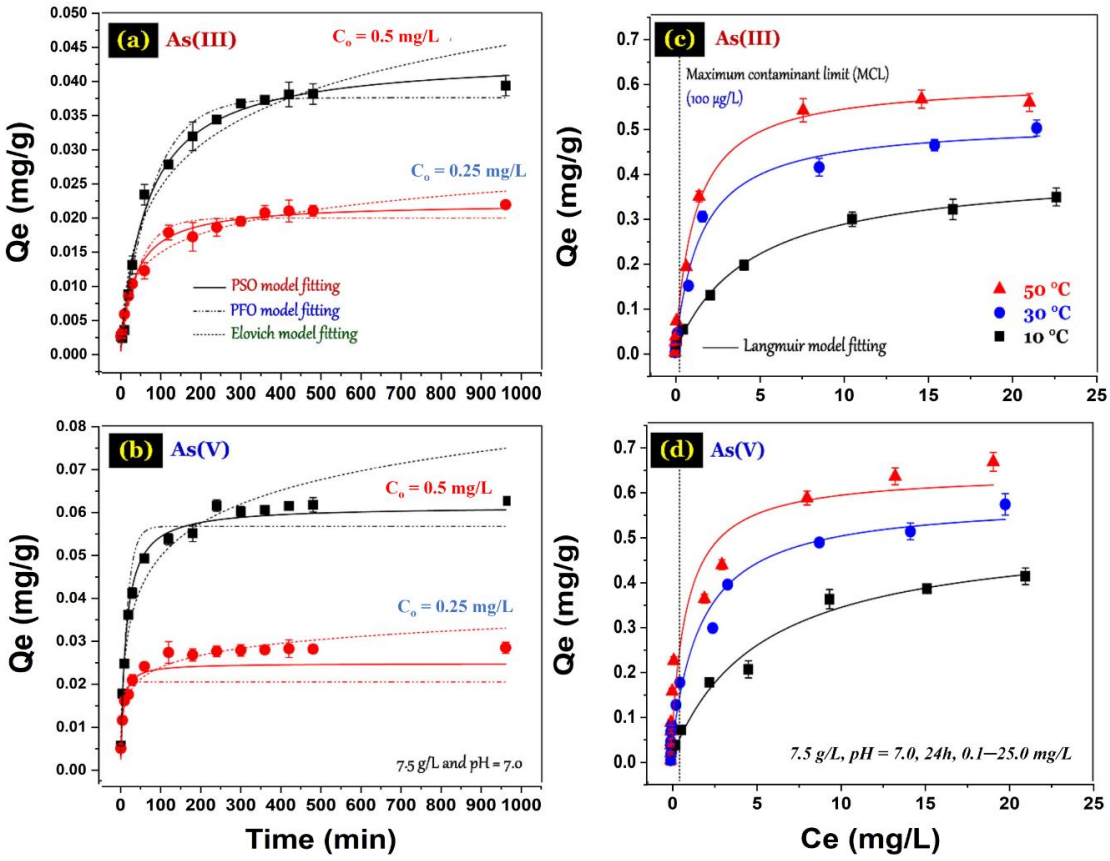

Figure 3.8. (a)–(b) Effect of contact time on the As adsorption process onto the NLTT at different initial As concentrations; and (c)–(d) isotherm of As adsorption onto the NLTT at different temperatures

Table 3.1. Relative adsorption kinetic parameters for the As(III) and As(V) adsorption by NLTT at different intial As concncetrations (0.25 and 0.50 mg/L)

	Unit	As(III)		As(V)	
		0.25 mg/L	**0.50 mg/L**	**0.25 mg/L**	**0.50 mg/L**
1. PFO model					
q_e	mg/g	0.020	0.038	0.021	0.057
k_1	1/min	0.021	0.013	0.168	0.064
R^2	—	0.944	0.988	0.829	0.976
χ^2	—	2.71*10^-6	2.46*10^-6	82.1*10^-6	58.5*10^-6
2. PSO model					
q_e	mg/g	0.022	0.044	0.025	0.062
k_2	g/mg × min	1.28	0.35	7.25	1.26
R^2	—	0.978	0.992	0.934	0.993
χ^2	—	1.03*10^-6	1.80*10^-6	10.2*10^-6	18.4*10^-6
3. Elovich model					
α	mg/g × min	0.002	0.001	0.019	0.010
β	mg/g	249	105	251	91
R^2	—	0.976	0.962	0.951	0.991
χ^2	—	1.14*10^-6	8.25*10^-6	22.5*10^-6	22.2*10^-6

3.3.6. Equilibrium adsorption isotherm

In essence, adsorption isotherm plays an important role in identify the region of As adsorption (i.e., Henry, Langmuir, or Freundlich) and the maximum contaminant limit (MCL) of As for drinking water (Simeonidis et al., 2016).

In this study, the Langmuir (Langmuir, 1918), Freundlich (Freundlich, 1907), and Redlich–Peterson (Redlich and Peterson, 1959) models were employed to describe the adsorptive behaviour of As ions onto the NLTT. To minimize the respective error functions, the non-linear optimization technique was used to calculate the adsorption parameters using these models. The relevant information of these models was provided in **Section 2.6.3.2**.

Figure 3.8 c–d and **Table 3.2** present the adsorption isotherms and the isotherm parameters for the adsorption of As by NLTT at three temperatures, respectively. The isotherm shapes of As(III) and As(V) can be classified into a L - type, suggesting that the NLTT has a strong affinity to As(III) and As(V) ions. The high R^2 indicates that the adsorption equilibrium data is adequately described by all three models **(Table 3.2**). Furthermore, the experimental data reveal that the adsorption capacity of NLTT, in general, increased with temperature for both As(III) and As(V).

As shown in **Table 3.2**, the Langmuir maximum adsorption capacity (Q_{max}) of NLTT towards As ions significantly increased from 0.409 to 0.602 mg/g for As(III) and from 0.514 to 0.638 mg/g for As(V) when the temperature increased from 10 °C to 50 °C. An identical adsorption tendency was reported by (Maiti et al., 2007) for the As(III) adsorption onto nature laterite at the temperatures: Q_{max} = 0.150 mg/g at 15 °C < 0.170 mg/g at 30 °C < 0.210 mg/g at 45 °C. These results suggest that the adsorption process

might be endothermic in nature and weak electrostatic attraction (also known as out-sphere complexation) might play a less important role than the others (inner-sphere complexation) i.e., complexation) in the adsorption process at pH 7.0. Furthermore, the Langmuir adsorption capacities determined for NLTT adsorption of As(III) and As(V) are generally similar or higher than those reported in literature for many of the other iron-containing low-cost adsorbents where adsorption experiments were conducted at the realistic As(III) or As(V) concentration (**Table 3.3**).

Notably, because the residual concentration of As ions plays an important role in designing and applying the adsorbent material for real water treatment, it may be necessary to estimate the index of regulation limit (Q_{RL}) of As pollutant as suggested in one study (Simeonidis et al., 2016). This index was obtained based on the maximum contaminant limit (MCL) of As for drinking water (0.01 mg/L WHO) and the equilibrium As concentration (C_e; mg/L). According to the experimental data of adsorption equilibrium and adsorption isotherm (**Figure 3.8c–d**), the Q_{RL} value was estimated to be approximately 0.033 mg/g for As(III) and 0.039 mg/g for As(V) at the operation conditions (i.e., 30 °C, pH = 7.0, and solid/liquid ratio of 7.5 g/L). The value for As(V) adsorption in our study is similar to the Q_{RL} values of 0.020–0.050 mg/g for As(V) adsorption on iron hydroxide modified activated carbon (Vitela-Rodriguez and Rangel-Mendez 2013), 0.025 mg/g for As(V) adsorption on iron oxide coated sand (Thirunavukkarasu et al., 2003) and 0.005–0.020 mg/g for As(V) adsorption on red mud (Genç et al., 2003).

Table 3.2. Relative isotherm parameters for the As(III) and As(V) adsorption by NLTT

	Unit	As(III) adsorption			As(V) adsorption		
		10 °C	30 °C	50 °C	10 °C	30 °C	50 °C
1. Langmuir model							
Q_{max}	mg/g	0.409	0.512	0.602	0.514	0.580	0.638
K_L ($\times 10^{-3}$)	L/mg	227	670	867	193	604	1170
R^2	—	0.99	0.99	0.99	0.98	0.97	0.93
χ^2	—	1.73*10^-4	4.70*10^-4	3.62*10^-4	4.98*10^-4	0.00152	0.00458
2. Freundlich model							
K_F	$(mg/g)(L/mg)^n$	0.093	0.179	0.280	0.107	0.218	0.307
n	—	0.43	0.35	0.31	0.46	0.33	0.28
R^2	—	0.98	0.95	0.94	0.97	0.98	0.99
χ^2	—	6.34*10^-4	2.18*10^-3	4.33*10^-3	9.36*10^-4	5.05*10^-4	8.39*10^-4
3. Redlich–Peterson model							
K_{RP}	L/g	0.05	0.43	0.36	0.12	18.18	29.38
a	$(mg/L)^{-g}$	0.05	1.03	0.42	0.32	80.02	88.46
g	—	1.22	0.93	1.11	0.89	0.69	0.75
R^2	—	0.99	0.99	0.99	0.98	0.98	0.99
χ^2	—	1.8*10^-4	5.10*10^-4	2.35*10^-4	5.83*10-4	5.53*10^-4	5.19*10^-4

Table 3.3. Comparison of the As adsorption capacities of iron-containing low-cost adsorbents

Adsorbent	Initial As(III)/As(V) concentration (mg/L)	Maximum adsorption capacity (mg/g) As(III)	Maximum adsorption capacity (mg/g) As(V)	Reference
NLTT	**0.1–25**	**0.51**	**0.58**	**This study**
Laterite soil	0.5	1.38	0.04	Maji et al. (2007)
Laterite iron concretions	0.1–2	0.909	0.714	Partey et al. (2008)
Raw laterite	0.25–5	0.128	0.301	Glocheux et al. (2013)
Sulphuric acid acidified laterite	0.25–5	0.172	0.924	Glocheux et al. (2013)
Iron oxide hydroxide nanoflower	0.1–1	1.31	-	Raul et al. (2014)
Fe-exchanged zeolite	0.1–20	0.10	0.05	Li et al. (2011)
Iron hydroxide modified activated carbon	0.025–1.5	-	0.37–1.25	Vitela-Rodriguez and Rangel-Mendez (2013)
Iron oxide coated sand	0.1	0.041	0.043	Thirunavukkarasu et al. (2003)
Hematite	10	-	0.205	Singh et al. (1996)

3.3.7. Adsorption thermodynamics

The thermodynamic variables (standard Gibbs free energy change (ΔG°), standard enthalpy change (Δ*H*°), and standard entropy change (Δ*S*°)) for the As adsorption by adsorbent were caculated to confirm the adsorption mechanism using the van't Hoff equation. Firstly, Δ*G*° was computed using **Equation 3.5.**

$$\Delta G^\circ = -RT\, ln K^o_{\text{Equilibrium}} \quad \textbf{(3.5)}$$

The relationship between three parameters (Δ*G*°, Δ*H*°, and Δ*S*°) is provided in **Equation 3.6**.

$$\Delta G^\circ = \Delta H^\circ - T\Delta S^\circ \quad \textbf{(3.6)}$$

The van't Hoff equation (**Equation 3.7**) is derived by substituting **Equation 3.5** in **Equation 3.6**. $K^o_{\text{Equilibrium}}$ is computed by **Equation 3.8.**

$$\text{Ln}K^o_{\text{Equilibrium}} = \frac{-\Delta H^\circ}{R} \times \frac{1}{T} + \frac{\Delta S^\circ}{R} \quad \textbf{(3.7)}$$

where R is a gas constant [0.00831 kJ/(mol×K)] and T is absolute temperature in degrees Kelvin (^0K)

$$K^o_{\text{Equilibrium}} \approx \frac{K_{\text{model}}(L/mol) \times C^o(mol/L)}{\gamma} \quad \textbf{(3.8)}$$

where K_{model} (L/mol), $K^{o}_{\text{Equilibrium}}$ (dimensionless) are the Langmuir constant (K_{L}) and thermodynamic equilibrium constant; $C°$ is the standard concentration of As ($C°$ = 1 mol/L); and γ is an activity coefficient of As in solution.

Table 3.4. Thermodynamic parameters for the adsorption of As on NLTT

	T (K)	Van't Hoff equation	ΔG° (kJ/mol)	ΔH° (kJ/mol)	ΔS° (kJ/mol)
As(III)	283	y = -3096x + 20.8	-22.9	25.7	0.173
	303	R^2 = 0.911	-27.3		
	323		-29.8		
As(V)	283	y = -4142x + 24.3	-22.5	34.4	0.202
	303	R^2 = 0.987	-27.0		
	323		-30.6		

Thermodynamic parameters for the adsorption of As on NLTT are presented in **Table 3.4.** The results show that the Δ$G°$ values for both As species at three studied temperatures are negative, implying that the adsorption process occurred spontaneously. In addition, the positive Δ$H°$ values indicate that the adsorption process of As(III) and As(V) are endothermic in nature. According to magnitude of Δ$H°$, it might conclude that the NLTT has a higher affinity to As(V) adsorption than As(III) in solution because its higher Δ$H°$ magnitude. Moreover, the positive Δ$S°$ values demonstrate an increase in randomness at the solid/solution interface during the adsorption process of As(III) and As(V). A similar conclusion was reported by Maiti et al. (2007) for As(III) adsorption

by natural laterite ($\Delta G°$ = from -5.22 to -6.65 kJ/mol, $\Delta H°$ = 35.6 kJ/mol, and $\Delta S°$ = 0.142 kJ/mol×K).

3.3.8. Desorption study

To explore the desorption efficiency of As from the laden NLTT samples, different solvents - deionized water (pH = 12), HCl, NaOH, NaCl, and EDTA - served as target desorbing agents. The experiment results demonstrated that the desorption efficiency of As(III) was considerably higher than that of As(V) for whole desorbing agents used (**Table 3.5**). This presumably because As(III) was weakly adsorbed by NLTT when compared to As(V). Of the agents, the desorption efficiency of both As(III) and As(V) was highest for 0.5M NaOH (approximately 48% and 29%, respectively). This is probably due to the electrostatic repulsion of the negatively charged As anions and increased surface negative charges on the adsorbent at high pHs caused by NaOH. It could also be due to the increased competition of As adsorption with the increased OH^- ions produced at high pHs. As adsorption process is expected to be irreversible in salt solution (0.5M of NaCl) because Cl^- is a weakly adsorbing anion and cannot compete with the strongly adsorbing As (as reported in **Section 3.3.4**). This explained the using inability of 0.5M NaCl to desorb As.

Table 3.5. Percentage of As desorption from the As-laden NLTT

Desorbing agents	As(V)	As(III)
Sodium chloride (0.5M)	0.01	0.04
EDTA (5%)	2.8	6.7
Hydrochloric acid (0.5M)	14.0	15.4
Deionized distilled water at pH12	12.6	18.5
Sodium hydroxide (0.5M)	29.0	47.8

3.3.9. Possible mechanism of As adsorption onto NLTT

In this study, a possible adsorption mechanism of As ions onto the collected NLTT was conducted with a pH level of pH 7.0. As discussed in **Section 3.3.2**, the NLTT exhibited a smaller specific surface area (155 m^2/g) than activated carbon (566–1302 m^2/g) (Tran et al., 2017b) and biochar (188–543 m^2/g) (Boakye et al., 2019); therefore, although the pore-filling mechanism might play an important role in the adsorption process, it is not significant. In this case, the surface interactions played a vital role rather than pore filling. The existence of As element on the surface of NLTT (**Figure 3.9**) after adsorption confirmed that the adsorption of As(III) and As(V) onto NLTT was successful and occurred mainly in the surface of NLTT.

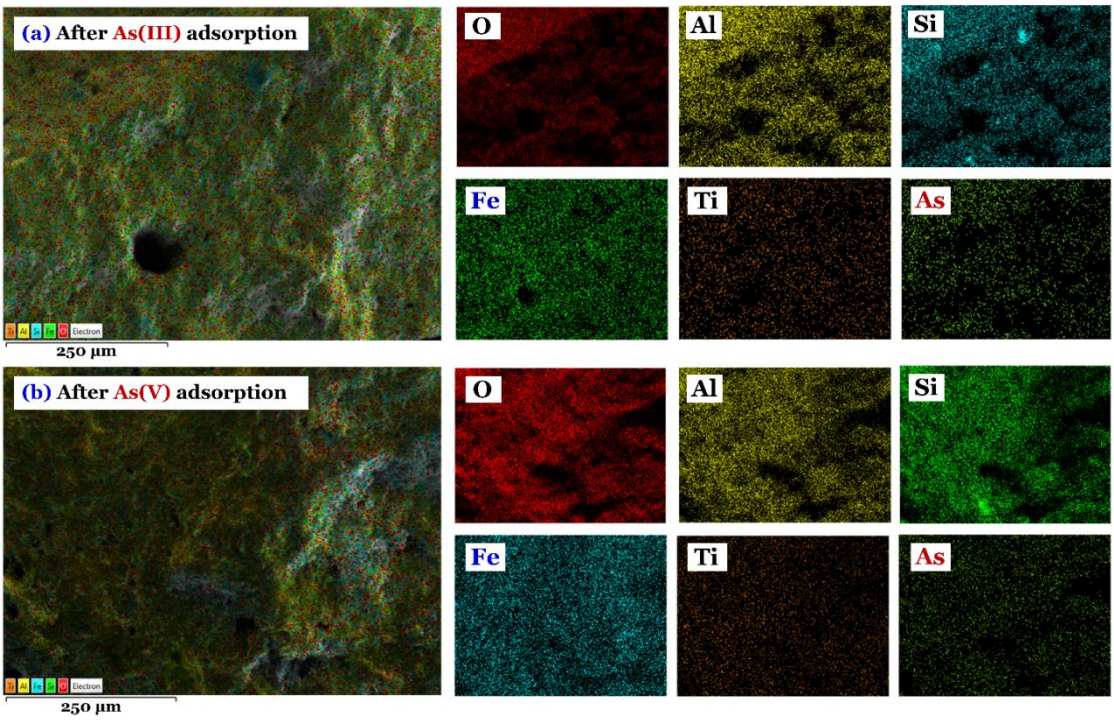

Figure 3.9. Elemental mapping analysis of the NLTT after adsorption of (a) As(III) and (b) As(V)

Notably, referring to the adsorption of As(V), the surface interaction possibly involved weak electrostatic attraction (outer-sphere complexation) and surface complexation (inner-sphere complexation). Meanwhile, the oxidation of As(III) to As(V) and the complexation between As ions in solution and the –OH groups on the surface of NLTT might be dominant reactions for the adsorption of As(III) (Partey et al., 2009; Pozdnyakov et al., 2016; Zhao et al., 2018; Cheng et al., 2019;).

3.3.10. Laboratory column adsorption study

3.3.10.1 Effect of initial As(V) concentration

Figure 3.10a and **Figure 3.10c** present the breakthrough curves taken at flow rate of 0.85 m/h, using a bed height of 0.15 m and at two different As(V) initial concentrations of 0.1 and 0.5 mg/L, respectively. The results show that an increase of As(V) initial concentration causes a visible change in the shape and gradient of the breakthrough curves. At higher As(V) initial concentration, the breakthrough curves was sharper and shifted to the left (**Figure 3.10c**). An increase in the As(V) initial concentration resulted in the breakthrough occurring earlier and the exhaustion time was smaller. The breakthrough time decreased from 144 h to 28 h when As(V) initial concentration increased from 0.1 mg/L to 0.5 mg/L. Similarly, the exhaustion time reduced from 450 h to 250 h as As(V) at higher initial concentration. These results suggest that the change in As(V) initial concentration affected the diffusion process of As(V) adsorption onto NLTT, leading to a change for parameters such as breakthrough and the exhaustion time. This is because a higher As(V) initial concentration resulted in a higher driving force, steeper adsorbate concentration gradient and a faster exhaustion rate. These outcomes agree with those of others (Aksu et al., 2007).

Figure 3.10b and Figure **3.10d** also show the breakthrough curves obtained at two As(V) concentrations (0.1 mg/L and 0.5 mg/L), with bed height of 0.41 m. A similar trend was obtained when the As(V) concentration increased from 0.1 mg/L to 0.5 mg/L.

3.3.10.2. Effect of bed height

The breakthrough curves of NLTT towards As(V) adsorption at different bed heights with As(V) initial concentration of 0.1 mg/L and flow rate of 0.85 m/h are presented in **Figure 3.10a** and **Figure 3.10b**. As portrayed in **Figure 3.10a** and **Figure 3.10b**, there were significant increases for both breakthrough and exhaustion time when bed height of column increased from 0.15 m to 0.41 m. Breakthrough times were 144 h and 240 h for 0.15 m and 0.41 m in lengths of bed, respectively. A similar trend occurred for the exhaustion times which were 450 h to 600 h, respectively. Steeper breakthrough curves were recorded where the bed heights were larger. An increase in bed height or adsorbent amount resulted in more adsorbent specific surfaces and more available active binding sites for As(V) ions. Consequently, the amount of As(V) adsorbed onto NLTT increased. These similar findings were found in the reports of Acheampong et al. (2013), Brion-Roby et al. (2018), and Vu et al. (2018).

Figure 3.10c and **Figure 3.10d** show the breakthrough curves of As(V) in the column adsorption studies at bed heights of 0.15 m and 0.41 m, flow rate of 0.85 m and As(V) initial concentration of 0.5 mg/L. A similar trend could be observed for both breakthrough time and exhaustion time when the bed height increased from 0.15 m (**Figure 3.10c**) to 0.41 m (**Figure 3.10d**). At an As(V) initial concentration of 0.5 mg/L, the breakthrough occurred at 28 h and 122 h at the bed height of 0.15 m and 0.41 m, respectively.

In addition, at As(V) initial concentrations of 0.1 mg/L, the NLTT column could treat up to 497 bed volumes until the filter column effluent started exceeding the Vietnam and WHO drinking water standard (0.01 mg/L).

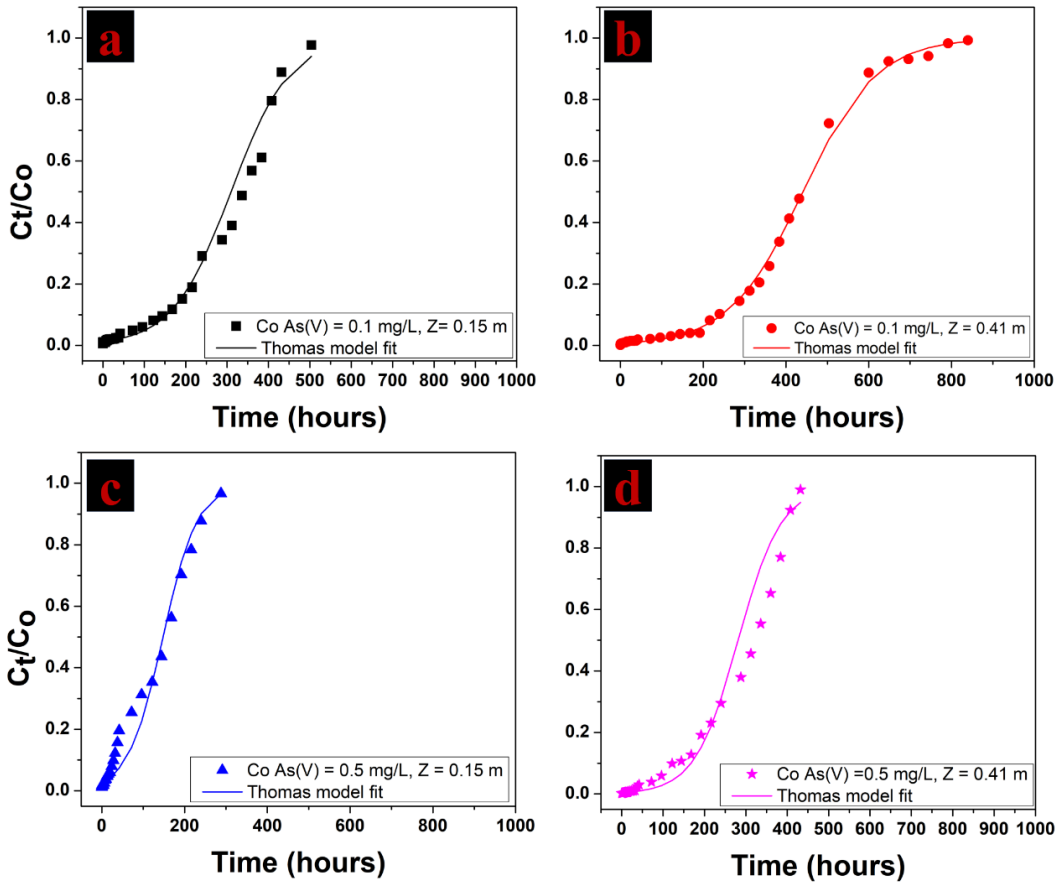

Figure 3.10. Breakthrough curves for As(V) adsorption on NLTT in term of different experimental conditions (initial concentrations and bed heights)

(Experimental conditions: Co: 0.1 mg/L and 0.5 mg/L; Bed height Z: 0.41 m and 0.15 m flow velocity 0.85 m/h; pH: 7.0; room temperature)

3.3.10.3. Breakthrough curve modeling

The Thomas model (Thomas, 1944) was used to describe the breakthrough curves. This model is the most popular and widely applied in column adsorption studies (Nur et al., 2015; Eeshwarasinghe et al., 2018). Furthermore, it accurately describes the column adsorption capacity unlike many others. The nonlinear and linear forms of the Thomas

model was described in **Section 2.6.3.3**. The Thomas parameters values (k_{TH} and q_{TH}) were determined from the linear plot of $\ln\left(\frac{C_0}{C_t} - 1\right)$ against t and are presented in **Table 3.6**. The model satisfactorily described the As(V) breakthrough in the column at the two inlet concentrations (0.1 and 0.5 mg/L) tested, as indicated by the high coefficient of determination values (R^2) (0.95, 0.98) (**Table 3.6, Figure 3.10**).

Table 3.6. Thomas model parameters for As(V) adsorption on NLTT

Co ***(mg/L)***	***Z*** ***(m)***	q_{exp} ***(mg/g)***	**Thomas model parameters**		
			k_{TH} (L/h.mg)	q_{TH} (mg/g)	R^2
0.1	0.41	0.05	0.117	0.058	0.98
0.5	0.41	0.20	0.038	0.198	0.95
0.1	0.15	0.11	0.146	0.113	0.97
0.5	0.15	0.26	0.046	0.285	0.96

The results show that the adsorption capacity of NLTT obtained at bed height of 0.41 m increased from 0.058 to 0.198 mg/g, and the kinetic coefficient, K_{TH}, decreased from 0.117 to 0.038 L/h.mg as the initial As(V) concentration rose from 0.1 mg/L to 0.5 mg/L, respectively (**Table 3.6**). The similar trend was found at two As(V) concentrations (0.1 mg/L and 0.5 mg/L), with bed height of 0.15 m. The higher values of q_{TH} at higher initial As(V) concentration are due to the higher driving force for adsorption of As(V) on

NLTT. This outcome agrees with previous studies (Nguyen et al., 2015; Abdolali et al., 2017). The Thomas adsorption capacities of NLTT are much lower than the Langmuir maximum adsorption capacity of NLTT for As(V) (Q_{max} = 0.580 mg/g) obtained in a static batch study. It is because the equilibrium As(V) concentration (> 10 mg/L) at the calculated Langmuir maximum adsorption value was much higher than the inlet As(V) concentrations used in the column experiment (0.1 and 0.5 mg/L). However, the adsorption capacities in the batch adsorption study at similar As(V) concentrations in solution phase of 0.25 mg/L and 0.5 mg/L as in the column study were 0.020 mg/g and 0.037 mg/g, respectively. These results show that the adsorption capacities derived from the batch adsorption process are lower than the Thomas adsorption capacities obtained in the column adsorption study at comparable solution As(V) concentrations. The reason for the higher values in the column study is that the driving force for adsorption is always constant, and this was made possible by the continuous mode of feeding the As(V) solution to the adsorbent fixed bed. Conversely, in the batch experiment the driving force diminishes progressively with time due to the removal of the As(V) from the solution by adsorption.

Table 3.7 summarizes a comparison of the Thomas adsorption capacities obtained for NLTT in this study with those reported for other adsorbents. The data indicate that NLTT possessed a higher adsorption capacity than that of manganese oxide ore (Nguyen et al., 2020b), natural pozzolan (Kofa et al., 2015), and iron mixed mesoporous pellet (Te et al., 2018). The reasons for higher Thomas adsorption capacity of NLTT could possibly be attributed by the higher concentration of Fe in NLTT's component. The amount of Fe_2O_3 in NLTT was 48.7% of its weight, which was higher

than that of manganese oxide ore (16.10%), natural pozzolan (21.19%) and iron mixed mesoporous pellet (25.78%).

Table 3.7. Comparison of Thomas adsorption capacities obtained in the current study with those reported in other studies

Adsorbent	As (V) concentration (mg/L)	Flow rate (L/h)	Thomas adsorption capacity (mg/g)	References
NLTT	0.5	0.6	**0.198**	**This study**
Manganese oxide ore	0.25	0.15	0.151	Nguyen et al. (2020b)
Natural pozzolan	0.40	0.24	0.003	Kofa et al. (2015)
Iron mixed mesoporous pellet	0.5	1.23	0.099	Te et al. (2018)

3.4. Conclusions

Among seven locally available low-cost materials in Vietnam, a natural laterite from Thach That district, Hanoi (NLTT) emerged as the most promising material for As removal from groundwater. The NLTT with PZC of pH 7.1 and composed of high weight percentages of iron and aluminium contained mainly goethite and hematite, and some minor minerals (titanium dioxide, manganese oxide), all of which play an important role in adsorbing As(V) and As(III). The batch experiment results demonstrated that the adsorption process of NLTT depended less on the solution pH when it ranged from 2.0 to

10. Coexisting anions competed with As(III) and As(V) in the following sequence: monohydrogen phosphate > silicate > carbonate > sulphate > chloride. The adsorption process reached a fast equilibrium at approximately 120–360 min, depending on the initial As concentrations. Adsorption of As(V) was higher than As(III). The Langmuir adsorption capacities of NLTT at pH 7 for As(III) and As(V) were 0.512 and 0.580 mg/g, respectively which were mostly higher than the values reported for many other low-cost adsorbents at realistic total As concentrations in water. Meanwhile, the thermodynamic study conducted at 10 °C, 30 °C, and 50 °C suggest that the adsorption process of As(III) and As(V) was spontaneous and endothermic. The main mechanisms of removing As(V) include weak electrostatic attraction (outer-sphere complexation) and surface complexation (inner-sphere complexation). For As(III), the oxidation of arsenite As(III) to arsenate As(V) and the complexation between As(III) ions in solution and the –OH groups on the surface of NLTT might be dominant reactions for As(III) adsorption. Results from the laboratory column study with NLTT at different experimental conditions (initial As(V) concentration: 0.1 and 0.5 mg/L; bed height: 0.15 and 0.41 m) indicate that at a very high As(V) concentration of 0.5 mg/L, adsorption breakthrough occurred at 28 h and 122 h for column heights of 0.15 m and 0.41 m, respectively. When the As(V) concentration was reduced to 0.1 mg/L, the breakthrough times increased to 144 h and 240 h, respectively. The breakthrough curves were found to fit the Thomas model very satisfactorily at all experimental conditions. The Thomas adsorption capacities at a flow velocity of 0.85 m/h and input As(V) concentration of 0.5 mg/L for bed height of 0.15 m and 0.41 m were 0.28 mg/g and 0.20 mg/g, respectively. When As(V) concentration fell

to 0.1 mg/L, the Thomas adsorption capacity was 0.113 mg/g for bed height of 0.15 m and 0.06 mg/g for bed height of 0.41 m.

This chapter focuses on As removal by NLTT, an adsorbent produced from natural mineral. Although NLTT has the potential to become a commercially As filter media because of its low cost (US$ 0.10/kg) and good performance, a new iron-based adsorbent with higher As adsorption capacity compared to NLTT should be developed and investigated. In other words, the new iron-based adsorbent can remove both As ions from higher contaminated water. It means that for practical application the replacement and maintenance time of filter media is expected to take longer to do. Moreover, a new iron-based adsorbent needs to possess several features such as cost-effectiveness, local availability, and environmental friendliness. The next chapter will present PPCI, a new adsorbent derived from pomelo peel, an agricultural waste.

CHAPTER 4. REMOVAL OF ARSENIC FROM WATER BY A POMELO PEEL BIOCHAR COATED WITH IRON

Chapter 4 presents the PPCI's performance on the removal of As from water. PPCI is a new adsorbent derived from pomelo peel, an agricultural waste. The results of the batch study in this chapter have been submitted in journal below and being in under review stage.

Nguyen, T. H., Loganathan P., Nguyen, T. V., Vigneswarana S., Nguyen, T. H. H., Tran, H. N., Nguyen, Q. B. Arsenic removal by a pomelo peel biochar coated with iron. *Chemical Engineering Research and Design (accepted).*

4.1. Introduction

A significant number of adsorbents have been used for As removal such as, natural adsorbents (laterite, zeolite, clay minerals) (Nguyen et al., 2020a); industrial by-products (red mud, iron mine waste sludge) (Nguyen et al., 2009; Yang et al., 2014); agricultural by-products (biomass-derived adsorbents, biochar, activated carbon) (Ahmad et al., 2022; Nguyen et al., 2020c; Nham et al., 2019); and synthetic materials (layered double hydroxides nanomaterials, iron-oxide coated materials) (Nguyen et al., 2021b). However, due to practical reasons, new adsorbents based on local and low-cost materials are still required. Compounds containing iron have been shown to be effective in removing As from drinking water (Pierce and Moore, 1982; Matis et al., 1997; Lakshmipathiraj et al., 2006; Aredes et al., 2013). Iron-based adsorbents can also be magnetically separated after the adsorption process, thereby minimizing secondary pollution and recycling exhausted

adsorbents (Zhang et al., 2013). However, one of the main weaknesses of these adsorbents is linked to their chemical and physical form in which they occur. For example, amorphous hydrous iron oxide (FeOOH) often exists in the form of fine powders or gel. Therefore, it is challenging for it to be completely removed from the treated solution after its use (Li et al., 2009). Another example is γ-Fe_2O_3 particles, with specific magnetic properties, which may easily form aggregates, thereby rapidly reducing their adsorption efficiency (Zhang et al., 2013). In general, iron and iron oxide particles are often not easily handled, which limits their practical applicability. This led to rising interest in combining iron with low-cost supporting media to remove As, including man-made materials such as: cement (Kundu and Gupta, 2006); sand (Chang et al., 2008; Herbel and Fendorf, 2006); activated carbon (Chang et al., 2010); activated alumina (Kuriakose et al., 2004); peat sorbent (Kasiuliene et al., 2018); slag (Zhang and Itoh, 2005); naturally-derived materials like cork granulates (Pintor et al., 2018); sugarcane bagasse (Pehlivan et al., 2013); rice husk (Cope et al., 2014; Pehlivan et al., 2013); seaweeds (Vieira et al., 2017); or zeolite (Jeon et al., 2009). The results from these studies demonstrated the high effectiveness of iron-impregnated adsorbents to remove As.

Biochar can provide an excellent matrix to load iron due to its enormous surface area and high porosity (Li et al., 2016a; He et al., 2018). Other studies show that biochar in combination with oxides/hydroxides functional groups could effectively remove As in aqueous solution through chemical adsorption (Aredes et al., 2013; Zhang et al., 2013). The utilization of biochar derived from agricultural residues could serve as a practical option for groundwater treatment in developing countries due to its abundant local availability, low-cost, simple preparation, and environmental friendliness.

Pomelo (*Citrus maxima* or *Citrus grandis*) is the largest citrus fruit abundantly available in tropical countries, including Vietnam. With its high biomass, pomelo peel (30% by weight of the fruit, (Tocmo et al., 2020)) can cause environmental pollution when disposed of as waste (Liang et al., 2014; Wu et al., 2017). Pomelo peel is a promising biomass-derived adsorbent because of its high content of polysaccharides, including cellulose, pectin, and lignin, which provide many functional groups (Zhang et al., 2019; Tocmo et al., 2020). Pomelo peels have been reported to have effectively removed lead (Lim et al., 2019), cadmium (Saikaew et al., 2009), copper (Tasaso, 2014), and dyes by adsorption (Jayarajan et al., 2011; Zhang et al., 2019). However, their adsorption efficiency towards anionic species such as arsenate is expected to be poor because they possess negative surface charges which do not favour the adsorption of similarly charged anionic species.

According to Cheng et al. (2020), activated biochar adsorbent produced from pomelo peel provided a high specific surface area (up to 2457 m^2/g) and total pore volume (1.14 cm^3/g), which were responsible for the large adsorption capacity of tetracycline antibiotic. The large surface area and pore volume as well as the presence of organic functional groups in the biochar can also help to adsorb iron compounds. Li et al. (2016b) successfully coated Fe_3O_4 on the porous surface of biochar derived from spongy pomelo pericarp. In other studies, iron oxide particles coated biochar obtained from the pomelo peel were successfully prepared and used for removing organic compounds such as Reactive Red 21 (Nguyen et al., 2020d), chrome, phenol (Dong et al., 2021), and rhodamine B (Liu et al., 2019a). Results of these studies indicate the huge potential of using pomelo peel-derived biochar as an iron-coating adsorbent. However, to the best of

our knowledge, no study has yet been published on using this adsorbent to remove As or any other inorganic anionic pollutants from water. The novelties of the study presented in this paper are that a locally available agricultural waste (pomelo peel) was used to prepare an activated biochar of very high surface area and iron with high adsorption capacity to As was successfully impregnated onto this biochar. For the first time such an adsorbent was used to remove an inorganic As pollutant and its mechanisms of removal was studied. The results of this study are also expected to provide valuable information for possibly using this adsorbent in removing other inorganic anionic pollutants in water. The practicality of the study is that pomelo peel is a huge agricultural waste in Vietnam, where serious As problem exists. Therefore, use of this locally available waste to ameliorate the As pollution is very cost effective and an easily acceptable technology by the local people.

In this research, pomelo peel biochar coated with iron (PPCI) was synthesized via the slow pyrolysis carbonization process and then impregnated with iron. Detailed batch tests were conducted to evaluate the PPCI's adsorption performance towards both As(III) and As(V) ions. The adsorption mechanisms were explored using morphological, textural, surface functionality, and surface charge characteristics of PPCI before and after adsorption.

4.2. Materials and methods

4.2.1. Chemicals

Iron chloride hexahydrate ($FeCl_3.6H_2O$) was purchased from GHTech (Guangdong Guanghua Sci-Tech Co. Ltd). Stock As(III) or As(V) solutions of 1000 mg/L

were obtained by dissolving 1730 mg of sodium arsenite ($NaAsO_2$, from ACE Chemical Co.) or 4160 mg of sodium arsenate heptahydrate ($Na_2HAsO_4 \cdot 7H_2O$, from BDH Chemical Ltd.) in 1 L distilled water, respectively. Feed solutions of As(III) or As(V) at different concentrations (from 0.05 to 20 mg/L) were prepared by diluting the As(III) or As(V) stock solutions with distilled water. All chemicals used in this study were analytical grade.

4.2.2. Preparation of adsorbents

4.2.2.1. Original pomelo peels

Raw pomelo peels (PP) were collected from fresh pomelo fruits in a supermarket in Hanoi, Vietnam, and subsequently washed three times with tap water, followed by three times with deionized water to remove any impurities. The raw PP was then cut into small pieces (2.5–5 mm) and placed inside an oven at 70 °C for 48 h. The dried PP was finally crushed and sieved into particle sizes varying from 0.25 to 0.5 mm. They were then placed in sealed plastic bags before being employed in subsequent experiments.

4.2.2.2. Pomelo peel biochar production

In this study, biochar productions from PP at different pyrolysis temperatures (350, 550, and 650 ºC) were developed to determine the optimum temperature of production. Briefly, 100 g dried PP of size 0.25–0.5 mm was subjected to slow pyrolysis carbonization for 3 h in an oxygen-free muffle furnace at 350, 550, or 650 ºC, respectively. Following the pyrolysis process, the PP biochar formed in the heating process was washed several times with deionized water and then placed inside an oven at

70 ºC for 48 h. The resultant biochar productions at 350, 550, and 650 ºC of pyrolysis were labelled as PPC-350, PPC-550, and PPC-650, respectively.

A scanning test was conducted to compare the removal efficiency of PP raw and its biochar samples (developed at three different pyrolysis temperatures of 350, 550, and 600 ºC) with As(V) solution. The experiment was implemented with 1 g/L of adsorbent dose, 24 h, pH = 7.0, temperature 30 ºC, and initial As(V) concentration of 0.4 mg/L. The results (presented in more detail in **Section 4.3.1**) indicated that the removal efficiency of PPC-350 for As(V) in solution were 12.43%, which was not much different with that of PPC-500 (12.50%) and PPC-600 (14.30%). In fact, increasing pyrolysis temperature increased the energy consumption. Although PPC-350 exhibited a slightly lower adsorption capacity than that of PPC-550 and PPC-650, PPC-350 samples were selected for the subsequent iron coating process due to its low energy consumption and its environmental friendliness.

4.2.2.3. Pomelo peel's modification with iron

In this study, the biochar produced at 350 ºC (PPC-350) was selected for its modification with iron. A PPC-350 sample was firstly dried inside the oven then coated with iron according to the method described by Nguyen et al. (2020c). The procedure used was as follows: 50 g of PPC-350 was soaked into a 150 mL solution of 0.1 M $FeCl_3.6H_2O$. The pH of the resulting suspension was set at approximately 7.0 by dropwise addition of 2 M NaOH solution. The mixture was then agitated at 160 rpm for 48 h at 30 ºC. The solids were separated from the suspension and dried at 70 ºC for 48 h. Then the dried solids were rinsed with deionized water several times until the brown colour was removed. All residual fibrous material was dried further at 70 ºC for 24 h. To enhance the

level of iron grafting, the grafting process was repeated three times. The final iron-modified PPC-350 adsorbents after coating once, twice, and thrice with iron were labelled PPCI-1, PPCI-2, and PPCI-3 and stored in airtight containers. The preparation procedure for the adsorbents is illustrated in **Figure 4.1**.

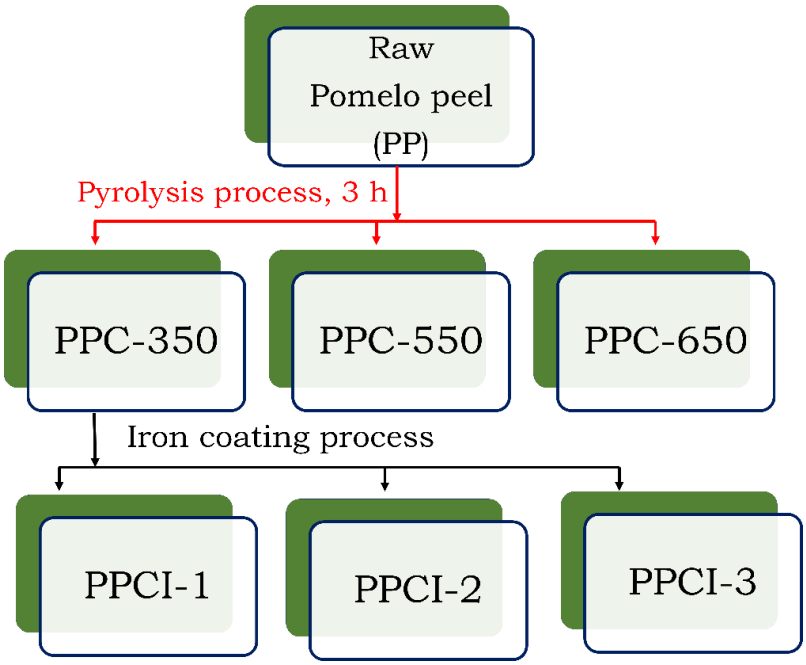

Figure 4.1. Schematic illustration of the preparation procedure of the adsorbents

4.2.3. Batch adsorption experiment

An initial adsorption test was conducted to identify the removal capacity of PP and its modified forms of adsorbents for removing As from synthetic water. The experimental conditions were similar to the scanning test described in **Section 4.2.2.2.** Approximately 0.1 g of adsorbent was added to 100 mL of As(V) solution in an Erlenmeyer flask. The initial As concentration was fixed at 0.4 mg/L. The flasks were sealed, and then placed on a mechanical shaker, and shaken at 160 rpm for 24 h at 30 ºC.

After the completion of the experiment, the samples were filtered through a 0.45 μm filter to analyse As(V) concentration in solution.

The equilibrium adsorption study was carried out by mixing either 0.5 g PP or 0.05 g PPCI with 50 mL of As(III) or As(V) solutions. The 100 mL flasks containing the mixed solutions were shaken for 24 h at 30 ^{o}C. The initial concentrations of As(III) and As(V) varied from 0.05 to 20 mg/L. Because the As contaminated natural surface and groundwater normally exist at neutral pH, the solution pH in the experiment was kept constant throughout the experiment at 7.0 ± 0.2 by monitoring the pH solution after 2–3 h and adjusting it to the initial value (pH ~ 7) by adding 0.1 M HNO_3 or 0.1 M NaOH.

The adsorption kinetics experiment was done by mixing 0.05 g PPCI with 50 mL of As(III) or As(V) solutions at initial concentrations of 0.5 mg/L and 1 mg/L, respectively. Samples were taken at 1, 10, 30, 60, 120, 240, 360, 480, 1200, and 1440 min intervals.

The influence of solution pH on As adsorption performance of PPCI was evaluated by changing the pH of the feed solution from 2.0 to 10.0. The adsorbent dosage was 1 g/L and the initial As(III) or As(V) concentration was 0.5 mg/L. The experimental procedure was similar to that used for the equilibrium adsorption experiment. The pHs of the experimental solutions were determined at the end of the experiment.

Sodium salts of five anions, including chloride (Cl^{-}), carbonate (CO_3^{2-}), monohydrogen phosphate (HPO_4^{2-}), sulphate (SO_4^{2-}), and silicate (SiO_3^{2-}) at concentrations of 10 mM and 100 mM were used to evaluate the effect of coexisting anions on As adsorption capacity of PPCI. As was added to all the solutions to create a

concentration of 0.5 mg As/L. The solutions' pH and temperature were kept at 7.0 and 30 °C, respectively.

In all experiments, the ratio of PPCI weight to As solution volume was 1 g to 1.0 L. At pre-determined times, samples of suspensions were withdrawn from the flask and immediately filtered through 0.45 μm filters to separate the solid and liquid components. The solid component was dried at 80 °C for 12 h and then examined for As-laden adsorbent features. The total As concentration in the liquid component (filtrate) was measured by Inductively coupled plasma mass spectrometry (ICPMS-NexION 2000, US). All tests were duplicated, and the mean data were displayed.

The amount of As adsorbed onto PP and PPCI at equilibrium, q_e (mg/g) and the amount of As uptake at time t, q_t (mg/g) were calculated using **Equations 3.1** and **3.2,** respectively, in **Section 3.2.3**.

Desorption experiments were conducted to determine the reversibility of the As adsorption process on PPCI. Firstly, about 1 g As-loaded PPCI was prepared by mixing 0.5 g PPCI with 500 mL solutions of As(III) or As(V) 0.5 mg/L during 24 hours. The NaOH solutions at different concentration of 0.1, 0.2, and 0.5M were used as desorbing agents. In this study, the flasks containing 0.025 L of different desorbing agents (V_2) and predetermined amount (approximately 0.025 g) of As loaded PPCI (m_2) were placed in a shaker and shaken at 160 rpm for 24 h. Afterwards, the solid and liquid parts were then separated from mixture solution by 0.45 μm syringe filters. The collected liquid was analysed to determine the total desorbed As concentration using ICPMS-NexION 2000, US. Meanwhile, the solid parts were dried in an oven at 80 °C for 12 h and then stored in tightly closed bags for re-adsorption experiment. The amount of As remained on PPCI

and the percentage of desorption were determine using **Equations 3.3** and **3.4,** respectively, in **Section 3.2.3**.

4.2.4. Characterization of adsorbents

The surface morphology and superficial main elements of PP and PPCI before and after adsorption were determined by Scanning electron microscope (SEM, Quanta-65, Thermo Fisher Scientific Inc., USA) and Energy dispersive spectroscopy (EDS), respectively. Their main surface functional groups were identified by Fourier transform infrared spectroscopy (FTIR; Nicolet iS5, Thermo Fisher Scientific Inc., USA) using their spectra in the 400 to 4000 cm^{-1} range. Their textural properties were analysed based on the physisorption isotherm of nitrogen at 77 ^{0}K (using NOVA touch 4LX, Anton Paar GmbH, Austria). Furthermore, the surface charge characteristics of adsorbents before and after adsorption were determined using the point of zero charge (pH at which the net surface charge is zero, pH_{PZC}) via the pH drift method. The procedure of this method has been mentioned in **Section 3.2.3**.

4.2.5. Column adsorption experiment

The column adsorption studies were conducted with both As(V) and As(III) solutions. In this experiment, two glass columns of 9 mm inner diameter and 0.09 m height were used. The experimental conditions in two columns were similar. Feed As(III) or As(V) solutions of 0.3 mg/L were pumped in an up-flow mode through the columns at a constant flow rate of 0.8 m/h by dosing pumps (Master flex L/S). The columns were packed with 1g of PPCI (corresponding to the bed height of 0.05 m and the EBCT of 4 min). 1.0 mm acrylic beads and cotton balls were placed at the bottom and top of the

column to prevent the release of the packed adsorbent. The fixed-bed adsorption tests were conducted continuously for 44 days and the samples were collected with an interval of 2 days until the As concentration in the effluent approached the influent concentration. The samples were filtered using 0.45 μm filters, and filtrates were analysed for As concentration by (ICPMS-NexION 2000, US).

4.3. Results and discussion

4.3.1. Comparison of As(V) adsorption capacity of pomelo peel and its modifications

The removal efficiency of As(V) by PP and its modifications is shown in **Figure 4.2**. Results show that removal efficiency of PP and its different modified adsorbents decreased in the order: PPCI-3 > PPCI-2 > PPCI-1 > PPC-650 > PPC-550 > PPC-350 > PP. Three PP's modification with iron adsorbents (PPCI-1, PPCI-2, PPCI-3) exhibited a remarkably higher adsorption capacity than that of PP and its biochar productions without iron (PPC-350, PPC-550, PPC-650). Additionally, the As(V) adsorption capacity of PP's modification with iron increased with the number of coatings. The removal efficiency of PPCI-3 for As(V) adsorption was 96.02% which is much higher compared to PPCI-2 (55.31%) and PPCI-1 (38.87%). A greater amount of Fe on the surface of adsorbent produced by three coating times had the highest removal capacity towards As(V). This trend is in line with that reported by Nguyen et al. (2020c). Thus, PPCI-3 was used in the subsequent experiments and with an alternative name as PPCI for more convenience.

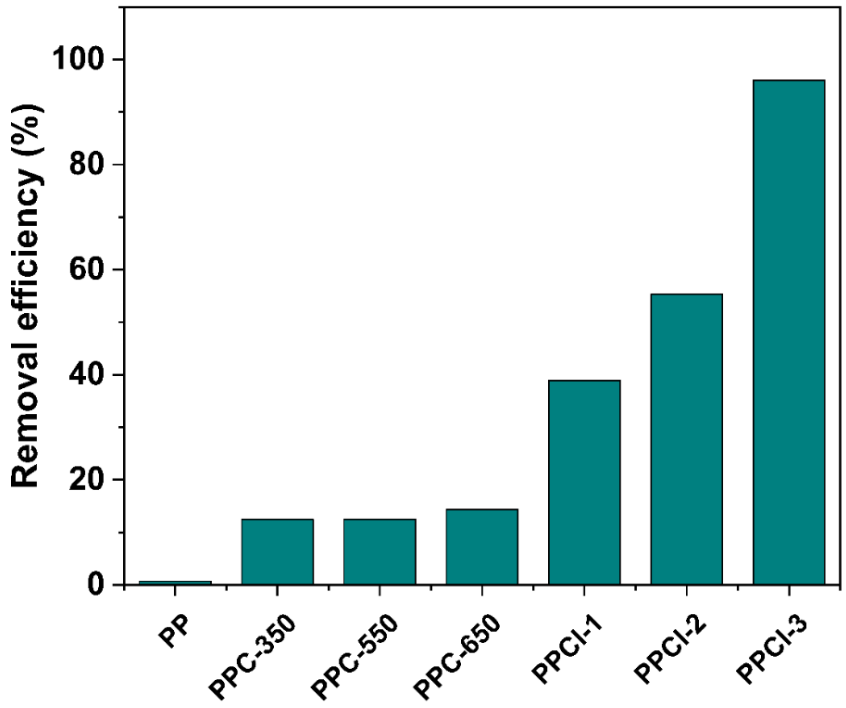

Figure 4.2. Removal efficiency of As(V) by PP and its modifications

4.3.2. Equilibrium adsorption isotherm

The isotherms for As(V) and As(III) adsorption by PP and PPCI are shown in **Figure 4.3**. The isotherm shapes of PPCI adsorbent are categorized as being L-shaped, suggesting that PPCI's surface has a strong affinity towards As(V) and As(III) ions at small concentrations, which then diminished as concentration increased. Three adsorption isotherm models, namely the Langmuir, Freundlich, and Redlich–Peterson models were applied to describe the adsorption data. Information on these models is presented in **Section 2.6.3.2**.

The high R^2 and low $\chi 2$ values (**Table 4.1**) indicate that the equilibrium adsorption data for both As(V) and As(III) adsorption on PP and PPCI very satisfactorily fitted to all

three adsorption models: Langmuir, Freundlich, and Redlich–Peterson. However, the data fits were slightly better with the Redlich–Peterson model, as demonstrated by the slightly greater coefficient of determination (R^2) values ≥ 0.98 (**Table 4.1**). As stated in **Table 4.1**, the maximum Langmuir adsorption capacity (Q_{max}) of modified PPCI towards As(V) and As(III) were 15.28 and 11.77 mg/g, respectively, which were extremely higher than those of the raw PP (Q_{max} = 0.034 mg/g for As(V) and Q_{max} = 0.033 mg/g for As(III)).

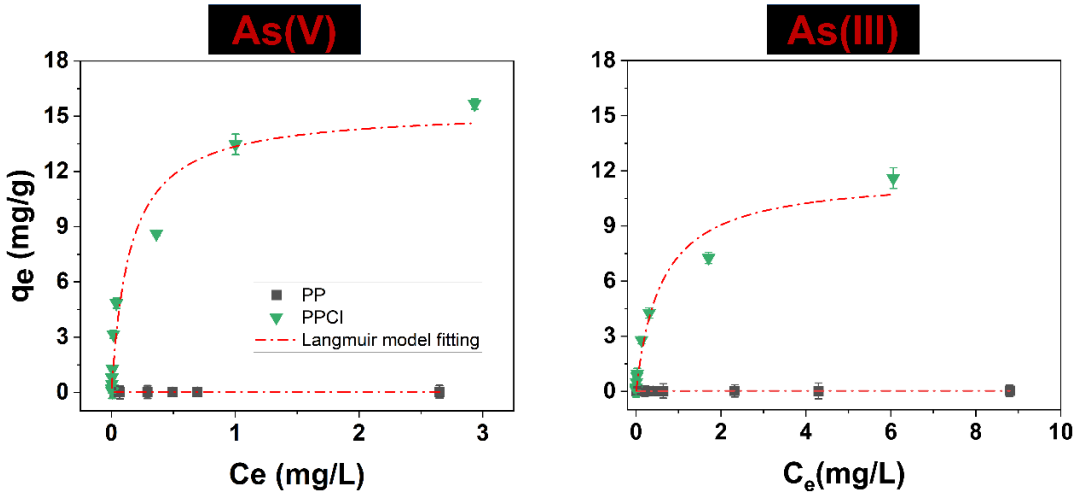

Figure 4.3. Adsorption isotherms for As(V) and As(III) removal by PP and PPCI

(experimental conditions: Co As(V) and As(III) = 0.05–20 mg/L, m/V = 1 g/L, t = 24 h, pH = 7 ± 0.2, temperature 30 oC)

The As adsorption performance of PPCI was compared to that of other adsorbents reported in the literature (**Table 4.2**). The modified PPCI material shows an excellent adsorption performance towards both As ions, as demonstrated by its superior adsorption capacity, compared to other adsorbents, including biomass-derived adsorbents (e.g. Luffa plant fibres (Nguyen et al., 2020c), iron oxy-hydroxides based biosorbents (e.g. Iron-

loaded walnut shell, Fe-modified corn straws, Fe-Luffa plant fibres) (Duan et al., 2017; Lin et al., 2017; Nguyen et al., 2020d), magnetic biochars (Tian et al., 2011; Cope et al., 2014; Kim et al., 2019), natural iron and manganese oxides minerals (Lenoble et al., 2004; Nguyen et al., 2020a; Nguyen et al., 2020b), activated carbon and its iron modified activated carbon adsorbents (Chang et al., 2010; Kalaruban et al., 2019), and iron coated zeolite adsorbents (Jiménez-Cedillo et al., 2011; Li et al., 2011; Pizarro et al., 2021).

Table 4.1. Adsorption isotherm model parameters for As(V) and As(III) removal by PP and PPCI

Adsorption parameters	Unit	PP		PPCI	
		As(V)	As(III)	As(V)	As(III)
1. Langmuir model					
Q_{max}	mg/g	0.034	0.033	15.28	11.77
K_L	L/mg	6.07	6.43	6.70	1.67
R^2	—	0.99	0.97	0.95	0.97
χ^2	—	1.81*10^-6	3.50*10^-6	1.60	0.50
2. Freundlich model					
K_F	$(mg/g)/(mg/L)^n$	0.03	0.0235	10.81	5.72
n_F	—	0.30	0.221	0.37	0.40
R^2	—	0.85	0.830	0.95	0.99
χ^2	—	2.36*10^-5	2.76*10^-5	1.43	0.19
3. Redlich–Peterson model					
K_{RP}	L/g	0.18	0.22	260.33	78.80
a_{RP}	$(mg/L)^{-g}$	4.90	6.69	20.70	11.54
g	—	1.00	0.99	0.78	0.70
R^2	—	0.98	0.98	0.98	0.99
χ^2	—	3.17*10^_6	4.06*10^-6	0.64	0.03

Note: R^2 is coefficient of determination and χ^2 is Chi-Square values

Table 4.2. Comparison of the Langmuir maximum adsorption capacity (Q_{max}) values of As(III) and As(V) for PPCI with values for other adsorbents reported in literature

Adsorbents	Adsorption condition					Q_{max} (mg/g)		Ref.
	m/V (g/L)	pH	T (°C)	t (h)	C_0 (mg/L)	As(V)	As(III)	
PP	1.0	7.0	30	24	0.05–20	**0.034**	**0.033**	**This study**
PPCI	1.0	7.0	30	24	0.05–20	**15.28**	**11.77**	**This study**
Natural laterite (NLTT)	7.5	7.0	25	24	0.1–25	**0.58**	**0.512**	**This study**
Luffa plant fibres	1–5	7	25	24	0.5	0.035		Nguyen et al. (2020c)
Iron-loaded walnut shell	1.0	7.0	30	24	0.1–5	—	1.24	Duan et al. (2017)
Fe-modified corn straws	1	7	—	—	0.2–50	8.25	—	Lin et al. (2017)

Adsorbents	Adsorption condition					Q_{max} (mg/g)		Ref.
	m/V (g/L)	pH	T (°C)	t (h)	C_o (mg/L)	As(V)	As(III)	
Fe-Luffa plant fibres (FLF-3)	0.003–0.07	7	25	24	0.5	2.55	—	Nguyen et al. (2020c)
Iron oxide amended rice husk char	0.4	6.9	—	—	0.1–2.5	—	1.46	Cope et al. (2014)
Fe-modified biochar beads	2.4	7.9	—	—	1–30	—	11.29	Kim et al. (2019)
Fe_3O_4 coated wheat straw	10	7	—	—	1–28	4.018	3.898	Tian et al. (2011)
VMO	2–14	7	25	24	0.5	0.11	-	
Fe-VMO	0.1–2.0	7	25	24	0.5	2.19	-	Nguyen et al. (2020b)
Mixed magnetite–maghemite nanoparticles	0.4	2	—	—	0.5–4	3.71	3.69	Chowdhury and Yanful (2010)

Adsorbents	Adsorption condition					Q_{max} (mg/g)		Ref.
	m/V (g/L)	pH	T (°C)	t (h)	C_0 (mg/L)	As(V)	As(III)	
GACs	0.1–0.8	6.0	25	24	0.1	—	1.01	Kalaruban et al. (2019)
GAC-Fe	0.1–0.8	6.0	25	24	0.1	—	1.43	
Fe-GACs	2.5	6.9	25	48	—	—	1.95	Chang et al. (2010)
Iron–manganese-modified zeolite-rich tuffs	10	6.5	18	24	0.05–2	0.06	0.10	Jiménez-Cedillo et al. (2011)
Fe-exchanged natural zeolite	20	—	—	24	0.1–20	0.10	0.05	Li et al. (2011)

4.3.3. Kinetic adsorption

Figure 4.4 presents the results of the experiments on the time-dependent adsorption of As(III) and As(V) ions by PPCI at two different initial As concentrations (0.5 mg/L and 1 mg/L). The adsorption rate of As(V) and As(III) onto PPCI was very rapid during the first 30 min of the experiment. Afterward, the adsorption process continued at a relatively slower rate until it reached a plateau and equilibrium after approximately 120 min. The initial fast adsorption is due to an ample amount of vacant adsorption sites on the PPCI surface at the initial stage, which shrank later on because the adsorption sites were progressively filled up. At a later stage, the remaining vacant surface sites are difficult to occupy due to repulsive forces occurring between the As species on the solid and bulk phases, and therefore the rate of adsorption dropped (Yao et al., 2014). Three common kinetic models, pseudo-first-order (PFO), pseudo-second-order (PSO), and Elovich models, were employed to describe the experimental data. The information on the non-linearized form of the three models is provided in **Section 2.6.3.1**.

The relevant kinetic model parameters for the As adsorption onto PPCI at two initial As concentrations are presented in **Table 4.3**. The PSO model with a high coefficient of determination value ($R^2 = 0.99$) and low Chi-square value ($\chi 2$ = 0.0001–0.001) described the kinetic adsorption data better than the PFO ($R^2 = 0.96$–0.97 and $\chi^2 =$ 0.0006–0.0029) and Elovich ($R^2 = 0.916$–0.950 and $\chi^2 < 0.004$) models. Others have reported that because the PSO model fitted adsorption of As on iron hydroxide/oxides better than PFO model the mechanism of As adsorption is probably chemical, presumably mediated by inner-sphere complexation of the As species with iron hydroxide/oxides (Hao et al., 2018; Kalaruban et al., 2019; Nguyen et al., 2020c). This interpretation is

consistent with that made from the point of zero charge data discussed later (**Section 4.3.7.3**) where As adsorption reduced the point of zero charge of PPCI and this was explained as due to chemical adsorption of As. Kalaruban et al. (2019) reported that the kinetics of As adsorption on granulated AC (GAC) were explained better by PFO, but when iron was coated on GAC the kinetic data fitted better to PSO. Based on these results, they reported that the adsorption on GAC was mostly physical whereas that on iron-coated GAC was chemical.

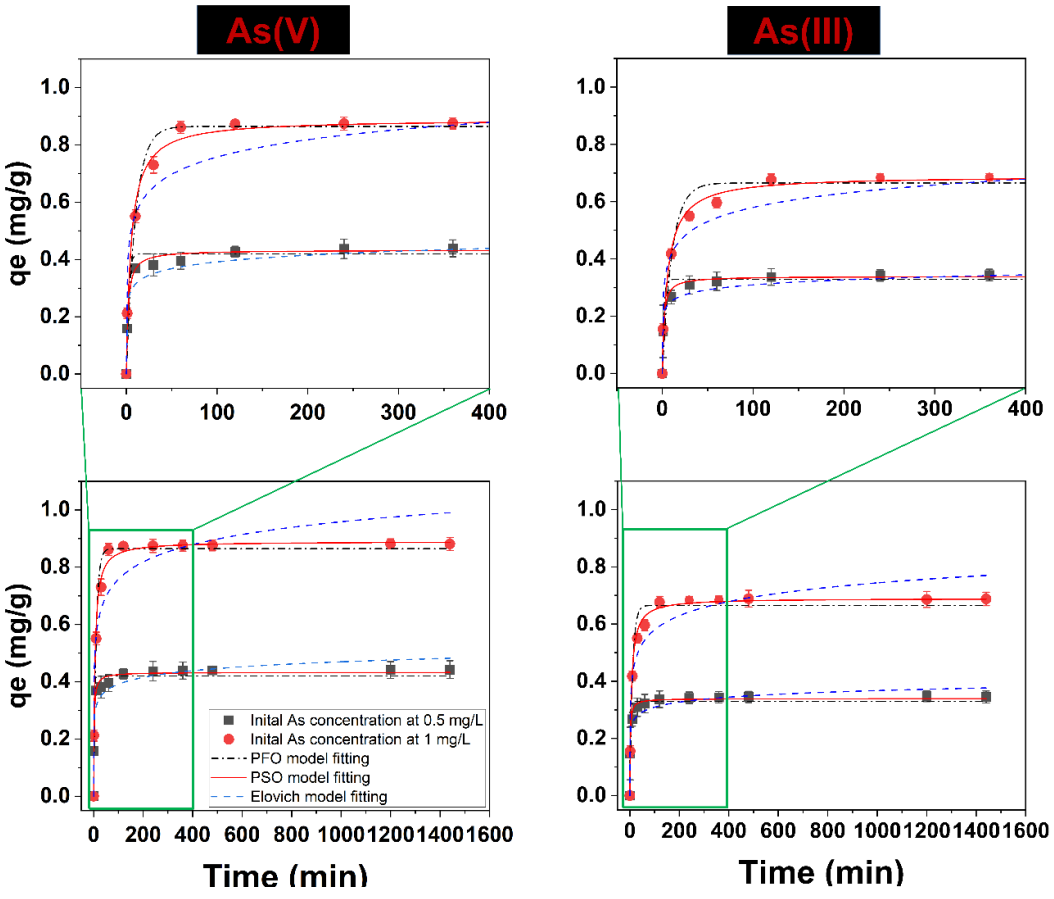

Figure 4.4. Adsorption kinetics for As(V) and As(III) adsorption onto PPCI (experimental conditions: Co As(V) and As(III) = 0.5 and 1 mg/L, m/V = 1 g/L, pH = 7 ± 0.2)

As shown in **Table 4.3**, there is a remarkable decrease in the PSO adsorption rate constant (k_2) value when the initial concentrations of As(III) and As(V) increased from 0.5 mg/L to 1 mg/L. At higher initial As concentration, there was greater competition for adsorption than at lower concentrations and this might have reduced the adsorption rate. A similar finding was documented by Yao et al. (2014).

Table 4.3. Kinetic model parameters for As(V) and As(III) uptake by PPCI

	Unit	Adsorbate			
		As(V)		As(III)	
		Co=0.5 mg/L	Co=1 mg/L	Co=0.5 mg/L	Co=1 mg/L
PFO model					
q_e	mg/g	0.420	0.865	0.329	0.665
k_1	1/min	0.444	0.100	0.573	0.093
R^2	—	0.969	0.972	0.955	0.962
χ^2	—	0.0007	0.0029	0.0006	0.0024
PSO model					
q_e	mg/g	0.433	0.890	0.339	0.689
k_2	g/(mg×min)	1.254	0.222	1.864	0.238
R^2	—	0.991	0.990	0.988	0.990
χ^2	—	0.0002	0.0010	0.0001	0.0006
Elovich model					
α	mg/(g×min)	35.083	5.164	57.415	2.420
β	mg/g	29.493	11.465	39.874	14.023
R^2	—	0.931	0.916	0.950	0.938
χ^2	—	0.0016	0.0091	0.0006	0.0040

4.3.4. Influence of solution pH on the adsorption of As ions and the stability of PPCI

The effect of solution pH (2.0–10) on the adsorption of As(III) and As(V) by PPCI is presented in **Figure 4.5.** The capacity of PPCI to adsorb As(III) and As(V) was insignificantly controlled by the pH within the 2.0 to 10 range. The efficiency of PPCI in adsorbing As(V) fell slightly when the pH solution rose from 2.0 to 10. In contrast, there was a minor increase in the adsorption capacity of As(III) by PPCI at low and high pHs.

In fact, within the pH solution range from 2 to 10, two anionic forms of As(V) tended to predominate, including monovalent $H_2AsO_4^-$ (pH= 3.0–6.0) and divalent $HAsO_4^{2-}$ (pH = 7.0–10) (Smedley and Kinniburgh, 2002). PPCI possessed a pH_{PZC} of 7.3, suggesting that the PPCI surface was positively charged at solution pH lower than 7.3 (detailed information on pH_{PZC} is presented in **Section 4.3.7.3**). Thus, at pH lower than 7.3, significant amounts of As(V) anions were probably removed by PPCI through electrostatic attraction (outer-sphere complexation). When pH was higher than 7.3, both the adsorbent and adsorbate had negative charges, and therefore the adsorption process is unlikely to occur through electrostatic attraction. Other adsorption mechanisms, namely inner-sphere complexation by ligand exchange (Hao et al., 2018; Kalaruban et al., 2019), and hydrogen bonding (Yee et al., 2019) might have largely operated in removing As(V) in the solution.

In the case of arsenite (As(III)), within the pH range of 1.0 to 9.0, only the uncharged form of As(III) ($H_3AsO_3^o$) is present (Smedley and Kinniburgh, 2002; Mondal et al., 2007). Thus, PPCI could not remove the uncharged $H_3AsO_3^o$ through the electrostatic attraction mechanism. **Figure 4.5** shows that the removal efficiency of PPCI towards As(III) was slightly lower than that of As(V). However, more than 82% of As(III) was removed. The significant amount of As(III) removal is possibly due to other

mechanisms of adsorption, such as hydrogen bonding (between oxygen in As(III) species and hydrogen in hydroxide group in biochar) (Yee et al., 2019).

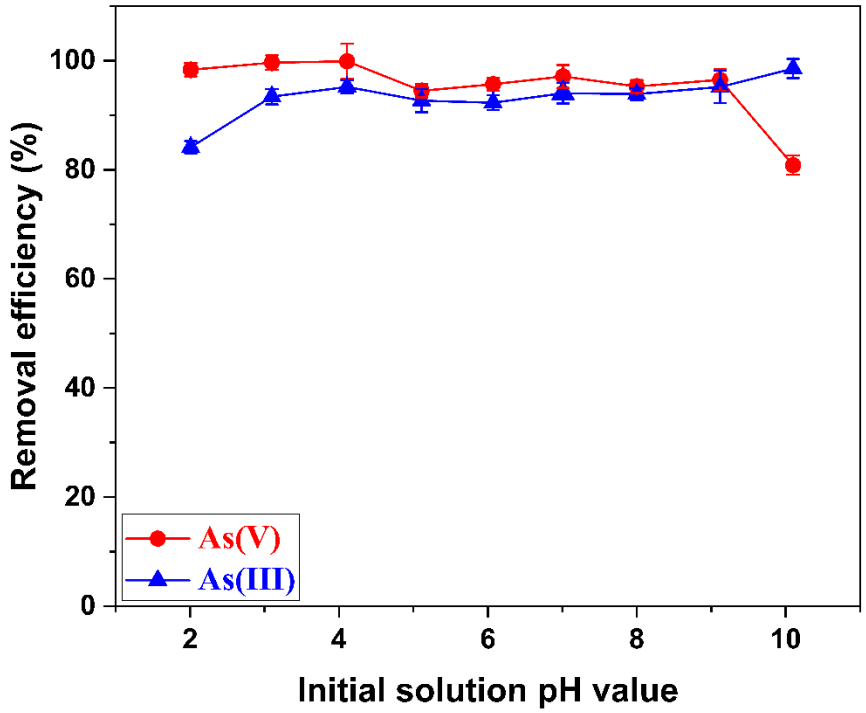

Figure 4.5. Effect of pH solution on the adsorption capacity of PPCI towards As(V) and As(III)

(experimental conditions: Co As(V) and As(III) = 0.5 mg/L, m/V = 1 g/L, t = 24 h)

4.3.5. Influence of coexisting single and mixed anions on As(III) and As(V) adsorption

To evaluate the influence of the presence of coexisting anions on As removal of PPCI, five anions (Cl^-, SO_4^{2-}, CO_3^{2-}, SiO_3^{2-}, and HPO_4^{2-}) were tested at two concentrations, these being 10 mM and 100 mM. These anions were mixed with As ions individually or in combination. **Figure 4.6** shows that the presence of coexisting anions

caused a remarkable reduction in the efficiency of removing As(III) and As(V). The adsorption capacity of PPCI towards both As(III) and As(V) decreased in the order, chloride (Cl^-) > sulphate (SO_4^{2-}) > carbonate (CO_3^{2-}) > silicate (SiO_3^{2-}) > monohydrogen phosphate (HPO_4^{2-}) > the five anions in combination (Cl^-, SO_4^{2-}, CO_3^{2-}, SiO_3^{2-}, and HPO_4^{2-}). As shown in **Figure 4.6**, the presence of HPO_4^{2-} had the greatest single anion influence on PPCI's efficiency in removing both As(III) and As(V). The similar tetrahedral structures of As(V) and HPO_4^{2-} and the presence of As and P in the same group in the periodic table (therefore, similar chemical properties) is probably the reason for the strong competition of HPO_4^{2-} with As ions in the adsorption process.

These ions have been reported to be chemically adsorbed by inner-sphere complexation usually involving the ligand exchange mechanism (adsorbent surface OH groups exchanging with As and monohydrogen phosphate anions) by Fe-based adsorbents (Loganathan et al., 2014; Hao et al., 2018; Kalaruban et al., 2019; Nguyen et al., 2020d). In contrast, the As removal efficiency by PPCI adsorbent was insignificantly affected by Cl^- in the solution. This is because the Cl^- is monovalent, possesses poorer ionic potential, lacks a tetrahedral structure, and adsorbed on adsorbents by physical processes (outer-sphere complexation/electrostatic forces). These results are consequently consistent with the results of other studies (Loganathan et al., 2014; Yao et al., 2014; Hongtao et al., 2018; Foroutan et al., 2019; Nguyen et al., 2020a).

The competition of coexisting single and mixed anions with As(V) adsorption was slightly stronger than that with As(III) adsorption. This is partly because As(V) ions are present as anions at pH 7, and this means they compete more with coexisting anions compared to As(III) which is present as uncharged $H_3AsO_3^{\circ}$.

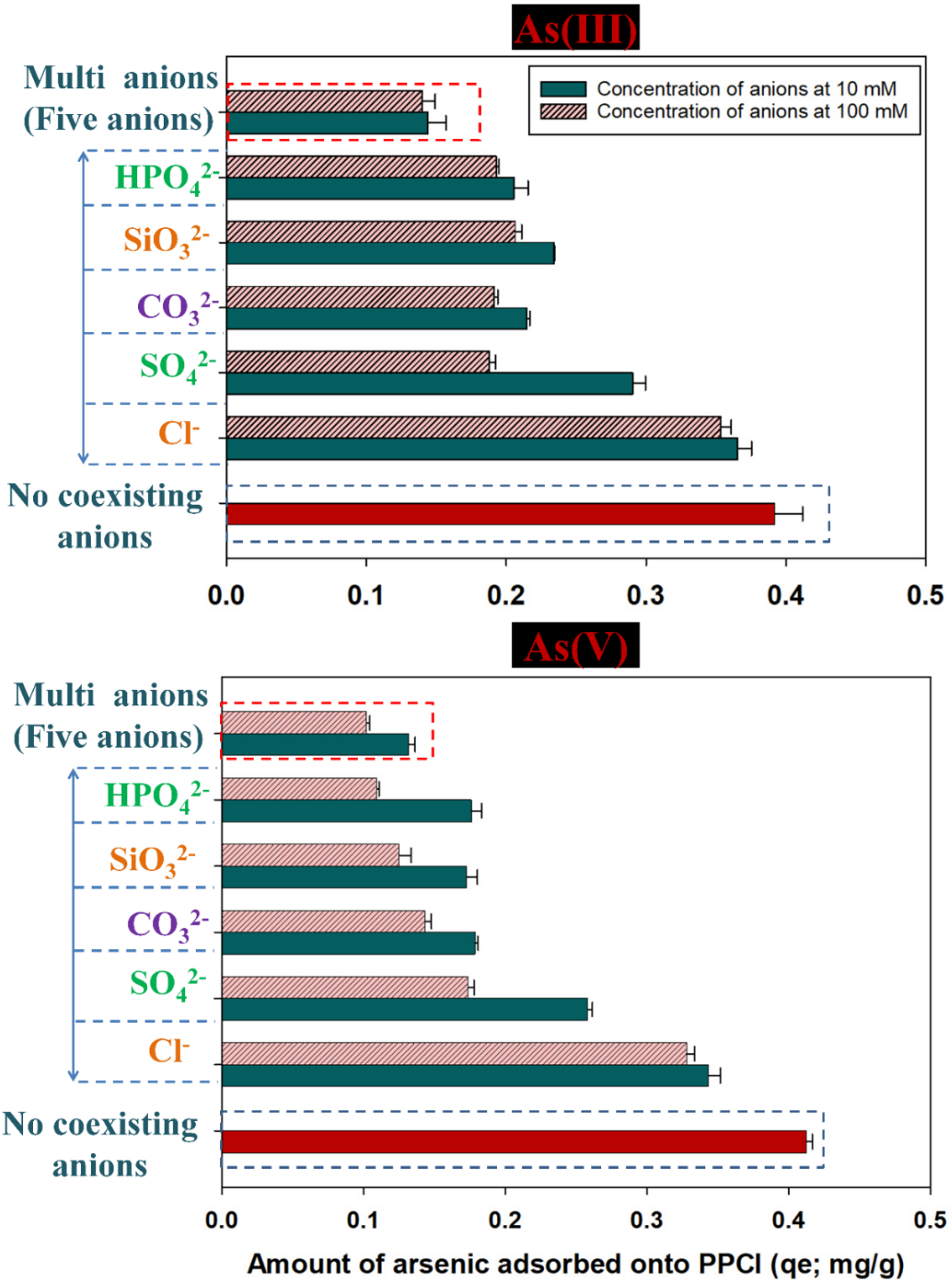

Figure 4.6. Influence of coexisting anions (at two initial concentrations of 10 mM and 100 mM) on the adsorption capacity of PPCI towards As(V) and As(III) ions

(experimental conditions: Co As(V)/As(III) = 0.05 mg/L, m/V = 1 g/L, t = 24 h, pH = 7 ± 0.2)

4.3.6. Desorption and reusability study

To explore the reusability of PPCI adsorbent, the desorption of As(V) and As(III) ions from the As - laden PPCI samples was investigated. NaOH solutions at three different concentrations of 0.1, 0.2, and 0.5 M were used as desorbing agents. The amount of As adsorbed into PPCI could be desorbed from exhausted PPCI by NaOH because of ion exchange between OH^- from NaOH solution with As ion in the As laden adsorbent (Patel, 2021). As shown in **Figure 4.7a**, the results indicate that increasing the NaOH concentration led to an increase in desorption efficiency. A similar trend was reported by Yang et al. (2014). For PPCI, the highest desorption efficiencies of both As(III) and As(V) were 57.82 % and 65.48%, respectively, which was observed when using desorbing agent of 0.5 M NaOH. The desorption efficiency of As - laden PPCI adsorbents after the As(III) adsorption process is slightly higher than that after As(V) adsorption process (**Figure 4.7a**).

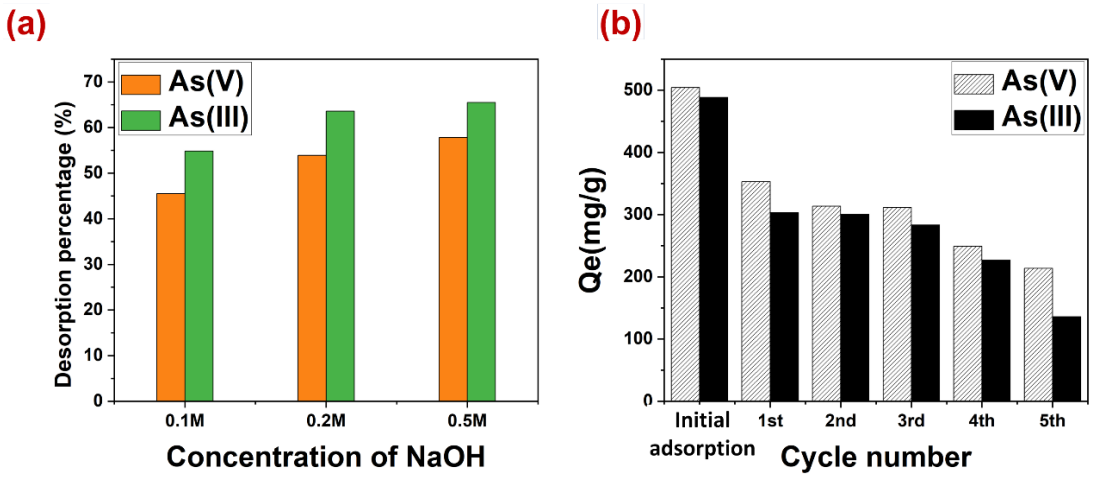

Figure 4.7. (a) Effect of NaOH concentration on desorption efficiency of As-laden PPCI after As(III) and As(V) adsorption; (b) Adsorption tests with regenerated PPCI

The adsorption capacities of regenerated PPCI after 5 regeneration cycles with As(V) and As(III) are presented in **Figure 4.7b**. Clearly, the adsorption capacity of PPCI for both As(V) and As(III) ions gradually diminished when the number of regeneration cycles rose. After five regeneration cycles, the adsorption capacity of PPCI remarkably dropped from 0.504 mg/g to 0.213 mg/g for As(V) adsorption and from 0.488 mg/g to 0.135 mg/g for As(III) adsorption. This corresponded to a substantial decrease to 42% and 28%, respectively. A similar trend was reported by previous studies such as Lin et al. (2012) who reported that the adsorption capacity of magnetic Fe_2O_3 nanoparticles partly decreased from 95.19 mg/g to 57.00 mg/g in removing As(V) and from 64.33 mg/g to 25.00 mg/g in removing As(III) ions. Elsewhere, Kundu and Gupta (2006) indicated that the adsorption capacity of regenerated IOCC adsorbent declined when the number of regeneration cycle increased.

4.3.7. Physico-chemical properties of adsorbent

4.3.7.1. Morphology and surface elemental composition (EDS)

The surface morphologies of raw PP and pristine PPCI are presented in **Figure 4.8**. The raw PP possessed a highly porous structure with a smooth surface, suggesting that it exhibits a large surface area. The heterogeneous surface is due to the aggregation/agglomeration of iron particles and their extensive uneven distribution on the PPCI surfaces. Most of the micropores and ultra-micropores of PPCI adsorbent were blocked or clogged by iron particles, leading to a shrinkage in surface area and pore volume of PPCI. This explanation is supported by textural properties data presented in the next section (**Section 4.3.7.2**). The As(III) and As(V)-laden PPCI also possessed a

wrinkled, irregular, and heterogeneous surface morphology, which did not differ much from that of PPCI before adsorption (**Figure 4.8**).

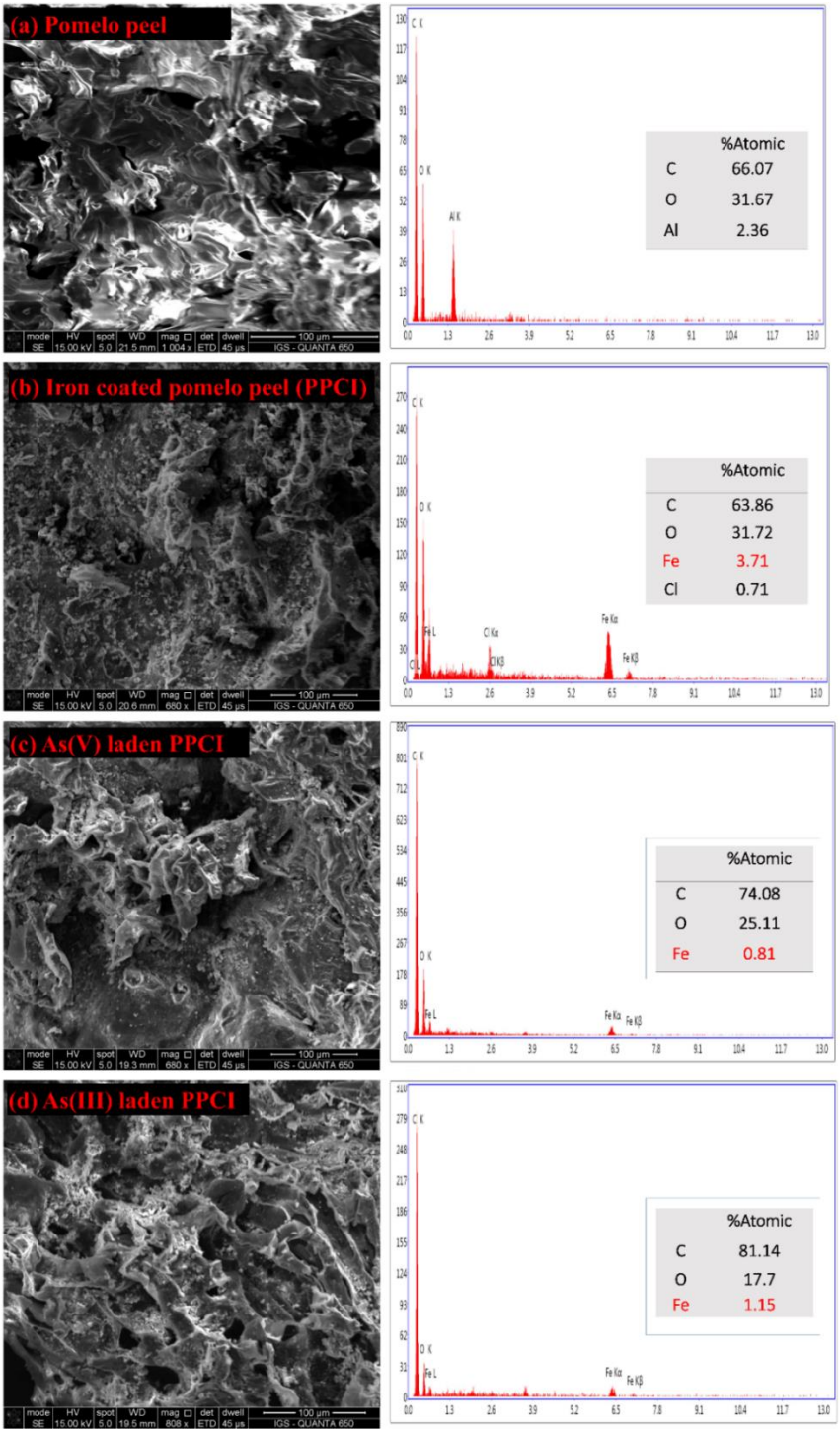

Figure 4.8. SEM-EDS data of (a) raw PP, (b) pristine PPCI, (c) As(V) - laden PPCI, and (d) As(III) - laden PPCI

In addition to morphology, element analysis (EDS) of the adsorbent surfaces was conducted (**Figure 4.8**). The results indicate that C is a predominant element in both PP and PPCI adsorbents (atomic percentage of 66.07% and 63.86%, respectively), reflecting the composition of pomelo peel biochar. PPCI possessed a small amount of Fe (3.71% in atomic composition, corresponding to 13.75% in total weight), suggesting that the iron was successfully incorporated onto PPCI during its synthesis. The original PP before incorporation of Fe contained no detectable amount of Fe.

4.3.7.2. Texture

The isotherm graphs of N_2 adsorption at 77 ^oK of PP and PPCI adsorbents are shown in **Figure 4.9.** Based on the IUPAC technical report by Thommes et al. (2015), N_2 adsorption and desorption isotherms of PP adsorbent are classified as II type with an H3 type hysteresis loop (relative pressure of p/p0 > 0.8). These results suggest that PP is a porous adsorbent. The N_2 adsorption and desorption graph for PPCI samples exhibited two things: a IV type physisorption isotherm and H3 type hysteresis loop. For this reason, it is expected that the PPCI adsorbent is mesoporous and this conclusion is consistent with what Coville and Tshavhungwe (2010) reported.

Table 4.4 presents the surface area (S_{BET}; determined from the Brunauter-Emmett-Teller and total pore volume (V_{total}; calculated from the BJH) of the adsorbents using the N_2 adsorption data. PP exhibited a S_{BET} of 48.65 m^2/g and a total pore volume of 0.13 cm^3/g, which were remarkably higher than those of PPCI (5.43 m^2/g and 0.0289 cm^3/g, respectively). A notable reduction in surface areas and pore volume of PPCI was probably due to iron particles and their aggregates dispersing widely on its surface and closely blocking most of its macropores and micropores. These results demonstrate that the

blockage process or pore filling of iron oxides inside the carbon matrix leads to remarkably increasing of the iron oxide content in PPCI. Other researchers also reported that a reduction in surface area and pore volume of adsorbent can occur after the iron-impregnation process. According to Kalaruban et al. (2019), BET surface and pore volume of the modified GAC-Fe were 876 m^2/g and 0.60 cm^3/g, which were much lower than that of GAC (1124 m^2/g and 0.62 cm^3/g). The surface area and pore volumes of As(V) and As(III)-laden adsorbents were not much different from those of PPCP before adsorption (As(V), 4.72 m^2/g and 0.0295 cm^3/g, respectively; As(III), 3.20 m^2/g and 0.0354 cm^3/g, respectively), which implies that the pores are still blocked, this time probably by Fe/As reaction products formed after adsorption.

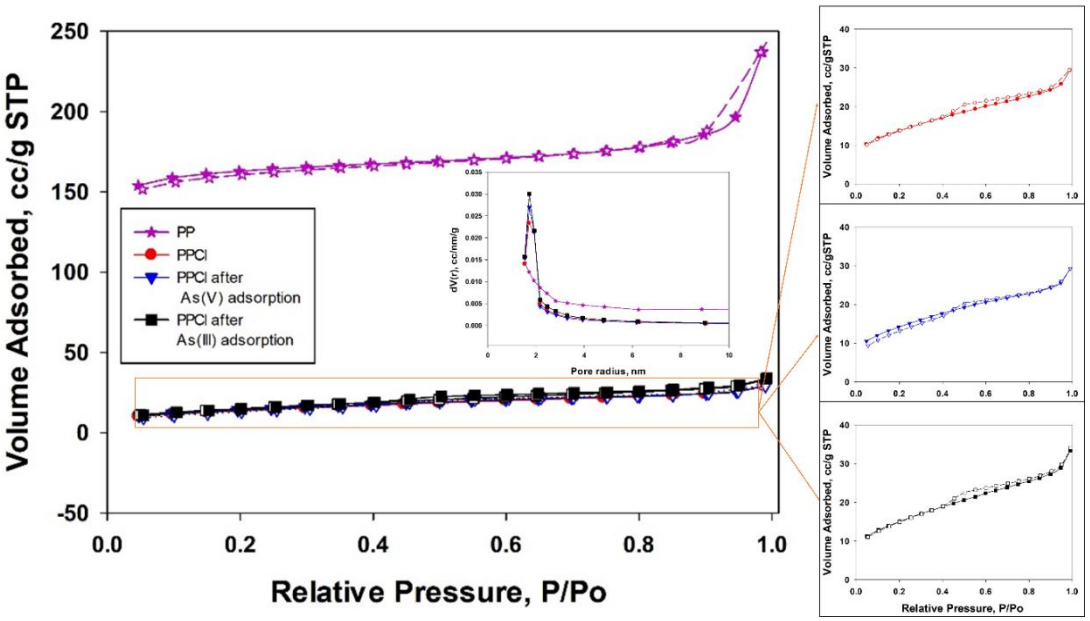

Figure 4.9. Nitrogen adsorption and desorption isotherms of raw PP, pristine PPCI and As-laden PPCI

Table 4.4. Physical properties of adsorbents

Adsorbents	BET surface area	Pore volume	Pore radius
	m^2/g	cm^3/g	nm
PP	48.65	0.13	1.53
PPCI	5.43	0.0289	1.709
PPCI after As(V) adsorption	4.72	0.0295	1.726
PPCI after As(III) adsorption	3.20	0.0354	1.721

4.3.7.3. Point of zero charge (pH_{PZC})

The point of zero charge (pH_{PZC}) of raw PP and PPCI before and after As adsorption was determined by the pH drift method. As shown in **Figure 4.10**, pH_{PZC} of the raw PP material was 4.8. This result agrees with the pH_{PZC} for other biomass-derived adsorbents such as raw orange peel (pH_{PZC} = 5.3) (Tran et al., 2016), and *Nauclea diderrichii* seed (pH_{PZC} = 4.9) (Omorogie et al., 2016). The PPCI had a pH_{PZC} of 7.3, which was significantly higher than that of raw PP. The higher pH_{PZC} of PPCI was caused by the iron-coating process where the impregnation of positively charged Fe caused increased positive charges on PPCI surface and therefore raised the pH at which the net surface charge is zero (pH_{PZC}). A similar increase was reported in a previous study on iron modified rice straw biochar, where the pH_{PZC} of raw rice straw biochar (BC) increased from 5.44 to 6.88 when Fe was incorporated into BC (Nham et al., 2019). Thus, the external surface of PPCI exhibited some positive charges in this study where the solution

pH value was maintained at 7. Therefore, PPCI could remove As(V) anions from solution through electrostatic attraction mechanism.

The pH_{PZC} values decreased from 7.3 to 5.8 and 5.4 after As(V) and As(III) adsorption, respectively as shown in **Figure 4.10**. This decrease in pH_{PZC} values suggests that both these As ions have reacted with PPCI by inner-sphere complexation adding negative charges to PPCI surface, thereby decreasing the pH at which the net surface charge became zero (pH_{PZC}). Decreases in pH_{PZC} after As adsorption were also reported for other Fe-based adsorbents (Faria et al., 2014; Pereira et al., 2019).

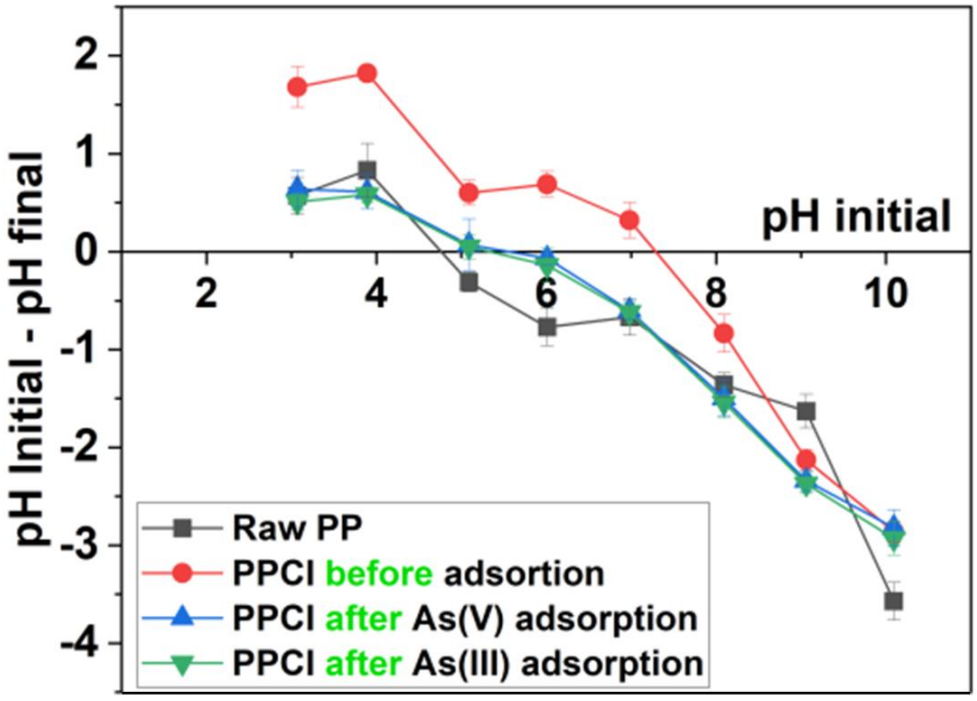

Figure 4.10. pH_{PZC} values of raw PP (pH_{PZC} = 4.8), pristine PPCI (pH_{PZC} = 7.3), PPCI after adsorption of As(V) (pH_{PZC} = 5.8), and PPCI after adsorption of As(III) (pH_{PZC} = 5.4)

4.3.7.4. Surface functionality

The main functional groups on adsorbents' surface were determined by the FTIR technique (**Figure 4.11**). The FTIR spectrum of raw PP (purple solid line) is presented in **Figure 4.11a**. The highlighted broad spectra band located at the peak around of 3390 cm^{-1} (corresponding to the presence of –OH groups) show the stretching vibrations of –OH group presented in adsorbed water (Oliveira et al., 2009; Nguyen et al., 2020a). The narrower peak at approximately 2930 cm^{-1} is attributed to the –CH stretching bond, which means $–CH_2$ and –CH groups are present (Oliveira et al., 2009). Two small spectral bands at 1738 cm^{-1} and 1417 cm^{-1} are assigned to the stretching of C=O and COO–, respectively, which were probably from carboxylic acids, esters, and anhydrides. A sharp peak at 1633 cm^{-1} is attributed to C=C surface functional groups (Tomul et al., 2020). The peak for the stretching vibration of C–O bonds could be seen at 1054 cm^{-1}. The peaks at around 618 cm^{-1} are ascribed to C–C bond (El-Naggar et al., 2020).

The FTIR spectrum of pristine and As-laden PPCI samples still exhibited several typical functional groups as in PP after the modification and adsorption process (**Figure 4.11b**). Some important functional groups on the pristine PPCI and As-laden PPCI's surface were well identified at several corresponding peaks at approximately 1630 cm^{-1} (C=C) and 1054 cm^{-1} (C–O). The broad spectra bands in the region between 3800 and 3000 cm^{-1} could be attributed to the –OH stretching vibration. The –CH stretching is detected at a broad band of 2800–2929 cm^{-1}. A peak, although small at 1737 cm^{-1} is attributed to C=O bond, which was quite hardly visible on the surface of pristine PPCI adsorbent. Particularly, the broad spectral band at around 500 cm^{-1} (including three small peaks at 445.17, 486.18, and 513.32 cm^{-1}) was assigned to the Fe–O groups (Baig et al., 2016; Chaudhry et al., 2017), which was well observed on pristine PPCI's surface but not

observed in raw PP. This result indicates that the iron grafting process on PPCI adsorbent was successful, and it is also supported by SEM results, as well as elemental analysis data (EDS) (**Section 4.3.7.1**). In addition, after As(V)/As(III) adsorption process, Fe–O groups were found to be absent on the surface of As-laden adsorbents, probably because Fe has reacted with As by breaking the Fe–O bond (**Figure 4.11b**).

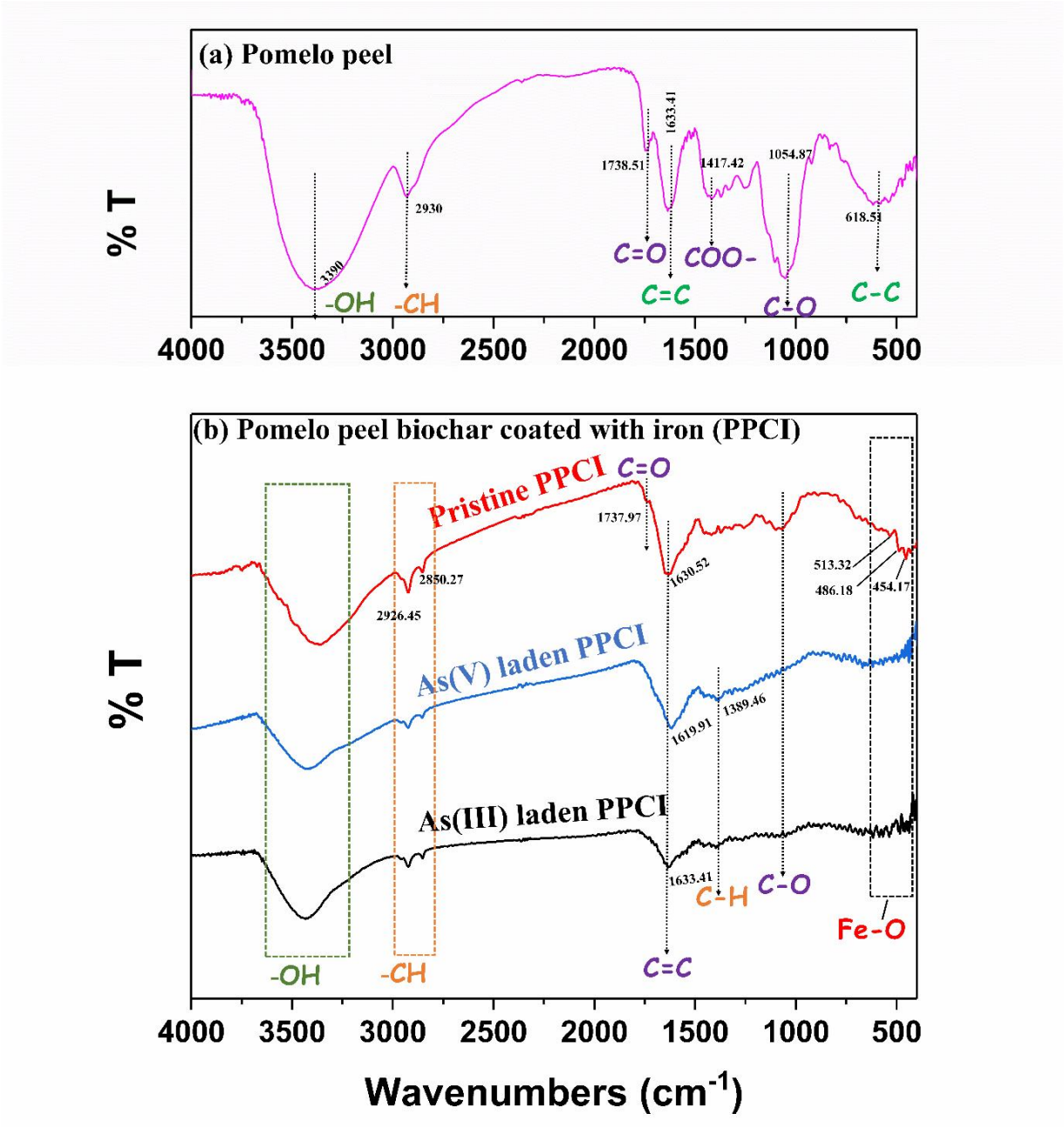

Figure 4.11. FTIR spectrum of (a) raw PP and (b) pristine and As-laden PPCI

4.3.8. Adsorption mechanisms

Generally, the possible mechanisms of As adsorption by iron-coated biochar includes a number of interactions. The S_{BET} of PPCI (5.43 m^2/g) is remarkably lower than that of typical commercial activated carbon (CAC) (>1000 m^2/g) (Lee et al., 2007), modified activated carbon (388 to 1747 m^2/g) (Arcibar-Orozco et al., 2014). Thus, the contribution of pore filling mechanism in removing As by PPCI from water is not important as other mechanisms, such as electrostatic attraction. The value of pH_{PZC} of PPCI (**Section 4.3.7.3**) prior to and after adsorption process suggest that electrostatic adsorption (outer-sphere complexation) probably occurred because the pH_{PZC} (pH 7.3) of PPCI was slightly higher than pH of the experimental solution (pH 7). Similar findings were reported elsewhere (Amen et al., 2020; Dixit and Hering, 2003; Samsuri et al., 2013; Vithanage et al., 2017; Yee et al., 2019).

Hydrogen bonding mechanism is considered as a predominant interaction between As and certain adsorbents. The main common feature of those adsorbents is that they possess abundant oxygen and hydrogen-containing functional groups in their surfaces. In this study, FTIR results also indicate that there was a remarkable number of oxygen and hydrogen-bearing functional groups (C–O, –OH, C=O) in pristine PPCI. These could be responsible for H-bonding with the hydrogen and oxygen atoms in As(III)/As(V) ions in solution. This explanation agrees with what has been intensively reported in several studies (Khatamian et al., 2017; Verma and Singh, 2019; Vithanage et al., 2017).

According to Vithanage et al. (2017), the iron-coating on the iron-coated biochar was present in the form of iron oxides largely as magnetite and hematite. Both the reduced form (Fe^{2+}) and the oxidized form (Fe^{3+}) of iron dominated the iron-coated biochar

adsorbents. These iron oxides could oxidize the more toxic As(III) ion into less toxic As(V) ion. The As(III) and oxidized As(V) were then probably chemically adsorbed on iron oxides by the inner-sphere complexation mechanism.

The possible inner-sphere complexation mechanisms of As(III) and As(V) adsorption on the iron-coated biochar are described by **Equations 4.1–4.5** given below:

For As(III) ions:

$$\text{Biochar - FeOH}_{(solid)} + \text{AsO}_3^{3-}{}_{(aqueous)} + 3\text{H}^+{}_{(aqueous)} \leftrightarrow \text{Biochar - FeH}_2\text{AsO}_{3(solid)} + \text{H}_2\text{O}_{(liquid)} \quad \textbf{(4.1)}$$

$$\text{Biochar - FeOH}_{(solid)} + \text{AsO}_3^{3-}{}_{(aqueous)} + 2\text{H}^+{}_{(aqueous)} \leftrightarrow \text{Biochar - FeHAsO}_3^-{}_{(solid)} + \text{H}_2\text{O}_{(liquid)} \quad \textbf{(4.2)}$$

For As(V) ions:

$$\text{Biochar - FeOH}_{(solid)} + \text{AsO}_4^{3-}{}_{(aqueous)} + 3\text{H}^+{}_{(aqueous)} \leftrightarrow \text{Biochar - FeH}_2\text{AsO}_{4\,(solid)} + \text{H}_2\text{O}_{(liquid)} \quad \textbf{(4.3)}$$

$$\text{Biochar - FeOH}_{(solid)} + \text{AsO}_4^{3-}{}_{(aqueous)} + 2\text{H}^+{}_{(aqueous)} \leftrightarrow \text{Biochar - FeHAsO}_4^-{}_{(solid)} + \text{H}_2\text{O}_{(liquid)} \quad \textbf{(4.4)}$$

$$\text{Biochar - FeOH}_{(solid)} + \text{AsO}_4^{3-}{}_{(aqueous)} + \text{H}^+{}_{(aqueous)} \leftrightarrow \text{Biochar - FeAsO}_4^{2-}{}_{(solid)} + \text{H}_2\text{O}_{(liquid)} \quad \textbf{(4.5)}$$

The chemical adsorption of As ions by inner-sphere complexation is supported by the reduction in pH_{PZC} observed when these ions were adsorbed (discussed in **Section 4.3.7.3**).

4.3.9. Column adsorption of As(V) and As(III)

The adsorption capacity of PPCI toward As(V) and As(III) ions in dynamic condition was investigated through the continuous fixed bed column. **Figure 4.12** shows the breakthrough curves of the As(V) and As(III) adsorption**.** The breakthrough curves were classified as having an "S shape" in both different As adsorption columns. The breakthrough curves of PPCI for As(III) ions were steeper than that of As(V) ions and the saturation time of PPCI for As(V) ions was 1056 h which was longer than that of As(III) (888 h). This is due to the higher adsorption capacity of PPCI for As(V). The column

could treat up to 3,840 bed volumes for As(V) solution of 0.3 mg/L mg/L and 1,536 bed volumes for As(III) solution of 0.3 mg/L to below WHO guidelines.

The Thomas model (Thomas, 1944) is one of the most widely used models to apply and describe the column performance and predict the breakthrough curves of the adsorption process (Nguyen et al., 2020c). The nonlinear form of the Thomas model is described in **Section 2.6.3.3**. The values of the Thomas model parameters including the Thomas adsorption rate constant-k_{TH} (L/h.mg) and the maximum column As(V) adsorption capacity - q_{TH} (mg/g) are given in **Table 4.5**.

Table 4.5. Thomas model parameters for As(V) and As(III) adsorption on PPCI

Adsorbate	Thomas model parameters		
	k_{TH} (L/h.mg)	q_{TH} (mg/g)	R^2
As(V)	0.028	9.46	0.97
As(III)	0.024	8.25	0.93

The results indicate that the breakthrough curves of PPCI for As(V) and As(III) adsorption in the continuous fixed-bed system were successfully described by the Thomas model because of the high coefficient of determination values (R^2) (0.97 for As(V) and 0.93 for As(III)) (**Table 4.5**). The adsorption capacities of PPCI for As(V) and As(III) in column experiment were 9.46 mg/g and 8.25 mg/g, respectively. The Thomas adsorption capacities of PPCI toward both of As(V) and As(III) ions were lower than the Langmuir maximum adsorption capacity of PPCI for As(V) (15.28 mg/g) and for As(III) (11.77 mg/g) calculated in the batch experiment. This many have been caused by the smaller As concentration used in the column experiment compared to that used in the isotherm study.

The Thomas adsorption capacities of PPCI adsorbent in this study and other adsorbents in the literature for As(V) and As(III) are summarized in **Table 4.6**. As shown in **Table 4.6**, only a few studies investigated the adsorption capacity of an adsorbent in removing both As ions (As(III) and As(V)) in the fixed bed column system. Most studies have only been done on As(V).

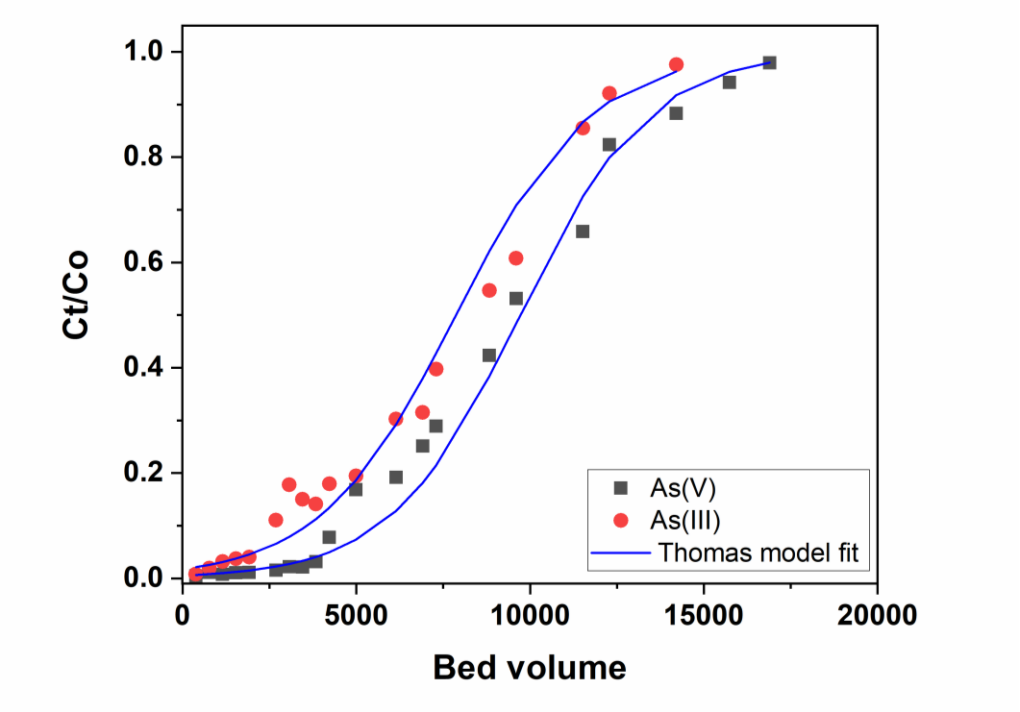

Figure 4.12. Breakthrough curves for As(III) and As(V) adsorption onto PPCI

The results in the above table show that PPCI revealed a higher adsorption capacity than many adsorbents derived from natural mineral sources, bio-sorbents (natural laterite, rice polish, crawfish shell biochar) and iron-based adsorbents (iron-loaded Azadirachta indica roots, iron modified manganese oxide ore (Fe-VMO), iron-impregnated granular activated carbon (GAC-Fe), and iron modified luffa fibre (FLF-3).

Table 4.6. The Thomas adsorption capacities of As(III) and As(V) by PPCI and other adsorbents

Adsorbent	As concentration (mg/L)		Thomas adsorption capacity q_{TH} (mg/g)		References
	As (V)	As (III)	As(V)	As (III)	
PPCI	0.3	0.3	**9.46**	**8.25**	**This study**
Natural laterite (NLTT)	0.5	-	0.198	-	**This study**
Crawfish shell biochar	20	-	2.10	-	Yan et al. (2018)
Rice polish	1	1	0.079	0.067	Ranjan et al. (2009)
Iron-loaded Azadirachta indica roots	1	-	0.09	-	Sawood and Gupta (2020)
Iron modified manganese oxide ore (Fe-VMO)	0.25	-	1.145	-	Nguyen et al. (2020b)
Iron-impregnated granular activated carbon (GAC-Fe)	0.25	-	0.470	-	Kalaruban et al. (2019)
Iron modified luffa fibre (FLF-3)	0.1	-	1.26	-	Nguyen et al. (2020c)

4.4. Conclusions

Pomelo peel biochar coated with iron (PPCI) was successfully produced by combining of slow pyrolysis and iron grafting processes. PPCI possessed a pH_{PZC} of 7.3, which suggests that its surface contains positive charges at natural water for favorable adsorption of the negatively charged As species. The batch experiment results confirm that the Langmuir maximum adsorption capacities of As(III) and As(V) on PPCI at pH = 7 and 30 ºC were 11.77 mg/g and 15.28 mg/g, respectively. The PPCI's capacity is noticeably higher than that of raw pomelo peel (PP) (0.033 mg/g and 0.034 mg/g for As(III) and As(V), respectively). PPCI had superior adsorption capacity compared to many other biomass-derived adsorbents including those modified with Fe reported in literature. Experiment results also show that pH solution (2.0–10) did not affect PPCI's adsorption capacity toward As ions. Significant amounts of O– bearing functional groups (C–O, –OH, C=O) in PPCI play a significant role in strong H-bonding and/or surface complexation formation with As(III) and As(V) ions in solution. However, the much higher adsorption capacity of PPCI compared to unmodified pomelo peel adsorbent is largely due to inner-sphere complexation of As species with Fe in PPCI. The presence of coexisting anions reduced the adsorption capacity of PPCI, with the effect being strong for other inner-sphere complexing anions (phosphate, silicate) and weak for outer-sphere complexing anions (chloride). The adsorption rate of As(V) and As(III) on PPCI was rapid and most ions were removed within the first 60 minutes of contact. The kinetic data of PPCI toward both As(V) and As(III) anions fitted better to the PSO model than the PFO and Elovich models. The good adsorption capacity of regenerated PPCI, even after five-cycle regeneration has demonstrated the promising application potential of PPCI. The results of column studies show that the saturation time of PPCI column for As(V)

ions was 1056 h, which was longer than that for As(III) (888 h). The adsorption breakthrough curves fitted the Thomas model very satisfactorily with respective adsorption capacities of 8.25 and 9.46 mg/g for As(III) and As(V) ions.

This chapter presents the results of As removal by a PPCI, an adsorbent derived from agriculture industry waste. Although NLTT and PPCI possess their unique properties and perform well, a new novel iron-based adsorbent derived commercial chemical should be developed to remove As from highly polluted water sources. It is expected to have a super-adsorption capacity for both As ions. Finally, the new adsorbent is expected to remove multiple contaminants (both toxic cation and anion) in the solution. The next chapter will present the removal of As using Mn/Mg/Fe-LDH, an adsorbent synthesized from commercial chemicals.

CHAPTER 5. REMOVAL OF ARSENIC FROM WATER BY Mn/Mg/Fe LAYERED DOUBLE HYDROXIDES

Chapter 5 presents the As adsorption capacity of Mn/Mg/Fe-LDH, an adsorbent synthesized from commercial chemicals. The results in this chapter, except the column study, were published in the below paper in Chemosphere journal (A-rated journal):

Nguyen, T. H., Tran, H. N., Nguyen, T. V., Vigneswaran, S., Trinh, V.T., Nguyen, T. D. Nguyen, T. H. H., Mai, T.N., Chao, H. P. (2021). Single-step removal of arsenite ions from water through oxidation-coupled adsorption using Mn/Mg/Fe layered double hydroxide as catalyst and adsorbent. Chemosphere, 133370 (IF: 8.943; SJR: Q1)

5.1. Introduction

Among existing adsorbents, layered double hydroxides (LDHs) have garnered much attention for the removal of both toxic cations and anions in aquatic environments due to their unique properties and simple synthesis processes (Asiabi et al., 2017; Wang et al., 2018; Tran et al., 2019). The LDHs belong to the synthetic clay group, one that possesses different ionic layer structures such as positively charged brucite like layers and non-framework charge compensating anions in their galleries. Specifically, the form of LDH can be expressed by the general formula $[M^{2+}_{1-x}M^{3+}_{x}(OH)_2]^{x+}(A^{n-})_{x/n}\bullet mH_2O$. In this formula, M^{2+} and M^{3+} are divalent metal cations (i.e., Mg^{2+}, Cu^{2+}, Zn^{2+}, Ni^{2+}, or Fe^{2+}) and trivalent metal cations (Al^{3+}or Fe^{3+}) in the brucite like layers, respectively. A^{n-} indicates the interlayer charge (NO_3^-, CO_3^{2-}, Cl^-, etc.), and x is the $M^{3+}/(M^{2+} + M^{3+})$ molar ratio (Huang et al., 2015; Pavlovic et al., 2016; Wang et al., 2018; Tran et al., 2019).

Thus, the positive charge of the material's brucite layers is favorable in reacting with toxic anions via electrostatic-attraction mechanism. Meanwhile, the host anions in the interlayer regions (i.e., CO_3^{2-} and NO_3^{2-} anions) play an important role in exchanging with toxic anions in solution through anion exchange mechanism (Asiabi et al., 2017; Hudcová et al., 2017; Mubarak et al., 2018; Varga et al., 2021; Wang et al., 2018).

Due to the neutral molecular forms of As(III), layered double hydroxides cannot remove As(III) based on the reaction of their positively charged surface or host anions in their interlayer region with As(III) ions. Thus, in order to successfully remove As(III), it is required to oxidize As(III) to As(V), and then remove the oxidized As(V) from water (also known as a two-step removal process). For example, Neppolian et al. (2008) applied peroxydisulfate ions to effectively oxidize As(III) into less toxic As(V) anions. However, after the oxidation process, an additional removal process (i.e., adsorption or coagulation) is required. In addition, activated carbon (AC) and biochar have been commonly used in water treatment, it has a low adsorption capacity to As(III) and As(V) in water. For this reason, it is necessary to make additional modifications or improve treatment, such as alumina composite-modified AC (Karmacharya et al., 2016), aluminum-enriched biochar (Ding et al., 2018), biochar modified with Fe/Mn (Lin et al., 2017), and the composite of Fe/Mn-LDH and carbon material (Fe/Mn-C-LDH) (Wang et al., 2021a; Wang et al., 2021b). As a result, the preparation costs of this material rise, and the two stage-preparation is very time-consuming.

To solve this problem, development a material exhibited superior properties to remove both As(III) and As(V) from water in a single process is necessary. It means that the new material not only acts as oxidant agent but also be a good adsorbent. A one-step removal process of both As(III) and As(V) using Fe(II)/Mn(II) oxides was reported by

Bai et al. (2016). Herein, As(III) ions in solution were firstly oxidized into As(V) anions when it contacted the Fe(II)/Mn(II) oxides oxides; subsequently, oxidized As(V) and As(V) in solution were adsorbed by this oxide material. This removal process involved a combination of mechanisms, namely oxidation-coupled adsorption.

Most previous researches on As removal by LDH-based adsorbents focused on only As(V) (Wang et al., 2009; Huang et al., 2015; Asiabi et al., 2017; Hudcová et al., 2017). There is only a few researches done on As(III) ions. In other words, the removal of toxic As(III) by the LDH-based materials is still a big challenge.

In this study, a clay-like sample (Mn/Mg/Fe-LDH) was simply prepared from three metals (Mn, Mg, and Fe) through a one-step coprecipitation process. The Mn and Fe metals were selected because their oxides have been acknowledged as effective oxidants to convert As(III) to As(V). The prepared Mn/Mg/Fe-LDH material was well characterized by various techniques and then applied to remove As(III) and As(V) from aqueous solution. The adsorption mechanism was deeply investigated. The effects of important operating parameters (such as solution pH, contact time, temperature, etc.) which have strong impacts on the adsorption process were tested under batch experiments. A column adsorption test for both As(III) and As(V) ions was also studied.

5.2. Material and methods

5.2.1. Reagents

All the chemicals and reagents used in this work were of an analytical grade and used without any further purification. $Mg(NO_3)_2.6H_2O$ (256.4 g/mol), $Mn(NO_3)_2$, $Fe(NO_3)_3.9H_2O$ (404 g/mol), sodium hydroxide NaOH, and sodium carbonate $NaCO_3$ were obtained from Sigma-Aldrich. Stock solutions of As(III) and As(V) were prepared

by dissolving sodium arsenite ($NaAsO_2$, from ACE Chemical Co.) and sodium arsenate heptahydrate ($Na_2HAsO_4.7H_2O$, from BDH Chemical Ltd.) in deionized water, respectively.

5.2.2. Synthesis of Mn/Mg/Fe layered double hydroxides

Manganese/magnesium/iron layered double hydroxides (Mn/Mg/Fe-LDH) were synthesized by co-precipitation method at different molar ratios of Mn/Mg/Fe, such as 2/1/1, 1/1/1, 2/1/2, and 1/1/2, respectively (Chao et al., 2018). The Mn/Mg/Fe sample prepared at the molar ratio of 1/1/1 was taken as a typical example. Namely, a 60 mL of the solution [containing 0.04 mol of $Mn(NO_3)_2$, 0.04 mol of $Mg(NO_3)_2.6H_2O$, and 0.04 mol of $Fe(NO_3)_3.9H_2O$] was added drop by drop into another 60 mL solution [containing 0.336 mol NaOH and 0.022 mol Na_2CO_3]. Continuous stirring was applied. The pH of the mixture was maintained at 12 ± 0.2 and aged at 45 °C for 3 h to maintain the precipitation. Le et al. (2009) reported that the Mg/Al-LDH precipitates were colloidal nanoparticles in solutions, with their average particle diameters ranging from 68.6 to 367 nm. The collected precipitate was centrifuged at 9000 rpm for 15 min. The concentrated precipitate was then washed several times with deionized water until the pH value of the filtrate reached a constant pH (approximately 7.0). The concentrated precipitate (Mn/Mg/Fe-LDH) was then dried at 80 °C for 48 h. After the drying process, the hard solids (~ 1.0–2.0 cm) were obtained because of the aggregation phenomenon of the Mn/Mg/Fe-LDH colloids. The hard solids were grinded and sieved into smaller particles (their sieve sizes ranging from 0.106 to 0.250 mm) and then stockpiled in tightly closed bags until further use. The other Mn/Mg/Fe samples at the molar ratios of 2/1/1, 2/1/2, and 1/1/2 were also synthesized in a similar way to that of Mn/Mg/Fe at 1/1/1.

A primary adsorption test (scanning experiment) was conducted to compare the adsorption capacity of Mn/Mg/Fe-LDH samples (prepared at four different molar ratios of Mn/Mg/Fe) with As(III) and As(V) solution. The adsorption conditions were fixed at 1.0 g/L of adsorbent dose, 24 h, 25 °C, pH = 7.0, and 3.5 mg/L of As(III) or As(V). The results (**Figure 5.1**) demonstrate that the Mn/Mg/Fe-LDH adsorbent prepared at the 1/1/1 ratio exhibited an efficiency in removing As ions similar to that prepared at the 2/1/1 ratio and higher than that prepared at 1/1/2 and 2/1/1. Therefore, Mn/Mg/Fe-LDH adsorbent (prepared at a ratio of 1/1/1) was selected in the subsequent batch adsorption experiments and material characterization.

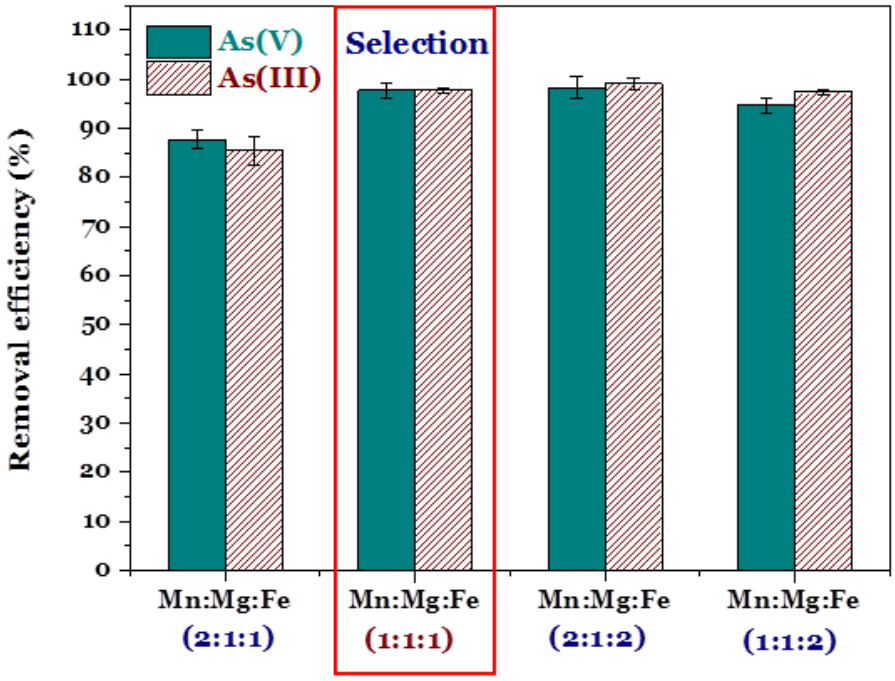

Figure 5.1. Effect of molar ratio of metals (Mn, Mg, and Fe) on the adsorption capacity of resultant Mn/Mg/Fe-LDH samples towards As(III) and As(V)

(Adsorption conditions: m/V = 1 g/L, t = 24 h, T = 25 °C, pH = 7.0, and Co = 3.5 mg/L)

5.2.3. Characterization of Mn/Mg/Fe-LDH

The crystal phases of Mn/Mg/Fe-LDH were characterized using an X-ray Diffractometer (XRD; Empyrean-PANalytical). Its main functional groups were detected by Fourier transform infrared instrument (FTIR; Nicolet iS5). Morphological features and element composition of Mn/Mg/Fe-LDH were determined by scanning electron microscope coupled with energy-dispersive X-ray spectroscopy (SEM-EDS; Quanta-650). Its textural properties such as Brunauer-Emmett-Teller surface area (S_{BET}) and total pore volume (V_{Total}) were determined from the N_2 adsorption/desorption isotherm at 77 K (using Micromeritics sorptometer; AccuPyr II 1340. V1.02). The pH value at the isoelectric point (pH_{IEP}) of Mn/Mg/Fe-LDH was measured by a zeta potential analyser (Colloidal Dynamics; ZED-3600) (Chao et al., 2018). The Mn/Mg/Fe-LDH solid was degassed under vacuum conditions at 105 °C for 24 h before it was characterized.

5.2.4. Batch adsorption experiment

As adsorption onto Mn/Mg/Fe-LDH was studied under batch experiments at different operating parameters such as solution pH, contact time, initial As concentration, temperature, coexisting anion, and desorbing agent. All adsorption studies were done in triplicate. The values were presented as average ± standard deviation (as error bars).

5.2.4.1. Effect of solution pH

Firstly, the effect of solution pH on As removal was studied at different pH values with an initial solution containing approximately 50 mg/L As (III) or As (V). The initial pH value of the As solutions was adjusted from 2.0 to 10 ± 0.2 by adding either 1 M NaOH or 1 M HNO_3.

5.2.4.2. Isotherm adsorption

Adsorption isotherm studies were conducted with initial As (III)/As (V) concentration ranging from 0 to 270 mg/L with an initial pH of 7 and at three temperature levels of 7 °C, 25 °C, and 50 °C, respectively. The pH of the solution was kept constant at around 7.0 during the adsorption process.

5.2.4.3. Kinetic adsorption

Kinetic studies were conducted at time intervals of 1, 5, 10, 30, 60, 120, 180, 240, 300, 360, 420, 480, 1320, and 1440 min at initial concentration of As (III) (70.47 mg/L) or As (V) (74.35 mg/L) at pH = 7 and at three temperatures of 7 °C, 25 °C, and 50 °C, respectively. Similar to the isotherm adsorption, during kinetic adsorption, the pH solution value was kept constant at around 7.0.

5.2.4.4. Effect of coexisting anions

The effect of coexisting anions on As adsorption capacity of Mn/Mg/LDH was carried out with the addition of different anions (including Cl^-, CO_3^{2-}, HPO_4^{2-}, SO_4^{2-}, SiO_3^{2-}), with the two levels of concentration of each anion at 10 mM and 100 mM.

In all the batch experiments above, approximately 0.1 g of Mn/Mg/Fe-LDH was added into a flask containing 100 mL of As(III) or As(V) solution. The solid/liquid (m/V) concentration of the adsorbent in this study amounted to 1.0 g/L. The flask was shaken using a mechanical shaker (Lab Tech LIS-2) at 150 rpm and 25 °C. After pre-determined shaking times, the solid and liquid parts were separated and used for different tasks. The liquid was filtered through a 0.45 μm filter to analyse residual As in solution. The solid part was dried at 105 °C for 24 h and then stockpiled in tightly plastic bags for further characterization of laden Mn/Mg/Fe-LDH (i.e., FTIR, the textural, morphological

properties, and desorption). The amount of As adsorbed by Mn/Mg/Fe-LDH at any time (q_t; mg/g) and equilibrium (q_e; mg/g) was calculated by **Equations 3.1** and **3.2**, respectively, in **Section 3.2.3**.

5.2.4.5. Desorption experiment

A desorption study was carried out after the equilibrium adsorption process. Several desorbing agents were used for this purpose, such as Na_2CO_3 (0.2 M), NaCl (0.2 M), EDTA (ethylenediaminetetraacetic; 0.2 M), NaOH (0.2 M), HCl (0.2 M), and deionized water (at pH = 12). After the adsorption process approximately 0.1 g of As-laden Mn/Mg/Fe-LDH was transferred into the flask containing 100 mL of each desorbing agent. The time set aside for the desorption study was 24 h at 25 °C. The concentration of As residue on LDH111 and the percentage of desorption were determined using **Equations (3.3)** and **(3.4)**, respectively, in **Section 3.2.3.**

5.2.4.6. Stability assessment

Stability assessment tests were conducted at two different conditional experiments as follows. For the first test, 0.05 g of the Mn/Mg/Fe-LDH was added into the flasks containing 0.05 L distilled water, which pH adjusted from 2 to 10. After 24 hours of contact, the concentration of metal ions (Fe, Mn, Mg) was determined. The second test is similar to the 1st test. However, the purpose is to determine the concentration of leaching metal ions during the As adsorption process. Then, after 24 hours of contact, the concentration of metal ions (Fe, Mn, Mg) was also examined.

5.2.5. Laboratory column adsorption study

Column adsorption studies were conducted using four glass columns of 9 mm inner diameter and 0.11 m height. Two different adsorbates, As(V) and As(III), were used

in the column adsorption studies at the same experimental condition. The feed solutions of As(III) or As(V) concentration of 0.33 mg/L were pumped in an up-flow mode through the column at constant flow rates of 1 m/h by dosing pumps (Master flex L/S). Each column was packed with 5 g of Mn/Mg/Fe-LDH, corresponding to the bed height of 0.09 m and the EBCT of 5 min. 1.0 mm acrylic beads and cotton balls were placed at the bottom and top of the column to prevent the release of the packed adsorbent.

The fixed-bed adsorption tests were conducted for 45 weeks and the samples were collected for 43 times with certain interval until the As concentration approached the initial concentration.

The samples were filtered using 0.45 μm filters, and filtrates were analyzed for As using an ICPMS (NexION 2000, US).

5.3. Results and discussion

5.3.1. Characterization of Mn/Mg/Fe-LDH

5.3.1.1. Crystalline structure and surface morphology

The crystal structure of Mn/Mg/Fe-LDH is detected by X-ray powder diffraction**.** **Figure 5.2** shows that Mn/Mg/Fe-LDH exhibited a typical structure of hydrotalcite-like material (Guo et al., 2017; Hudcová et al., 2017; Mubarak et al., 2018; Wang et al., 2021a; Wang et al., 2021b). This finding was confirmed from its morphology that was detected through SEM imaging (**Figure 5.3**). Two diffraction peaks (**Figure 5.2**) well-identified at 11.68° and 23.4° were regarded as the typical characteristics (the (003) and (006), respectively) of LDH solid (Vucelic et al., 1997; Huang et al., 2015; Pavlovic et al., 2016; Tran et al., 2019; Zhang et al., 2022), suggesting that the LDH was successfully synthesized from three metal ions (Mn, Mg, and Fe). According to Bragg's law, the basal

spacing (d_{003}) of Mn/Mg/Fe-LDH was 0.757 nm (**Figure 5.2**). The d_{003} value (0.757 nm) of Mn/Mg/Fe-LDH was similar to that of some other LDH materials reported in the literature, such as Mg/Fe-LDH (0.768 nm) (Vucelic et al., 1997), Mg/Al-LDH (0.781nm) (Huang et al., 2015), and Mg/Fe-LDH (0.87 nm) (Mubarak et al., 2018).

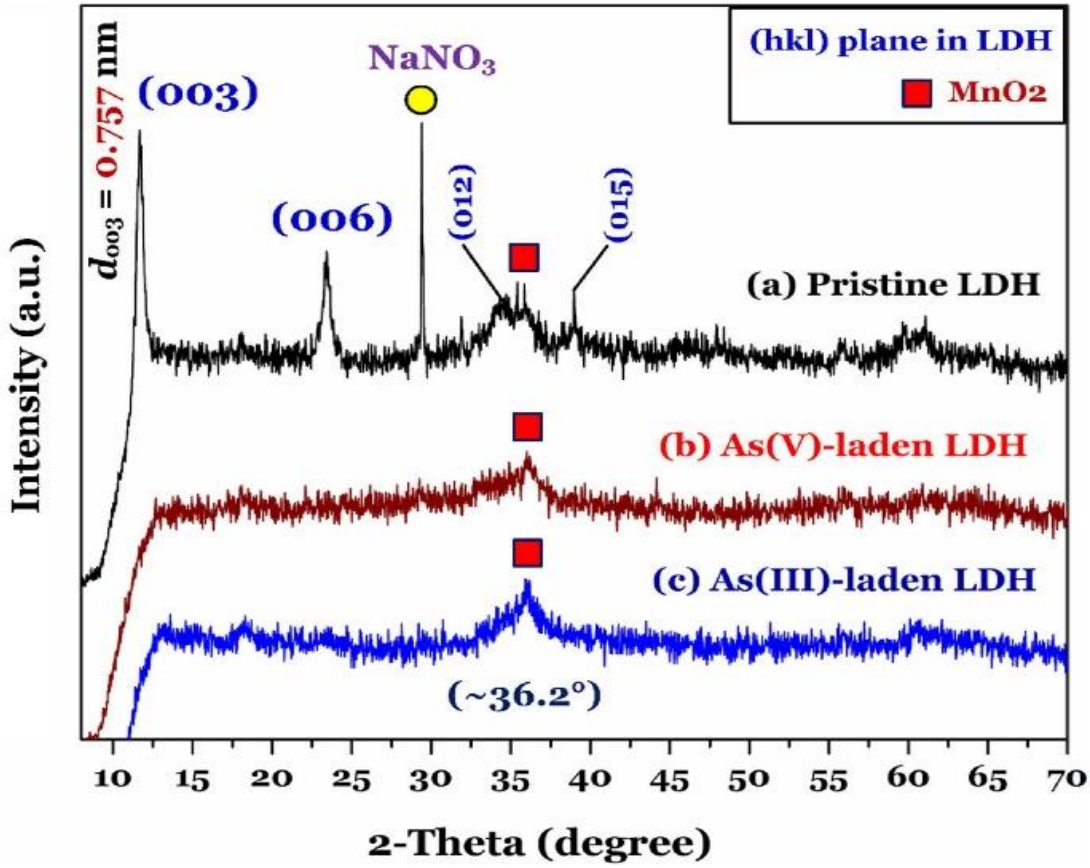

Figure 5.2. XRD pattern of Mn/Mg/Fe-LDH before and after adsorption of As(III) ions or As(V) anions

(adsorption conditions: 1.0 g/L, C_o = 50 mg/L, 24 h, pH = 7.0, and 25 °C)

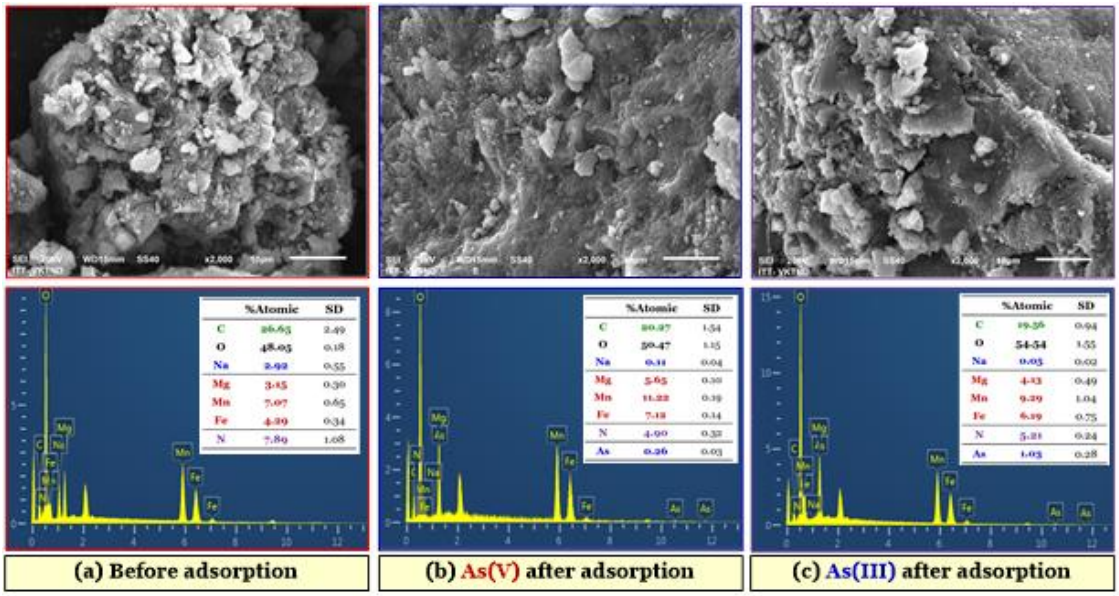

Figure 5.3. SEM-EDS data of (a) pristine Mn/Mg/Fe-LDH, (b) As(V) laden Mn/Mg/Fe-LDH, and (c) As(III) laden Mn/Mg/Fe-LDH

(adsorption conditions: 1.0 g/L, C_o = 50 mg/L, 24 h, pH = 7.0, and 25 °C)

Notably, a strong diffraction peak at 29.4° indicates the crystal nature of nitratite mineral ($NaNO_3$) (Córdova et al., 2014; Reyes et al., 2014; Ferrer, 2016; Triviño et al., 2018) in the dried Mn/Mg/Fe-LDH. In addition, a peak at 36.2° might belong to the (110) plane of birnessite-type MnO_2 (Mohammadi et al., 2021). Those solids ($NaNO_3$ and MnO_2) that were naturally generated during the synthesis of Mn/Mg/Fe-LDH played an important role in adsorbing As(V) and As(III) in this study (**Sections 5.3.9** and **5.3.10**).

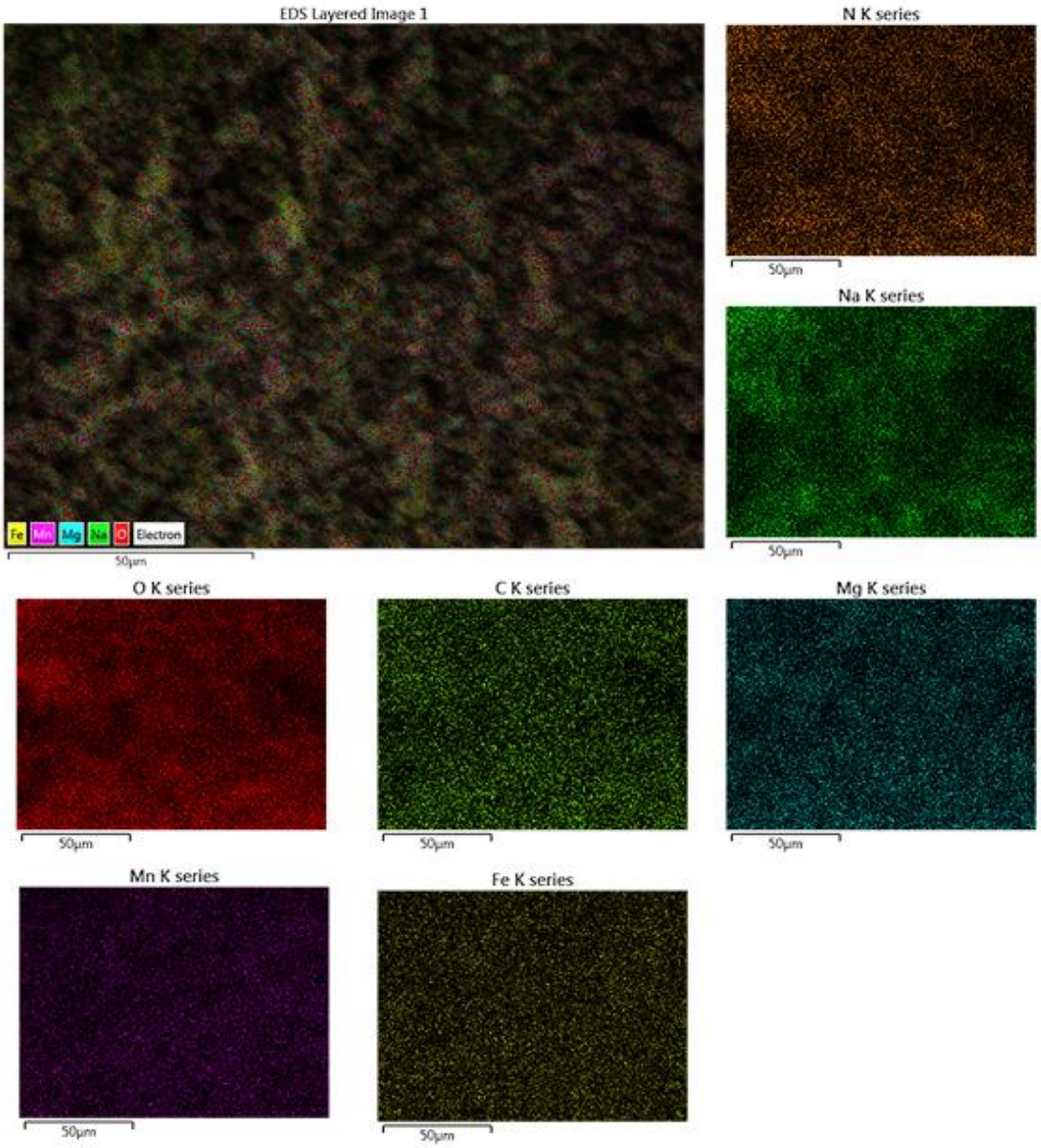

Figure 5.4. Energy-dispersive X-ray spectroscopy (EDS) mapping of the composition of Mn/Mg/Fe-LDH

5.3.1.2. Textural property

The textural property of Mn/Mg/Fe-LDH was analysed by nitrogen adsorption/desorption isotherm (**Figure 5.5**). This physical sorption belongs to the Type

IV isotherm and presents Type H3 hysteresis, suggesting that Mn/Mg/Fe-LDH was a mesoporous material (average pore with ~ 14.2 nm) with slit-shaped pores (Varga et al., 2021; Wang et al., 2021a; Wang et al., 2021b). Mn/Mg/Fe-LDH exhibited a low BET surface area (S_{BET} = 75.2 m^2/g; **Figure 5.5**). This is a typical future of hydrotalcite like-materials such as Mg/Al-LDH (95.7 m^2/g) (Huang et al., 2015), Mn/Fe-LDH (82.6 m^2/g) (Wang et al., 2021a; Wang et al., 2021b), Ni/Al-LDH (61.05 m^2/g) (Asiabi et al., 2017), Mg/Zn/Fe-LDH (48.4 m^2/g) (Liu et al., 2019b), Ca/Fe-LDH (43.3 m^2/g) (Lu et al., 2018), Mg/Fe-LDH (40.1 m^2/g) (Hudcová et al., 2017), and granular Mg/Fe-LDH (1.37 m^2/g) (Choong et al., 2021). This particular result suggests that the adsorption of As ions onto Mn/Mg/Fe-LDH through pore-filling mechanism might be negligible.

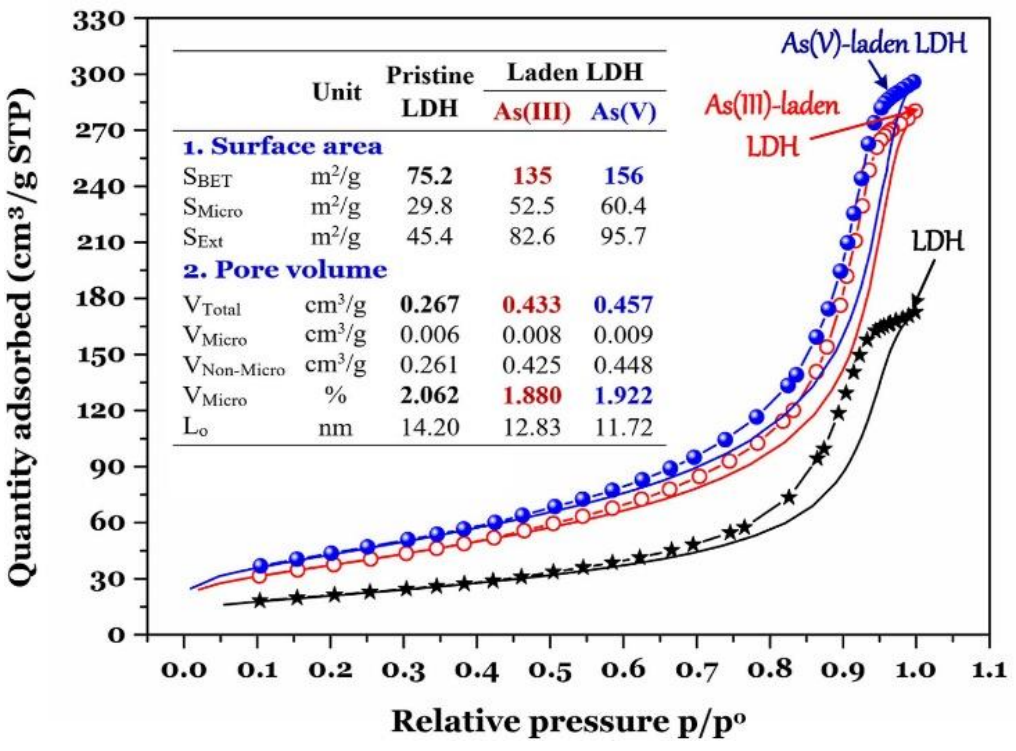

	Unit	Pristine LDH	Laden LDH	
			As(III)	As(V)
1. Surface area				
S_{BET}	m^2/g	**75.2**	**135**	**156**
S_{Micro}	m^2/g	29.8	52.5	60.4
S_{Ext}	m^2/g	45.4	82.6	95.7
2. Pore volume				
V_{Total}	cm^3/g	**0.267**	**0.433**	**0.457**
V_{Micro}	cm^3/g	0.006	0.008	0.009
$V_{Non-Micro}$	cm^3/g	0.261	0.425	0.448
V_{Micro}	%	**2.062**	**1.880**	**1.922**
L_o	nm	14.20	12.83	11.72

Figure 5.5. Nitrogen adsorption/desorption isotherm at 77 K of pristine and laden Mn/Mg/Fe-LDH adsorbents

(adsorption conditions: 1.0 g/L, C_o = 50 mg/L, 24 h, pH = 7.0, and 25 °C)

5.3.1.3. Surface functionality

The main functional groups on the surface of Mn/Mg/Fe-LDH were identified by FTIR. **Figure 5.6** shows that a broad band at approximately 3430 cm^{-1} is attributed to the O–H stretching vibrations derived from the OH^- groups on the surface of Mn/Mg/Fe-LDH or from the OH^- anions on its interlayer region (Chubar et al., 2013; Lu et al., 2018). Meanwhile, the presence of Fe–O groups on the surface of Mn/Mg/Fe-LDH is typically identified at 594 cm^{-1} (Huang et al., 2015; Wang et al., 2021a; Wang et al., 2021b). Lastly, a band located at around 420 cm^{-1} is assigned to the M–O and M–OH vibrations (where M is Mg, Mn, or Fe), which is related to metal-oxygen bond and the metal hydrogen-oxygen stretching vibration (Asiabi et al., 2017; Huang et al., 2015).

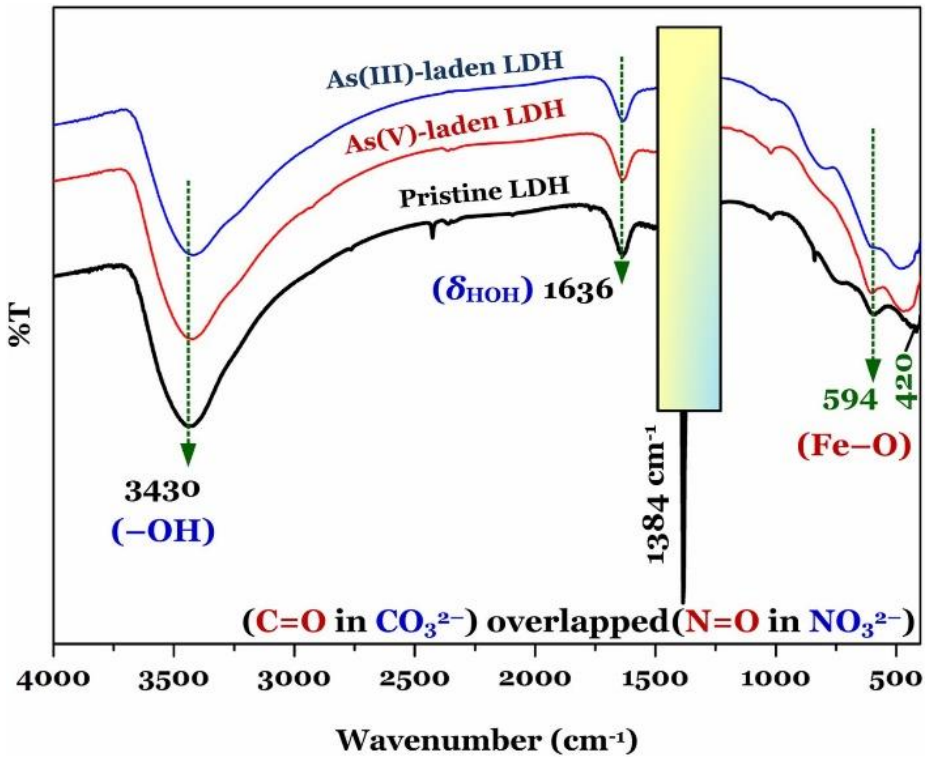

Figure 5.6. FTIR spectrum of Mn/Mg/Fe-LDH before and after adsorption of As ions

(adsorption conditions: 1.0 g/L, C_o = 50 mg/L, 24 h, pH = 7.0, and 25 °C)

Notably, an observed band at approximately 1384 cm^{-1} corresponds to the host anions in the interlayer anions of Mn/Mg/Fe-LDH that is C=O (derived from CO_3^{2-} ions) overlapped with N=O (NO_3^- ions) (Chao et al., 2018; Goh et al., 2008; 2009; Li et al., 2009a). The identification of this band plays an important role in identifying the adsorption mechanisms in this study (**Sections 5.3.9 and 5.3.10**).

5.3.1.4. Chemical state of the main elements in Mn/Mg/Fe-LDH

The element valences and elemental compositions (**Table 5.1**) in Mn/Mg/Fe-LDH were explored through the corresponding XPS data. The high-resolution scans of core-level photoelectron spectrum (C 1s, O 1s, N 1s, Mg 1s, Fe 2p, and Mn 2p) are explored.

The XPS spectrum of C 1s (**Figure 5.7**) for Mn/Mg/Fe-LDH shows two peaks of binding energy (BE) at 284.30 eV and 287.98 eV attributed to the C–C bond in adventitious carbon (Mubarak et al., 2018) and the C=O bond in the host CO_3^{2-} anion in its interlayer region (Liu et al., 2006; Liu et al., 2019b), respectively. The presence of another important host NO_3^- anion in this interlayer region was confirmed through N=O bond at 407.03 eV in the N 1s XPS spectrum (**Figure 5.8**) or **Table 5.1** (Goh et al., 2009). The CO_3^{2-} ions generated by CO_2 from atmosphere into the interlayer region during the synthesis of Mn/Mg/Fe-LDH (**Section 5.2.2**) (Mubarak et al., 2018); meanwhile, NO_3^- ions were derived from the metal salts of Mg, Fe, and Mn used (**Section 5.2.1**). The presence of C and N elements, which was obtained from the EDS data (**Figure 5.3**) and the XPS data (**Table 5.1**); and also visible in mapping pictures (**Figure 5.4**), might result from the CO_3^{2-} and NO_3^- anions in its interlayer region. The host CO_3^{2-} and NO_3^- anions have been acknowledged as active anions for efficiently exchanging hexavalent chromium anions (CrO_4^{2-} and $Cr_2O_7^{2-}$) (Tran et al., 2019; Varga et al., 2021) and As(V) anions ($H_2AsO_4^-$ and $HAsO_4^{2-}$) (Yu et al., 2012; Lee et al., 2018) in water environments.

Table 5.1. Low resolution XPS data for Mn/Mg/Fe-LDH and As-laden Mn/Mg/Fe-LDH samples

		Pristine LDH	As(III)-laden LDH-10min	As(III)-laden LDH-48h	As(V)-laden LDH-48h
1. C 1s	BE (eV)	284.55	285.26	284.48	284.48
	At.%	**58.26**	**58.02**	**71.67**	**60.2**
	FWHM (eV)	1.63	2.9	1.76	1.7
2. O 1s	BE (eV)	531.78	531.79	531.84	531.11
	At.%	**31.74**	**32.67**	**24.76**	**32.64**
	FWHM (eV)	3.96	4.14	3.78	4.2
3. Mg 1s	BE (eV)	1303.26	1303.86	1303.3	1303.66
	At.%	**1.43**	**3.33**	**1.15**	**1.89**
	FWHM (eV)	2.84	3.11	2.88	1.61
4. Mn 2p	BE (eV)	641.96	642.52	641.78	641.94
	At.%	**2.0**	**2.94**	**1.0**	**2.24**
	FWHM (eV)	3.69	3.98	4.22	3.61
5. Fe 2p	BE (eV)	711.54	712.24	711.0	711.34
	At.%	**1.61**	**2.02**	**0.62**	**1.98**
	FWHM (eV)	4.71	4.79	4.73	5.05
6. N 1s	BE (eV)	407.03	401.93	401.91	401.09
	At.%	**2.54**	**0.03**	**0.07**	**0.14**
	FWHM (eV)	2.69	0.45	1.84	1.02
7. Na 1s	BE (eV)	1071.22	NA	NA	NA

		Pristine LDH	As(III)-laden LDH-10min	As(III)-laden LDH-48h	As(V)-laden LDH-48h
	At.%	**2.0**	**NA**	**NA**	**NA**
	FWHM (eV)	2.74	NA	NA	NA
8. As (Total)	**At.%**	—	**0.77**	**0.53**	**0.41**
8.1. As 2p3	BE (eV)	—	1326.79	1325.74	—
	At.%	—	0.21	0.08	—
	FWHM (eV)	—	0.95	0.99	—
8.3. As 3p1	BE (eV)	—	149.2	—	149.24
	At.%	—	0.02	—	0.02
	FWHM (eV)	—	0.25	—	0
8.4. As 3p3	BE (eV)	—	143.95	143.13	143.51
	At.%	—	0.1	0.14	0.16
	FWHM (eV)	—	1.33	2.33	2.58
8.5. As 3d3	BE (eV)	—	**44.89**	**44.17**	**43.93**
	At.%	—	0.35	0.03	0.02
	FWHM (eV)	—	1.16	0	0
8.5. As 3d5	BE (eV)	—	44.96	44.21	44.61
	At.%	—	0.09	0.28	0.21
	FWHM (eV)	—	0.58	2.17	0.89

Note: BE = Binding energy (eV) and At.% = Atomic percentage (%). FWHM = Full width at half maximum

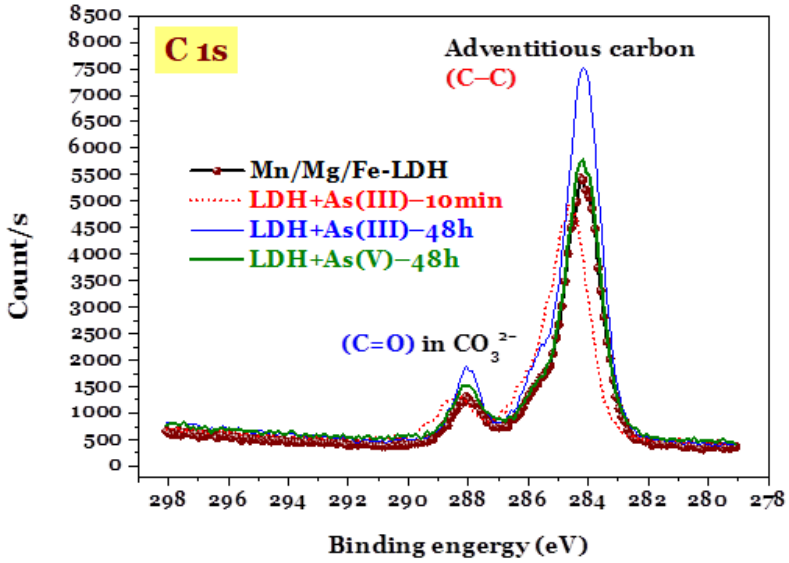

Figure 5.7. Raw XPS spectra of C 1s of Mn/Mg/Fe-LDH before and after adsorption of As(III) (10-min contact time and 48-h contact time) and As(V) (48-h contact time)

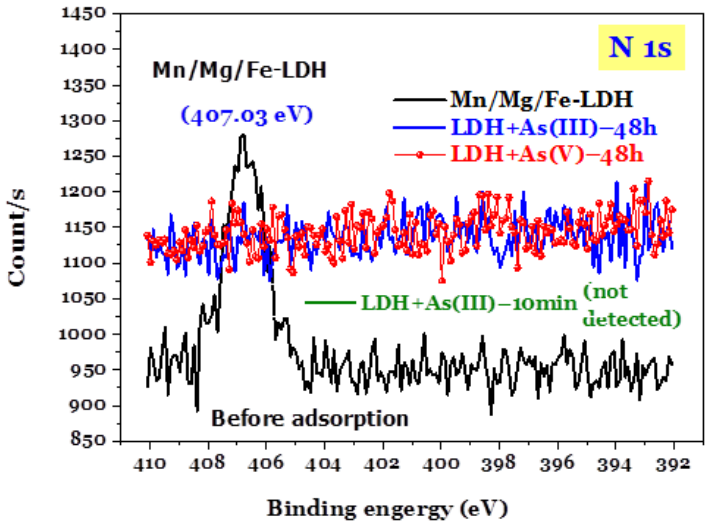

Figure 5.8. Raw XPS spectra of N 1s of Mn/Mg/Fe-LDH before and after adsorption of As(III) (10-min contact time and 48-h contact time) and As(V) (48-h contact time)

Note: The BE of N 1s of the Mn/Mg/Fe-LDH sample at 407.03 eV belongs to the host NO_3^- anions in the interlayer region of Mn/Mg/Fe-LDH). The N 1s XPS spectrum of the laden Mn/Mg/Fe-LDH sample after 10-min contact was not detected because %N was only 0.03% in **Table 5.1.**

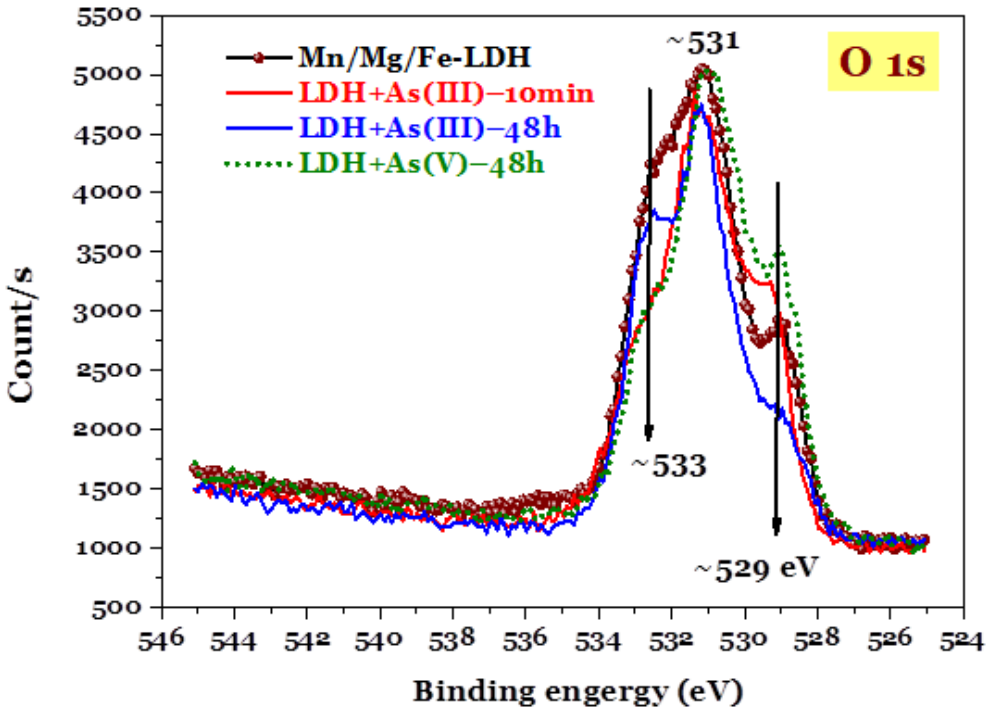

Figure 5.9. Raw XPS spectra of O 1s of Mn/Mg/Fe-LDH before and after adsorption of As(III) (10-min contact time and 48-h contact time) and As(V) (48-h contact time)

The high-resolution O 1s spectrum (**Figure 5.11a** or **Figure 5.9**) can be divided into three distinct peaks. Two BE peaks at 529.05 and 530.97 eV correspond to the M–O–M (or M–O where M represents for Mg, Mn, or Fe) and M–O–H (hydroxyl group). Another peak at 532.52 eV is the overlap of the M–O–H^+_2 (protonated hydroxyl group),

H–O–H (water molecule), and C=O (carbonate) bonds (Goh et al., 2009; Ferrer, 2016; Hudcová et al., 2017; Penke et al., 2021; Wang et al., 2021a; Zhang et al., 2022).

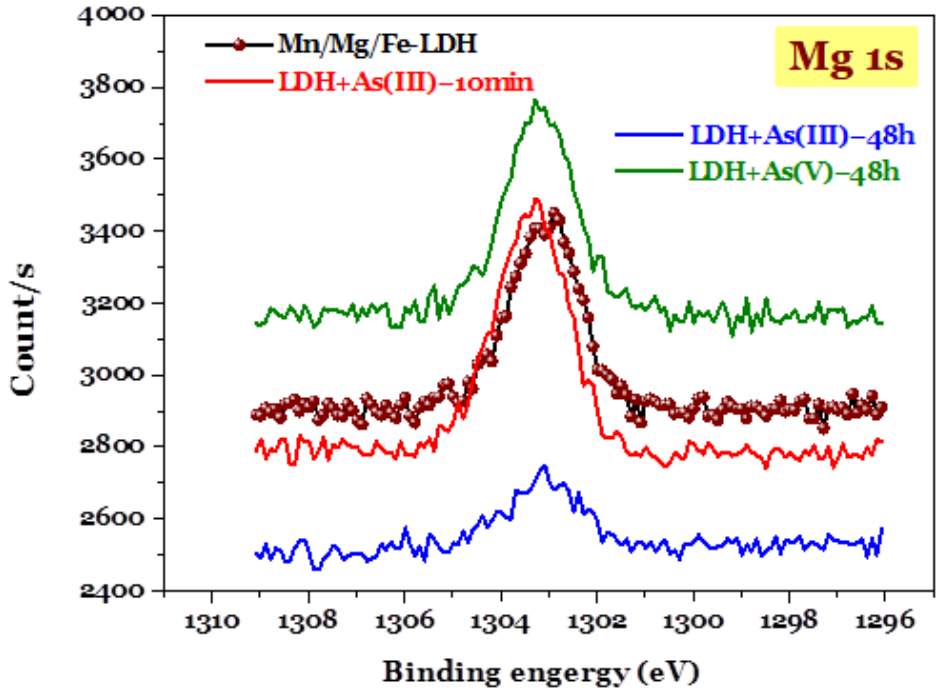

Figure 5.10. Raw XPS spectra of Mg 1s of Mn/Mg/Fe-LDH before and after adsorption of As(III) (10-min contact time and 48-h contact time) and As(V) (48-h contact time)

For magnesium, the BE value at 1303.3 eV (the XPS spectrum of Mg 1s in **Figure 5.10**) is related to the form of hydroxide of $Mg(OH)_2$ in Mn/Mg/Fe-LDH. In contrast, Fe and Mn are transition metals, so they can change their oxidation states under suitable conditions. Thus, it is necessary to consider both their raw XPS spectra and deconvoluted XPS spectra.

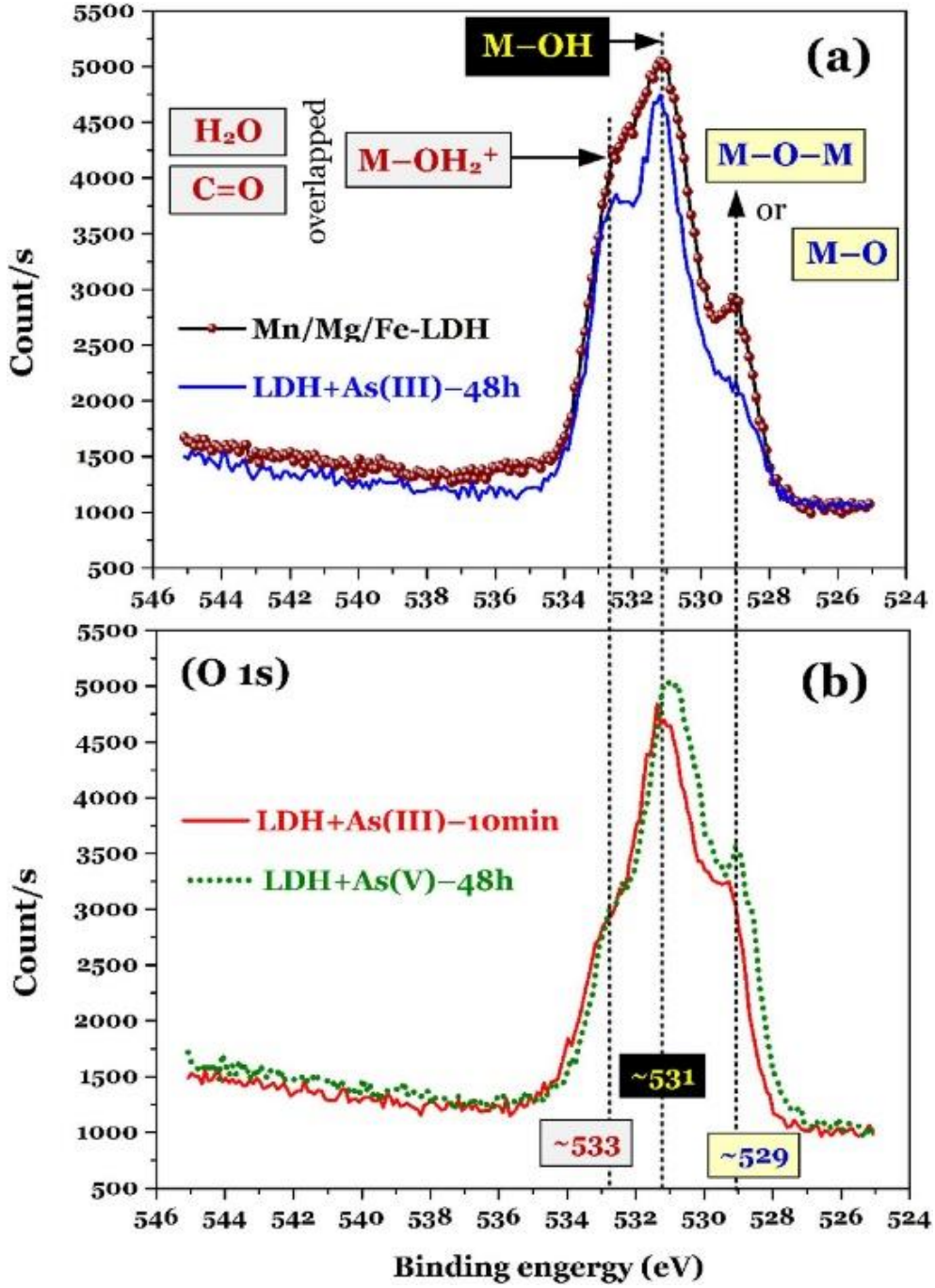

Figure 5.11. High-resolution spectrum of O 1s of Mn/Mg/Fe-LDH before adsorption and after adsorption of As(III) for 10 min, As(III) for 48h, and As(V) for 48h

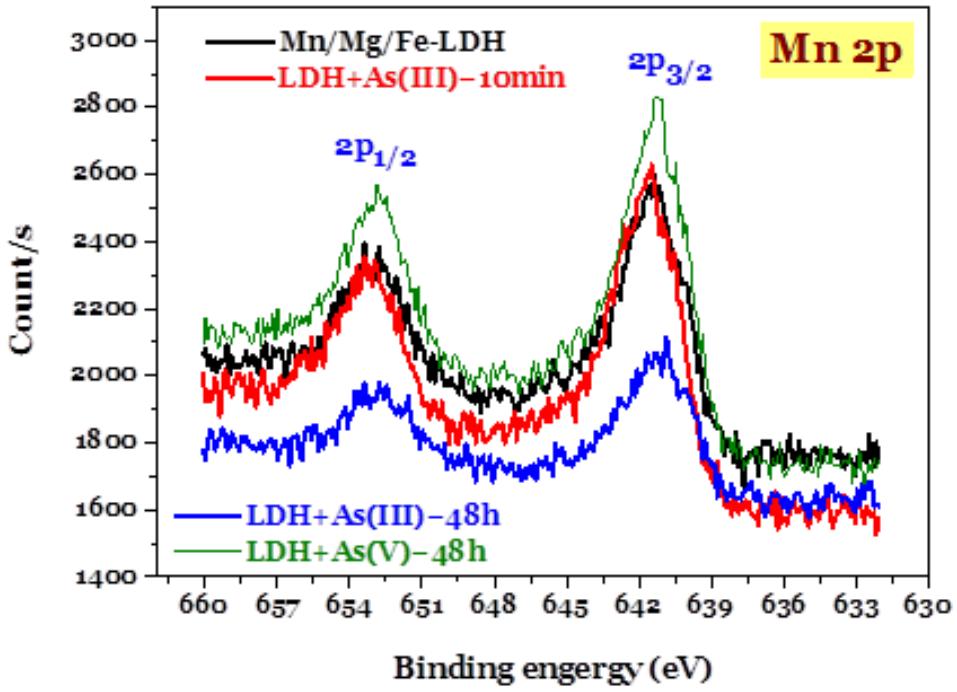

Figure 5.12. Raw XPS spectra of Mn 2p of Mn/Mg/Fe-LDH before and after adsorption of As(III) (10-min contact time and 48-h contact time) and As(V) (48-h contact time)

The raw spectrum of Mn 2p (**Figure 5.12**) indicate two BE peaks at 641.29 eV (Mn $2p_{3/2}$) and 652.91 eV (Mn $2p_{1/2}$), which implies the existence of the dominant Mn^{3+} oxidation state in Mn/Mg/Fe-LDH (Guo et al., 2016; Zhang et al., 2022). Although the $Mn(NO_3)_2$ salt used for preparing Mn/Mg/Fe-LDH, under high alkaline aqueous condition at pH 12 (**Section 5.2.2**), Mn^{2+} was easily oxidized to Mn^{3+}. This is because such reaction (**Equation 5.1**) occurs with a low standard reduction potential (E^o_{red}) (Haynes, 2014; Guo et al., 2016). However, highly unstable Mn^{3+} can continue to be oxidized to Mn^{4+} (Zhang et al., 2022). Many other authors reported a similar oxidation phenomenon when preparing LDH solids (Guo et al., 2016; Zhou et al., 2021; Zhang et

al., 2022). For example, Zhang et al. (2022) prepared Ni/Mn-LDH from $Ni(NO_3)_2$ and $MnSO_4$. The XPS spectrum indicate the attribution of Mn^{3+} at 641.75 eV (Mn $2p_{3/2}$) and 652.60 eV (Mn $2p_{1/2}$).

$$Mn(OH)_3 + e^- \rightleftharpoons Mn(OH)_2 + OH^- \quad (E^o_{red} = 0.15\ V) \qquad \textbf{(5.1)}$$

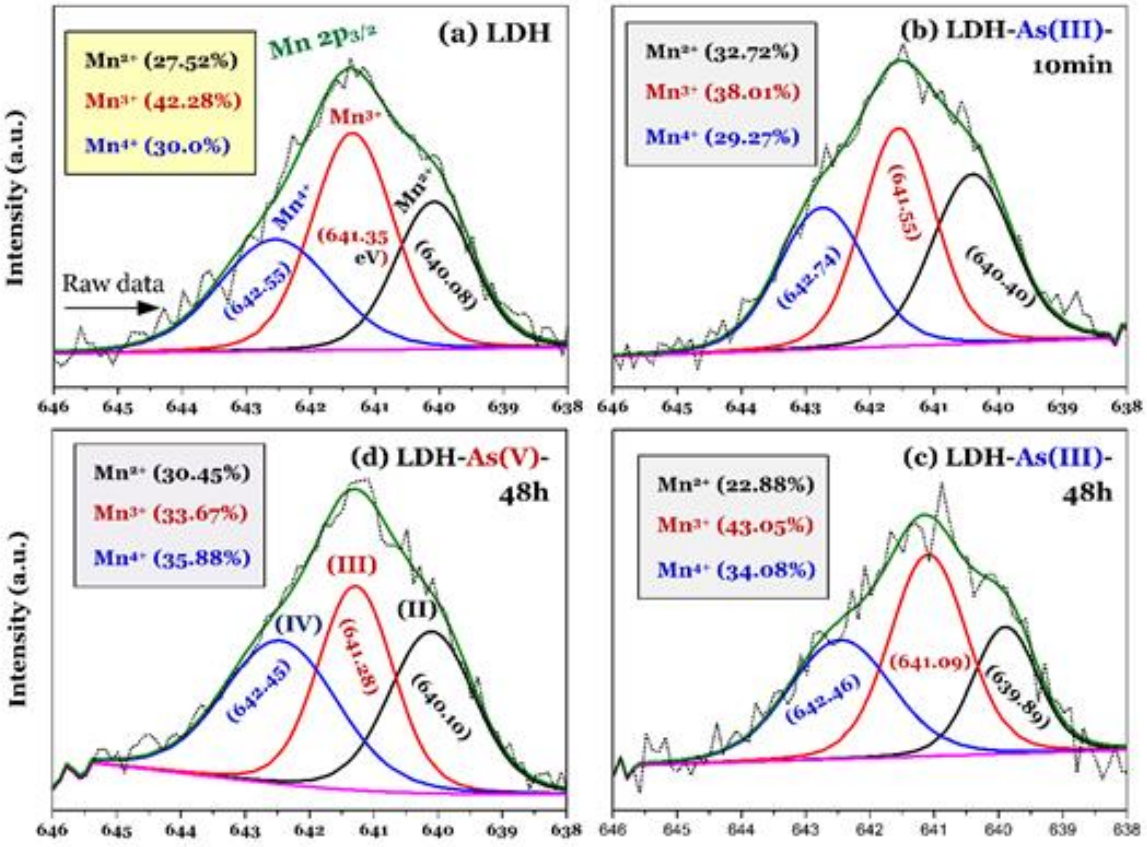

Figure 5.13. The deconvolution of XPS spectra of Mn 2p of Mn/Mg/Fe-LDH before and after adsorption of As(III) (10-min contact time and 48-h contact time) and As(V) (48-h contact time)

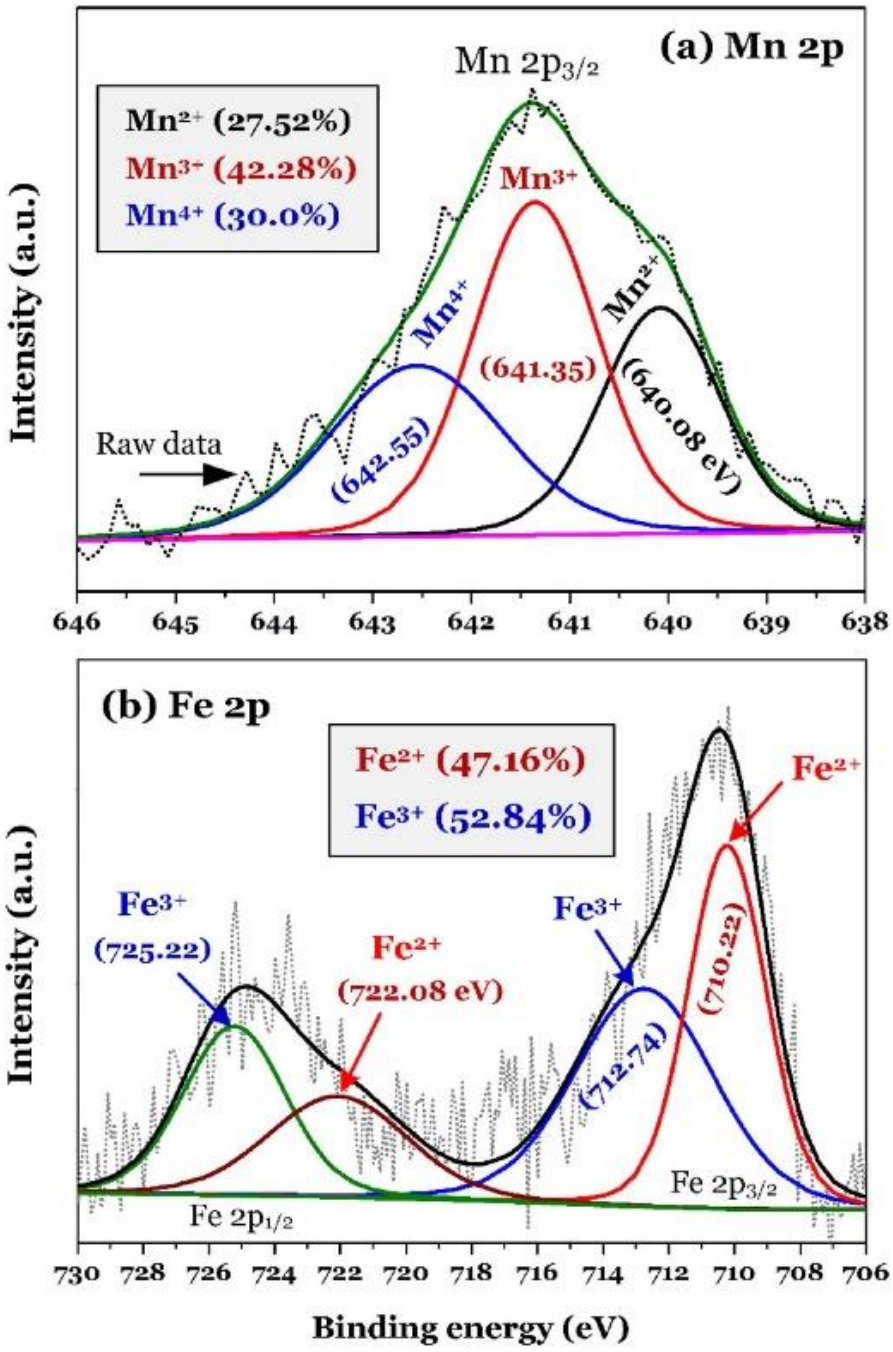

Figure 5.14. High-resolution spectrum of (a) Mn 2p and (b) Fe 2p of Mn/Mg/Fe LDH

(Corresponding data for Mn/Mg/Fe-LDH after adsorption of As(III) for 10 min, As(III) for 48 h, and As(V) 48 h are presented in **Figures 5.13** and **5.16**)

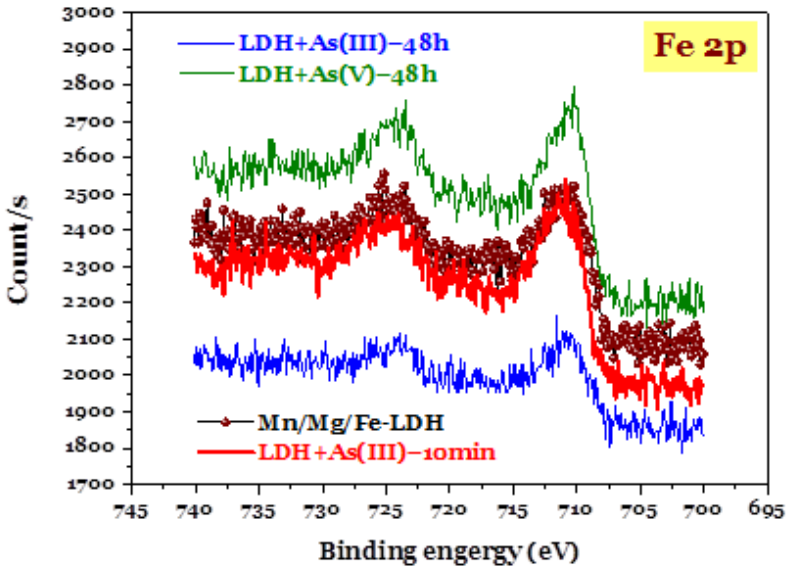

Figure 5.15. Raw XPS spectra of Fe 2p of Mn/Mg/Fe-LDH before and after adsorption of As(III) (10-min contact time and 48-h contact time) and As(V) (48-h contact time)

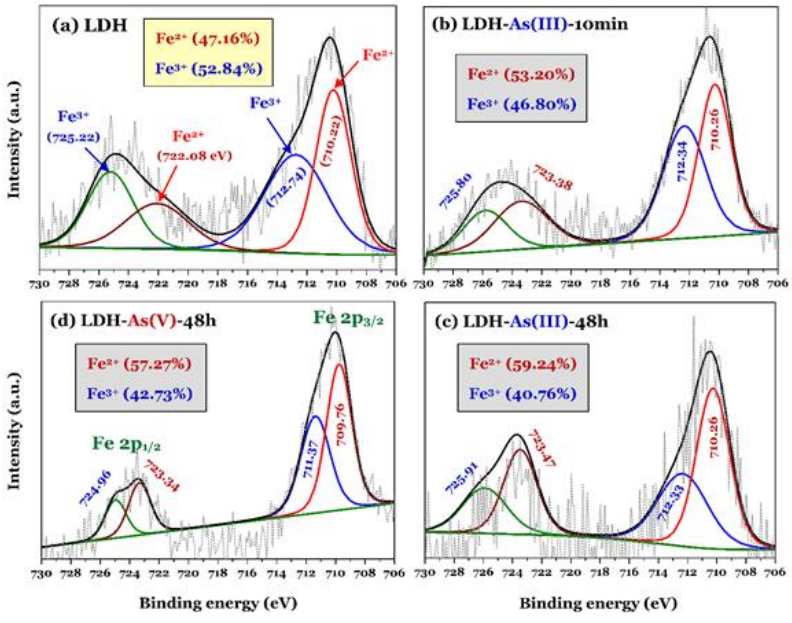

Figure 5.16. The deconvolution of raw XPS spectra of Fe 2p of Mn/Mg/Fe-LDH before and after adsorption of As(III) (10-min contact time and 48-h contact time) and As(V) (48-h contact time)

To verify the oxidation state of Mn in Mn/Mg/Fe-LDH, the narrowed scan of Mn $2p_{3/2}$ was applied based on the recommendations of previous studies (**Figure 5.13a** or **Figure 5.14a**). The oxidation states of Mn^{2+} [in the form of $Mn(OH)_2$ solid], Mn^{3+} [in $Mn(OH)_3$ solid], and Mn^{4+} in MnO_2 solid] were observed at the corresponding BE peaks at 640.08, 641.35, and 642.55 eV, respectively (Mohammadi et al., 2021; Zhou et al., 2021). The percentages of Mn^{2+}, Mn^{3+}, Mn^{4+} in Mn/Mg/Fe-LDH that were calculated based on the area of the corresponding peaks in the core level spectrum of the Mn $2p_{3/2}$ region were 27.52%, 42.28%, and 30.20%, respectively. Similarly, Zhou et al. (2021) concluded that Ni/Mn-LDH contained 57% for Mn^{3+} and 43% for the others (Mn^{2+} and Mn^{4+}) based on the Mn $2p^{3/2}$ data.

The raw XPS spectrum of Fe 2p indicate two BE peaks at 711.02 and 724.38 eV (**Figure 5.15**). Those peaks are typical characteristics for the Fe^{3+} oxidation state in some LDH materials such as Co/Fe-LDH (Wang et al., 2021a; Wang et al., 2021b), Mg/Fe-LDH (Mubarak et al., 2018), and Mg/Zn/Fe (Liu et al., 2019b). The high-resolution Fe 2p XPS spectrum was deconvoluted into four peaks (**Figure 5.14b** or **Figure 5.16**). The result of the detail deconvolution suggests that both Fe^{3+} (52.84%) and Fe^{2+} (47.16%) coexisted in Mn/Mg/Fe-LDH. Similarly, Wang et al. (2021a; b) prepared Co/Fe-LDH from two salts ($CoCl_2$ and $FeCl_3$) and concluded the coexistence of Fe^{3+} and Fe^{2+} in Co/Fe-LDH (based on their XPS data). A similar conclusion was reported by other scholars (Mubarak et al., 2018) for Mg/Fe-LDH. They found that the Fe^{3+}/Fe^{2+} ratio in Mg/Fe-LDH that was obtained based on the relative areas of the Gaussian peaks in the Fe 2p XPS spectrum was 0.34/1 (Mubarak et al., 2018). The presence of Fe^{2+} in Mn/Mg/Fe-LDH might result from some reduction reactions (**Equation 5.2** and **Equation 5.3**) (Haynes, 2014).

$Fe(OH)_3 + e^- \rightleftharpoons Fe(OH)_2 + OH^-$ (E^o_{red} = –0.56 V) **(5.2)**

$Fe^{3+} + e^- \rightleftharpoons Fe^{2+}$ (E^o_{red} = 0.15 V) **(5.3)**

In essence, a reduction–oxidation (redox) reaction is spontaneous if the standard electrode potential for this reaction (E^o_{redox}) is positive and vice versa. Possible redox reactions between Mn^{2+} and Fe^{3+} are expressed as **Equation 5.4** and **5.5** (Haynes, 2014). Considering the sign of E^o_{redox}, it can be concluded that the redox reaction (**Equation 5.5**) occurred spontaneously during the synthesis process of Mn/Mg/Fe-LDH.

$Mn(OH)_2 + Fe(OH)_3 \rightleftharpoons Mn(OH)_3 + Fe(OH)_2$ ($E^o_{redox} = -0.71\ V$) **(5.4)**

$Mn(OH)_2 + Fe^{3+} + OH^- \rightleftharpoons Mn(OH)_3 + Fe^{2+}$ ($E^o_{redox} = 0.621\ V$) **(5.5)**

5.3.1.5. Electrical state of the surface of Mn/Mg/Fe-LDH solution

The change of the external surface charge of Mn/Mg/Fe-LDH with changing solution pH is defined by its pH_{IEP}. **Figure 5.17a** shows that the Mn/Mg/Fe-LDH material had a high pH_{IEP} of 10.15 ± 0.06, which is similar to earlier studies done with Mg/Al-LDH (pH_{IEP}= 10.9) (Li et al., 2009a), in-situ synthesized Mg/Al-LDH (pH_{IEP} = 11.5) (Chao et al., 2018), and Mg/Fe-LDH (pH_{IEP} > 12; its zeta potential at pH 12 = 8.67 mV) (Mubarak et al., 2018). In addition, Chubar et al. (2013) reported that the pH_{IEP} value of Mg/Al-LDH (pH_{IEP} ≈ 9.7) was not affected by the preparation methods (i.e., alkoxide sol–gel method, alkoxide-free sol–gel synthesis, and hydrothermal precipitation). The outcome suggests that Mn/Mg/Fe-LDH exhibited a positive charge on its external surface with solution pH values lower than its pH_{IEP} (**Figure 5.17a**). This is because of the protonation of abundant –OH groups (its pKa ranging from 9.0 to 10) on its external surface (Jiao and Hou, 2007; Li et al., 2009a; Tran et al., 2019). Therefore, it is expected that As(V) anions can be effectively removed from solution by the $–OH_2^+$ groups on the external surface of Mn/Mg/Fe-LDH (also known as electrostatic attraction).

5.3.2. Effect of solution pH on the adsorption process

The effect of different initial solutions pH (2.0–10) on removal efficiency of As(III) and As(V) by Mn/Mg/Fe-LDH for two initials As concentrations (i.e., 3.5 and 55 mg/L) is presented in **Figure 5.17b.** At initial As concentration (*Co*) of ~3.5 mg/L, the removal efficiency of As(III) and As(V) using Mn/Mg/Fe-LDH is nearly similar because Mn/Mg/Fe-LDH exhibited a very high affinity to the As contaminants. An analogous result was reported by Wang and co-workers (2021b) for adsorption of As(III) and As(V) at different Co values (i.e., 5, 10, and 50 mg/L) onto Fe/Mn-C-LDH. Consequently, the influence of different solutions pH on the adsorption process was not clear in a low initial As concentration scenario.

Figure 5.17b shows that the adsorption capacity of Mn/Mg/Fe-LDH at very high initial As concentration (~55 mg/L) dramatically decreased when the solution pH increased from 2.0 to 10. A similar tendency was found for the As(III) and As(V) adsorption onto Mn/Fe-LDH (Otgonjargal et al., 2012), Mg/Fe-LDH (Hong et al., 2014), and α-alanine-intercalated Mg/Fe-LDH (Hong et al., 2014). Under strong acidic conditions (i.e., pH 2.0), the structure of Mn/Mg/Fe-LDH might not be stable (Wang et al., 2021a; Wang et al., 2021b) because it was synthesized through the co-precipitation method at pH 12 (**see Section 5.2.2**). This means that the components (Fe, Mg, and Mn) in its structure were released into the solution (**Table 5.3**).

The released Fe ions might then react with As(III) and As(V) in solution to form precipitates such as such as $FeAsO_4 \cdot 2H_2O$ (Lenoble et al., 2005), $Fe_3(AsO_4)_2 \cdot 8H_2O$, and amorphous ferric As(V) (Tian et al., 2017). In addition, the concentrations of Fe after adsorption of As(III) (0.071 mg/L) and As(V) (0.045 mg/L) were significantly lower than

that of the blank sample (11.25 mg/L; **Table 5.3**), confirming the existence of certain reactions (possible co-precipitation) between Fe and As.

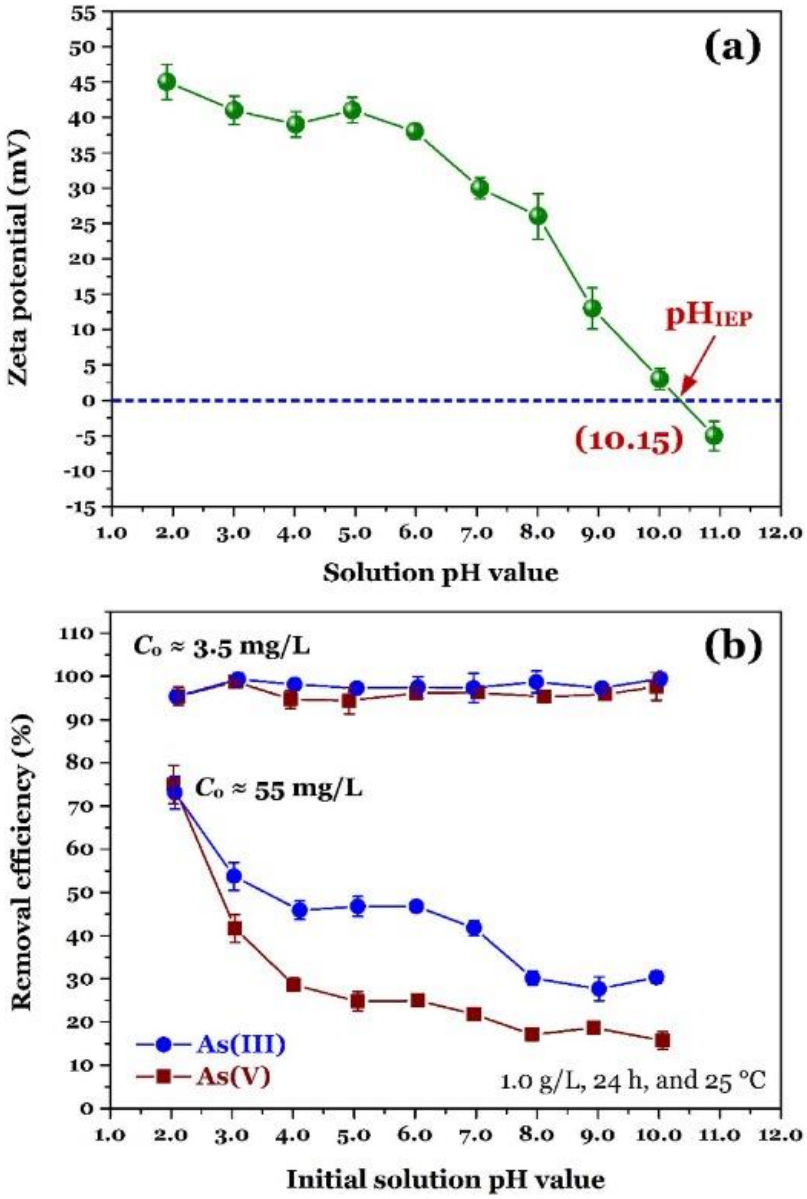

Figure 5.17. Effect of pH solution on (a) the zeta potential of Mg/Mn/Fe-LDH and (b) the adsorption capacity of Mg/Mn/Fe-LDH towards As(V) or As(III) ions

To evaluate the feasibility of reaction between the leached metals and As ions in solution, adsorption and removal studies of As ions from solutions were carried out

at pH 2.0. The concentrations of the leached metals were prepared based on the result in **Table 5.3**. The results (**Table 5.2**) show that a presence of certain reaction between Fe ions and As ions in solution. However, the removal efficiency of As by the metal ions from water was remarkably lower than using the Mn/Mg/Fe-LDH material. For example, the percentages of As(III) and As(V) ions in solution removed by the percentages of Fe^{3+} ions were only 9.17% and 5.16%, respectively. In contrast, the corresponding removal efficacies of As(III) and As(V) by the Mn/Mg/Fe-LDH solid were 80% and 84.8%, respectively (**Table 5.2**). The result suggests that reactions between the leached metals and As ions in solution at pH 2.0 were not a main removal mechanism. In addition, the mass loss of Mn/Mg/Fe-LDH (calculated based on the dry mass) after adsorption at pH 2.0 was only around 5%. This means that the amounts of the metals leached from Mn/Mg/Fe-LDH were not enough to remove effectively As ions from water. Therefore, the highest removal percentage of As(III) or As(V) by Mn/Mg/Fe-LDH (**Figure 5.17b**) at pH 2.0 mainly resulted from the adsorption mechanism of As ions in solution onto the material. In fact, **Figure 5.17a** shows that Mn/Mg/Fe-LDH exhibited the highest positive value of zeta potentials (+45.2 mV; **Figure 5.17a**) at pH 2.0. As a result, electrostatic attraction between the positively charged surface of Mn/Mg/Fe-LDH and As(V) anions in solutions played a critical role in adsorption mechanism.

Although at solution pH 2.0, the removal efficiency was the highest, the structure of Mn/Mg/Fe-LDH was relatively less stable. As well, the removal mechanism was the combination of adsorption and other chemical reactions (i.e., precipitation). For a real-life application the solution pH value often ranges from 6.0 to 8.0 (especially for groundwater; **Section 5.3.11**). Therefore, the subsequent study was conducted with an initial solution pH of 7.0.

Table 5.2. Removal of As from water by different systems using Fe^{3+} ions to remove As, Mn^{3+} ions to remove As, Mg^{3+} ions to remove As, three metal ions (Fe^{3+}, Mn^{2+}, Mg^{2+}) to remove As, and the Mn/Mg/Fe-LDH solid to adsorbing As (≈ 1.0 g/L)

	Before reaction (mg/L)				After reaction (mg/L)				% Removal			
	As	**Fe**	**Mn**	**Mg**	**As**	**Fe**	**Mn**	**Mg**	**As**	**Fe**	**Mn**	**Mg**
1. For adsorbing As (V)												
Two ions (Fe^{3+} and As)	50.50	15.34	—	—	45.87	<0.01	—	—	**9.17**	99.9	—	—
Two ions (Mn^{2+} and As)	50.50	—	139.1	—	50.03	—	132.1	—	**0.93**	—	5.0	—
Two ions (Mg^{2+} and As)	50.50	—	—	54.7	50.32	—	—	54.09	**0.36**	—	—	1.12
Four ions (Fe^{3+}, Mn^{2+}, Mg^{2+}, and As)	50.50	15.34	142.9	55.7	45.33	4.89	133.1	54.82	**10.2**	68.1	6.9	1.58
Mn/Mg/Fe-LDH solid + As ion	50.50	—	—	—	10.08	0.09	48.65	45.39	**80.0**	—	—	—
2. For adsorbing As (III)												
Two ions (Fe^{3+} and As)	46.30	15.34	—	—	43.91	0.0395	—	—	**5.16**	99.7	—	—
Two ions (Mn^{2+} and As)	46.30	—	139.1	—	43.39	—	132.3		**6.29**	—	4.9	—
Two ions (Mg^{2+} and As)	46.30	—	—	54.7	44.83	—	—	54.11	**3.17**	—	—	1.08
Four ions (Fe^{3+}, Mn^{2+}, Mg^{2+}, and As)	46.30	15.34	142.9	56.04	40.15	4.30	131.6	55.71	**13.28**	72.0	7.9	0.59
Mn/Mg/Fe-LDH solid + As ion	46.30	—	—	—	7.05	0.16	47.27	42.7	**84.8**	—	—	—

Note: Experimental conditions: the volume of solution used (100 mL), pH = 2.0, 30 °C, and 24 h

Table 5.3. The effect of solution pH on the structural stability of Mn/Mg/Fe-LDH and the release of metal ions (mg/L) from Mn/Mg/Fe-LDH after an equilibrium adsorption

pH	Distilled water			As(V) solution			As(III) solution		
	Fe	Mn	Mg	Fe	Mn	Mg	Fe	Mn	Mg
2	11.25	150	50.0	0.045	35.8	30.1	0.071	58.5	40.1
3	<0.01	<0.01	11.7	0.045	0.63	8.14	0.048	0.76	8.72
4	<0.01	<0.01	4.96	0.039	0.26	4.22	0.060	0.25	4.36
5	<0.01	<0.01	4.30	0.093	0.33	3.34	0.050	0.31	4.07
6	<0.01	<0.01	3.59	0.050	0.22	3.05	0.057	0.26	3.98
7	<0.01	<0.01	3.91	0.044	0.22	1.79	0.065	0.25	3.40
8	<0.01	<0.01	3.54	0.077	0.14	1.63	0.059	0.15	3.26
9	<0.01	<0.01	3.47	0.065	0.17	1.16	0.056	0.15	2.67
10	<0.01	<0.01	2.63	0.101	0.11	—	0.063	0.051	1.95

Note: The concentrations of metal ions (mg/L) were released from distilled water were denoted as the blank sample (without As adsorption). The limitation (established by the Vietnam national technical regulation on drinking water quality; QCVN 01:2009/BYT) for both total Fe (Fe^{2+} and Fe^{3+}) and Mn in drinking water was 0.3 mg/L.

5.3.3. Effect of foreign anions on the adsorption process of As(III) or As(V)

The (inhibitory) effect of the presence of foreign anions on the As removal process was explored by using five anions (Cl^-, SO_4^{2-}, CO_3^{2-}, SiO_3^{2-}, and HPO_4^{2-}) at two initial concentrations (10 mM and 100 mM). Results indicate that the strong competition between foreign anions and As ions in aqueous solution led to a remarkable decline in the efficiency of removing As(III) and As(V) (**Figure 5.18**).

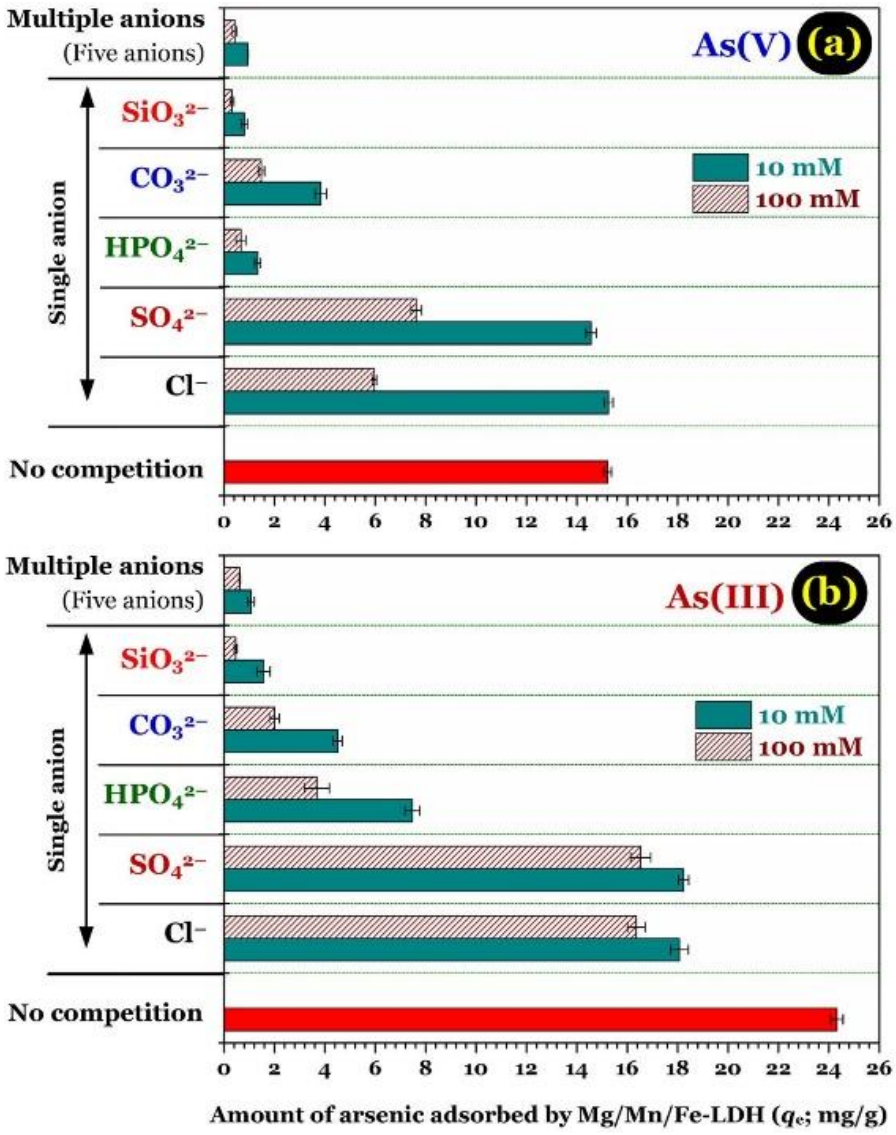

Figure 5.18. Effect of co-existing anions (at two concentrations of 10 mM and 100 mM) on the capacity of As adsorption by Mn/Mg/Fe-LDH

(Experimental conditions: $C_o \approx 50$ mg/L for As(III) or As(V), pH 7.0, 25 °C, and 24 h)

In general, the adsorption capacity of Mn/Mg/Fe-LDH followed the order of no competition (absence of foreign anions) > chloride (the presence of Cl^- anion) > sulphate (SO_4^{2-}) > monohydrogen phosphate (HPO_4^{2-}) > carbonate (CO_3^{2-}) > silicate (SiO_3^{2-}) >

five foreign anions (Cl^-, SO_4^{2-}, CO_3^{2-}, SiO_3^{2-}, and HPO_4^{2-}). An identical adsorption tendency has been reported in the literature (Hong et al., 2014; Lu et al., 2018).

Among coexisting single anions, the presence of Cl^- anions has the lowest inhibitory effect on the removal efficiency of As ions by Mn/Mg/Fe-LDH. This is because of chloride is monovalent anion with its lower ionic charge density than As(V) anions and lacking tetrahedral structure. In contrast, SiO_3^{2-} and CO_3^{2-} were the strongest competing anions. As discussed in **Section 5.3.2**, CO_3^{2-} was the host anions in the interlayer region of Mn/Mg/Fe-LDH; therefore, it was more favorable to this region than guest As(V) anions. In addition, SiO_3^{2-} and $CO3^{2-}$ exhibited a similarity in their structure and chemical behavior because they are the same group in the periodic table. Therefore, SiO_3^{2-} and CO_3^{2-} had a stronger competitive adsorption than As(V) anions in the interlayer region. For competitor anion (HPO_4^{2-}), monohydrogen phosphate and As(V) exhibit similar tetrahedral structures and are listed in the same group in the periodic table (Hong et al., 2014; Lu et al., 2018). Therefore, they have the same adsorption competition to the exchange sites in the interlayer region of Mn/Mg/Fe-LDH (Lu et al., 2018).

The results suggest an integral role of anion exchange in the adsorption process of As ions onto the interlayer region of Mn/Mg/Fe-LDH. As(V) anions in solution are easily exchanged with the host anions in the interlayer region of Mn/Mg/Fe-LDH. In contrast, As(III) ions might be firstly oxidized into As(V) anions. Subsequently, oxidized As(V) anions were exchanged with the host anions present in the Mn/Mg/Fe-LDH material.

5.3.4. Adsorption kinetics

The adsorption kinetics results are provided in **Figure 5.19.** The reaction between the Mn/Mg/Fe-LDH and the adsorbate [As(III) or As(V)] remarkably increased within the first contact period of 60 min, and then it proceeded at a relatively slower rate before

achieving equilibrium at approximately 20 h. Other scholars also reported that the adsorption process of As ions [As(III) and As(V)] onto Mn/Fe-LDH and α-alanine intercalated Mg/Fe-LDH reached an equilibrium within 30 h (Otgonjargal et al., 2012) and 24 h (Hong et al., 2014), respectively. In this work, four common kinetic models, namely pseudo-first-order (PFO), pseudo-second-order (PSO), Avrami and Elovich models were applied to describe the experimental data of adsorption with time. The relevant information concerning the non-linearized form of those models is given in **Section 2.6.3.1**.

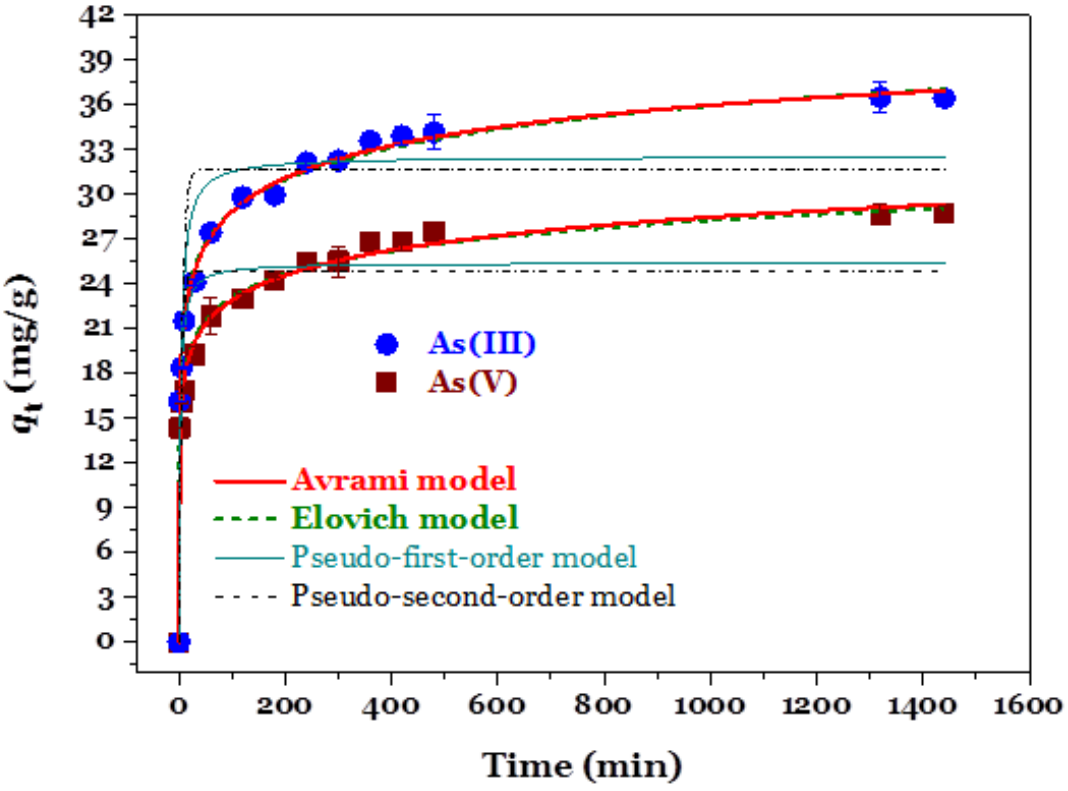

Figure 5.19. Adsorption kinetics for As(V) and As(III) adsorption onto Mg/Mn/Fe-LDH

(Experimental conditions: 0.5 g/L, pH 7.0, 25 °C, and Co ~ 70 mg/L)

Table 5.4. Kinetic parameters for As(V) and As(III) uptake by Mg/Mn/Fe-LDH

	Unit	Adsorbate	
		As(V)	As(III)
1. PFO model			
q_e	mg/g	24.9	31.7
k_1	1/min	0.233	0.174
R^2	—	0.726	0.774
χ^2	—	15.8	21.8
2. PSO model			
q_e	mg/g	25.4	32.5
k_2	g/(mg×min)	0.019	0.009
R^2	—	0.837	0.865
χ^2	—	9.37	13.03
3. Avrami model			
q_e	mg/g	41.0	44.1
k_{AV}	1/min	0.003	0.013
$t_{1/2}$	min	231	53.3
n_{AV}	—	0.160	0.202
R^2	—	0.992	0.996
χ^2	—	0.438	0.395
4. Elovich model			
α	mg/(g×min)	707	378
β	mg/g	0.448	0.326
R^2	—	0.990	0.994
χ^2	—	0.576	0.561

Table 5.4 provides the values of kinetic parameters of the selected kinetic models. On the basis of the statistics (R^2 and χ^2), the Avrami and Elovich models described the experimental data of time-dependent adsorption (adsorption kinetics) better than the PSO and PFO models. The adsorption rate constant (k_{AV}) of the Avrami model indicates that the adsorption process of As(III) (0.013/min) onto Mn/Mg/Fe-LDH was faster than that of As(V) (0.003/min). A similar conclusion was reported by (Wang et al., 2021a; Wang et al., 2021b). However, at the beginning the adsorption process of As(V) occurred more rapidly than that of As(III) because the initial adsorption rate constant (α) of As(V) adsorption [707 mg/(g×min)] was overwhelmingly higher than that of As(III) one [378 mg/(g×min)]. This might be because As(III) ions in solution were oxidized into As(V) when they came into contact with the Mn/Mg/Fe-LDH material first. Subsequently, the oxidized As(V) ions and As(III) ions in solution were removed from solution.

5.3.5. Adsorption isotherm

Adsorption isotherms for As(V) and As(III) by Mn/Mg/Fe-LDH at different solution temperatures are provided in **Figure 5.20**. The isotherms are categorized as H-shaped (Lyklema, 1995). Therefore, Mn/Mg/Fe-LDH can effectively remove both As(V) and As(III) from water even at small initial concentrations. Yang et al. (2005) also reported that calcined and uncalcined LDH materials can effectively eliminate As ions from aqueous water under trace levels. Five adsorption isotherm models are applied to describe the experimental data of adsorption equilibrium. They (the Langmuir, Freundlich, Langmuir–Freundlich, Redlich–Peterson, and Khan models) are introduced in **Section 2.6.3.2**.

According to higher R^2 and lower χ^2 (**Table 5.5**), the three-parameter models of adsorption isotherm (i.e., the Langmuir–Freundlich, Redlich–Peterson, and Khan models)

well fitted to the experimental data of adsorption equilibrium compared to the two-parameter models (Langmuir and Freundlich). Although the parameters (Q_{LF}, Q_{Khan}, and Q_{max}) of the models (Langmuir–Freundlich, Khan, and Langmuir, respectively) can provide information on the maximum adsorption capacity of LDH to As(III) and As(V), the parameter Q_{max} of the Langmuir model is more consistent with the experimental data in **Figure 5.20**. In fact, the adsorption capacity of As(V) and As(III) onto Mn/Mg/Fe-LDH at 25 °C was higher than at 50 °C and 7 °C (**Figure 5.20**). Therefore, the values of Q_{LF}, Q_{Khan}, and Q_{max} should follow the order of 25 °C > 50 °C > 7 °C to be consistent with the experimental data in **Figure 5.20**. However, the Q_{LF} value followed the decreasing order: 25 °C > 7 °C > 50 °C, while the Q_{Khan} follows the order of 50 °C > 25 °C > 7 °C for the As(V) adsorption. Therefore, the adsorption capacity of Mn/Mg/Fe-LDH towards As(III) or As(V) was reflected through the Q_{max} of the Langmuir model. Thus, the parameter Q_{max} is used for discussion and comparison.

As shown in **Table 5.5**, Mn/Mg/Fe-LDH exhibited a higher affinity of As(III) than As(V) in solution. For example, the Q_{max} value for As(III) adsorption (56.1 mg/g) by Mn/Mg/Fe-LDH at 25 °C was higher than that for As(V) adsorption (32.2 mg/g). This means that Mn/Mg/Fe-LDH exhibited a high affinity for As(III) compared to As(V). This finding was similar to that of other researchers (Hong et al., 2014; Kong et al., 2014; Bai et al., 2016; Guo et al., 2017; Wang et al., 2021a; Wang et al., 2021b) on the adsorption of As(III) and As(V) onto some similar LDH-based materials. However, an opposite tendency was reported by Choong et al. (2021) using Mg/Fe-LDH embedded by polyacrylamide and polyvinyl alcohol and (Bagherifam et al., 2014) using SO_4-intercalated Zn/Al-LDH. If anion exchange plays an important role in the adsorption process, the amount of As(V) anions adsorbed by Mn/Mg/Fe-LDH (exchanged with the

host anions in its interlayer region) would have been higher than that of As(III) ions. This is because As(III) might be partly oxidized into As(V) but not totally. Therefore, it was evident that other dominant adsorption mechanisms (i.e., inner-sphere complexation) existed, not just anion exchange in adsorbing As(III) onto Mn/Mg/Fe-LDH.

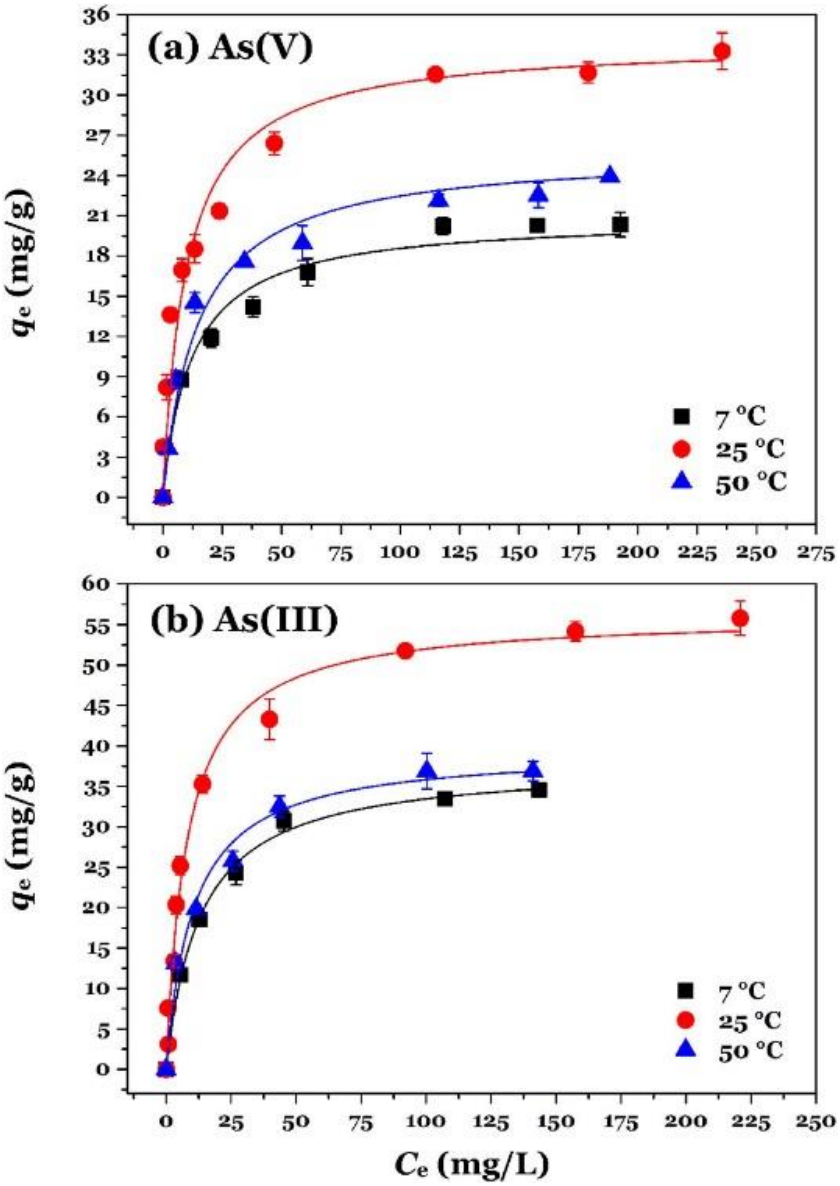

Figure 5.20. Adsorption isotherm of (a) As(V) and (b) As(III) onto Mn/Mg/Fe-LDH at different temperatures

(Experimental conditions: 1.0 g/L, C_o = 0–270 mg/L, 24 h, and 25 °C)

Table 5.5. Isotherm adsorption parameters for As(V) and As(III) uptake onto Mn/Mg/Fe-LDH

	Unit	As(V)			As(III)		
		7 °C	25 °C	50 °C	7 °C	25 °C	50 °C
1. Langmuir model							
Q_{max}	mg/g	21.9	32.2	24.0	37.8	56.1	39.6
K_L	L/mg	0.063	0.138	0.096	0.076	0.126	0.096
R^2	—	0.981	0.954	0.990	0.996	0.988	0.984
χ^2	—	0.964	6.096	0.790	0.682	5.230	3.066
2. Freundlich model							
K_F	$(mg/g)/(mg/L)^n$	5.61	9.89	5.96	9.32	13.3	10.8
n_F	—	0.255	0.232	0.272	0.275	0.283	0.261
R^2	—	0.987	0.977	0.949	0.959	0.927	0.974
χ^2	—	0.662	3.096	3.838	6.591	32.065	4.891
3. Redlich–Peterson model							
K_{RP}	L/g	3.20	16.3	2.90	2.88	8.32	6.20
a_{RP}	$(mg/L)^{-g}$	0.345	1.192	0.172	0.076	0.195	0.279
g	—	0.838	0.832	0.930	1.000	0.945	0.883
R^2	—	0.991	0.986	0.992	0.995	0.989	0.988
χ^2	—	0.460	1.792	0.607	0.854	4.695	2.239
4. Langmuir-Freundlich model							
Q_{LF}	mg/g	29.1	45.4	25.0	38.1	58.0	46.4
K_{LF}	L/mg	0.027	0.038	0.086	0.075	0.112	0.062
n_{LF}	—	0.568	0.474	0.882	0.977	0.895	0.686
R^2	—	0.993	0.993	0.989	0.995	0.988	0.991
χ^2	—	0.356	0.989	0.827	0.845	5.395	1.630
5. Khan model							
Q_K	mg/g	10.7	13.4	17.8	39.4	44.3	24.4
K_K	L/mg	0.248	0.897	0.156	0.072	0.181	0.227
n_K	—	0.819	0.826	0.911	1.016	0.931	0.865
R^2	—	0.990	0.985	0.993	0.995	0.990	0.987
χ^2	—	0.485	1.937	0.560	0.844	4.589	2.400

Note: Average Q_{max} ± SE values: 37.8 ± 0.80, 56.1 ± 1.47, and 39.6 ± 1.58.

The maximum adsorption capacity of Mg/Fe-LDH to As(III) and As(V) ions is compared to some other materials investigated in the literature (**Table 5.6**). As expected, the prepared Mn/Mg/Fe-LDH material (Q_{max} = 56.1 mg/g) exhibited higher adsorption capacity of toxic As(III) ions than others such as the composite of Fe/Mn-LDH and carbon (36.1 mg/g) (Wang et al., 2021a; Wang et al., 2021b), Zn/Al-LDH (34.2 mg/g) (Bagherifam et al., 2014), aluminum-enriched biochar prepared from Tetra Paks (24.2 mg/g) (Ding et al., 2018), alumina composite modified activated carbon (14.3 mg/g), tire rubber alumina composite (13.51 mg/g) (Karmacharya et al., 2016), Fe/Mn modified biochar (8.25 mg/g) (Lin et al., 2017), natural laterite (0.52 mg/g) of this study (**Chapter 3**).

Furthermore, under the same experimental conditions (i.e., ~50 mg/L, 30 °C, pH = 7.0, 1.0 g/L, and 24 h), the adsorption capacity of Mn/Mg/Fe-LDH towards As(III) or As(V) ions (21.3 or 11.2 mg/g; **Figure 5.21**) exceeded commercial activated carbon (0.205 or 0.309 mg/g, respectively). Therefore, it can be concluded that Mn/Mg/Fe-LDH was a promising material for the remediation of As-contaminated water.

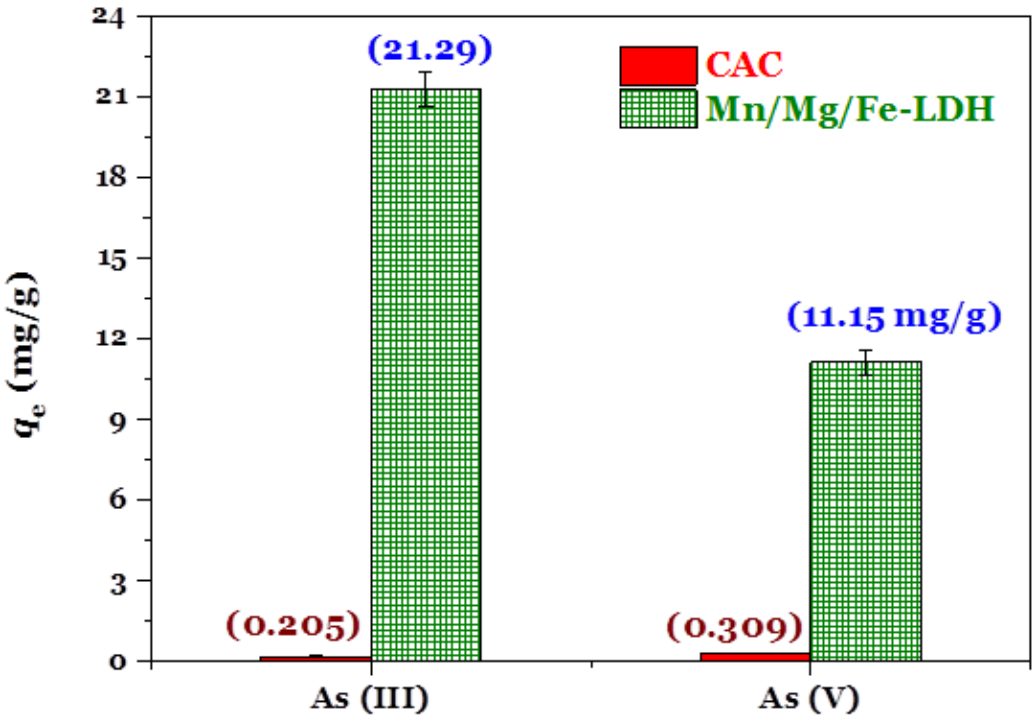

Figure 5.21. Comparison of the adsorption capacity of As ions between commercial activated carbon (CAC) and Mn/Mg/Fe-LDH

(Experimental conditions: Co = 46.1 mg/g for As (III) and 50.5 mg/g for As (V), 24 h, pH ≈ 7.0, 30 °C, and m/V ≈ 1.0 g/L)

Table 5.6. The Langmuir maximum adsorption capacity (Q_{max}) of As(III) and As(V) from water environment by the prepared Mn/Mg/Fe-LDH material and other materials in the literature

	Adsorption condition					Q_{max} (mg/g)		Ref.
	m/*V* (g/L)	pH	T (°C)	t (h)	C_o (mg/L)	As(III)	As(V)	
Mn/Mg/Fe-LDH	1.0	7.0	25	24	4–270	**56.1**	**32.2**	**This study**
Calcined Mg/Zn/Fe-LDH	0.5	6.0	30	12	1–100	54.36	72.16	Liu et al. (2019b)
Composite (Fe/Mn-LDH + carbon)	1.4	7.0	25	2	5–100	36.1	22.2	Wang et al. (2021b)
Mg/Fe-LDH	1.0	7.5	Room	2	1–450	—	30.8	Hudcová et al. (2017)
Mg/Al-LDH	0.12	4.2–5.4	25	120	20–200	—	4.55	Yang et al. (2005)
Calcined Mg/Al-LDH	0.12	4.2–5.4	25	120	20–200	—	5.61	Yang et al. (2005)
Mg/Al-LDH	5.0	—	10	24	0.15–150	—	76.9	Rahman et al. (2017)
Calcined Mg/Al-LDH	0.35	7.0	25	24	0–400	—	216	Yu et al. (2012)
Calcined Mg/Fe-LDH(400 °C)	1.0	7.0	25	10	—	—	50.2	Kang et al. (2013)
Mg/Al-LDH	0.5	6.0	25	48	—	—	44.7	Wu et al. (2013)
Zn/Al-LDH	2.0	—	—	24	0.3–1.5	34.2	47.4	Bagherifam et al. (2014)
Mg/Al-LDH	0.5	6.0	25	48	—	—	88.3	Wu et al. (2013)
Uncalcined Zn/Fe-LDH	0.2	7.0	25	—	2–100	—	151	Lu et al. (2015)
Uncalcined Mg/Fe -LDH	—	6.0	20	24	30–750	—	195	Caporale et al. (2011)
MnO_2	1.6	—	—	—	3–150	9.75	7.5	Lenoble et al. (2004)

	Adsorption condition					Q_{max} (mg/g)		Ref.
	m/V (g/L)	pH	T (°C)	t (h)	C_o (mg/L)	As(III)	As(V)	
Corn stem	1.0	7.0	25	24	0.2–50	2.89	—	Lin et al. (2017)
Perrilla leaf-biochar	1.0	7.0	20	2	0.05 –7.0	11.0	7.21	Niazi et al. (2018)
Tetra paks-biochar	1.0	—	22	24	5–1000	24.2	33.2	Ding et al. (2018)
Fe/Mn modified biochar	1.0	7.0	25	24	0.2–50	8.25	—	Lin et al. (2017)
Iron-loaded walnut shell	1.0	7.0	30	24	0.1–5	—	1.24	Duan et al. (2017)
Iron oxide amended rice husk char	0.4	6.9	—	—	0.1–2.5	—	1.46	Cope et al. (2014)
GACs	0.1–0.8	6.0	25	24	0.1	—	1.01	Kalaruban et al. (2019)
Fe-loaded IAC	0.01–0.6	3.0	25	24	4.5	—	2.02	Tuna et al. (2013)
Fe(III)-loaded IAC	0.01–0.6	3.0	25	24	4.5	—	3.01	Tuna et al. (2013)
GAC-Fe	0.1–0.8	6.0	25	24	0.1	—	1.43	Kalaruban et al. (2019)
Fe-GACs	2.5	6.9	25	48	—	—	1.95	Chang et al. (2010)
Zeolite	10	5.5	25	3	1–450	—	0.32	Pizarro et al. (2021)
Iron–manganese-modified zeolite-rich tuffs	10	6.5	18	24	0.05–2	0.06	0.10	Jiménez-Cedillo et al. (2011)
Fe-exchanged natural zeolite	20	—	—	24	0.1–20	0.10	0.05	Li et al. (2011)
Nanomagnetite-zeolite composite	10	5.5	25	3	1–450	—	6.21	Pizarro et al. (2021)

5.3.6. Adsorption thermodynamics

The effect of solution temperatures on the adsorption process was investigated at 7 °C, 25 °C, and 50 °C (**Figure 5.20**). Results indicate that an increase in temperature from 7 °C to 25 °C increased the amounts of As(V) and As(III) removed from solution (adsorbed onto LDH). However, a further rise to 50 °C caused a significant reduction in the amount of As(V) and As(III) removed. This might be due to the desorption phenomena occurring at the high temperature of 50 °C. The thermodynamic parameters ($\Delta G°$, $\Delta H°$, and $\Delta S°$) of the As adsorption by Mn/Mg/Fe-LDH are computed using the van't Hoff equation (**Equations 3.5**–**3.8**). The relevant information of van't Hoff equation were provided in **Section 3.3.7**.

Table 5.7 shows the thermodynamics parameters for the adsorption process (7 °C, 25 °C, and 50° C) obtained based on the equilibrium constant of the adsorption isotherm models (K_L, K_{LF}, and K_{Khan}). Because the R^2 value of the van't Hoff equation is very low (**Table 5.7**), the $\Delta H°$ and $\Delta S°$ parameters cannot be obtained for whole adsorption process. **Table 5.8** provides the thermodynamics parameters calculated at two ranges of temperatures: 7 °C and 25 °C (280–298 K); and 25 °C and 50 °C (298–323 K). Of the three equilibrium constants, only the Langmuir constant K_L was suitable for application as $K^{o}_{\text{Equilibrium}}$ because the sign of $\Delta H°$ is consistent with the experimental data depicted in **Figure 5.20**. For example, the adsorption capacity of Mn/Mg/Fe-LDH towards As(V) and As(III) decreased when temperature increased from 25 °C to 50 °C; therefore, $\Delta H°$ must be negative. In this study, standard enthalpy change ($\Delta H°$) was calculated for each two-temperature using **Equation 4.1,** in **Section 4.3.5,** and standard entropy change ($\Delta S°$) was computed from **Equation 3.6,** in **Section 3.3.7.**

Table 5.7. Thermodynamic parameters [ΔH° and ΔS°; kJ/mol and J/(mol×K)] of the As(III) or As(V) adsorption by Mg/Mn/Fe-LDH at all operation temperatures

	Adsorption of As(V)					Adsorption of As(III)				
	$K_{Equilibrium}$	van't Hoff equation	$\Delta G°$	$\Delta H°$	$\Delta S°$	$K_{Equilibrium}$	van't Hoff equation	$\Delta G°$	$\Delta H°$	$\Delta S°$
1. Based on the Langmuir constant (K_L)										
280 K	2369	y = –809.8x + 10.88	**–18.1**	6.73	90.4	5713	–426.4x + 10.32	**–20.1**	3.54	85.7
298 K	5161	R^2 = 0.2446	**–21.2**			9428	R^2 = 0.1639	**–22.7**		
323 K	3610		**–22.0**			7171		**–23.8**		
2. Based on the Langmuir-Freundlich constant (K_{L-F})										
280 K	2809	y = 446.6x + 6.52	–18.5	–3.71	54.2	2046	y = –2425x + 16.2	–17.7	20.15	134.8
298 K	4191	R^2 = 0.1273	–20.7			2875	R^2 = 0.9695	–19.7		
323 K	2340		–20.8			6409		–23.5		
3. Based on the Khan constant (K_{Khan})										
280 K	2680	y = –2374x + 16.52	–18.4	19.73	137.3	18604	y = 1168x + 6.201	–22.9	-9.71	51.5
298 K	6789	R^2 = 0.8535	–21.8			67176	R^2 = 0.0944	–27.5		
323 K	8494		–24.3			11705		–25.1		

Note: The unit of $\Delta G°$ (kJ/mol), $\Delta H°$ (kJ/mol), and ΔS°[J/(mol×K)

The results (**Table 5.7**) indicate that the adsorption process of As ions by Mn/Mg/Fe-LDH occurred favorably because of the negative values of $-\Delta G°$ (calculated based on the Langmuir constant, for example, $\Delta G°$ for: As(V) adsorption (–18.1 kJ/mol at 280 K, –21.2 kJ/mol at 298 K, and –22.0 at 323 K); and As(III) adsorption (–20.1 kJ/mol at 280 K, –22.7 kJ/mol at 298 K, and –23.8 kJ/mol at 323 K).

Table 5.8. Thermodynamic parameters [ΔH° and ΔS°; kJ/mol and J/(mol×K)] of the As(III) or As(V) adsorption by Mn/Mg/Fe-LDH at two operation temperatures

Temperature	As(III)		As(V)	
	$\Delta H°$	$\Delta S°$	$\Delta H°$	$\Delta S°$
1. Based on K_L of the Langmuir model				
280–298 K	19.3	141	29.9	172
298–323 K	–8.75	46.7	–11.44	32.3
2. Based on K_{LF} the Langmuir–Freundlich model				
280–298 K	13.1	110	15.41	121
298–323 K	25.7	152	–18.64	6.75
3. Based on K_K the Khan model				
280–298 K	49.5	258	35.81	194
298–323 K	–55.9	–95.2	7.17	97.4

As shown in **Table 5.8**, the adsorption process of As(V) onto Mn/Mg/Fe-LDH was endothermic within the 280-298 K temperature range ($\Delta H°$ = +29.9 kJ/mol) and exothermic within 298 K and 323 K ($\Delta H°$ = –11.4 kJ/mol). A similar tendency was observed for As(III) adsorption that was $\Delta H°$ = +19.3 kJ/mol (280–298 K) and $\Delta H°$ = –8.75 kJ/mol (298–323K). Furthermore, the positive values of $\Delta S°$ suggest that the

organization of As at the solid/liquid interface during the process of As(III) and As(V) adsorption become more random. A positive value of $\Delta S°$ was reported for the adsorption of As(III) and As(V) onto Mn/Fe-LDH (Otgonjargal et al., 2012).

5.3.7. Desorption study

Different solvents (Na_2CO_3, NaCl, EDTA, NaOH, deionized water adjusted to pH 12, and HCl) were used to examine the desorption efficiency of As from the laden Mn/Mg/Fe-LDH. The result demonstrated that the desorption efficiency of both As(III) and As(V) was negligible (lower than 1%) for all desorbing agents used (**Table 5.9**), suggesting that the adsorption was highly irreversible. Subsequently, reusing Mn/Mg/Fe-LDH samples after adsorption was not feasible. In contrast, Goh et al. (2009) found that the adsorption process of As(V) by nitrate-intercalated Mg/Al-LDH was reversible, with the desorption efficiency being 68.3% or 76.6% (using 0.1 M NaOH or Na_2CO_3, respectively). High desorption efficiency resulted from the reversible adsorption mechanism that was anion exchange between As(V) anions and the host NO_3^- anions in its interlayer region (Goh et al., 2009).

Table 5.9. Desorption efficiency of As(III) or As(V) from laden Mg/Mn/Fe-LDH

Desorbing agent	Concentration	Desorption efficiency (%)	
		As(V)	As(III)
Na_2CO_3	0.2 M	0.05	0.10
NaCl	0.2 M	0.11	0.18
EDTA	0.2 M	0.19	0.41
HCl	0.2 M	0.43	0.67
NaOH	0.2 M	0.55	0.77
Pure water (pH 12)	—	0.35	0.44

5.3.8. Leaching test after the adsorption process

The stability of synthesized Mn/Mg/Fe-LDH at different pH solutions was evaluated through the leaching test. Because the pH value of drinking water often ranges from 6.0 to 8.0, the data obtained from this pH range were used for discussion. **Table 5.3**'s results show that the amount of Fe and Mn leached from Mn/Mg/Fe-LDH after adsorption of As(V) and As(III) was smaller than that established by the Vietnamese government's national technical regulation on drinking water quality (<0.3 mg/L for total Fe or Mn). Magnesium ions are necessary for good human health. However, too high a level of Mg (10–100 mg/L) in drinking water can pose serious health risks such as heart disease (Rosanoff, 2013). The Mg concentrations after the adsorption process ranged from 1.79 to 3.98 mg/L (**Table 5.3**). Therefore, the concentrations of Mg, Mn, Fe ions leached from the Mn/Mg/Fe-LDH after adsorption are in the safe range limit for drinking water.

5.3.9. Possible adsorption mechanism of soluble As(V) oxyanions by Mn/Mg/Fe-LDH

The adsorption mechanism of As(V) oxyanions by Mn/Mg/Fe-LDH was discussed at pH 7.0. Under neutral pH, inorganic As(V) species exist as predominantly monovalent $H_2As^VO_4^-$ anion and divalent $HAs^VO_4^{2-}$ anion (**Figure 2.2**).

5.3.9.1. Reduction of As(V) to As(III) by Mn/Mg/Fe-LDH

An important question is whether (1) As(V) was reduced into As(III) by LDH-based materials and (2) the As(V) and reduced As(III) ions are adsorbed onto the materials. To confirm the reduction phenomenon, the speciation of As present in the As(V)-laden LDH materials is confirmed by relevant techniques: X-ray absorption near edge structure (XANES) and XPS. It is hypothesized that the presence of As(V) in the LDH materials

does not destroy their unique layer structure. This means that the XRD patterns of LDH solids before and after adsorption of As(V) are nearly the same (the original layer structure of LDH is preserved). In this case, the (003) plane is still detected in the As(V)-laden LDH samples.

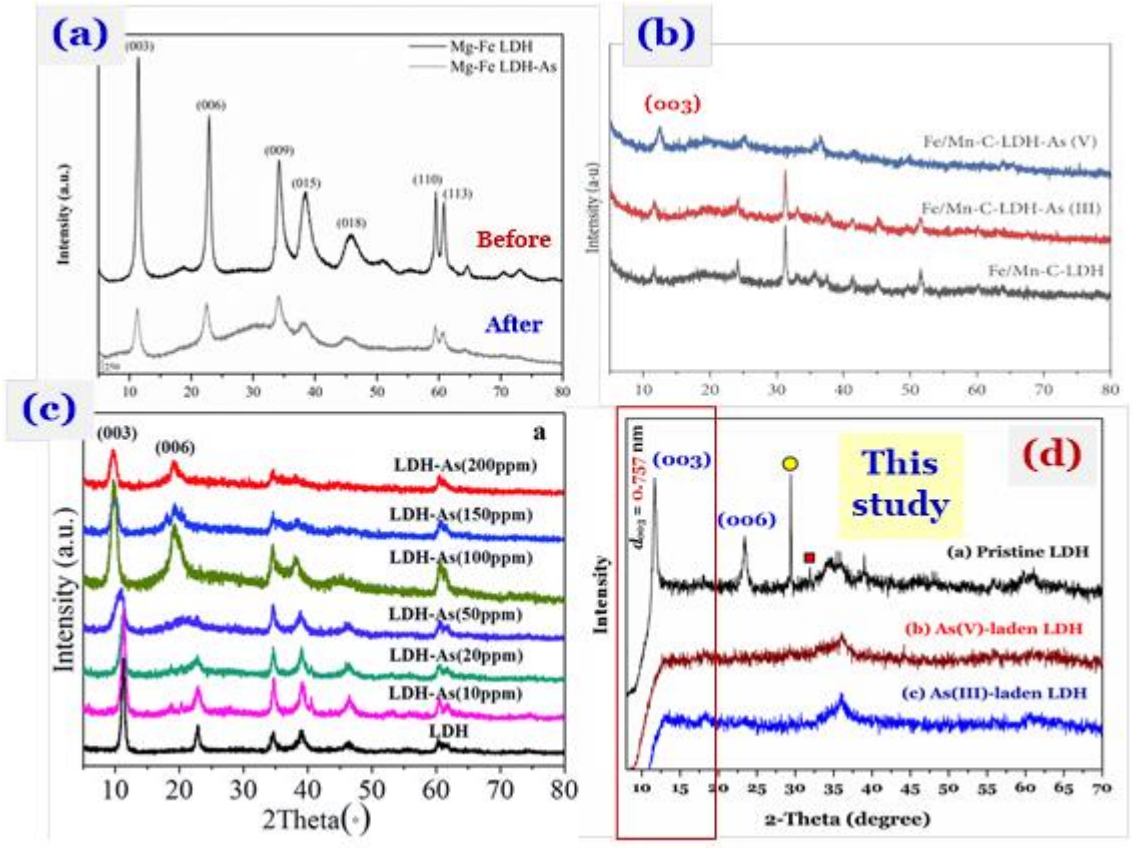

Figure 5.22. XRD patterns of the materials before and after adsorption of As(V): (a) Mg/Fe-LDH (Hudcová et al., 2017), (b) composite of Fe/Mn and carbon

For example, Wang et al. (2021a, b) applied XPS to identify the reduction process of As(V) by the composite of Fe/Mn-LDH and bamboo carbon. They found that only As(V) speciation existed in the composite. The As 3d spectrum of the laden composite indicates one peak at 44.32 eV. The original layer structure of the material (XRD data)

was still maintained after adsorption (**Figure 5.22b**). The results suggest that As(V) was not reduced to As(III) during the adsorption process. A similar conclusion was obtained for adsorption As(V) by Mg/Fe-LDH (Hudcová et al., 2017), Mg/Al-LDH (Huang et al., 2015), Cl-intercalated Mg/Fe-LDH (Guo et al., 2017), NO_3-intercalated Mg/Al-LDH (Goh et al., 2009), Mg/Fe-LDH embedded with polymers (Choong et al., 2021), and SO4-intercalated Zn/Al-LDH (Bagherifam et al., 2014).

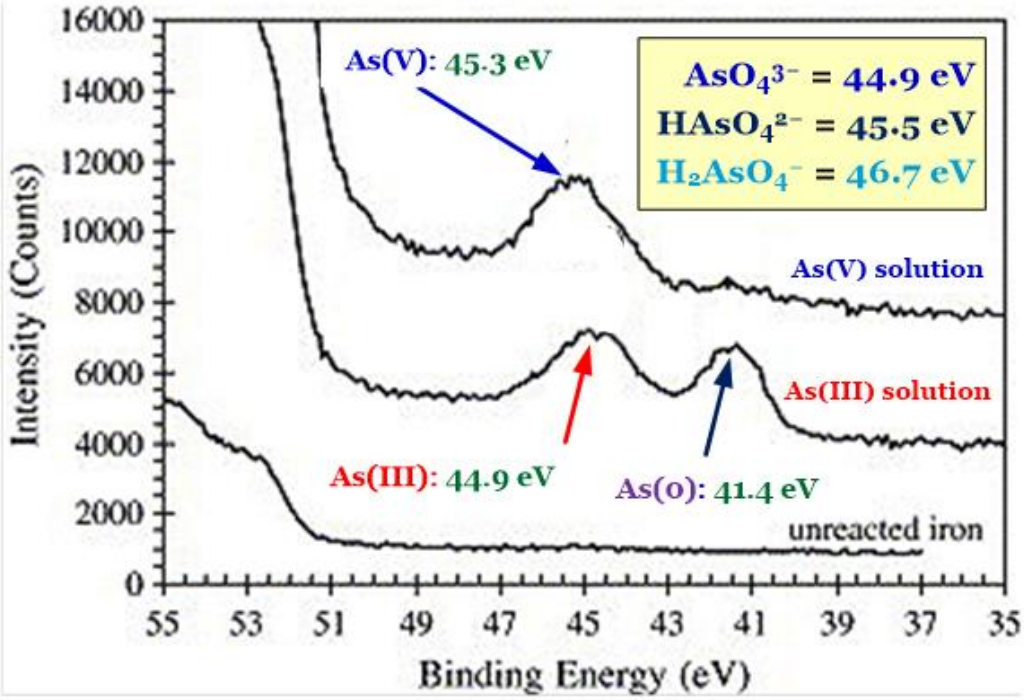

Figure 5.23. High-resolution XPS spectra of the iron coupons in the range of the As 3d photoelectron peak (Bang et al., 2005)

Similarly, Wang et al. (2009) applied (XANES) to identify this reduction process. Their results on the comparison on XANES spectra of As(III) standard, As(V) standard, and As(V)-laden Mg/Al-LDH indicated that As(V) was not reduced into As(III) following the process of As(V) adsorption by Mg/Al-LDH. An analogous conclusion was

reported by some researchers who used XANES to identify the reduction process of As(V) by Li/Al-LDH (Liu et al., 2006) and Cl-intercalated Mg/Fe-LDH (Guo et al., 2017).

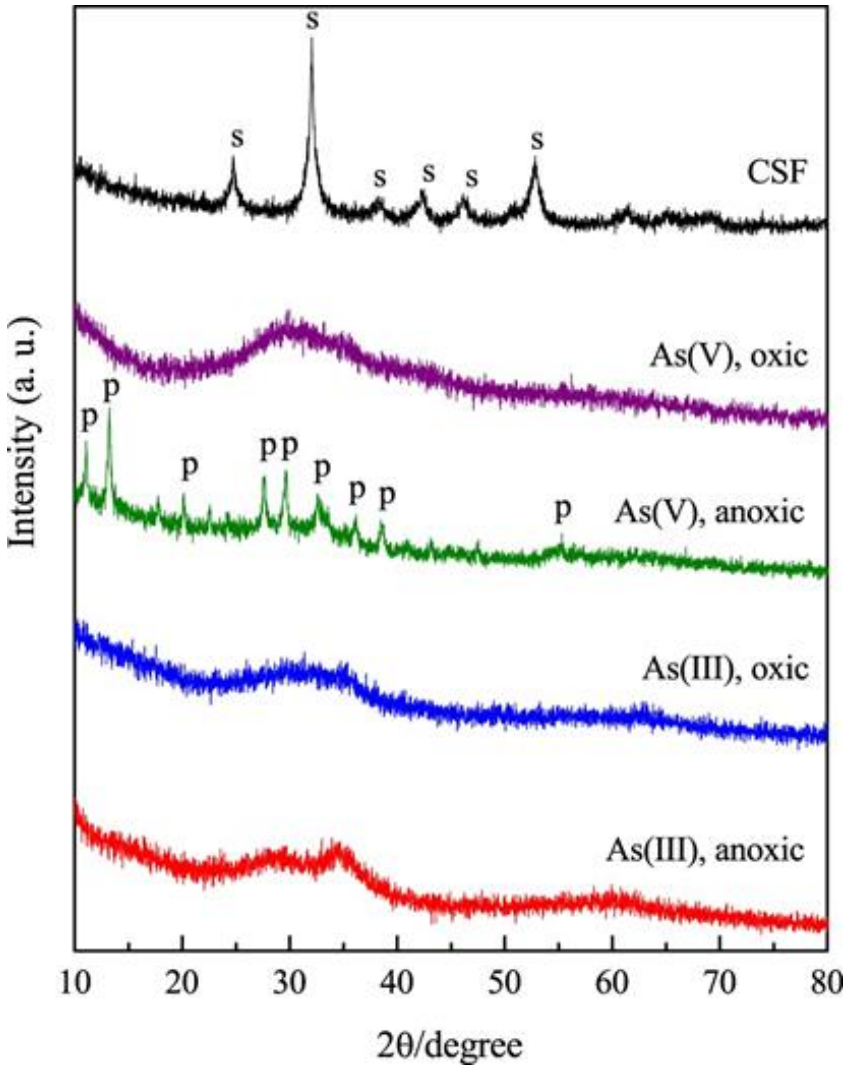

Figure 5.24. XRD patterns of pristine (carbonate structural Fe(II); CSF) and As-loaded CFS under oxic and anoxic conditions

(As(V) = 100 mg/L, As(III) = 50 mg/L, CSF = 0.1 g-Fe/L, initial pH = 9.0). The peaks indicate siderite (s) and parasymplesite (p).

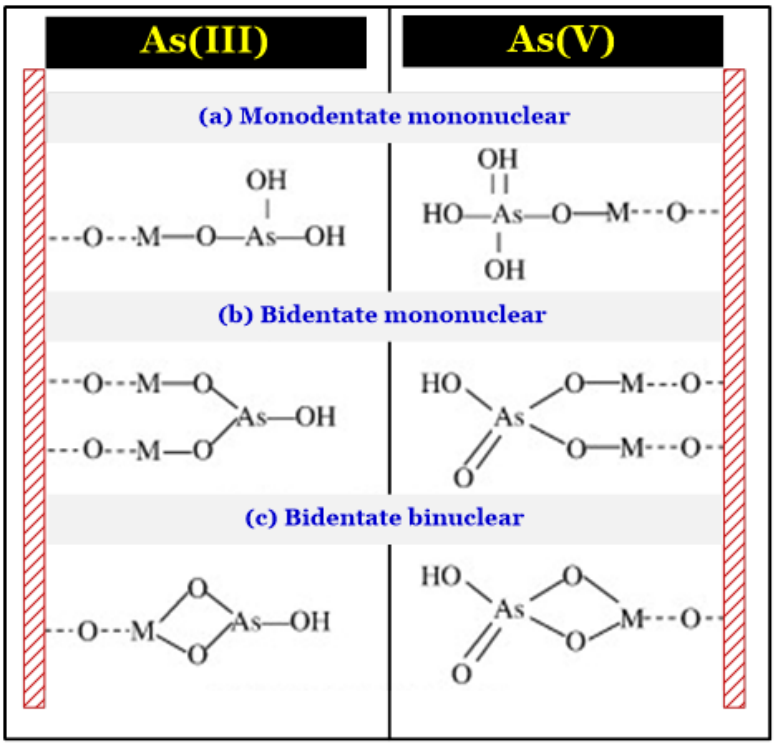

Figure 5.25. Schematic configuration of the inner-sphere surface complexes of As(III) and As(V) formed on the surfaces of the solid (M = Al, Fe, etc.) (Wang and Mulligan, 2008**)**

However, the reduction of As(V) to As(III) after the equilibrium adsorption was identified in this study through the XPS data. In essence, the binding energy (BE) of As(III) is lower than that of As(V). For example, the BE value of As(III) derived from the pure chemical $NaAsO_2$ was 44.2 eV (Bang et al., 2005), while the corresponding value for As(V) from $Na_2HAsO_4 \cdot 7H_2O$ was 45.6 eV (Soma et al., 1994). **Figure 5.26a** shows that the dominant As species in Mn/Mg/Fe-LDH was As(III), with the BE value in the low resolution XPS survey being 44.17 eV (**Table 5.1**). The deconvoluted result of the high resolution of As 3d spectrum (**Figure 5.26d**) show that after adsorption As(V), the percentage of As(III) species (64.02%) in Mn/Mg/Fe-LDH dominated than that of As(V)

species (35.98%). In addition, previous study reported the photoelectron peak for As(0) was at 41.4 eV (**Figure 5.23**) (Bang et al., 2005). However, there was not existence of As(III) species in the laden Mn/Mg/Fe-LDH (**Figure 5.26d**). The results suggest that As(V) was only reduced to As(III) when As(V) in solutions contacted with Mn/Mg/Fe-LDH. The reduction mechanism of inorganic As(V) species to As(III) species might be expressed as **Equations 5.6–5.7** (Bang et al., 2005). As(V) and reduced As(III) were adsorbed by Mn/Mg/Fe-LDH through some below mechanisms.

$$H_2AsO_4^- + 2Fe^{2+} + 3H^+ \rightleftharpoons H_3AsO^o + 2Fe^{3+} + H_2O \quad \textbf{(5.6)}$$

$$HAsO_4^{2-} + 2Fe^{2+} + 4H^+ \rightleftharpoons H_3AsO^o + 2Fe^{3+} + H_2O \quad \textbf{(5.7)}$$

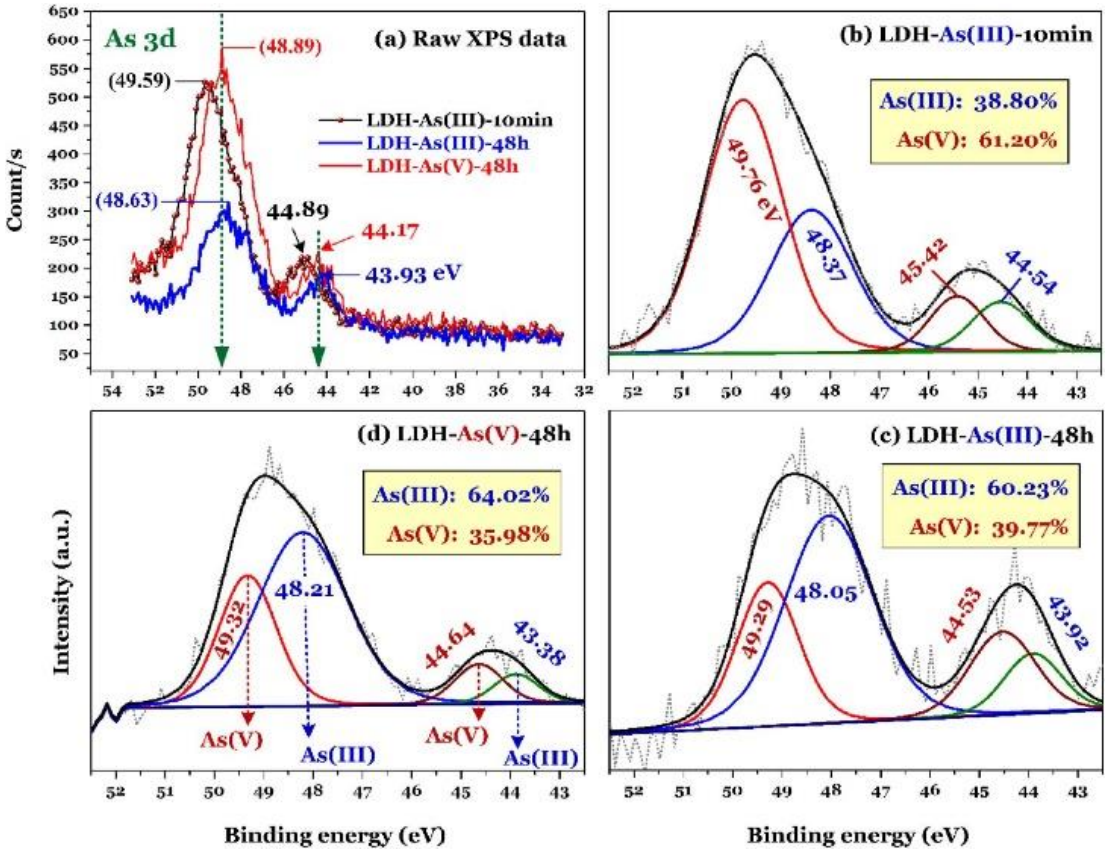

Figure 5.26. High-resolution spectrum of As 3d of Mn/Mg/Fe-LDH after adsorbing As(V) for 48 h [LDH-As(V)-48h], As(III) for 10 min [LDH-As(III)-10min], and As(III) for 48 h [LDH-As(III)-48h]

5.3.9.2. Dissolution–precipitation mechanism

Some authors reported that reactions between Fe-containing materials (i.e., ferrihydrite) and As(V) (prepared from Na_3AsO_4•$12H_2O$) can generate a scorodite ($FeAsO_4$•$2H_2O$ and its pKa = 20.24) (Frau et al., 2010). They authors reported that the BE of As(V) in the scorodite (the As 2p spectrum) was approximately 46 eV (Frau et al., 2010). Furthermore, based on the XRD data of the carbonate structural Fe(II) material (CSF) before and after adsorption of As(V), Tian et al. (2017) concluded that the existence of adsorption mechanism involved in surface precipitation. Their XRD data (**Figure 5.24**) confirmed the formation of the crystalline parasymplesite ($Fe_3(AsO_4)_2$•$8H_2O$ and its pKa = 33.25) on the As(V)-laden material. This reaction between Fe^{2+} and As(V) (from NaH_2AsO_4) in solutions to form the precipitation of ferrous As(V) is expressed as **Equation 5.8** (Johnston and Singer, 2007).

$$2HAsO_4^{2-} + 3Fe^{2+} \rightarrow Fe_3(AsO_4)_2 + 2H^+ \quad \textbf{(5.8)}$$

Furthermore, Tournassat et al. (2002) investigated the adsorption of As(III) by birnessite (MnO_2•nH_2O). They found that As(III) was oxidized to As(V) by birnessite. The oxidized As(V) reacted to Mn^{2+} ions (released from birnessite) through the krautite reaction to form the precipitation of manganese(II) As(V) ($MnHAsO_4$•H_2O; **Equation 5.9**) (Tournassat et al., 2002).

$$H_2AsO_{4-} + Mn^{2+} + H_2O \rightarrow MnHAsO_4 \bullet H_2O + H^+ \quad \textbf{(5.9)}$$

Guo et al. (2017) studied the adsorption of As(V) or As(III) by Cl-intercalated Mg/Fe LDH. The presence of precipitates of hornesite ($Mg_3(AsO_4)2$•$8H_2O$) or ($Fe_4(AsO_4)_2O_3$) in the As(V)-laden LDH solid was identified by XRD at a peak of ~30°. However, the relevant peak at around 30° was not observed in the As(II) laden LDH material.

In this study, the leaching test indicated that the structure of Mn/Mg/Fe-LDH was highly stable under pH 7.0 (**Table 5.3**). The reactions between the dissolved metals (i.e., Mg, Fe, and Mn) from Mn/Mg/Fe-LDH and As(V) in solution had a minor contribution to the removal efficiency of As(V) (**Section 5.3.2**). Therefore, the dissolution–precipitation mechanism was less important (or possibly ruled out) in this study. The conclusion was supported by the XRD data of Mn/Mg/Fe-LDH before and after adsorption (**Figure 5.2**) and the XPS data (**Figure 5.26).** An analogous conclusion was stated by many researchers (Wang et al., 2009; Guo et al., 2017; Choong et al., 2021; Wang et al., 2021a; Wang et al., 2021b).

5.3.9.3. Outer-sphere and inner-sphere complexation

The out-sphere surface complex (also known as weak electrostatic attraction) that occurred between the positively charged surface of Mn/Mg/Fe-LDH and As(V) anions in solution was highly expected as a primary adsorption mechanism of As(V) anions (Wang et al., 2009; Choong et al., 2021). This interaction was supported by the positively charged surface of Mn/Mg/Fe-LDH confirmed by its zeta potentials (**Figure 5.17a**). In contrast, the XPS and FTIR techniques did not give a reliable information on this weak interaction. A similar identification on this mechanism has reported by other scholars for studying the adsorption of As(V) anions onto some materials with similar properties (Tian et al., 2017). However, this attraction (weak and reversible) might only exist in the first period of the adsorption process. This conclusion was confirmed by the desorption study (**Section 5.3.8**). After the 24 h-equilibrium adsorption, the presence of As ions in the laden Mn/Mg/Fe-LDH material was very strong. This might be because As(V) anions were reduced to As(III) ions, and the reduced As(III) ions were strongly adsorbed by

Mn/Mg/Fe-LDH through stronger interactions (or irreversible adsorption mechanism). Therefore, the desorption efficiency was negligible (only 0.5%; **Table 5.9**).

With regard to inner-sphere complex, Wang et al. (2009) found that As(V) can react with the oxygen-containing functional groups of Mg/Al-LDH (mainly –OH groups on its surface) through this complexation. The dominant inner-sphere complexation through ligand exchange was confirmed by As K-edge XAS (X-ray absorption spectroscopy) spectrum**. Figure 5.11** shows that after adsorption of As(V), the intensity of the BE peak at approximately 533 eV ($M–OH_2^+$) decreased, but that at around 529 eV (M–O–M) increased (**Figure 5.9**). The changes of relevant peak intensities in the O 1s spectrum after the 48 h-adsorption of As(V) suggest the existence of inner-sphere complexation between As(V) oxyanions or reduced As(III) ions and the hydroxyl groups on the surface of LDH. The different kinds of inner-sphere surface complexes of As summarized in **Figure 5.25** (Wang and Mulligan, 2008). This complexation was found in the adsorption process of As(V) and As(III) using LDH-based materials (Liu et al., 2006; Goh et al., 2009; Wang et al., 2009; Liu et al., 2019b; Choong et al., 2021) and other (Penke et al., 2021).

5.3.9.4. Anion exchange

In general, LDH contains abundant host anions (i.e., NO_3^- and CO_3^{2-}), so anion exchange between As(V) anions in solution and its host anions in the interlayer region is highly feasible (Goh et al., 2009; Huang et al., 2015; Asiabi et al., 2017; Hudcová et al., 2017). This conclusion was confirmed by the results of competitive adsorption of foreign anions (**Figure 5.18**). The adsorption capacity of Mn/Mg/Fe-LDH (**Figure 5.18**) declined remarkably due to the presence of foreign anions in solution (competitive adsorption). For example, it fell from 14.5 mg/g (no competition) to approximately 1.5 mg/g

(competition between As(V) and phosphate anions for exchangeable sites in Mn/Mg/Fe-LDH). Some other techniques were also helpful to identity this mechanism, such as FTIR (**Figure 5.6**), XRD (**Figure 5.2**), and XPS (**Figures 5.7–5.8**)

The FTIR data (**Figure 5.6**) show that the intensity of the bands at around 1384 cm^{-1} (N=O in NO_3^- overlapped C=O in CO_3^{2-}) decreased markedly after adsorption of As(V). This result suggests a significant decrease in the host anions in the interlayer region of Mn/Mg/Fe-LDH that resulted from the anion exchange phenomenon. However, the FTIR data cannot distinguish between NO_3^- and CO_3^{2-} anions (Goh et al., 2009).

The XPS data (**Figure 5.8**) indicate that NO_3^- anions in its interlayer region played a more important role in exchanging As(V) anions than CO_3^{2-} anions. This is because a remarkable decease in (1) the atomic percentage of N element (**Table 5.1**) from 2.54% to 0.14% after adsorption of As(V) and (2) the intensity of the important peak at approximately 407 eV (**Figure 5.8**). Goh et al. (2009) also reported a remarkable decrease in N% from 2.9% to nearly 0% (XPS data) after adsorbing As(V) by NO_3-intercalated Mg/Al-LDH. **Equation 5.10** gives an anion exchange stoichiometry between As(V) anions in solution and the host NO_3^- anions in the interlayer region of Mn/Mg/Fe-LDH without considering exchange between As(V) and CO_3^{2-} anions (Goh et al., 2009).

$$HAsO_4^{2-}{}_{(aq)} + 2NO_3^- - LDH_{(s)} \rightleftharpoons 2NO_3^-{}_{(aq)} + HAsO_4^{2-} - LDH_{(s)} \quad \textbf{(5.10)}$$

Furthermore, the XRD data (**Figure 5.2**) confirms that the import role of anion exchange between As(V) anions and NO_3^- anions because of the disappearance of the relevant peak at 29.4° ($NaNO_3$) for As(V)-laden Mn/Mg/Fe-LDH. In contrast, **Figure 5.7** and **Table 5.1** show that after adsorption of As(V), the presence of the host CO_3^{2-} anions in the interlayer region of Mn/Mg/Fe-LDH still maintained. As discussed at **Section 5.3.9.1**, the anion exchange does not make Mn/Mg/Fe-LDH in loss of its original

structure. However, **Figure 5.2** shows that Mn/Mg/Fe-LDH lost its original structure after adsorption of As(V). The result suggests that anion exchange might occur in the first period of the adsorption process. This hypothesis can be supported by the desorption study (**Section 5.3.8**). After the exchange process, the guest As(V) anions in the interlayer region of Mn/Mg/Fe-LDH contacted to Fe^{2+} in this material. The reduction of As(V) to As(III) was described in **Equations 5.6–5.7**. The redox reactions that occurred in the interlayer region might lead to destroy the original layer structure of Mn/Mg/Fe-LDH (**Figure 5.2**). This conclusion might be support by changing the textural properties (i.e., S_{BET}) of Mn/Mg/Fe-LDH after adsorbing As(V) anions (**Figure 5.5**).

5.3.9.5. Pore-filling mechanism

In essence, pore filling often plays a more important role in the adsorption mechanism of organic pollutants than inorganic pollutants. Many authors ignored the role of pore-filling mechanism when they interpreted the adsorption process of As (Liu et al., 2006; Huang et al., 2015; Guo et al., 2017; Ding et al., 2018; Mubarak et al., 2018; Lu et al., 2018; Choong et al., 2021). If pore-filling mechanism is dominant, the S_{BET} value of LDH should decease after adsorption. For example, Wang et al. (2021a, b) found that the S_{BET} value of Fe/Mn-C-LDH decreased from 170.5 to 68.2 m^2/g after absorbing As(III) or to 92.1 m^2/g after absorbing As(V). However, **Figure 5.5** shows that the S_{BET} value of Mn/Mg/Fe-LDH remarkably increased from 75.2 to 156 m^2/g after the adsorption process. The result might because Mn/Mg/Fe-LDH lost its original layer structure caused by the redox reactions **Section 5.3.9.4**.

5.3.9.6. Isomorphic substitution

Isomorphic substitution is commonly found for the adsorption of cation metals (Cr^{3+}, Pb^{2+}, Cd^{2+}, etc.) by clay minerals like LDH. For example, Cr^{3+} ions in solution can isomorphically substitute to Al^{3+} in the LDH structure (i.e., Mg/Al-LDH) after the adsorption process. This is because of a similar radius between them (Cr^{3+} and Al^{3+} of 0.052 nm and 0.054 nm, respectively) (Chao et al., 2018; Tran et al., 2019). Although As(V) anions were reduced to As(III) ions when they contact with Mn/Mg/Fe-LDH, As(III) exists as a charge- neutral species. Therefore, adsorption mechanism involved in isomorphic substitution was ruled out in this study. This mechanism was not reported for adsorbing As ions onto other LDH materials (Liu et al., 2006; Bagherifam et al., 2014; Huang et al., 2015; Guo et al., 2017; Hudcová et al., 2017; Lu et al., 2018; Mubarak et al., 2018; Liu et al., 2019b; Choong et al., 2021; Wang et al., 2021a; Wang et al., 2021b).

5.3.9.7. Hydrogen bonding interaction

Some authors reported that the adsorption of As(III) and As(V) by LDH-based materials through hydrogen bonding (Hudcová et al., 2017; Liu et al., 2019b; Choong et al., 2021). For example, Choong et al. (2021) concluded that hydrogen bonding is one of the most important adsorption mechanisms of As(III) and As(V) onto the polymers-embedded Mg/Fe-LDH. However, the authors did not give any convincing evidence for the existence of such interaction (Choong et al., 2021). In fact, it is very hard to interpret the presence of H-bonding interactions between Mn/Mg/Fe-LDH and As by FTIR, XPS, or even EXAFS (Wang and Mulligan, 2008; Wang et al., 2009). In contrast, many researchers ignored this interaction when they discussed the adsorption mechanisms of As by the LDH-based materials (Liu et al., 2006; Goh et al., 2009; Wang et al., 2009;

Bagherifam et al., 2014; Huang et al., 2015; Guo et al., 2017; Lu et al., 2018; Mubarak et al., 2018; Wang et al., 2021a; Wang et al., 2021b) and other materials such as zero-valent iron (Bang et al., 2005), birnessite (Tournassat et al., 2002), gibbsite (Liu et al., 2006), and aluminum-enriched biochar (Ding et al., 2018). This mechanism might also exit in the adsorption systems. However, its contribution might be negligible.

5.3.10. Possible adsorption mechanism of As(III) ions by Mn/Mg/Fe-LDH

Some authors reported that As(III) was reduced to As(0) after adsorption (Bang et al., 2005). However, this reduction was ruled out in this study. **Figure 5.26** shows that As(0) species did not exist in the As(III)-laden Mn/Mg/Fe-LDH. As(0) has been previously identified at 41.4 eV. As(III) exits as a predominantly no charged species ($H_3AsO_3^{\circ}$; **Figure 2.2**) in aqueous *s*olution at pH 7.0. Therefore, the out-sphere surface complex was ruled out. However, the adsorption phenomenon of As(III) by Mn/Mg/Fe-LDH was very similar to that of As(V), especially the adsorption studies of effects of pH and foreign anions. Therefore, it is highly expected that As(III) ions were oxidized to As(V) anions during the adsorption process of As(III). The oxidation phenomenon of As(III) to As(V) by LDH-based materials have been reported by many scholars, such as Cl-intercalated Mg/Fe (Guo et al., 2017) and granular Mg/Fe-LDH (Choong et al., 2021). The oxidation process by Mn(IV) can occur two steps (**Equations 5.11–5.12**). The redox reaction can be overall expressed as **Equation 5.13** (Tournassat et al., 2002).

$$H_3AsO_3^{o} + 2MnO_2 + H_2O \rightleftharpoons H_2AsO_4^{-} + 2MnOOH + H^{+} \quad \textbf{(5.11)}$$

$$H_3AsO_3^{o} + 2MnOOH + 3H^{+} \rightleftharpoons H_2AsO_4^{-} + 2Mn^{2+} + 3H_2O \quad \textbf{(5.12)}$$

$$H_3AsO_3^{o} + MnO_2 + H^{+} \rightleftharpoons H_2AsO_4^{-} + Mn^{2+} + H_2O \quad \textbf{(5.13)}$$

However, the oxidation process might occur at the first period of the adsorption process (i.e., 10 min contact). The XPS data show BE [As 3d] = 49.59 eV and 44.89 eV

(Figure 5.26a) and BE [As 2p3] = 1327.8 eV (**Table 5.1**). Those values are close the BE values of As(V) that have been reported elsewhere (Choong et al., 2021; Wang et al., 2021a; Wang et al., 2021b). For example, Choong et al. (2021) reported that the As species in the polymers-embedded Mg/Fe-LDH after adsorption were As(V) [BE at 1326.1 eV (As 2p3) and 44.72 eV (As 3d3)] and As(III) [1325.6 eV (As 2p3) and 43.97 eV (As 3d3)].

In addition, **Figure 5.26b** shows that after the 10-min adsorption of As(III), the As(V) species (61.20%) predominated in Mn/Mg/Fe-LDH compared to As(III) one (38.80%). However, after the 48-h adsorption of As(III), the percentages of As(V) only accounted for 39.77% (**Figure 5.26c**). The result suggests the existence of the first redox reaction (**Equation 5.12**); as a result, As(III) was oxidized to As(V). The adsorption mechanisms of the oxidized As(V) anions Mn/Mg/Fe-LDH might occur as the case of adsorbing As(V) (**Section 5.3.9**). The XPS data (**Figure 5.26c**) confirmed that there was the existence of the second redox reaction (**Equations 5.6–5.7**); as a result, the oxidized As(V) was then reduced to As(III). The original and reduced As(III) ions were adsorbed by Mn/Mg/Fe-LDH through the dominant inner-sphere complexation. As(III) is often more favorable than As(V) in complexing with the OH groups in adsorbents. Some authors (Hong et al., 2014; Penke et al., 2021) found that As(III) was more easily to adsorbed by LDH through the strong in-sphere surface complexation. This conclusion was supported by the O 1s spectrum in **Figure 5.11** (or **Figure 5.9**) through a remarkable decrease in the density of the peaks at ~529 eV (M–O or M–O–M) and ~533 eV (M–OH_2^+).

Figure 5.8 and **Table 5.1** show that two involved processes—the oxidation of As(III) to As(V) anions as well as anion exchange between the oxidized As(V) anions

and the host anions (NO_3^-) in the interlayer region of Mn/Mg/Fe-LDH—occurred very fast (~10 min). After 10-min contact, the species of As(V) in the laden Mn/Mg/Fe-LDH were dominant (61.20%; **Figure 5.26b**) than those of As(III). The oxidation and reduction occurred simultaneously in the adsorption system along with the other phenomena (adsorption and desorption). As a result, Mn/Mg/Fe-LDH lost its original structure after the completed adsorption process of As(III) (**Figure 5.2**).

5.3.11. Application of Mn/Mg/Fe-LDH for eliminating As from groundwater

Mn/Mg/Fe-LDH was applied for removing As from real groundwater. The groundwater samples from the wells of ten households were collected in the Phuong Tu commune, Ung Hoa district, Hanoi, Vietnam. The basic characteristics of the groundwater are presented in **Table 5.10**. The batch adsorption experiment was contacted under the following conditions: 1.0 g/L, room temperature (~31 °C), pH (not adjusted; pH = 6.81–7.32), and 24 h. The concentrations of the raw groundwaters from ten local wells (before sand filtration) ranged from 0.045-0.092 mg/L (**Table 5.11**). After the adsorption process, the residual As concentrations (0.00035–0.0079 mg/L) were detected below the Vietnam and WHO drinking water standards (0.01 mg/L). Similarly, Lu et al. (2018) used the calcinated Ca/Fe LDH (1.0 g/L) for the decontamination of As (mainly As(V) form) from the water samples of the river. They found that the concentrations of As after adsorption were 0.0017 mg/L (Co = 0.03 mg/L and pH = 7.12) and 0.009 mg/L (Co = 1.11 mg/L and pH = 7.62). **Table 5.11** shows that the removal efficiency of As from the groundwaters ranged from 91.41% to 99.22%. Therefore, Mn/Mg/Fe-LDH can serve as a promising material for the real applications.

Table 5.10. Basic characteristics of groundwater in the Phuong Tu commune, Ung Hoa district, Hanoi, Vietnam before treatment by a traditional sand filter

Parameters	Unit	Concentrations	Standard for drinking water*
		Before sand filter	
pH	—	6.81–7.32	6.0–7.0
As	mg/L	**0.045–0.093**	**0.01**
Iron	mg/L	0.06–3.87	0.3
Manganese	mg/L	12.48–13.44	-
Calcium	mg/L	44.80–51.21	300
Permanganate	mg/L	1.60–5.76	2
Ammonium	mg/L	7.98–18.67	3
Coliform	CFU/100mL	89–126	0
E. Coli	CFU/100mL	36–237	0

Note: *Vietnamese standard for drinking water (QCVN 01:2009/BYT).

Table 5.11. The results of applying the prepared Mn/Mg/Fe-LDH for removing As using from real groundwater (collected from 10 household wells) in the Phuong Tu commune, Ung Hoa district, Hanoi, Vietnam

	m (g)	*V* (L)	As concentrations		Removal efficiency (%)	q_e (mg/g)
			Input (mg/L)	Output (mg/L)		
Sample 1	0.0519	0.05	0.077	0.0044	94.29	0.0699
Sample 2	0.0504	0.05	0.045	0.00035	99.22	0.0443
Sample 3	0.0502	0.05	0.087	0.0051	94.14	0.0816
Sample 4	0.0513	0.05	0.082	0.0061	92.56	0.0740
Sample 5	0.0509	0.05	0.053	0.0045	91.51	0.0476
Sample 6	0.0508	0.05	0.092	0.0079	91.41	0.0828
Sample 7	0.0516	0.05	0.076	0.0047	93.82	0.0691
Sample 8	0.0514	0.05	0.065	0.0044	93.23	0.0589
Sample 9	0.0512	0.05	0.049	0.0005	98.98	0.0474
Sample 10	0.0511	0.05	0.089	0.0053	94.04	0.0819

5.3.12. Laboratory column adsorption study

An adsorption column study was conducted using Mn/Mg/Fe-LDH as the adsorbent for As removal from synthetic water. The breakthrough curves of the As(V) and As(III) adsorption by Mn/Mg/Fe-LDH are presented in **Figure 5.27**. Results show

that the breakthrough curves for both As ions are classified as having an S shape. However, the curves of Mn//Mg/Fe-LDH for As(V) ions were steeper than that of As(III) ions. Subsequently, the breakthrough time and saturation time of Mn//Mg/Fe-LDH for As(III) ions were longer than that of As(V). The saturation time of Mn/Mg/Fe for As(III) and As(V) ions were 6,720 h and 4,320 h, respectively, corresponding to the bed volumes of 134,400 and 86,400, respectively. This is because the Langmuir maximum adsorption capacity of Mn/Mg/Fe-LDH towards As(III) (Q_{max} = 56.1 mg/g) was much higher than that towards As(V) (Q_{max} = 32.2 mg/g). The bed volume that Mn/Mg/Fe-LDH could treat As(III) and As(V) solution of 0.33 mg/L to As concentration of below the WHO guideline were very high; respectively. They were 13,920 and 21,600 for As(V) and As(III).

The Thomas model (Thomas, 1944) was implemented to describe the column's performance and predict the breakthrough curves of the As adsorption process on Mn/Mg/Fe-LDH. The relevant information concerning the Thomas model is described in **Section 2.6.3.3**.

Table 5.12. Thomas model parameters for As(V) and As(III) adsorption on Mn/Mg/Fe-LDH

Adsorbate	Thomas model parameters		
	k_{TH} (L/h.mg)	q_{TH} (mg/g)	R^2
As(V)	0.006	10.42	0.96
As(III)	0.004	15.25	0.95

Table 5.12 shows the values of the Thomas model parameters of Mn/Mg/Fe-LDH for As adsorption. The high determination coefficient value (R^2 > 0.95) indicate that As(V) and As(III) adsorption in the continuous Mn/Mg/Fe-LDH fixed-bed system were

successfully described by the Thomas model. The Thomas adsorption capacity of Mn/Mg/Fe-LDH for As(III) was 15.25 mg/g, which is higher than that of As(V) (q_{TH} = 10.42 mg/g). The smaller concentration of As solution and less contact between adsorbate and adsorbent in the column experiment than that used in isotherm experiment could explain the lower Thomas adsorption capacity value for both As ions than their Langmuir maximum adsorption capacity of both As ions on Mn/Mg/Fe-LDH.

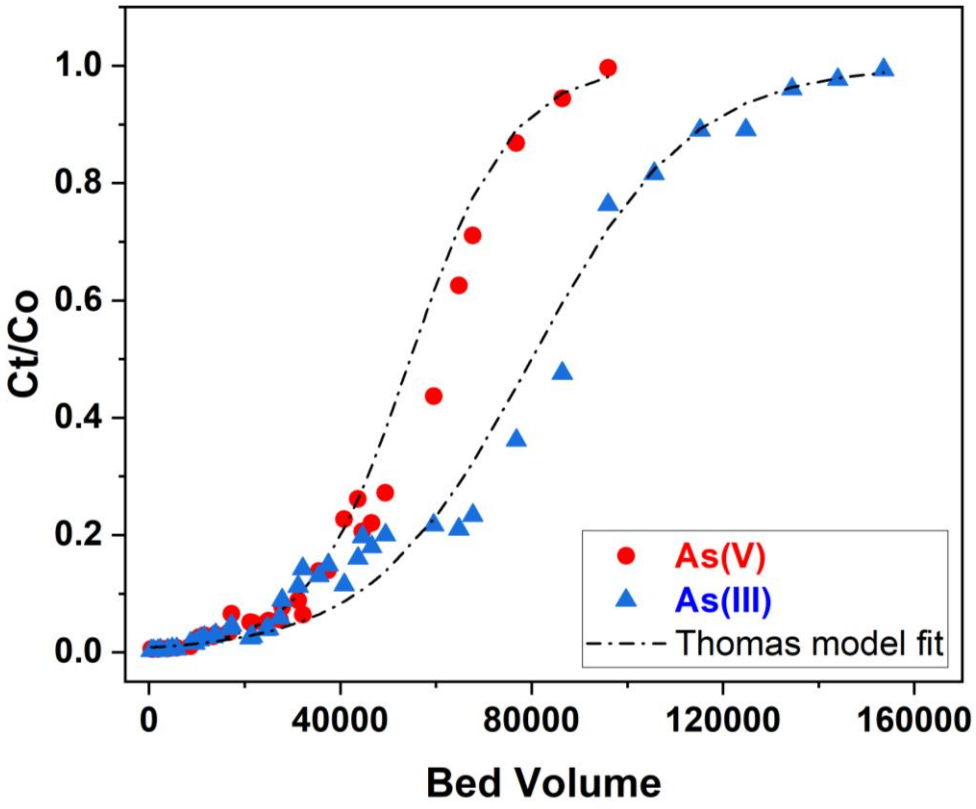

Figure 5.27. Breakthrough curves for As(III) and As(V) adsorption onto Mn/Mg/Fe-LDH

5.4. Conclusions

The Mn/Mg/Fe-LDH material (acting as catalyst and adsorbent) was successfully synthesized from three salts of metals [i.e., $Mg(NO_3)_2$, $Mn(NO_3)_2$, and $Fe(NO_3)_3$] through

a simple co-precipitation process. The optimum Mg/Mn/Fe molar ratio for synthesizing Mn/Mg/Fe-LDH was 1/1/1. The basal spacing of Mn/Mg/Fe-LDH amounted to 0.757 nm. The host anions (NO_3^- and CO_3^{2-}) in its internal region were identified by the XRD, FTIR, and XPS techniques. Both Fe^{2+}/Fe^{3+} and $Mn^{2+}/Mn^{3+}/Mn^{4+}$ coexisted in Mn/Mg/Fe-LDH, which possessed a positively charged surface when the pH solution was lower than its pH_{IEP} of 10.15. The Mn/Mg/Fe-LDH adsorbent was mesoporous material (average pore width of 14.2 nm), with its S_{BET} and V_{Total} being 75.2 m^2/g and 0.267 cm^3/g. The adsorption capacity of Mn/Mg/Fe-LDH was significantly affected by the presence of foreign anions in solution. The adsorption trend followed the order of no competition (absence of foreign anions) > the presence of Cl^- anion > SO_4^{2-} anion > HPO_4^{2-} anion > CO_3^{2-} anion > SiO_3^{2-} anion > five foreign anions (Cl^-, SO_4^{2-}, CO_3^{2-}, SiO_3^{2-}, and HPO_4^{2-}). The Langmuir maximum adsorption capacity of Mn/Mg/Fe-LDH to As was superior (56.1 mg/g for As(III) and 32.2 mg/g for As(V) at pH 7.0 and 25 °C), much higher than the popular adsorbents cited in the literature. In this pH scenario, the amounts of Mn, Mg and Fe leached after the adsorption process were smaller than the Vietnamese government's standard limit according to the QCVN 01:2009/BYT: National Technical Regulation on Drinking Water Quality. The desorption study demonstrated that adsorption is highly irreversible. This meant that the release of As from laden Mn/Mg/Fe-LDH into the environment was negligible. Mn/Mg/Fe-LDH can efficiently remove As from groundwater, with the initial As concentrations diminishing from 0.045–0.092 mg/L to 0.00035–0.0079 mg/L after adsorption. X-ray photoelectron spectroscopy was applied to identify the oxidation states of As in laden Mn/Mg/Fe-LDH. The key removal mechanism of As(III) by Mn/Mg/Fe-LDH was oxidation-coupled adsorption. Here, the Mn/Mg/Fe-LDH was found to be able to oxidize As(III) ions into As(V) anions. The

As(III) and oxidized As(V) were then adsorbed on Mn/Mg/Fe-LDH. Conversely, the main As(V) removal mechanism by Mn/Mg/Fe-LDH was reduction-coupled adsorption. The As(V) mechanism adsorption mainly involved: (1) the inner-sphere and outer-sphere complexation with OH groups of Mn/Mg/Fe-LDH; and (2) anion exchange with host anions (NO_3^-) in its interlayer. The primary mechanism adsorption of As(III) was only the inner-sphere complexation. The redox reactions made Mn/Mg/Fe-LDH lose its original layer structure after adsorbing As(V) or As(III). Mn/Mg/Fe-LDH can serve as a promising catalyst and adsorbent for removing highly toxic As(III) ions and As(III) anions from water. The adsorption column results show that the exhaustion times of Mn/Mg/Fe-LDH for As(III) and As(V) ions were extremely high, 6720 h and 4320 h, respectively. These exhaustion times were much longer than that of NLTT, PPCI, and many other adsorbents reported previously. The breakthrough curves were well described by the Thomas model and the respective Thomas adsorption capacities were 10.41 mg/g and 15.25 mg/g for As(V) and As(III) ions.

Chapter 3, 4, and 5 present the As adsorption capacity of three novel adsorbents including NLTT, PPCI, and Mn/Mg/Fe-LDH in the different conditions of batch and column experiments. Among them, NLTT material can be applied in water filtration systems at household and community levels in As contaminated rural areas in Vietnam due to it's initial favorable laboratory results (Chapter 3), as well as its local availability and low-cost (US$ 0.10/kg). Thus, next chapter (Chapter 6) presents the application of NLTT in the field and waste management of exhausted NLTT.

CHAPTER 6. APPLICATION OF NATURAL LATERITE IN DRINKING WATER TREATMENT IN VIETNAM AND WASTE MANAGEMENTS

This chapter presents the application of NLTT in the field and waste management of spent NLTT. The performance of a community filtration system packed with NLTT for removal of real As-contaminated groundwater in Ha Nam province, Vietnam was published in the following paper in the journal Science of the Total Environment.

1. Nguyen, T. H., Tran, H. N., Vu, H. A., Trinh, M. V., Nguyen, T. V., Loganathan, P., Vigneswarana S., Nguyen, T.M., Trinh, V.T., Vu, D.L., Nguyen, T. H. H. (2020). Laterite as a low-cost adsorbent in a sustainable decentralized filtration system to remove arsenic from groundwater in Vietnam. Science of the Total Environment, 699, 134267 (IF: 10.753; SJR: Q1)

The performance of the household filtration systems packed with NLTT for removal of real As-contaminated groundwater in Ha Nam province and Hanoi' suburb, Vietnam and waste management were published in the journal Process Safety and Environmental Protection.

2. Nguyen, T. H., Nguyen, A. T., Loganathan, P., Nguyen, T. V., Vigneswaran, S., Nguyen, T. H. H., & Tran, H. N. (2021). Low-cost laterite-laden household filters for removing arsenic from groundwater in Vietnam and waste management. Process Safety and Environmental Protection, 152, 154-163 (IF: 7.926; SJQ:Q1)

6.1. Introduction

In the Red River Delta in the north of Vietnam, As contamination of groundwater is a serious problem and it is estimated that nearly ten million people are affected. Millions of people in this area are unable to access clean water from the existing centralized water treatment systems. Hanoi's suburb and Ha Nam province have now emerged as the two areas most affected by As contaminated groundwater. According to Agusa et al. (2006), total As concentration varied from below 0.001 to 0.33 mg/L in Hanoi's suburb groundwater. This is up to 33 times higher than the WHO's guidelines and Vietnam drinking water quality standards of 0.01 mg/L. Moreover, around 40% of collected samples containing As concentrations exceeded 0.01 mg/L. These results agree with the data in the study done by Berg et al. (2001), which recorded As contamination in groundwater in the city and rural districts of Hanoi. The total As concentration of 0.037–0.32 mg/L was detected in raw groundwater used in eight drinking water treatment plants in Hanoi. In Ha Nam province, approximately 52% groundwater samples was found to be higher in total As concentration than what Vietnam drinking water quality standards specify (Tran, 2008).

A large number of commercial, synthetic, and natural adsorbents have been used as filter media for removing As. Activated carbon and activated alumina are popular commercial adsorbents, which have been identified as highly effective media for removing toxic As(III) and As(V) (Kalaruban et al., 2019). However, they are expensive, and there are high regeneration costs involved. This means their practical application might be restricted in low-income villages. Unlike commercial products, many low-cost natural adsorbents or industrial/agricultural waste products (e.g., clay, goethite, zeolites, laterite, red mud, fly ash, etc.) possess outstanding characteristics, including their local

availability, inexpensiveness, and moderately high As removal efficiency (Nguyen et al., 2020a; Nguyen et al., 2009). This has heightened their usefulness as alternative adsorbents for removing As from contaminated water and wastewater (Mohan and Pittman, 2007). However, the applications of those low-cost adsorbents in pilot-scale and full-scale scenarios are still limited.

Based on NLTT's initial favorable laboratory results (**Chapter 3**), as well as its local availability and low-cost (US$ 0.10/kg), NLTT material has been applied in many water filtration systems at household and community levels in As contaminated rural areas in the Red River Delta, Vietnam. In the rural areas of Red River Delta, households and community facilities are traditionally using only simple sand filters to remove As, Fe and other contaminants from groundwater. These sand filters can only remove some of the contaminants and As level in the effluent, yet many sand filters cannot meet the Vietnam government's drinking water standards. Many households in the As contaminated rural areas cannot afford to buy expensive household water filters and consequently there is a high demand for low-cost As filter media for water treatment systems. Thus, in the first part of this chapter, the application of NLTT on household and communities water filtration systems was evaluated. The performance of NLTT on As removal from real contaminated groundwater was investigated through long-term (6–7 months) monitoring of four representative household water filtration systems and a childcare water filtration system in Ha Nam province and Hanoi's suburb.

One of the problems with using adsorbents to remove As is disposal of the exhausted adsorbent. Many As waste disposal methods have been proposed to prevent the release of toxic As from solid wastes into the environment, which include landfill, mixing with livestock waste, desorption/regeneration, and encapsulation within

construction materials (Sullivan et al., 2010). Of these methods, encapsulation through solidification/stabilization (S/S) has received much attention mainly due to its cost-effectiveness, significantly preventing As mobility and generating a new building material. The encapsulation technique through the S/S process is also identified as the Best Demonstrated Available Technology (BDAT) for hazardous waste disposal by the United States Environmental Protection Agency (USEPA) (Kundu and Gupta, 2008). In this process, normally, As-bearing waste is mixed with some common locally available building materials (e.g., cement, lime, sand, gravel, slag, or polymer) to produce new solidified products. Nguyen et al. (2020c) reported that products made by mixing As-bearing manganese oxides with cement and sand were suitable as building materials in the construction industry. They also reported that As leaching from the encapsulated products was negligible because Ca reacted with As to form calcium arsenate $Ca_3(AsO_4)_2$ precipitate in the concrete. This suggestion is tested in this study by: firstly, mixing the exhausted NLTT with cement and lime ($Ca(OH)_2$) at different ratios; and secondly, measuring As leaching and compressive strength of the encapsulated product to determine its suitability as a construction material. Although a previous study was conducted on mixing exhausted adsorbent with lime, cement, and fly ash to determine As leaching behavior, the mixed products' compressive strength, which is an important property related to its suitability for use as a construction material was not reported.

The main objectives of this chapter are to: (i) evaluate the performance of the household and community water filters packed with NLTT in treating As-contaminated groundwater in Vietnam; and (ii) determine the efficiency of the S/S process in managing the spent adsorbent by mixing it with Portland cement and lime at different ratios.

Management of the spent adsorbent was evaluated by measuring As leaching potential and compression strength of the brick product formed in this mixture.

6.2. Materials and methods

6.2.1. Field studies

The field studies were carried out in Hoang Tay commune (Kim Bang rural district, Ha Nam province) and Phuong Tu commune (Ung Hoa rural district, Hanoi city). They are the poor communes which are affected by As contaminated groundwater. Most households and community places in these 2 communes are using rainwater and contaminated groundwater as their main water sources for daily activities. Similar to other communes in Vietnam, people in here used sand filters as a solution to treat contaminated water. However, this treatment method generally cannot produce safe drinking water, so there has been a failure to keep the total As concentration below the Vietnam drinking water quality standard for the local villagers.

6.2.1.1. Field study with community filter treatment systems in Hoang Tay commune, Ha Nam province

Hoang Tay childcare was selected to receive a new community water filtration system in 2018 due to the water quality issue in this area and insufficiency of previous water treatment system. The characteristics of the groundwater before and after old sand filter in Hoang Tay childcare are presented in **Table 6.1**. The results show that the total As concentrations of groundwater in the childcare centre varied around from 0.122 to 0.237 mg/L. Notably, the previous treatment system using the sand filter did not provide safe drinking water for the childcare centre. This is because the total As concentrations

(0.042–0.110 mg/L; **Table 6.1**) after passing the traditional sand filter-based treatment system were dramatically higher than the WHO regulation (0.01 mg/L).

Figure 6.1. Digital picture of real water treatment system at the Hoang Tay children care centre, located at Ha Nam province in Vietnam

In order to supply safe water for the childcare, a new water supply system (**Figure 6.1**) was designed and installed by the cooperation between the University of Technology Sydney and the Institute of Environmental Technology (Vietnam Academy of Science and Technology). The designed system can supply 500 L/h to meet the water demand of around 440 children and 32 staff members in the investigated childcare centre. NLTT has been used as As filter media in the newly developed community water treatment system. The performance of the new filtration system as well as NLTT in removing As was

evaluated over a period of 6 months, since June 2018 to January 2019. The community filtration system has also incorporated the simultaneous removal of iron and pathogens from groundwater.

Table 6.1. Basic characteristics of groundwater in the childcare center (located at Hoang Tay commune, Kim Bang, Ha Nam, Vietnam) before and after using the traditional sand filter-based treatment system

Parameter	Unit	Concentration		Standard for drinking water*
		Before sand filter	After sand filtration	
pH	—	6.7–7.4	7.3–8.4	6.0–7.0
As	mg/L	**0.122–0.237**	**0.042–0.11**	**0.01**
Iron	mg/L	3.8–7.2	0.47–0.64	0.3
Manganese	mg/L	0.19	0.17	0.3
Phosphate	mg/L	0.179–1.5	0.021–0.29	—
Chloride	mg/L	197–759	163–361	250
Sulphate	mg/L	7.97*	2.13	250
Ammonia	mg/l	21–80	16–42	3
Silica	mg/L	3.2	2.60	—
Coliform	CFU/100mL	10–100	0–60	0
E. Coli	CFU/100mL	10–20	0–20	0

Note: *Vietnamese standard for drinking water (QCVN 01:2009/BYT: Vietnam Technical Regulation on Drinking Water Quality).

The designed water treatment system principally includes: a combined aeration and clarifier tank (main purpose for the simulation of coprecipitation process between iron and As as well as the removal of the Fe-As precipitates, respectively), an adsorption column (for the removal of As and other pollutants), an ultrafilter (for the removal of microorganisms), and a storage tank. **Figure 6.2** and **Figure 6.1** illustrate the schematic

diagram and digital picture of the designed system, respectively. Notably, in this system, the up-flow adsorption column comprises three ordering layers: sand, NLTT, and commercial GAC, with their bed height being 0.5 m, 0.4 m, and 0.3 m, respectively. The adsorption column with its diameter of 0.76 m contained approximately 288 kg of sand (particle size: 2–4 mm), 220 kg of NLTT (0.5–1.0 mm), and 140 kg of GAC (0.5–2.5 mm) in each layer. The EBCT of adsorption column is 20 min. To evaluate how well the childcare centre functioned, the water samples were collected weekly from six different positions (from **C1** to **C6** in **Figure 6.2**) for around six months. A commercial granular activated carbon (GAC) used as a second adsorbent in the community filtration system was purchased from the Phuong Nam Company Limited in Vietnam.

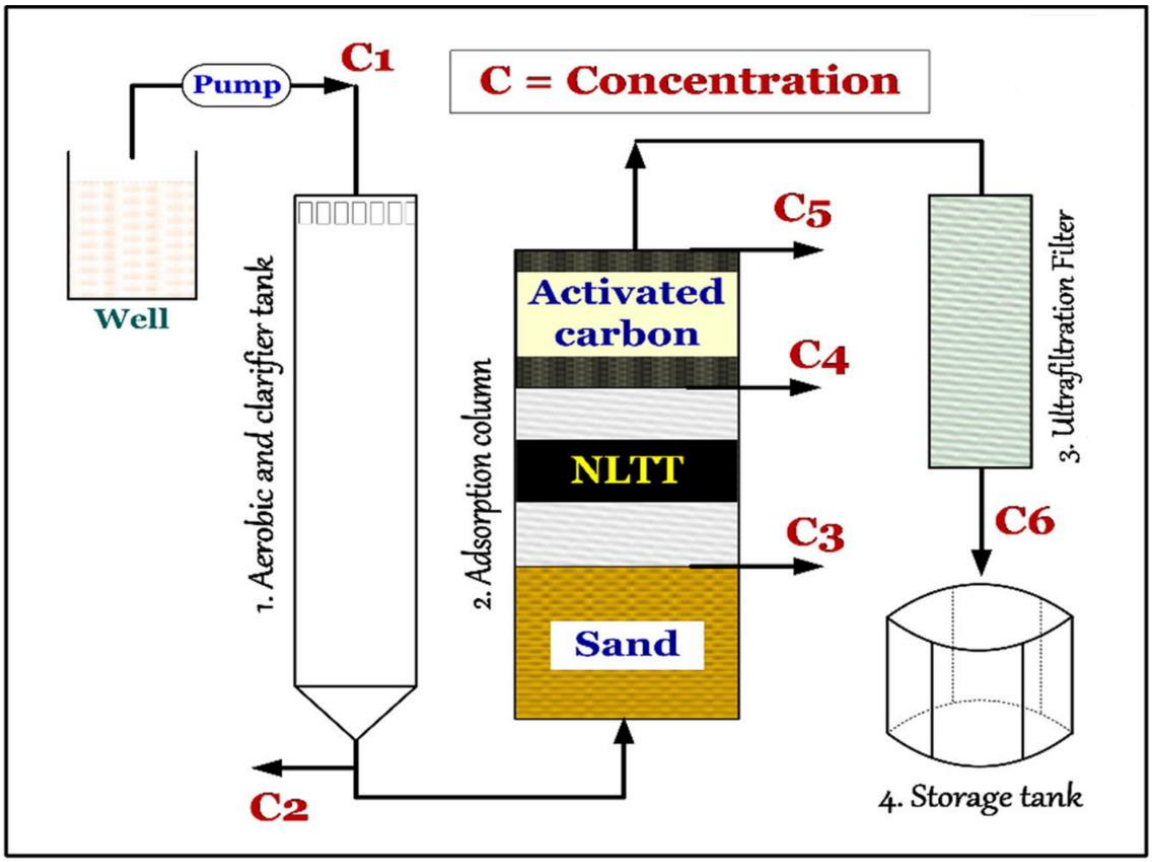

Figure 6.2. Schematic diagram of the water treatment system

6.2.2.2. Field study with household filter treatment systems in Hoang Tay commune, Ha Nam and Phuong Tu commune, Hanoi

The results of a water quality survey carried out by the University of Technology Sydney and its partners in Hoang Tay commune, Ha Nam, from June to September 2017 and Phuong Tu commune, Hanoi from November to December 2019 indicated that the total As concentration in some local wells ranged from 0.028 to 0.447 mg/L, remarkably higher than the As safety limit, which is approximately 3 to 45 times, respectively, than the As safety limit recommended by the World Health Organization (WHO) and the Vietnam drinking water quality standard (QCVN01:2009/BYT).

The household filter system used in this field study had a filter cartridge packed with 15 kg NLTT (particle size of 1–2 mm) and 1 kg of sand, as shown in **Figure 6.3**. The sand was placed at the bottom of the filter cartridge, and NLTT media was then placed above the sand layer. The filter cartridge was prepared from a PVC water pipe with an inner diameter of 14 cm and 65 cm height. Four such filters were installed, two in Hoang Tay commune, Kim Bang district, Ha Nam province, and two in Phuong Tu commune, Ung Hoa district, Hanoi, Vietnam. Groundwaters that were pre-treated with traditional sand filters were passed through the NLTT filter at a filtration rate of 10 L/h (0.65 m/h), corresponding to a EBCT of 45 min.

Groundwater samples before and after treatment by, firstly, the traditional sand filters and secondly, NLTT filter system were collected fortnightly over 7 months. The sand filter, which has been traditionally used in Vietnam, comprised two main containers: sand filter tank (about 0.5 – 1 m^3) and water storage tank (0.5 – 1 m^3). The sand filter tank was constructed above a water storage tank and filled with locally available sand

(approximate 300–600 kg). The groundwater is pumped from the tube well into the sand filter tank and allowed to trickle through the sand layers into the water storage tank. The samples were filtered using 0.45 µm filters, and filtrates were analyzed for As using inductively coupled plasma mass spectrometry (ICPMS, NexION 2000, US) ICPMS and Fe using an Atomic Absorption Spectrometer (PinAAcle 900T, USA). The As-laden NLTT adsorbent samples at the second household (H2) in Hoang Tay commune were collected and characterized after three months and six months operation. At each collection time, two As-laden NLTT adsorbent samples were collected, one from the bottom layer (approximately 55 cm from the lip of the filter column) and the other from the top layer (approximately 10 cm from the lip of the filter column).

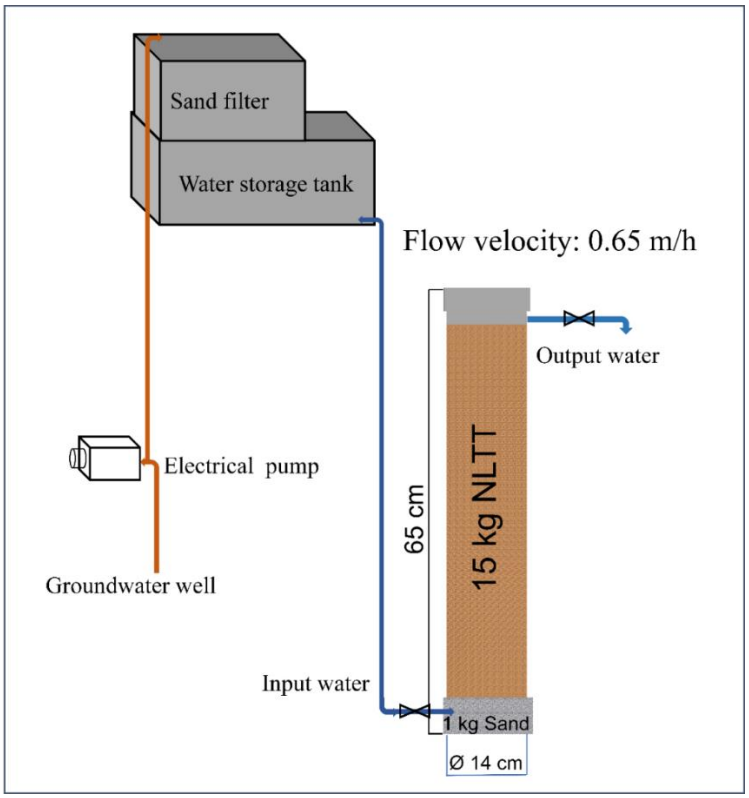

Figure 6.3. Schematic diagram of household filter system

6.2.2. Solidification/stabilization

An analysis of the management of exhausted NLTT was carried out using the solidification/stabilization method. Schematic diagram of solidification/stabilization study is shown in **Figure 6.4.** The exhausted NLTT media was prepared by soaking 5 kg NLTT material into 5 L of synthetic As(V) solutions of 4.5 g/L concentration. After 40 days soaking, the solid phase (adsorbent containing adsorbed As(V)) of the mixture was separated by filtration, dried in an oven for 48 h at 50 °C, and stored in tightly closed bags for later use in the solidification/stabilization process.

In this study, microwave digestion technique was applied to prepare the digested sample. The combination of three types of acids, including HNO_3, HCl, and HF were used for extraction process (Kailasa and Wu, 2012). Among them, HCl was used for extraction of salts (carbonate, phosphates), some oxides and sulfides. HF was needed for digestion of silica-based compounds. HNO_3 then extracts other compounds that were not extracted by HCl and HF. Briefly, 0.15 g of NLTT samples containing the adsorbed As(V) were digested in an acid solution consisting of a mixture of 2 mL concentrated HNO_3, 4 mL concentrated HCl, and 2 mL concentrated HF using a microwave digester for 3 h (Kailasa and Wu, 2012). The digested solutions were diluted to an appropriate volume and the As concentration was determined. Results show that the digested NLTT had 0.564 mg/g NLTT for As(V). This value is approximately the same as the Langmuir maximum adsorption capacity of 0.58 mg/g for As(V) at pH 7 and 30 °C reported for NLTT (**Section 3.3.6**). This confirms that 40 days soaking of NLTT in 4.5 g/L As(V) solution completely saturated the adsorption sites of NLTT with As(V). Therefore, the adsorbent material prepared by this method can be used as a material representing exhausted adsorbent.

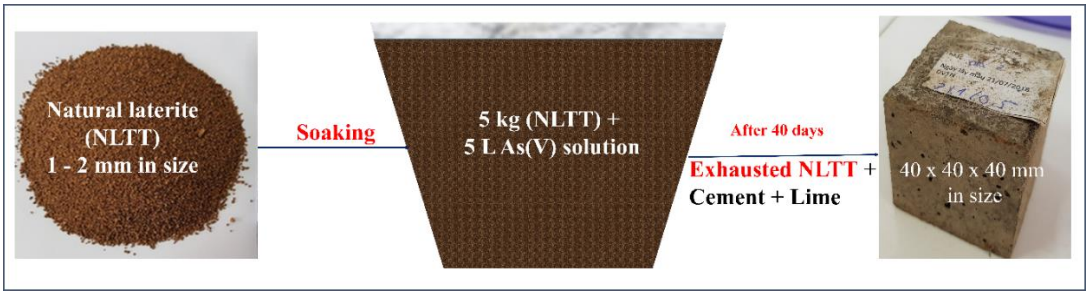

Figure 6.4. Schematic diagram of solidification/stabilization study

6.2.2.1. Preparation of concrete bricks

Three different concrete brick products, namely NLTT3C1L0, NLTT3C1L1, and NLTT3C1L0.5, were prepared by mixing exhausted NLTT, Portland cement (C), and lime (L) at NLTT : C : L mass ratios of 3:1:0, 3:1:1, and 3:1:0.5, respectively. Portland cement and lime used in the mixture were purchased from a local construction material store. Initially, 1.8 kg of exhausted NLTT adsorbent was mixed with 0.5 L of deionized water, and then cement and lime were added to this mixture at the specified ratios. Then, the composite materials were thoroughly mixed using a laboratory concrete mixer. The mixed slurries were cured by placing them inside 40 × 40 × 40 mm cement cube moulds for 24 hours, as shown in **Figure 6.4.** The concrete bricks formed were taken out from the moulds and soaked in water for 27 days before conducting tests on them.

6.2.2.2. Leaching test

To determine the amount of As leaching to the environment from the concrete brick samples, a leaching test was conducted on all concrete samples. In this test, the concrete bricks samples with sizes of 40 × 40 × 40 mm were cut into smaller ones of 20 × 20 × 20 mm size with weights of approximately 75 g each. These small concrete bricks

were then washed with deionized (DI) water to eliminate any adhering dirt before placing them inside closed vessels without agitation that contained different leachants, such as distilled water (DW), 0.1 M HNO_3, and 0.1 M NaOH (Kundu and Gupta, 2008).

6.2.2.3. Physical properties of concrete bricks

The compressive strength property of the final concrete brick samples was determined using Vietnam standard methods, namely the Brick test method (TCVN 6355:2-2009). The compressive strength of concrete brick samples was measured using a concrete compressor TYA-300 LUDA.

6.3. Results and discussion

6.3.1. Field studies

6.3.1.1. Field study with community filter treatment system in Hoang Tay commune, Ha Nam province

Based on the batch adsorption experiments, a field trial was conducted to remove groundwater As contamination at Hoang Tay Childcare Centre for over 6 months. **Figure 6.5** shows the performance of the community water filter system. In general, the As concentration in groundwater is strongly dependent on the groundwater levels (or water aquifer) that often remarkably vary between dry and rainy seasons (Berg et al., 2007). In this study, total As concentration in the feedwater (the **C1** position in **Figure 6.2**) ranged from 0.122 mg/L to 0.237 mg/L (average 0.165±0.0389 mg/L). In addition, the groundwater contained a high concentration of total iron (3.78–7.24 mg/L). In essence, a Fe/As atomic ratio (ranging from 40.4 to 41.1) higher than 40 is expected to efficiently remove As from groundwater through common co-precipitation mechanism.

The above assumption was well consistent with the total As concentration in the **C2** position. As previously mentioned, after the groundwater has been extracted from the well, it was oxygenated through the aeration tank. The essential role of aeration tank (using as a typical pre-treatment process) in a groundwater treatment system has been reported and discussed in the literature (Rott et al., 2002; Farrell and Chaudhary, 2013; Luong et al., 2018). This tank is mainly responsible for successfully remove some parts of certain pollutants (i.e., As, iron, manganese, etc.) and enhance the effectiveness of the whole system (especially, the adsorption column). In essence, when the iron-groundwater was exposed to natural air through the aeration tank, the oxidation process of Fe^{2+} into Fe^{3+} can spontaneously occur. In addition, As(III) was oxidized to As(V) under this condition (Berg et al., 2007; Luong et al., 2018). The co-precipitation process neither between Fe^{3+} (oxidized) and As(V) nor Fe^{2+} (un-oxidized) and As(V) was primarily regarded as the removal mechanism of As from water in the **C2** position. This mean that the aeration tank can effectively simulate the co-precipitation process between As and iron to form the precipitates of $FeAsO_4 \circ 2H_2O$ and $Fe_3(AsO_4)_2 \circ 8H_2O$ through **Equations 6.3–6.4** (Lenoble et al., 2005). However, such co-precipitation process is strongly dependent on the Fe/As ratio and oxidation conditions (i.e., contact time and oxygen concentration). For example, the Fe/As atomic ratio in water dramatically decreased from 40 in the **C1** position to 2.4 (a Fe/As range from 2.3 to 2.5) in the **C2** one. Although the total As concentration passed through the aeration tank significantly decreased by approximately 70%±13%, its concentration (0.0232–0.0892 mg/L; average 0.0537±0.0.0229 mg/L) still exceeds the Vietnamese drinking water standard and WHO guideline (0.010 mg/L). Therefore, it is necessary to apply the adsorption column with certain appropriate adsorbent to remove As from water.

$$Fe^{2+} \rightleftharpoons Fe^{3+} + 1e^{-} \quad \textbf{(6.1)}$$

$$H_3AsO_3° + H_2O \rightleftharpoons HAsO_4^{2-} + 4H^{+} + 2e^{-} \quad \textbf{(6.2)}$$

$$Fe^{3+} + HAsO_4^{2-} \rightleftharpoons FeAsO_4 + H^{+} \quad \textbf{(6.3)}$$

$$3Fe^{2+}\ (\text{un-oxidized}) + 2HAsO_4^{2-} \rightleftharpoons Fe_3(AsO_4)_2 + 2H^{+} \quad \textbf{(6.4)}$$

After the aeration and clarifier tank, the supplied water was passed through the adsorption filter containing three material layers (i.e., sand, NLTT, and activated carbon). Firstly, the total As concentration after passing the sand layer (the **C3** position) varied from 0.00805 to 0.0849 mg/L (average 0.0325±0.00194 mg/L), which was lower than the As concentration in **C2** position (0.0232–0.0892 mg/L). In addition, the data collected at the different operation times indicate that the total As concentration decreased gradually (data not shown). Such decrease might result from a common reaction between uncomplete reaction between iron and As in the **C2** position. Another reason might result for the iron (III) formed by the oxidation of dissolved iron (II) was slowly getting deposited on the sand layer, which might act as an As adsorbent (Gibbons and Gagnon, 2010; Nur et al., 2019). Secondly, the total As concentration in the **C4** position (0.00097–0.00987 mg/L; average 0.00486±0.00338 mg/L) was always lower than 0.01 mg/L during the first 6 months operational period with a continuous input of water of more than 206 m^3. The result suggests that the NLTT can serve a promising to efficiently remove the As contaminant from real groundwater. Thirdly, the total As concentration in the **C5** position (0.00117–0.00970 mg/L; average 0.00454±0.00294 mg/L) was relatively similar to the **C4** one, suggesting that the used GAC exhibited poor adsorption capacity to As ions in solution. Similarity, the efficient removal of As by the ultra-membrane was negligible,

with the total As concentration ranging from 0.00169 to 0.00950 mg/L (average 0.00444±0.00349 mg/L).

The NLTT in the filter was replaced after 7 months of operation due to receiving the new batch of NLTT and availability of technical staff. At the replacement time, the filtration system continued to function providing a total of 240 m^3 of water with less than 0.010 mg/L of As. The cost of locally available NLTT adsorbent for providing water for 7 months with this low As concentration is 0.09 US$/$m^3$ (220 kg x 0.10 US$/kg/240 m^3). This cost is less than that of commercial 'imported' adsorbents such as Bayoxide. For example, (Katsoyiannis et al., 2015) reported that the cost of Bayoxide in treating water containing 41 ug/L to the permissible level of 10 ug/L was 0.09 Euro/m^3 (0.10 US$/$m^3$). The exhausted spent adsorbent is carefully stored in containers and will be used for producing concrete for road construction.

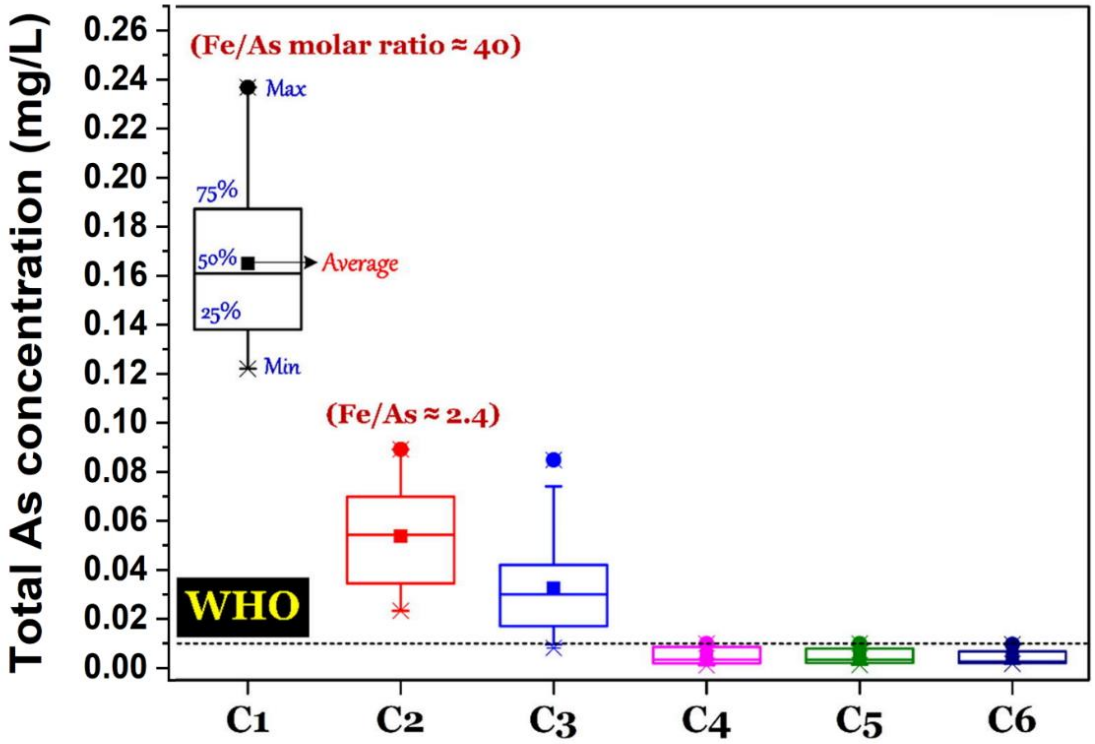

Figure 6.5. The performance of the system during six-month operation period

(The horizontal line in each graph represents the World Health Organization (WHO) As concentration limit (0.01 mg/L)**)**

To sum up, the experimental results after approximately the six-month period demonstrated that the total As (0.00169–0.0095 mg/L) and Fe (0.020–0.130 mg/L) concentrations remained below the upper permitted limits (0.01 mg/L and 0.3 mg/L, respectively). In addition, the concentrations of other cations (total Fe, Mn, Cu, total Cr, Pb, Hg, Ni, and Cd) and anions in the treated water were below the Vietnamese drinking water quality standard (**Table 6.2**). Especially, there was not the existence of Coliform and E. Coli in the treated water after the ultrafilter unit.

Table 6.2. Water quality parameter concentrations from the water treatment system and Vietnam regulation concentration limits

Parameter	Unit	Value	Standard*
Antimony	mg/L	0.0023	0.02
Barium	mg/L	0.0078	0.7
Boron	mg/L	<0.01	0.5
Bromide	mg/L	0.023	0.01
Cadmium	mg/L	0.00025	0.003
Iron	mg/L	0.130	0.3*
Chromium	mg/L	0.0026	0.05
Copper	mg/L	<0.01	2.0
Cyanide	mg/L	<0.005	0.07
Lead	mg/L	0.0048	0.01
Manganese	mg/L	0.0093	0.4
Mercury	mg/L	0.0002	0.006
Molybdite	mg/L	0.0047	0.07
Nickel	mg/L	0.0012	0.07
Selenium	mg/L	0.0044	0.01
Total Coliform	CFU/100mL	0	0
E. Coli	CFU/100mL	0	0

Note: *Based on Vietnam Standard for Drinking Water QCVN 01:2009/BYT.

6.3.1.2. Field study with household filter systems in Hoang Tay commune, Ha Nam province and Phuong Tu commune, Hanoi

a. Performance of NLTT filter system

Figure 6.6 presents the NLTT filter effectiveness in removing As in four different households - H1, H2, H3, and H4 (H1 and H2: two households in Hoang Tay commune; H3 and H4: two households in Phuong Tu commune). Over the seven months of operation in Hoang Tay commune (May 2019 to January 2020), the results show that the total As concentration (mg/L) in groundwater feed to filters in H1 and H2 houses ranged from 0.156 to 0.235 (median 0.19) and 0.114 to 0.17 (median 0.15), respectively. The disparity in total As concentration in the two households is probably due to spatial hydrological and geochemical differences between the locations of the households. Such differences even within short distances apart in Vietnam were reported by Berg et al. (2007).

During the 6-month operation period (September 2020 to February 2021) in Phuong Tu commune, the total As concentration in groundwater (mg/L) in H3 and H4 houses ranged from 0.047 to 0.056 (median 0.052), and 0.027 to 0.05 (median 0.040), respectively. The total As concentrations in groundwater in the two households in this commune were much lower with reduced variability compared to those in the two households in Hoang Tay commune.

As clearly evident in **Figure 6.6**, the concentration of total As passing through the sand filter had diminished considerably. However, they were still 2.6 to 5.4 times higher than that of the Vietnamese drinking water standard and WHO guideline (0.01 mg/L). Therefore, it is necessary to apply another household filter that can provide safe and sustainable drinking water at a decentralized scale.

To reduce As concentration further, the sand filter treated water was passed through the NLTT filter system. The results show that total As concentration in the output water in the H1 and H2 households ranged from 0.004 to 0.009 mg/L (median 0.006 mg/L) and 0.003 to 0.01 mg/L (median 0.0066 mg/L), respectively. The average As removal efficiency was 88%. The total As concentration in the output water in the H3 and H4 households ranged from 0.0004 to 0.009 mg/L and 0.0004 to 0.003 mg/L, respectively. The average As removal efficiency in these two household filters amounted to 92%.

Modelling of the data from the household filter system could not be conducted because generally all values for *Ct/Co* were less than 0.1. This is due to the low influent As concentrations that entered the NLTT column (0.02–0.05 mg/L compared to 0.1 and 0.5 mg/L used in the laboratory column study) and adsorption of very high proportion of the As that entered. As a consequence of this, significant breakthrough of As did not occur. There was also high variability in the influent concentration because the pre-treatment of the water with sand filter removed variable amounts of As.

The average Fe concentrations in the H1 and H2 households' effluents were 0.13 mg/L and 0.167 mg/L, respectively. The output filtered water in the H3 and H4 households had a much smaller concentration of Fe (0.05 mg/L). The range of Mn concentration in the treated water in all households was 0.17–0.24 mg/L. Both the concentrations of Fe and Mn were below the Vietnamese drinking water quality standard (QCVN 01:2009/BYT) (0.3 mg/L for both of Fe and Mn). During the 7 months when the filters were operating, at each household a total of approximately 2.1 m^3 water was treated to produce safe drinking water (As concentration below the Vietnam and WHO drinking

water standard of 0.01 mg/L). The cost of treating 1 m^3 water using NLTT is estimated to be lower than US$ 0.71/m^3 ((US$ 0.1/1 kg NLTT × 15 kg)/2.1 m^3).

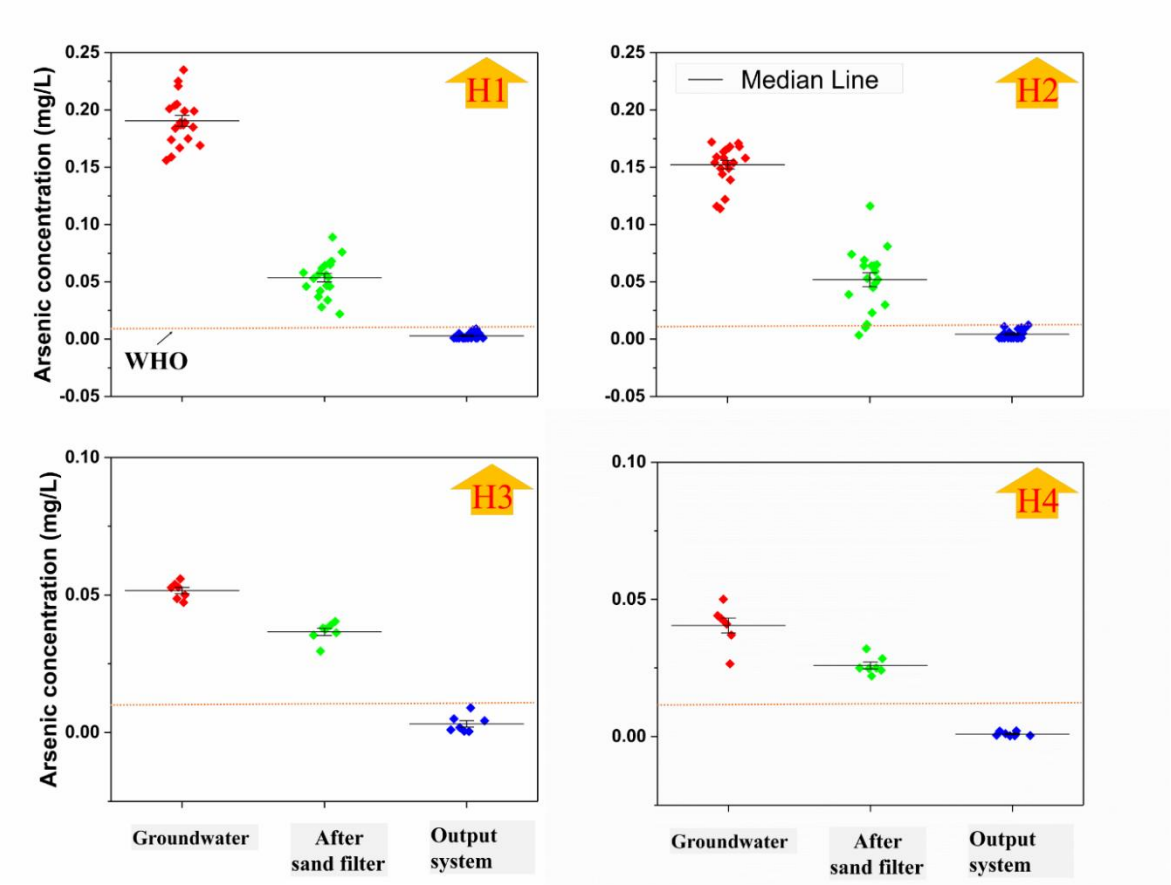

Figure 6.6. As concentration in groundwater (red dots), after sand filter (green dots), and in the output of NLTT filters (blue dots).

(The horizontal line in each graph represents the World Health Organization (WHO) As concentration limit (0.01 mg/L))

b. NLTT characterization after As adsorption

The mineralogy of NLTT before and after adsorption in field filters was determined using X-Ray powder diffraction. **Figure 6.7** shows five different XRD patterns: (1) pristine NLTT; (2) As-laden NLTT at the top layer (approximately 10 cm

from the lip of the filter column) after three months; (3) As-laden NLTT at the bottom layer (approximately 55 cm from the lip of the filter column) after three months; (4) As-laden NLTT at the top layer after six months; and (5) As-laden NLTT at the bottom layer after six months. The peaks for the main component minerals such as goethite (FeOOH), hematite (Fe_2O_3), nacrite ($AlSiO_5(OH)_4$), quartz (SiO_4), and anatase (TiO_2) of NLTT adsorbent after the field test appeared again after adsorption. However, the peak intensities of goethite, hematite, and nacrite of As-laden NLTT after three months and six months were slightly reduced from that of pristine NLTT. The peak intensity of As-laden NLTT at the bottom layer was lower than that of As-laden NLTT at the top layer after three months.

The same trend was also observed for the two layers after six months. The reduction in peak intensity of the minerals is probably due to As(V) reacting with Fe oxide/hydroxide sites in goethite and hematite and Al oxide/hydroxide sites in nacrite, slightly altering these minerals' crystal structures. The adsorbent at the bottom layer had lower peak intensities compared to that at the top layer. This is because the filter system was operated in the up-flow mode (solution moving from bottom of the column to top). In this mode of operation, the NLTT adsorbent at the bottom layer would have had contact with water containing a higher As concentration than that at the top layer, because by the time the water reached the top layer some of the As in the water would have been removed by the bottom layer. Moreover, the XRD patterns of NLTT after six months **(Figure 6.7** - [4] and [5]**)** possess a clear peak intensity change from those of NLTT after three months. This was due to NLTT interacting with a larger amount of As that passed through the column during the longer period of time (Rout et al., 2015).

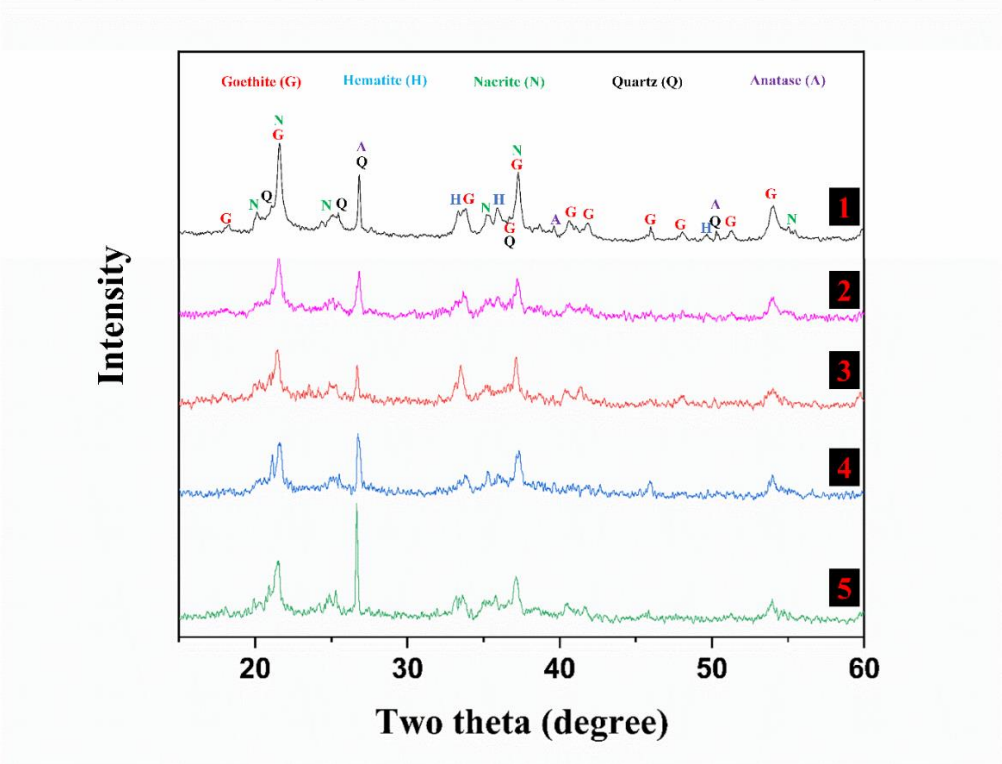

Figure 6.7. XRD pattern of (1) pristine NLTT; (2) As-laden NLTT at the top layer after 3 months, (3) As-laden NLTT at the bottom layer after 3 months, (4) As-laden NLTT at the top layer after 6 months, and (5) As-laden NLTT at the bottom layer after 6 months

The main functional groups on the surface of the pristine NLTT, and As-laden NLTT at the top and bottom layers at 3 months and 6 months after adsorption were determined by FTIR. **Figure 6.8** shows that the surfaces of all As-laden NLTT possess similar main functional groups, such as Si–O–Fe (at approximately 1100 cm^{-1}), Si–O (at 1030 cm^{-1}), Al–OH (at 910 cm^{-1}), Fe–OH (at 798 cm^{-1}), Fe–O (at 460 cm^{-1}), and -O-H (at the region of 3730 cm^{-1} and 3100 cm^{-1}) as those of pristine NLTT. Additionally, the results show no change occurred in the intensities of FTIR spectra of As-laden NLTT after three months operation compared to that of pristine NLTT adsorbent. On the other

hand, the FTIR spectrum of As-laden NLTT after six months of operation (**Figure 6.8** – (4) and (5)) reveals there was a remarkable decline in absorbance for all the main functional groups. This is due to the longer period of interaction between As and NLTT leading to larger amounts of As being adsorbed. Both the XRD and FTIR data showed that As was adsorbed onto the Fe and Al containing minerals in NLTT, while the amount adsorbed was higher at the bottom layer and at the longer operation time.

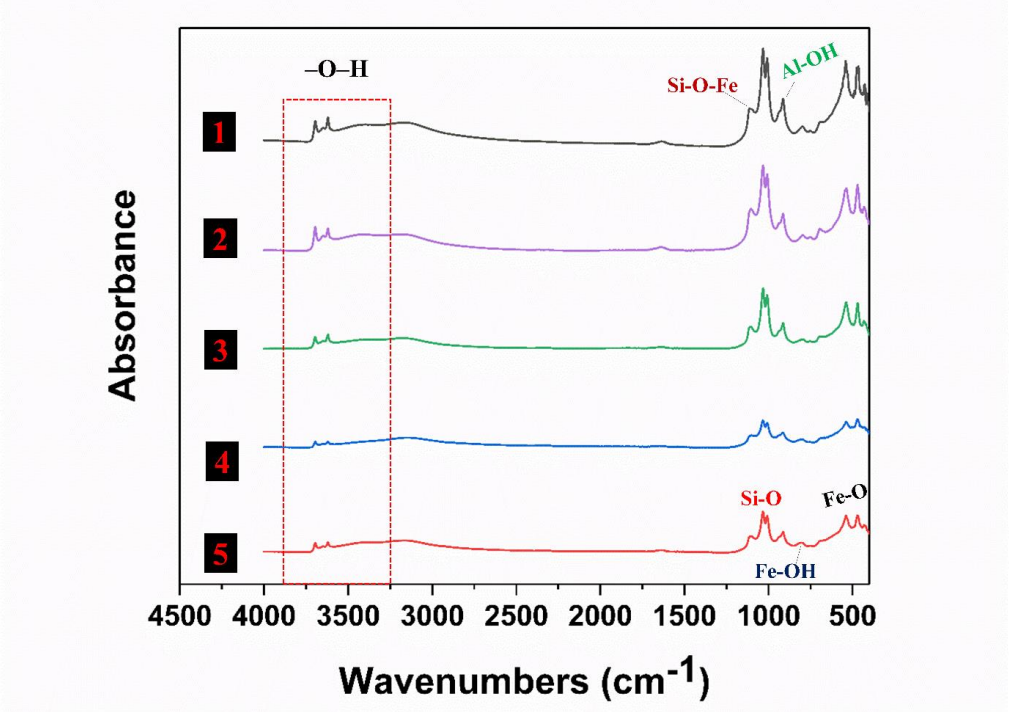

Figure 6.8. FTIR spectrum of (1) pristine NLTT; (2) As-laden NLTT at the top layer after 3 months, (3) As-laden NLTT at the bottom layer after 3 months, (4) As-laden NLTT at the top layer after 6 months, and (5) As-laden NLTT at the bottom layer after 6 months

c. Mechanisms of As removal by the filters

In this study, the existing household sand filters were utilized as a beneficial pre-treatment step to enhance the removal efficiency and extend the lifetime of the new household-scale NLTT treatment system. According to Nitzsche et al. (2015), sand filter plays an important role in the efficient removal of As, Fe, and Mn in groundwater. Apart from the enhanced removal of As by the sand filters presented in **Figure 6.6**, the average of Fe concentration (mg/L) after sand filtration in the four households **(**H1, H2, H3, and H4**)** also dropped significantly, from 10.3 to 0.39, 9.76 to 0.17, 1.44 to 0.036, and 0.914 to 0.030, respectively. Moreover, the average Fe/As ratio in the effluents of sand filters of the four households also fell to 7.3, 11, 1.0, and 1.2, respectively, which are much lower than the respective influent concentration ratios (**Figure 6.9**). The simultaneous decrease in the total As concentration, iron concentration, and the Fe/As ratio can be explained by the co-precipitation mechanism of Fe and As in water. This mechanism was also discussed in detail in my previous parts in community filter treatment system. Briefly, when groundwater containing soluble Fe^{2+} and As(III) was pumped into the sand filter tank containing natural air, these ions were oxidized to insoluble Fe^{3+} and As(V) and coprecipitated. The co-precipitation process resulted in the formation of $FeAsO_4.2H_2O$ and $Fe_3(AsO_4)_2.8H_2O$ precipitates. Thus, large amounts of both Fe and As were removed from the water.

Meng and Korfiatis (2001) reported that an Fe/As ratio ≥ 40 was needed to effectively remove As from groundwater by co-precipitation. The average Fe/As ratio in groundwater of the H1 and H2 households were 54 and 64, respectively, which were higher than that of H3 and H4 households of 27 and 24, respectively (**Figure 6.9**). The higher percentage removal of As by sand filters in H1 and H2 households (**Figure 6.5**)

than in H3 and H4 households is due to the higher Fe/As ratio in the groundwaters of H1 and H2 households.

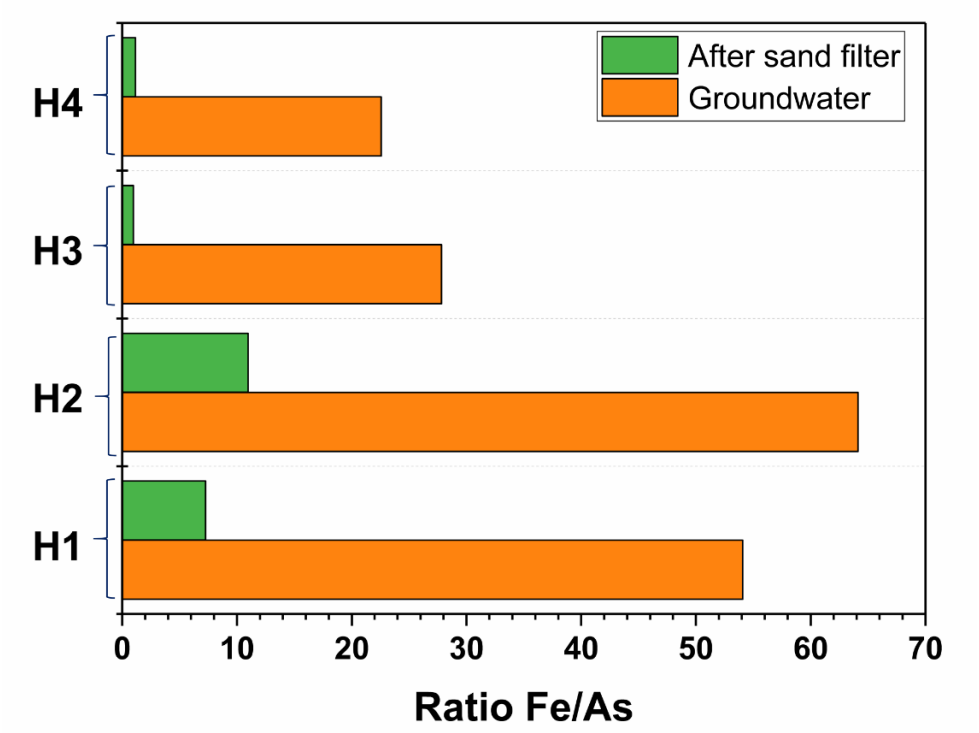

Figure 6.9. Ratio of Fe/As in ground water, after sand filtration in the four households

When the sand filter treated water was passed through the NLTT filter, most of the remaining As in the form of As(V) in the water was removed by adsorption on the Fe and Al oxides/hydroxides in the laterite by inner-sphere complexation as explained by others (Kalaruban et al., 2019; Mohan and Pittman Jr, 2007; Nguyen et al., 2020a). The reactions are represented by the following **Equations (6.5–6.6)**:

$$-\mathbf{X}OH + As(V)^{-} \rightarrow -\mathbf{X}As(V) + OH^{-} \quad \textbf{(6.5)}$$

$$-\mathbf{X}OH + As(V)^{2-} \rightarrow -\mathbf{X}As(V)^{-} + OH^{-} \quad \textbf{(4.6)}$$

where X represents Fe in goethite/hematite or Al in nacrite, and $As(V)^{-}$ and $As(V)^{2-}$ represent $H_2AsO_4^-$ and $HAsO_4^{2-}$, respectively. Both these species of As(V) are present at the neutral pH of the ground waters. At slightly lower pH, the monovalent species predominates and at slightly higher pH, the divalent species predominates.

6.3.2. Solidification/Stabilization

6.3.2.1. Compressive strength of concrete bricks made from spent adsorbent

The compressive strength of NLTT3C1L0 (20.67 MPa) was higher than that of the other two concrete bricks, NLTT3C1L0.5 (15.30 MPa), and NLTT3C1L1 (18.27 MPa). The results suggest that adding lime materials into concrete components could slightly undermine the bricks' compressive strength. According to the Vietnam concrete bricks and interlocking concrete bricks standard (TCVN 6477:2016), the compressive strength of concrete products should be in the 3.5 MPa to 20 MPa range. Concrete bricks are commonly used in construction work. According to the British concrete standard (BS 8500: 2002, Part 1 and 2), concrete with the compressive strength of 10–20 MPa, can be used for non-structural works such as patio slabs and pathways (10MPa), pavement kerbs, and floor blinding (15MPa), and international floor slabs, flooring for the workshops, garages, and driveways (20MPa). Therefore, all three concrete products created in this study can be used for pavement kerbs, garages, and driveways, which have limited contact times with people.

6.3.2.2. As leaching from concrete bricks

The concentration of As leached from concrete products in three different leachates (0.1 M NaOH, distilled water, and 0.1 M HNO_3) at different leaching times is presented in **Figure 6.10**. The results indicate that strong alkaline and acid conditions

could lead to significant leaching of As from the concrete mixtures. In general, the As leachability from all three concrete bricks followed the order of 0.1 M NaOH > 0.1 M HNO_3 > distilled water. As concentration increased rapidly during the first seven days and then slowly in the next 35 days. A similar trend was reported in other studies (Kundu and Gupta, 2008; Singh and Pant, 2006). In all three leachates, the highest concentration of As in the leachate was observed from the NLTT3C1L1 sample. The lowest leaching was observed for NLTT3C1L0.5 in acid and distilled water environments and for NLTT3C1L0 in a strong alkaline environment. The maximum As concentrations in the 0.1 M NaOH leachate from NLTT3C1L1, NLTT3C1L0.5, and NLTT3C1L0 were 1.705 mg/L, 0.993 mg/L, and 0.54 mg/L, respectively. The corresponding concentrations from 0.1 M HNO_3 leachant were 0.0632 mg/L, 0.0362 mg/L, and 0.0511 mg/L, respectively. Notably, the As concentrations in the leachates from the samples using distilled water were extremely low.

Although the As concentration in the leachates was over 0.01 mg/L after only one day, the As concentration in the leachates from all three solidified/stabilized products was always well below the recommended limit of 5 mg/L stipulated in the TCLP (toxicity characteristic leaching procedure) of USEPA (Jing et al., 2005). TCLP is the most widely used method for determination of leaching from solid phase. It was also used to categorize the spent adsorbent media as hazardous or non-hazardous waste. For As, the regulated level for TCLP is 5 mg/L. If the leachate contains As concentration of lower than 5 mg/L, it sugessted that the waste can be categoried as non- hazardous and can be legally disposed of in a normal landfill. Thus, solidification/stabilization method used in this study is feasible.

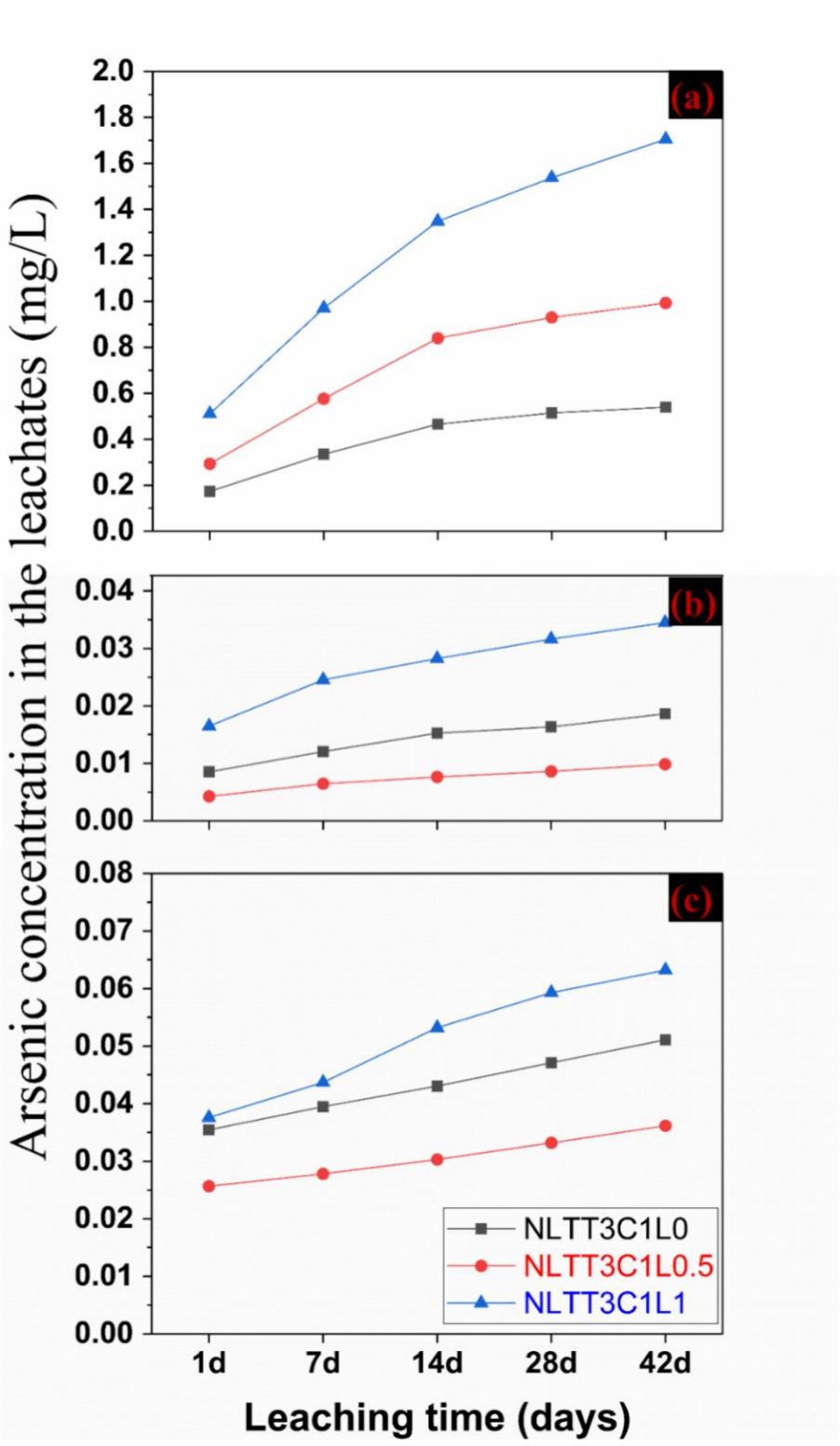

Figure 6.10. Leachability of As from concrete bricks using different leachants: (a) 0.1M NaOH, (b) distilled water, and (c) 0.1M HCl

Of the three products, the one with the higher rate of lime addition had the highest As leached by all three leachants. Kundu and Gupta (2008) also reported that when a large amount of lime was added to concrete, As leaching increased because of higher diffusivity of As through the concrete matrix. Taking these results into account, NLTT3C1L0.5 and NLTT3C1L0 appear to be the best products able to prevent As leaching into the environment. For the As leaching with distilled water and acid leachant, the pH conditions generally prevalent in most environments, NLTT3C1L0.5 produced less leaching than NLTT3C1L0. Therefore, adding lime to cement at this ratio is recommended for mixing with the exhausted adsorbent before disposing of this waste.

During the 42 days leaching trial, the pH of the leachates in 0.1 M NaOH, HNO_3, and distilled water were 12–13, 1–3, and 10–11, respectively. The reduction of pH of acid leachate and increase of pH of alkali leachate is expected because they are consistent with the pH of the leachants. The increase in pH of the distilled water (pH around 7) leachate is due to the dissolution of calcium (Ca) hydroxide present in cement and added lime. A similar increase in pH of water leachate from concrete bricks was reported by Nguyen et al. (2020b). An increase of leachate pH and the presence of Ca in concrete and added lime would have resulted in the formation of Ca-As precipitates (calcium arsenate, calcium arsenite, calcium hydrogen arsenate hydrate, and calcium hydrogen arsenate). This scenario might have reduced the concentration of As in the leachate (Jing et al., 2005; Silva et al., 2019).

6.4. Conclusions

The results from field studies show that NLTT adsorbent could be used as low-cost As filter medium. Both community and household water filtration systems packed

with NLTT (material cost of US$ 22 for a childcare in Hoang Tay commune and US$ 1.5 for a household water filtration) could produce safe drinking water continuously for at least six months with the As level remaining below the WHO and Vietnam drinking water limits. The detailed field study on household filters' performance at four different sites in the Red River Delta show that the median As concentration in groundwaters (0.04–0.19 mg/L) only dropped to 0.026–0.054 mg/L after traditional sand filtration. However, following subsequent NLTT filtration through simple household filter columns (14 cm inner diameter, 65 cm height, capacity of 12 L/h), the effluent satisfied the Vietnam and WHO drinking water standard (0.01 mg/L) during seven months of continuous operation at four different sites. The monitoring of a community water filtration treatment system (capacity of 500 L/h) packed with NLTT in Ha Nam province, Vietnam was also carried out during six months. The findings show that the community filter system could reduce total As concentration in groundwater from 0.122 – 0.237 mg/L to below 0.01 mg/L - the Vietnam and WHO drinking water standard. A traditional sand filtration unit at the household level and aeration tank in community facilities in Vietnam could contribute to As removal from groundwater and it should be used as a pre-treatment system. The main mechanisms in removing As from groundwater in both contexts are the co-precipitation process of Fe and As in groundwater and inner-sphere complexation of As with the Fe and Al oxides/hydroxides in NLTT. The characterization of NLTT after household scale testing revealed no visible change in terms of mineral composition and main function groups on the surface of As-laden NLTT.

Spent adsorbent waste could be managed through the solidification/stabilization technique to prevent As ending up in the natural environment. The mass ratio of As solid waste: Portland cement: lime of 3: 1: 0.5 was determined to be a favorable ratio for

producing good concrete bricks that also restrain the mobility of As. The concrete bricks had acceptable compressive strength for use as a building material in the construction industry.

CHAPTER 7. CONCLUSIONS AND RECOMMENDATIONS

7.1. Conclusions

This study examines the development of three novel iron-based adsorbents and evaluates their performance for As removal from water. In order to achieve these objectives, the development and performance of three novel adsorbents namely NLTT (originated from natural mineral), PPCI (originated from agricultural waste), and Mn/Mg/Fe-LDH (synthesized from commercial chemicals) in removing both As ions (As(V) and As(III)) were investigated in detail. They are presented in Chapters 3, 4, and 5, respectively. The practical application of the low-cost adsorbent, NLTT was also assessed through applying this adsorbent as a filter medium in household and community water filtration systems installed in As contaminated groundwater areas in Vietnam (see Chapter 6). The effects of environmental conditions such as pH solution, contact time, initial As concentration, coexisting anions, temperature on As(III) and As(V) removal of these 3 new adsorbents were studied. The adsorption mechanisms of each adsorbent were investigated in detail through batch experiments and characterization (before and after adsorption). Following the batch experiments, column studies were conducted using different experimental conditions. The data of batch and column studies was described by relevant models (pseudo-first-order, pseudo-second-order, Elovich, Avrami, Langmuir, Freundlich, Redlich-Peterson, Langmuir-Freundlich, Khan, and Thomas). The following are the main findings of this study:

1. NLTT from Thach That rural district, Hanoi was the most promising material for removing As from groundwater compared to the other six low-cost materials originating from natural minerals and industrial waste materials in Vietnam. The

NLTT contains a high percentage of iron (48.7% Fe_2O_3), aluminium (18.2% Al_2O_3) and a small proportion of titanium (2.89% TiO_2) and manganese (0.37% MnO), which play an essential role in oxidizing As(III) into As(V) and adsorbing both As(III) and As(V) ions. As adsorption on these adsorbents quickly reached equilibrium within 120–360 min of contact, depending less on the solution pH from 2.0 to 10, yet strongly affected by the presence of co-existing anions. The Langmuir adsorption capacities of NLTT at pH 7 for As(III) and As(V) were 0.512 and 0.580 mg/g, respectively, which are significantly higher than the values reported for many other low-cost adsorbents. The batch adsorption and material characterization results show that the weak electrostatic attraction (outer-sphere complexation) and surface complexation (inner-sphere complexation) were the main adsorption mechanisms of NLTT for As(V) ions. Meanwhile, the oxidation of As(III) to As(V) and the complexation between As ions in solution and the –OH groups on the NLTT's surface might be dominant reactions for the adsorption of As(III). Results derived from the laboratory filter column study with NLTT indicate that the adsorption breakthrough curves of As(V) at all experimental conditions fitted well with the Thomas model. At As(V) initial concentrations of 0.1 mg/L, the NLTT column could treat up to 497 bed volumes until the filter column effluent started exceeding the Vietnam and WHO drinking water standard (0.01 mg/L).

2. Pomelo peel biochar coated with iron (PPCI) was successfully synthesized through a combination of slow pyrolysis and iron grafting processes. The maximum adsorption capacity of PPCI to As(V) and As(III) calculated by the Langmuir model were 15.28 mg/g and 11.77 mg/g, respectively. These outcomes

are remarkably higher than that of raw pomelo peel, NLTT and many other biomass-derived adsorbents and iron-coated biosorbents reported in the literature. This is because PPCI's surface possesses special functional groups (e.g., O–bearing functional group, and Fe–O group), which play an important role in removing As from aqueous solution. The presence of foreign anions strongly influenced the As removal capacity of PPCI. The pH_{PZC} of PPCI was 7.3, indicating that the PPCI surface was positively charged in natural water. This result is a favourable adsorption scenario for adsorption of negatively charged As. The main adsorption mechanisms of As(V) and As(III) were inner-sphere complexation (ligand exchange, hydrogen bonding) and outer-sphere complexation (electrostatic attraction). Exhausted PPCI could be regenerated using 0.5 M NaOH solution as a desorbing agent. Column experiment results suggest that the Thomas adsorption capacity of PPCI for As(III) and As(V) at a filtration rate of 0.8 m/h was 8.25 mg/g and 9.46 mg/g, respectively. The column could treat up to 3840 bed volumes for As(V) solution of 0.3 mg/L mg/L and 1536 bed volumes for As(III) solution of 0.3 mg/L to below the WHO guidelines. The bed volume value for As(V) is approximately 8 times higher than that of NLTT adsorbent.

3. The new layered double hydroxides - Mn/Mg/Fe-LDH - was successfully prepared from three inorganic salts, namely $Mg(NO_3)_2$, $Mn(NO_3)_2$, and $Fe(NO_3)_3$ through a simple co-precipitation method. Mn/Mg/Fe-LDH exhibits a very high capacity to adsorb As(III) and As(V) ions. The Langmuir maximum adsorption capacities at 25 °C and pH 7.0 were 56.1 mg/g for As(III) and 32.2 mg/g for As(V), which is much higher than that of NLTT and PPCI. The amounts of Mn,

Mg and Fe leached after the adsorption process were very minimal and smaller than Vietnam's National Technical Regulation on Drinking Water Quality. Results of the desorption study indicate that the adsorption process for both As(III) and As(V) was highly irreversible, suggesting that the release of As from laden Mn/Mg/Fe-LDH into the environment was negligible. The main adsorption mechanisms of As(III) and As(V) ions were oxidation-coupled adsorption and reduction-coupled adsorption, respectively, which was confirmed by XPS data. Mn/Mg/Fe-LDH could remove As efficiently from highly contaminated water (for example, from a very high concentration of 0.045–0.092 mg/L to a low concentration of 0.0035-0.0079 mg/L). The column adsorption results obtained with columns packed with as small as 5 g of Mn/Mg/Fe-LDH show that the exhaustion time of Mn/Mg/Fe-LDH for As removal at a filtration rate of 1 m/h was extremely high, 6720 h for As(III) and 4320 h for As(V). The bed volumes with which Mn/Mg/Fe-LDH could treat As(III) and As(V) solution of 0.33 mg/L to a As concentration of below the WHO guideline were 13,920 and 21,600 for As(V) and As(III), respectively. This is approximately 4 times higher for As(V) and 14 times higher for As(III) when compared to PPCI. The results suggest that Mn/Mg/Fe-LDH is a promising catalyst as well as adsorbent for removing both highly toxic As(III) ions and As(III) anions from water.

4. NLTT has been applied successfully as an As filter medium in both household and community water filtration systems. For households, 7-month monitoring results of 4 filter cartridges (capacity of 12 L/h) packed with 15 kg of NLTT show that the filters did successfully remove As from groundwater at four contaminated sites in two communes in Ha Nam province and Hanoi's suburb from an average

of 0.17 mg/L (at Hoang Tay commune) and 0.046 mg/L (at Phuong Tu commune) to below 0.01 mg/L — the As limit in the Vietnam and WHO drinking water guidelines. A community water filtration system (capacity of 500 L/h) packed with 220 kg of NLTT was installed at a childcare centre in Ha Nam province, Vietnam in 2018. Results for a 6-month monitoring period from June, 2018 to January, 2019 showed that the adsorption filter column could reduce As in groundwater from an average of 0.165 mg/L to less than 0.01 mg/L — the requirement of As concentration in drinking water. Experimental results also reveal that exhausted NLTT, after As adsorption, could be successfully managed using the solidification/stabilization technique. The mass ratio of As solid waste : Portland cement : lime of 3: 1: 0.5 was found to be the best ratio for producing good quality concrete bricks. The compressive strength of the concrete bricks at this ratio met the requirement of building material in the construction industry. That bricks could also restrain the mobility of As.

In summary, this study shows that all iron-based adsorbents developed in this thesis can be used to remove As from water environment. A concise summary of the study is shown in **Figure 7.1**. Among the three adsorbents developed and investigated in this study, *Mn/Mg/Fe-LDH exhibited the highest adsorption capacity for both As ions and could be used for very highly polluted water sources*. *PPCI could be a new solution of reusing pomelo peel, an agricultural waste for As remediation of contaminated water*. *NLTT could become a popular commercial As filter media and its practical application has been proven through a long-term study with real As contaminated groundwater at different scales and different locations in Vietnam*.

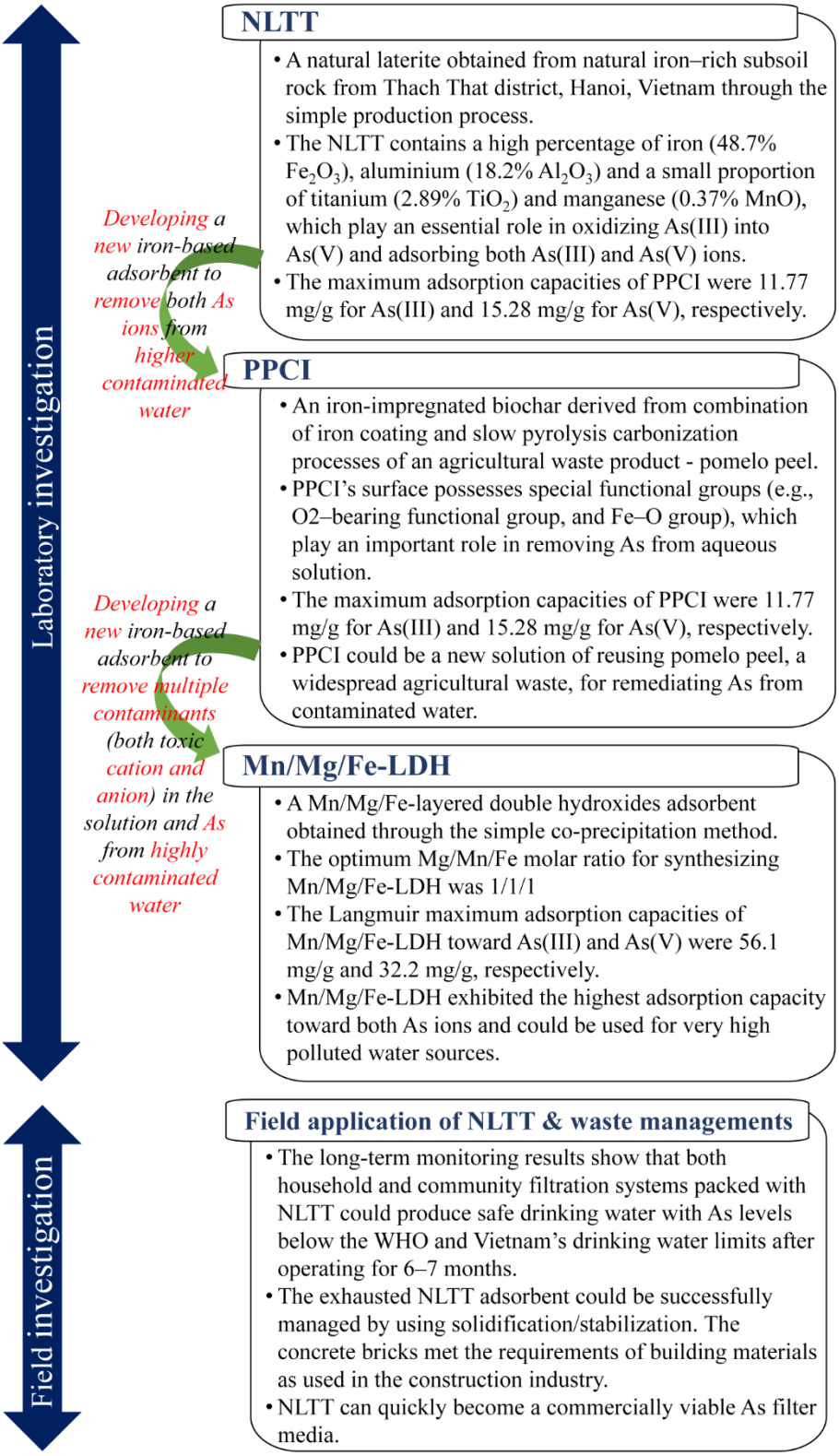

Figure 7.1. Summary diagram of the thesis

7.2. Recommendations

NLTT performed well in removing As from contaminated groundwater. Although NLTT is a low-cost medium and in its exhausted state could be safely managed by stabilisation/solidification with cement, the regeneration of exhausted NLTT is recommended in the future. The economic and technical feasibility of NLTT's regeneration should be evaluated and compared with that of using new NLTT plus stabilizing/solidifying exhausted NLTT. It is furthermore recommended to study the regeneration procedure for exhausted NLTT using a variety of desorbing agents in the future.

The good management of exhausted adsorbents after the As adsorption process is necessary in order to prevent the release of toxic As back into the environment. While spent NLTT was successfully managed through the solidification/stabilization technique, the management of exhausted PPCI and Mn/Mg/Fe-LDH adsorbents containing As has not been investigated in this study. Thus, further research is recommended on how to manage exhausted PPCI and Mn/Mg/Fe-LDH adsorbents after the As adsorption process. Spent Mn/Mg/Fe-LDH could be encapsulated through the solidification/stabilization method, while, the exhausted PPCI could be managed through phytoremediation. This is because the PPCI adsorbent was derived from agricultural waste and contained organic components, suggesting that it could be a soil-friendly product and a suitable bio material.

Due to the recent Covid-19 restrictions, the column studies with NLTT, PPCI, and Mn/Mg/Fe-LDH could only be carried out with restricted conditions. An additional fixed bed column test of NLTT with As(III) ions under various operation conditions is suggested. More column studies on As removal by PPCI and Mn/Mg/Fe-LDH at different

conditions of filtration rate, column bed height, and initial As concentration are suggested in the future to comprehensively investigate the adsorption behaviors of these adsorbents.

Two novel iron-based adsorbents - PPCI and Mn/Mg/Fe-LDH - exhibited superior adsorption capacity towards both As(III) and As(V) ions. It is recommended that pilot field trials of these adsorbents in removing As from real contaminated water be conducted. In addition, the calculation of material and treatment cost is strongly advised to fully evaluate the feasible application of these materials.

Although PPCI and Mn/Mg/Fe-LDH exhibited a very high adsorption capacity in removing As, the mass fabrication process is still a big challenge. For practical application purposes, it is suggested to improve the fabrication procedure towards a mass production and cost reduction. Finally, the water in some regions contains ammonium and pathogens as well as to As. Thus, hybrid processes should be developed to remove all contaminants simultaneously.

References

Abdolali, A., Ngo, H. H., Guo, W., Zhou, J. L., Zhang, J., Liang, S., Chang, S. W., Nguyen, D. D., and Liu, Y. 2017. Application of a breakthrough biosorbent for removing heavy metals from synthetic and real wastewaters in a lab-scale continuous fixed-bed column. Bioresource Technology. 229, 78-87.

Acheampong, M.A., Pakshirajan, K., Annachhatre, A.P. and Lens, P.N.L. 2013. Removal of Cu(II) by biosorption onto coconut shell in fixed-bed column systems. Journal of Industrial and Engineering Chemistry. 19(3), 841-848.

Agusa, T., Kunito, T., Fujihara, J., Kubota, R., Minh, T.B., Trang, P.T.K., Iwata, H., Subramanian, A., Viet, P.H. and Tanabe, S. 2006. Contamination by arsenic and other trace elements in tube-well water and its risk assessment to humans in Hanoi, Vietnam. Environmental Pollution. 139(1), 95-106.

Ahmad, I., Farwa, U., Khan, Z. U. H., Imran, M., Khalid, M. S., Zhu, B., Rasool, A., Shah, G.M., Tahir, M., Ahmed, M., and Bulgariu, L. 2022. Biosorption and health risk assessment of arsenic contaminated water through cotton stalk biochar. Surfaces and Interfaces, 29, 101806.

Akhter, H., Butler, L.G., Branz, S., Cartledge, F.K. and Tittlebaum, M.E. 1990. Immobilization of As, Cd, Cr and PB-containing soils by using cement or pozzolanic fixing agents. Journal of Hazardous Materials. 24(2), 145-155.

Aksu, Z., Çağatay, Ş.Ş. and Gönen, F. 2007. Continuous fixed bed biosorption of reactive dyes by dried Rhizopus arrhizus: Determination of column capacity. Journal of Hazardous Materials. 143(1). 362-371.

Al-Ghouti, M.A. and Da'ana, D.A. 2020. Guidelines for the use and interpretation of adsorption isotherm models: A review. Journal of Hazardous Materials. 393, 122383.

Ali, I. 2018. Microwave assisted economic synthesis of multi walled carbon nanotubes for arsenic species removal in water: batch and column operations. Journal of Molecular Liquids. 271, 677-685.

Altundoğan, H.S., Altundoğan, S., Tümen, F. and Bildik, M. 2000. Arsenic removal from aqueous solutions by adsorption on red mud. Waste Management. 20(8), 761-767.

Amen, R., Bashir, H., Bibi, I., Shaheen, S.M., Niazi, N.K., Shahid, M., Hussain, M.M., Antoniadis, V., Shakoor, M.B., Al-Solaimani, S.G., Wang, H., Bundschuh, J. and Rinklebe, J. 2020. A critical review on arsenic removal from water using biochar-based sorbents: The significance of modification and redox reactions. Chemical Engineering Journal. 396, 125195.

Anirudhan, T. and Unnithan, M.R. 2007. Arsenic (V) removal from aqueous solutions using an anion exchanger derived from coconut coir pith and its recovery. Chemosphere. 66(1), 60-66.

Aredes, S., Klein, B. and Pawlik, M. 2013. The removal of arsenic from water using natural iron oxide minerals. Journal of Cleaner Production. 60, 71-76.

Arencibia, A., López-Gutiérrez, M.S. and Arsuaga, J.M. 2020. Efficient aqueous As(III) removal by adsorption on thiol-functionalized mesoporous silica. Journal of Chemical Technology & Biotechnology. 95(7), 1883-1891.

Asiabi, H., Yamini, Y. and Shamsayei, M. 2017. Highly selective and efficient removal of arsenic (V), chromium (VI) and selenium (VI) oxyanions by layered double

hydroxide intercalated with zwitterionic glycine. Journal of Hazardous Materials. 339, 239-247.
Asmel, N.K., Yusoff, A.R.M., Krishna, L.S., Majid, Z.A. and Salmiati, S. 2017. High concentration arsenic removal from aqueous solution using nano-iron ion enrich material (NIIEM) super adsorbent. Chemical Engineering Journal. 317, 343-355.
Asif, Z., and Chen, Z. 2017. Removal of arsenic from drinking water using rice husk. Applied Water Science. 7(3), 1449-1458.
Bagherifam, S., Komarneni, S., Lakzian, A., Fotovat, A., Khorasani, R., Huang, W., Ma, J. and Wang, Y. 2014. Evaluation of Zn–Al–SO_4 layered double hydroxide for the removal of arsenite and arsenate from a simulated soil solution: isotherms and kinetics. Applied Clay Science. 95, 119-125.
Bai, Y., Yang, T., Liang, J. and Qu, J. 2016. The role of biogenic Fe-Mn oxides formed in situ for arsenic oxidation and adsorption in aquatic ecosystems. Water Research. 98, 119-127.
Baig, S.A., Lou, Z., Hayat, M.T., Fu, R., Liu, Y. and Xu, X. 2016. Characterization of magnetic biochar amended with silicon dioxide prepared at high temperature calcination. Materials Science Poland. 34(3), 597-604.
Banerjee, K., Amy, G.L., Prevost, M., Nour, S., Jekel, M., Gallagher, P.M. and Blumenschein, C.D. 2008. Kinetic and thermodynamic aspects of adsorption of arsenic onto granular ferric hydroxide (GFH). Water Research. 42(13), 3371-3378.
Bang, S., Johnson, M.D., Korfiatis, G.P. and Meng, X. 2005. Chemical reactions between arsenic and zero-valent iron in water. Water Research. 39(5), 763-770.
Berg, M., Stengel, C., Trang, P.T.K., Hung Viet, P., Sampson, M.L., Leng, M., Samreth, S. and Fredericks, D. 2007. Magnitude of arsenic pollution in the Mekong and Red River Deltas — Cambodia and Vietnam. Science of The Total Environment. 372(2), 413-425.
Berg, M., Tran, H.C., Nguyen, T.C., Pham, H.V., Schertenleib, R. and Giger, W. 2001. Arsenic contamination of groundwater and drinking water in Vietnam: a human health threat. Environmental Science & Technology. 35(13), 2621-2626.
Bhattacharyya, K.G. and Gupta, S.S. 2008. Adsorption of a few heavy metals on natural and modified kaolinite and montmorillonite: a review. Advances in Colloid and Interface Science. 140(2), 114-131.
Bilici, M. and Pala, A. 2011. Removal of arsenic from drinking water using modified natural zeolite. Desalination. 281, 396-403.
Blanchard, G., Maunaye, M. and Martin, G. 1984. Removal of heavy metals from waters by means of natural zeolites. Water Research. 18(12), 1501-1507.
Boakye, P., Tran, H.N., Lee, D.S. and Woo, S.H. 2019. Effect of water washing pretreatment on property and adsorption capacity of macroalgae-derived biochar. Journal of Environmental Management. 233, 165-174.
Brion-Roby, R., Gagnon, J., Deschênes, J.S. and Chabot, B. 2018. Investigation of fixed bed adsorption column operation parameters using a chitosan material for treatment of arsenate contaminated water. Journal of Environmental Chemical Engineering. 6(1), 505-511.
Bujňáková, Z., Baláž, P., Zorkovská, A., Sayagués, M.J., Kováč, J. and Timko, M. 2013. Arsenic sorption by nanocrystalline magnetite: An example of environmentally promising interface with geosphere. Journal of Hazardous Materials. 262, 1204-1212.

Bundschuh, J., Schneider, J., Alam, M.A., Niazi, N.K., Herath, I., Parvez, F., Tomaszewska, B., Guilherme, L.R.G., Maity, J.P. and López, D.L. 2021. Seven potential sources of arsenic pollution in Latin America and their environmental and health impacts. Science of the Total Environment. 146274.

Caporale, A., Pigna, M., Dynes, J., Cozzolino, V., Zhu, J. and Violante, A. 2011. Effect of inorganic and organic ligands on the sorption/desorption of arsenate on/from Al–Mg and Fe–Mg layered double hydroxides. Journal of Hazardous Materials. 198, 291-298.

Chang, Q., Lin, W. and Ying, W.C. 2010. Preparation of iron-impregnated granular activated carbon for arsenic removal from drinking water. Journal of Hazardous Materials. 184(1), 515-522.

Chang, Y.Y., Song, K.H. and Yang, J.K. 2008. Removal of As (III) in a column reactor packed with iron-coated sand and manganese-coated sand. Journal of Hazardous Materials. 150(3), 565-572.

Chao, H.P., Wang, Y.C. and Tran, H.N. 2018. Removal of hexavalent chromium from groundwater by Mg/Al-layered double hydroxides using characteristics of in-situ synthesis. Environmental Pollution. 243, 620-629.

Chaudhry, S.A., Zaidi, Z. and Siddiqui, S.I. 2017. Isotherm, kinetic and thermodynamics of arsenic adsorption onto Iron-Zirconium Binary Oxide-Coated Sand (IZBOCS): modelling and process optimization. Journal of Molecular Liquids. 229, 230-240.

Chen, W., Parette, R., Zou, J., Cannon, F.S. and Dempsey, B.A. 2007. Arsenic removal by iron-modified activated carbon. Water Research. 41(9), 1851-1858.

Cheng, D., Ngo, H.H., Guo, W., Chang, S.W., Nguyen, D.D., Zhang, X., Varjani, S. and Liu, Y. 2020. Feasibility study on a new pomelo peel derived biochar for tetracycline antibiotics removal in swine wastewater. Science of The Total Environment. 720, 137662.

Cheng, Y., Zhang, S., Huang, T. and Li, Y. 2019. Arsenite removal from groundwater by iron–manganese oxides filter media: Behavior and mechanism. Water Environment Research. 91(6), 536-545.

Choong, C.E., Wong, K.T., Jang, S.B., Saravanan, P., Park, C., Kim, S.H., Jeon, B.H., Choi, J., Yoon, Y. and Jang, M. 2021. Granular Mg-Fe layered double hydroxide prepared using dual polymers: Insights into synergistic removal of As (III) and As (V). Journal of Hazardous Materials. 403, 123883.

Chowdhury, S.R. and Yanful, E.K. 2010. Arsenic and chromium removal by mixed magnetite–maghemite nanoparticles and the effect of phosphate on removal. Journal of Environmental Management. 91(11), 2238-2247.

Chubar, N., Gerda, V., Megantari, O., Mičušík, M., Omastova, M., Heister, K., Man, P. and Fraissard, J. 2013. Applications versus properties of Mg–Al layered double hydroxides provided by their syntheses methods: Alkoxide and alkoxide-free sol–gel syntheses and hydrothermal precipitation. Chemical Engineering Journal. 234, 284-299.

Cope, C.O., Webster, D.S. and Sabatini, D.A. 2014. Arsenate adsorption onto iron oxide amended rice husk char. Science of The Total Environment. 488-489, 554-561.

Córdova Reyes, I., Salmones, J., Zeifert, B., Contreras, J.L. and Rojas, F. 2014. Transesterification of canola oil catalized by calcined Mg-Al hydrotalcite doped with nitratine. Chemical Engineering Science. 119, 174-181.

Coville, N.J. and Tshavhungwe, A.M. 2010. Mesoporous ethanesilica materials with bimodal and trimodal pore-size distributions synthesised in the presence of cobalt ions. South African Journal of Science. 106(7), 1-5.

Dai, M., Xia, L., Song, S., Peng, C., and Lopez-Valdivieso, A. 2016. Adsorption of As(V) inside the pores of porous hematite in water. Journal of Hazardous Materials. 307, 312-317.

Ding, Z., Xu, X., Phan, T., Hu, X. and Nie, G. 2018. High adsorption performance for As (III) and As (V) onto novel aluminum-enriched biochar derived from abandoned Tetra Paks. Chemosphere. 208, 800-807.

Dixit, S. and Hering, J.G. 2003. Comparison of arsenic (V) and arsenic (III) sorption onto iron oxide minerals: implications for arsenic mobility. Environmental Science Technology. 37(18), 4182-4189.

Dong, F.X., Yan, L., Zhou, X.H., Huang, S.T., Liang, J.Y., Zhang, W.X., Guo, Z.W., Guo, P.R., Qian, W. and Kong, L.J. 2021. Simultaneous adsorption of Cr (VI) and phenol by biochar-based iron oxide composites in water: Performance, kinetics and mechanism. Journal of Hazardous Materials. 416, 125930.

Dorraji, M.S., Mirmohseni, A., Tasselli, F., Criscuoli, A., Carraro, M., Gross, S. and Figoli, A. 2014. Preparation, characterization and application of iron (III)-loaded chitosan hollow fiber membranes as a new bio-based As (V) sorbent. Journal of Polymer Research. 21(4), 1-13.

Duan, X., Zhang, C., Srinivasakannan, C. and Wang, X. 2017. Waste walnut shell valorization to iron loaded biochar and its application to arsenic removal. Resource-Efficient Technologies. 3(1), 29-36.

Dutre, V. and Vandecasteele, C. 1998. Immobilization mechanism of arsenic in waste solidified using cement and lime. Environmental Science & Technology. 32(18), 2782-2787.

Eeshwarasinghe, D., Loganathan, P., Kalaruban, M., Sounthararajah, D. P., Kandasamy, J., and Vigneswaran, S. 2018. Removing polycyclic aromatic hydrocarbons from water using granular activated carbon: kinetic and equilibrium adsorption studies. Environmental Science and Pollution Research. 25(14), 13511-13524.

El-Naggar, N.E.A., Rabei, N.H. and El-Malkey, S.E. 2020. Eco-friendly approach for biosorption of Pb^{2+} and carcinogenic Congo red dye from binary solution onto sustainable Ulva lactuca biomass. Scientific Reports. 10(1), 1-22.

Faria, M.C., Rosemberg, R.S., Bomfeti, C.A., Monteiro, D.S., Barbosa, F., Oliveira, L.C., Rodriguez, M., Pereira, M.C. and Rodrigues, J.L. 2014. Arsenic removal from contaminated water by ultrafine δ-FeOOH adsorbents. Chemical Engineering Journal. 237, 47-54.

Farrell, J. and Chaudhary, B.K. 2013. Understanding arsenate reaction kinetics with ferric hydroxides. Environmental Science & Technology. 47(15), 8342-8347.

Ferrer, D.I. 2016. Supported Layered Double Hydroxides as CO_2 Adsorbents for Sorption-enhanced H_2 Production. Springer.

Foroutan, R., Mohammadi, R., Adeleye, A.S., Farjadfard, S., Esvandi, Z., Arfaeinia, H., Sorial, G.A., Ramavandi, B. and Sahebi, S. 2019. Efficient arsenic (V) removal from contaminated water using natural clay and clay composite adsorbents. Environmental Science and Pollution Research. 26(29), 29748-29762.

Frau, F., Addari, D., Atzei, D., Biddau, R., Cidu, R. and Rossi, A. 2010. Influence of major anions on As (V) adsorption by synthetic 2-line ferrihydrite. Kinetic

investigation and XPS study of the competitive effect of bicarbonate. Water, Air, and Soil Pollution. 205(1), 25-41.
Freundlich, H. 1907. Über die adsorption in lösungen. Zeitschrift für physikalische Chemie. 57(1), 385-470.
Gibbons, M.K. and Gagnon, G.A. 2010. Adsorption of arsenic from a Nova Scotia groundwater onto water treatment residual solids. Water Research. 44(19), 5740-5749.
Giles, D.E., Mohapatra, M., Issa, T.B., Anand, S. and Singh, P. 2011. Iron and aluminium based adsorption strategies for removing arsenic from water. Journal of Environmental Management. 92(12), 3011-3022.
Glocheux, Y., Pasarín, M.M., Albadarin, A.B., Allen, S.J. and Walker, G.M. 2013. Removal of arsenic from groundwater by adsorption onto an acidified laterite by-product. Chemical Engineering Journal. 228, 565-574.
Glodowska, M., Stopelli, E., Straub, D., Thi, D.V., Trang, P.T., Viet, P.H., Berg, M., Kappler, A. and Kleindienst, S. 2021. Arsenic behavior in groundwater in Hanoi (Vietnam) influenced by a complex biogeochemical network of iron, methane, and sulfur cycling. Journal of Hazardous Materials. 407, 124398.
Goh, K.H., Lim, T.T. and Dong, Z. 2008. Application of layered double hydroxides for removal of oxyanions: A review. Water Research. 42(6), 1343-1368.
Goh, K.H., Lim, T.T. and Dong, Z. 2009. Enhanced arsenic removal by hydrothermally treated nanocrystalline Mg/Al layered double hydroxide with nitrate intercalation. Environmental Science & Technology. 43(7), 2537-2543.
Goldberg, S. 2002. Competitive Adsorption of Arsenate and Arsenite on Oxides and Clay Minerals Contribution from the George E. Brown Jr., Salinity Laboratory. Soil Science Society of America Journal. 66(2), 413-421.
Guan, X., Du, J., Meng, X., Sun, Y., Sun, B. and Hu, Q. 2012. Application of titanium dioxide in arsenic removal from water: A review. Journal of Hazardous Materials. 215-216, 1-16.
Guo, H., Stüben, D. and Berner, Z. 2007. Adsorption of arsenic(III) and arsenic(V) from groundwater using natural siderite as the adsorbent. Journal of Colloid and Interface Science. 315(1), 47-53.
Guo, J., Yan, C., Luo, Z., Fang, H., Hu, S., and Cao, Y. 2019. Synthesis of a novel ternary HA/Fe-Mn oxides-loaded biochar composite and its application in cadmium(II) and arsenic(V) adsorption. Journal of Environmental Sciences. 85, 168-176.
Guo, Q., Cao, Y., Yin, Z., Yu, Z., Zhao, Q. and Shu, Z. 2017. Enhanced removal of arsenic from water by synthetic nanocrystalline iowaite. Scientific Reports. 7(1), 1-10.
Guo, X.L., Liu, X.Y., Hao, X.D., Zhu, S.J., Dong, F., Wen, Z.Q. and Zhang, Y.X. 2016. Nickel-manganese layered double hydroxide nanosheets supported on nickel foam for high-performance supercapacitor electrode materials. Electrochimica Acta. 194, 179-186.
Guo, Y., Zhu, Z., Qiu, Y. and Zhao, J. 2012. Adsorption of arsenate on Cu/Mg/Fe/La layered double hydroxide from aqueous solutions. Journal of Hazardous Materials. 239, 279-288.
Gupta, P. K. 2018. Chapter 6 - Metals and micronutrients. In P. K. Gupta (Ed.), Illustrated Toxicology. 195-223.

Gupta, V.K., Saini, V.K. and Jain, N. 2005. Adsorption of As(III) from aqueous solutions by iron oxide-coated sand. Journal of Colloid and Interface Science. 288(1), 55-60.
Hao, L., Liu, M., Wang, N. and Li, G. 2018. A critical review on arsenic removal from water using iron-based adsorbents. RSC Advances. 8(69), 39545-39560.
Haynes, W.M. 2014. CRC handbook of chemistry and physics, CRC press.
He, R., Peng, Z., Lyu, H., Huang, H., Nan, Q. and Tang, J. 2018. Synthesis and characterization of an iron-impregnated biochar for aqueous arsenic removal. Science of the Total Environment. 612, 1177-1186.
Herbel, M. and Fendorf, S. 2006. Biogeochemical processes controlling the speciation and transport of arsenic within iron coated sands. Chemical Geology. 228(1-3), 16-32.
Hering, J. G., Chen, P. Y., Wilkie, J. A., and Elimelech, M. 1997. Arsenic removal from drinking water during coagulation. Journal of Environmental Engineering, 123(8), 800-807.
Hong, H.J., Farooq, W., Yang, J.S. and Yang, J.W. 2010. Preparation and evaluation of Fe-Al binary oxide for arsenic removal: comparative study with single metal oxides. Separation Science and Technology. 45(12-13), 1975-1981.
Hong, J., Zhu, Z., Lu, H. and Qiu, Y. 2014. Synthesis and arsenic adsorption performances of ferric-based layered double hydroxide with α-alanine intercalation. Chemical Engineering Journal. 252, 267-274.
Hongtao, L., Shuxia, L., Hua, Z., Yanling, Q., Daqiang, Y., Jianfu, Z. and Zhiliang, Z. 2018. Comparative study on synchronous adsorption of arsenate and fluoride in aqueous solution onto MgAlFe-LDHs with different intercalating anions. RSC Advances. 8(58), 33301-33313.
Hsu, J.C., Lin, C.J., Liao, C.H. and Chen, S.T. 2008. Removal of As(V) and As(III) by reclaimed iron-oxide coated sands. Journal of Hazardous Materials. 153(1), 817-826.
Huang, P.P., Cao, C.Y., Wei, F., Sun, Y.B. and Song, W.G. 2015. MgAl layered double hydroxides with chloride and carbonate ions as interlayer anions for removal of arsenic and fluoride ions in water. RSC Advances. 5(14), 10412-10417.
Hudcová, B., Veselská, V., Filip, J., Číhalová, S. and Komárek, M. 2017. Sorption mechanisms of arsenate on Mg-Fe layered double hydroxides: A combination of adsorption modeling and solid state analysis. Chemosphere. 168, 539-548.
Jain, N. and Chandramani, S. 2018. Arsenic poisoning-An overview. Indian Journal of Medical Specialities. 9(3), 143-145.
Jang, Y. C., Somanna, Y., and Kim, H. J. I. J. 2016. Source, distribution, toxicity and remediation of arsenic in the environment–a review. International Journal of Applied Environmental Sciences, 11(2), 559-581.
Jayarajan, M., Arunachalam, R. and Annadurai, G. 2011. Use of low cost nano-porous materials of pomelo fruit peel wastes in removal of textile dye. Research Journal of Environmental Sciences. 5(5), 434.
Jeon, C.S., Baek, K., Park, JK., Oh, Y.K. and Lee, S.D. 2009. Adsorption characteristics of As (V) on iron-coated zeolite. Journal of Hazardous Materials. 163(2-3), 804-808.
Jiao, Y.N. and Hou, W.G. 2007. Effects of structural charges on points of zero charge and intrinsic surface reaction equilibrium constants of Zn–Al and Zn–Al–Fe

hydrotalcite-like compounds. Colloids and Surfaces A: Physicochemical and Engineering Aspects. 296(1-3), 62-66.
Jiménez-Cedillo, M., Olguín, M., Fall, C. and Colín, A. 2011. Adsorption capacity of iron-or iron–manganese-modified zeolite-rich tuffs for As (III) and As (V) water pollutants. Applied Clay Science. 54(3-4), 206-216.
Jing, C., Liu, S., and Meng, X. 2005. Arsenic leachability and speciation in cement immobilized water treatment sludge. Chemosphere, 59(9), 1241-1247.
Jing, C., Korfiatis, G.P. and Meng, X. 2003. Immobilization mechanisms of arsenate in iron hydroxide sludge stabilized with cement. Environmental Science & Technology. 37(21), 5050-5056.
Johnston, R.B. and Singer, P.C. 2007. Solubility of symplesite (ferrous arsenate): implications for reduced groundwaters and other geochemical environments. Soil Science Society of America Journal. 71(1), 101-107.
Kailasa, S. K., and Wu, H.F. 2012. 3.37 - Inorganic Contaminants: Sample Preparation Approaches. In J. Pawliszyn (Ed.), Comprehensive Sampling and Sample Preparation. 743-782.
Kalaruban, M., Loganathan, P., Nguyen, T.V., Nur, T., Hasan Johir, M.A., Nguyen, T.H., Trinh, M.V. and Vigneswaran, S. 2019. Iron-impregnated granular activated carbon for arsenic removal: Application to practical column filters. Journal of Environmental Management. 239, 235-243.
Kanel, S.R., Greneche, J.M. and Choi, H. 2006. Arsenic (V) removal from groundwater using nano scale zero-valent iron as a colloidal reactive barrier material. Environmental Science & Technology. 40(6), 2045-2050.
Kanel, S.R., Manning, B., Charlet, L. and Choi, H. 2005. Removal of arsenic (III) from groundwater by nanoscale zero-valent iron. Environmental Science & Technology. 39(5), 1291-1298.
Kang, D., Yu, X., Tong, S., Ge, M., Zuo, J., Cao, C. and Song, W. 2013. Performance and mechanism of Mg/Fe layered double hydroxides for fluoride and arsenate removal from aqueous solution. Chemical Engineering Journal. 228, 731-740.
Karmacharya, M.S., Gupta, V.K., Tyagi, I., Agarwal, S. and Jha, V.K. 2016. Removal of As(III) and As(V) using rubber tire derived activated carbon modified with alumina composite. Journal of Molecular Liquids. 216, 836-844.
Kartinen, E.O. and Martin, C.J. 1995. An overview of arsenic removal processes. Desalination. 103(1), 79-88.
Kasiuliene, A., Carabante, I., Bhattacharya, P., Caporale, A.G., Adamo, P. and Kumpiene, J. 2018. Removal of metal (oid) s from contaminated water using iron-coated peat sorbent. Chemosphere. 198, 290-296.
Katsoyiannis, I.A., Mitrakas, M. and Zouboulis, A.I. 2015. Arsenic occurrence in Europe: emphasis in Greece and description of the applied full-scale treatment plants. Desalination and Water Treatment. 54(8), 2100-2107.
Khan, A.R., Ataullah, R. and Al-Haddad, A. 1997. Equilibrium adsorption studies of some aromatic pollutants from dilute aqueous solutions on activated carbon at different temperatures. Journal of Colloid and Interface Science. 194(1), 154-165.
Khan, M.A. and Ho, Y.S. 2011. Arsenic in drinking water: a review on toxicological effects, mechanism of accumulation and remediation. Asian Journal of Chemistry. 23(5), 1889.

Khaskheli, M.I., Memon, S.Q., Siyal, A.N. and Khuhawar, M. 2011. Use of orange peel waste for arsenic remediation of drinking water. Waste and Biomass Valorization. 2(4), 423-433.

Khatamian, M., Khodakarampoor, N. and Saket-Oskoui, M. 2017. Efficient removal of arsenic using graphene-zeolite based composites. Journal of Colloid and Interface Science. 498, 433-441.

Kim, J., Song, J., Lee, S.M. and Jung, J. 2019. Application of iron-modified biochar for arsenite removal and toxicity reduction. Journal of Industrial Engineering Chemistry. 80, 17-22.

Kim, K.W., Chanpiwat, P., Hanh, H.T., Phan, K. and Sthiannopkao, S. 2011. Arsenic geochemistry of groundwater in Southeast Asia. Frontiers of medicine. 5(4), 420-433.

Koble, R.A. and Corrigan, T.E. 1952. Adsorption isotherms for pure hydrocarbons. Industrial & Engineering Chemistry. 44(2), 383-387.

Kofa, G. P., NdiKoungou, S., Kayem, G. J., and Kamga, R. 2015. Adsorption of arsenic by natural pozzolan in a fixed bed: determination of operating conditions and modeling. Journal of Water Process Engineering, 6, 166-173.

Kong, S., Wang, Y., Hu, Q. and Olusegun, A.K. 2014. Magnetic nanoscale Fe–Mn binary oxides loaded zeolite for arsenic removal from synthetic groundwater. Colloids and surfaces A: Physicochemical and Engineering Aspects. 457, 220-227.

Kumar, A.S.K. and Jiang, S.J. 2017. Synthesis of magnetically separable and recyclable magnetic nanoparticles decorated with β-cyclodextrin functionalized graphene oxide an excellent adsorption of As(V)/(III). Journal of Molecular Liquids. 237, 387-401.

Kundu, S. and Gupta, A.K. 2006. Adsorptive removal of As(III) from aqueous solution using iron oxide coated cement (IOCC): Evaluation of kinetic, equilibrium and thermodynamic models. Separation and Purification Technology. 51(2), 165-172.

Kundu, S. and Gupta, A.K. 2008. Immobilization and leaching characteristics of arsenic from cement and/or lime solidified/stabilized spent adsorbent containing arsenic. Journal of Hazardous Materials. 153(1), 434-443.

Kuriakose, S., Singh, T.S. and Pant, K.K. 2004. Adsorption of As (III) from aqueous solution onto iron oxide impregnated activated alumina. Water Quality Research Journal. 39(3), 258-266.

Lagergren, S.K. 1898. About the theory of so-called adsorption of soluble substances. Sven. Vetenskapsakad. Handingarl. 24, 1-39.

Lakshmipathiraj, P., Narasimhan, B., Prabhakar, S. and Raju, G.B.J.J.o.h.m. 2006. Adsorption of arsenate on synthetic goethite from aqueous solutions. Journal of Hazardous Materials. 136(2), 281-287.

Langmuir, I. 1918. The adsorption of gases on plane surfaces of glass, mica and platinum. Journal of the American Chemical Society. 40(9), 1361-1403.

Lata, S. and Samadder, S. 2016. Removal of arsenic from water using nano adsorbents and challenges: a review. Journal of Environmental Management. 166, 387-406.

Lee, S.H., Tanaka, M., Takahashi, Y. and Kim, K.W. 2018. Enhanced adsorption of arsenate and antimonate by calcined Mg/Al layered double hydroxide: Investigation of comparative adsorption mechanism by surface characterization. Chemosphere. 211, 903-911.

Lenoble, V., Bouras, O., Deluchat, V., Serpaud, B. and Bollinger, J.C. 2002. Arsenic Adsorption onto Pillared Clays and Iron Oxides. Journal of Colloid and Interface Science. 255(1), 52-58.

Lenoble, V., Laclautre, C., Deluchat, V., Serpaud, B. and Bollinger, J.C. 2005. Arsenic removal by adsorption on iron (III) phosphate. Journal of Hazardous Materials. 123(1-3), 262-268.

Lenoble, V., Laclautre, C., Serpaud, B., Deluchat, V. and Bollinger, J.C. 2004. As (V) retention and As (III) simultaneous oxidation and removal on a MnO_2-loaded polystyrene resin. Science of the Total Environment. 326(1-3), 197-207.

Li, J.H, Lv, G.H., Bai, W.B, Liu, Q., Zhang, Y.C. and Song, J.Q. 2016a. Modification and use of biochar from wheat straw (*Triticum aestivum L.*) for nitrate and phosphate removal from water. Desalination Water Treatment. 57(10), 4681-4693.

Li, T., Bai, X., Qi, Y.X., Lun, N. and Bai, Y.J. 2016b. Fe_3O_4 nanoparticles decorated on the biochar derived from pomelo pericarp as excellent anode materials for Li-ion batteries. Electrochimica Acta. 222, 1562-1568.

Li, Y., Gao, B., Wu, T., Sun, D., Li, X., Wang, B. and Lu, F. 2009a. Hexavalent chromium removal from aqueous solution by adsorption on aluminum magnesium mixed hydroxide. Water Research. 43(12), 3067-3075.

Li, Y., Zhang, F.S. and Xiu, F.R. 2009b. Arsenic (V) removal from aqueous system using adsorbent developed from a high iron-containing fly ash. Science of the Total Environment. 407(21), 5780-5786.

Li, Z., Jean, J.S., Jiang, W.T., Chang, P.H., Chen, C.J. and Liao, L. 2011. Removal of arsenic from water using Fe-exchanged natural zeolite. Journal of Hazardous Materials. 187(1), 318-323.

Liang, Q., Ye, L., Huang, Z.H., Xu, Q., Bai, Y., Kang, F. and Yang, Q.H. 2014. A honeycomb-like porous carbon derived from pomelo peel for use in high-performance supercapacitors. Nanoscale. 6(22), 13831-13837.

Lim, L.B., Priyantha, N., Lu, Y. and Zaidi, N. 2019. Adsorption of heavy metal lead using *Citrus grandis* (Pomelo) leaves as low-cost adsorbent. Desalin. Water Treat. 166, 44-52.

Lin, L., Qiu, W., Wang, D., Huang, Q., Song, Z. and Chau, H.W. 2017. Arsenic removal in aqueous solution by a novel Fe-Mn modified biochar composite: characterization and mechanism. Ecotoxicology Environmental Safety. 144, 514-521.

Lin, S., Lu, D. and Liu, Z. 2012. Removal of arsenic contaminants with magnetic γ-Fe_2O_3 nanoparticles. Chemical Engineering Journal. 211, 46-52.

Litter, M.I., Ingallinella, A.M., Olmos, V., Savio, M., Difeo, G., Botto, L., Torres, E.M.F., Taylor, S., Frangie, S. and Herkovits, J. 2019. Arsenic in Argentina: technologies for arsenic removal from groundwater sources, investment costs and waste management practices. Science of the Total Environment. 690, 778-789.

Liu, D.X., Mu, J., Yao, Q., Bai, Y., Qian, F., Liang, F., Shi, F.N. and Gao, J. 2019a. Design of iron-ion-doped pomelo peel biochar composites towards removal of organic pollutants. SN Applied Sciences. 1(2), 184.

Liu, J., Wu, P., Li, S., Chen, M., Cai, W., Zou, D., Zhu, N. and Dang, Z. 2019b. Synergistic deep removal of As (III) and Cd (II) by a calcined multifunctional MgZnFe-CO_3 layered double hydroxide: photooxidation, precipitation and adsorption. Chemosphere. 225, 115-125.

Liu, Y.T., Wang, M.K., Chen, T.Y., Chiang, P.N., Huang, P.M. and Lee, J.F. 2006. Arsenate sorption on lithium/aluminum layered double hydroxide intercalated by chloride and on gibbsite: sorption isotherms, envelopes, and spectroscopic studies. Environmental Science & Technology. 40(24), 7784-7789.

Loganathan, P., Vigneswaran, S., Kandasamy, J. and Bolan, N.S. 2014. Removal and recovery of phosphate from water using sorption. Critical Reviews in Environmental Science and Technology. 44(8), 847-907.

Lu, H., Liu, S., Zhang, H., Qiu, Y., Zhao, J. and Zhu, Z. 2018. Decontamination of arsenic in actual water samples by calcium containing layered double hydroxides from a convenient synthesis method. Water. 10(9), 1150.

Lu, H., Zhu, Z., Zhang, H., Zhu, J. and Qiu, Y. 2015. Simultaneous removal of arsenate and antimonate in simulated and practical water samples by adsorption onto Zn/Fe layered double hydroxide. Chemical Engineering Journal. 276, 365-375.

Luengo, C., Puccia, V. and Avena, M. 2011. Arsenate adsorption and desorption kinetics on a Fe(III)-modified montmorillonite. Journal of Hazardous Materials. 186(2), 1713-1719.

Luong, V.T., Cañas Kurz, E.E., Hellriegel, U., Luu, T.L., Hoinkis, J. and Bundschuh, J. 2018. Iron-based subsurface arsenic removal technologies by aeration: A review of the current state and future prospects. Water Research. 133, 110-122.

Lyklema, J. 1995 Fundamentals of Interface and Colloid Science (FICS). vol. II, Academic Press, London, San Diego, New York, Boston, Sydney, Tokyo, Toronto.

Maiti, A., Basu, J.K. and De, S. 2010. Removal of arsenic from synthetic and natural groundwater using acid-activated laterite. Environmental Progress & Sustainable Energy. 29(4), 457-470.

Maiti, A., Basu, J.K. and De, S. 2012. Experimental and kinetic modeling of As(V) and As(III) adsorption on treated laterite using synthetic and contaminated groundwater: Effects of phosphate, silicate and carbonate ions. Chemical Engineering Journal. 191, 1-12.

Maiti, A., DasGupta, S., Basu, J.K. and De, S. 2007. Adsorption of arsenite using natural laterite as adsorbent. Separation and Purification Technology. 55(3), 350-359.

Maiti, A., Thakur, B.K., Basu, J.K. and De, S. 2013. Comparison of treated laterite as arsenic adsorbent from different locations and performance of best filter under field conditions. Journal of Hazardous Materials. 262, 1176-1186.

Maji, S.K., Pal, A. and Pal, T. 2007. Arsenic removal from aqueous solutions by adsorption on laterite soil. Journal of Environmental Science and Health Part A. 42(4), 453-462.

Maji, S.K., Pal, A. and Pal, T. 2008. Arsenic removal from real-life groundwater by adsorption on laterite soil. Journal of Hazardous Materials. 151(2), 811-820.

Malik, A.H., Khan, Z.M., Mahmood, Q., Nasreen, S. and Bhatti, Z.A. 2009. Perspectives of low cost arsenic remediation of drinking water in Pakistan and other countries. Journal of Hazardous Materials. 168(1), 1-12.

Manning, B.A. and Goldberg, S. 1997. Adsorption and stability of arsenic(III) at the clay mineral−water interface. Environmental Science & Technology. 31(7), 2005-2011.

Masuda, H. 2018. Arsenic cycling in the Earth's crust and hydrosphere: interaction between naturally occurring arsenic and human activities. Progress in Earth and Planetary Science. 5(1), 1-11.

Matis, K., Zouboulis, A., Malamas, F., Afonso, M.R. and Hudson, M. 1997. Flotation removal of As (V) onto goethite. Environmental Pollution. 97(3), 239-245.
McCann, C.M., Peacock, C.L., Hudson-Edwards, K.A., Shrimpton, T., Gray, N.D. and Johnson, K.L. 2018. In situ arsenic oxidation and sorption by a Fe-Mn binary oxide waste in soil. Journal of Hazardous Materials. 342, 724-731.
McLintock, I.S. 1967. The Elovich equation in chemisorption kinetics. Nature. 216, 1204.
Meng, X., Korfiatis, G. P., Christodoulatos, C., and Bang, S. 2001. Treatment of arsenic in Bangladesh well water using a household co-precipitation and filtration system. Water Research. 35(12), 2805-2810.
Mishra, T. and Mahato, D.K. 2016. A comparative study on enhanced arsenic (V) and arsenic (III) removal by iron oxide and manganese oxide pillared clays from ground water. Journal of Environmental Chemical Engineering. 4(1), 1224-1230.
Mitra, S., Thakur, L.S., Rathore, V.K. and Mondal, P. 2016. Removal of Pb(II) and Cr(VI) by laterite soil from synthetic waste water: single and bi-component adsorption approach. Desalination and Water Treatment. 57(39), 18406-18416.
Mohammadi, N., Pourreza, K., Adeh, N.B. and Omidvar, M. 2021. Defective mesoporous carbon/MnO_2 nanocomposite as an advanced electrode material for supercapacitor application. Journal of Alloys and Compounds. 160874.
Mohan, D. and Pittman Jr, C.U. 2007. Arsenic removal from water/wastewater using adsorbents—A critical review. Journal of Hazardous Materials. 142(1-2), 1-53.
Mollah, M.Y.A., Lu, F. and Cocke, D.L. 1998. An X-ray diffraction (XRD) and Fourier transform infrared spectroscopic (FT-IR) characterization of the speciation of arsenic (V) in Portland cement type-V. Science of The Total Environment. 224(1), 57-68.
Mondal, P., Balomajumder, C. and Mohanty, B. 2007. A laboratory study for the treatment of arsenic, iron, and manganese bearing ground water using Fe^{3+} impregnated activated carbon: effects of shaking time, pH and temperature. Journal of Hazardous Materials. 144(1-2), 420-426.
Mubarak, M., Jeon, H., Islam, M.S., Yoon, C., Bae, J.S., Hwang, S.J., San Choi, W. and Lee, H.J. 2018. One-pot synthesis of layered double hydroxide hollow nanospheres with ultrafast removal efficiency for heavy metal ions and organic contaminants. Chemosphere. 201, 676-686.
Muthu Prabhu, S., Park, C.M., Shahzad, A. and Lee, D.S. 2019. Designed synthesis of sulfide-rich bimetallic-assembled graphene oxide sheets as flexible materials and self-tuning adsorption cum oxidation mechanisms of arsenic from water. Journal of Materials Chemistry A. 7(19), 12253-12265.
Neppolian, B., Celik, E. and Choi, H. 2008. Photochemical oxidation of arsenic (III) to arsenic (V) using peroxydisulfate ions as an oxidizing agent. Environmental Science & Technology. 42(16), 6179-6184.
Tran, T.V.N. 2008. Groundwater Management in Asian Cities: Technology and Policy for Sustainability. Takizawa, S. (ed), pp. 273-299, Springer Japan, Tokyo.
Ngo, H., Vigneswaran, S., Hu, J., Thirunavukkarasu, O. and Viraraghavan, T. 2002. A comparison of conventional and non-conventional treatment technologies on arsenic removal from water. Water Science and Technology: Water Supply. 2(5-6), 119-125.
Nguyen, T.H., Nguyen, A.T., Loganathan, P., Nguyen, T.V., Vigneswaran, S., Nguyen, T.H.H. and Tran, H.N. 2021a. Low-cost laterite-laden household filters for

removing arsenic from groundwater in Vietnam and waste management. Process Safety Environmental Protection.

Nguyen, T.H., Tran, H.N., Nguyen, T.V., Vigneswaran, S., Nguyen, T.D., Nguyen, T.H.H., Mai, T.N. and Chao, H.P. 2021b. Single-step removal of arsenite ions from water through oxidation-coupled adsorption using Mn/Mg/Fe layered double hydroxide as catalyst and adsorbent. Chemosphere. 133370.

Nguyen, T.H., Tran, H.N., Vu, H.A., Trinh, M.V., Nguyen, T.V., Loganathan, P., Vigneswaran, S., Nguyen, T.M., Trinh, V.T., Vu, D.L. and Nguyen, T.H.H. 2020a. Laterite as a low-cost adsorbent in a sustainable decentralized filtration system to remove arsenic from groundwater in Vietnam. Science of The Total Environment. 699, 134267.

Nguyen, T.T.Q., Loganathan, P., Nguyen, T.V. and Vigneswaran, S. 2020b. Removing arsenate from water using modified manganese oxide ore: Column adsorption and waste management. Journal of Environmental Chemical Engineering. 8(6), 104491.

Nguyen, T.T.Q., Loganathan, P., Nguyen, T.V., Vigneswaran, S. and Ngo, H.H. 2020c. Iron and zirconium modified luffa fibre as an effective bioadsorbent to remove arsenic from drinking water. Chemosphere. 258, 127370.

Nguyen, V.H., Van, H.T., Nguyen, V.Q., Dam, X.V., Hoang, L. and Ha, L. 2020d. Magnetic Fe_3O_4 Nanoparticle Biochar Derived from Pomelo Peel for Reactive Red 21 Adsorption from Aqueous Solution. Journal of Chemistry.

Nguyen, T. A. H., Ngo, H. H., Guo, W. S., Pham, T. Q., Li, F. M., Nguyen, T. V., and Bui, X. T. 2015. Adsorption of phosphate from aqueous solutions and sewage using zirconium loaded okara (ZLO): fixed-bed column study. Science of the Total Environment, 523, 40-49.

Nguyen, T.V., Nguyen, T.V.T., Pham, T.L., Vigneswaran, S., Ngo, H.H., Kandasamy, J., Nguyen, H.K. and Nguyen, D.T. 2009. Adsorption and removal of arsenic from water by iron ore mining waste. Water Science and Technology. 60(9), 2301-2308.

Nham, N.T., Al Tahtamouni, T., Nguyen, T.D., Huong, P.T., Jitae, K., Viet, N.M., Van Noi, N., Phuong, N.M. and Anh, N.T.H. 2019. Synthesis of iron modified rice straw biochar toward arsenic from groundwater. Materials Research Express. 6(11), 115528.

Niazi, N.K., Bibi, I., Shahid, M., Ok, Y.S., Burton, E.D., Wang, H., Shaheen, S.M., Rinklebe, J. and Lüttge, A. 2018. Arsenic removal by perilla leaf biochar in aqueous solutions and groundwater: An integrated spectroscopic and microscopic examination. Environmental Pollution. 232, 31-41.

Nitzsche, K. S., Lan, V. M., Trang, P. T. K., Viet, P. H., Berg, M., Voegelin, A., Friedrich, B. P., Zahoransky, J., Müller, S.K., Byrne, J.M., Schröder, C., Behrens S., Kappler, A. 2015. Arsenic removal from drinking water by a household sand filter in Vietnam—Effect of filter usage practices on arsenic removal efficiency and microbiological water quality. Science of the Total Environment. 502, 526-536.

Nur, T., Loganathan, P., Ahmed, M.B., Johir, M.A.H., Nguyen, T.V. and Vigneswaran, S. 2019. Removing arsenic from water by coprecipitation with iron: Effect of arsenic and iron concentrations and adsorbent incorporation. Chemosphere. 226, 431-438.

Nur, T., Shim, W. G., Loganathan, P., Vigneswaran, S., and Kandasamy, J. 2015. Nitrate removal using Purolite A520E ion exchange resin: batch and fixed-bed column

adsorption modelling. International Journal of Environmental Science and Technology, 12(4), 1311-1320.
Ociński, D., Jacukowicz-Sobala, I., Mazur, P., Raczyk, J. and Kociołek-Balawejder, E. 2016. Water treatment residuals containing iron and manganese oxides for arsenic removal from water–characterization of physicochemical properties and adsorption studies. Chemical Engineering Journal. 294, 210-221.
Oliveira, L.C.A., Pereira, E., Guimaraes, I.R., Vallone, A., Pereira, M., Mesquita, J.P. and Sapag, K. 2009. Preparation of activated carbons from coffee husks utilizing $FeCl_3$ and $ZnCl_2$ as activating agents. Journal of Hazardous Materials. 165(1), 87-94.
Omorogie, M.O., Babalola, J.O., Unuabonah, E.I., Song, W. and Gong, J.R. 2016. Efficient chromium abstraction from aqueous solution using a low-cost biosorbent: Nauclea diderrichii seed biomass waste. Journal of Saudi Chemical Society. 20(1), 49-57.
Otgonjargal, E., Kim, Y.S., Park, S.M., Baek, K. and Yang, J.S. 2012. Mn–Fe layered double hydroxides for adsorption of As (III) and As (V). Separation Science and Technology. 47(14-15), 2192-2198.
Palfy, P., Vircikova, E. and Molnar, L. 1999. Processing of arsenic waste by precipitation and solidification. Waste Management. 19(1), 55-59.
Partey, F., Norman, D., Ndur, S. and Nartey, R. 2008. Arsenic sorption onto laterite iron concretions: Temperature effect. Journal of Colloid and Interface Science. 321(2), 493-500.
Partey, F., Norman, D.I., Ndur, S. and Nartey, R. 2009. Mechanism of arsenic sorption onto laterite iron concretions. Colloids and Surfaces A: Physicochemical and Engineering Aspects. 337(1), 164-172.
Patel, H. 2021. Review on solvent desorption study from exhausted adsorbent. Journal of Saudi Chemical Society. 25(8), 101302.
Pavlovic, M., Huber, R., Adok-Sipiczki, M., Nardin, C. and Szilagyi, I. 2016. Ion specific effects on the stability of layered double hydroxide colloids. Soft Matter. 12(17), 4024-4033.
Pehlivan, E., Tran, H., Ouédraogo, W., Schmidt, C., Zachmann, D. and Bahadir, M. 2013a. Sugarcane bagasse treated with hydrous ferric oxide as a potential adsorbent for the removal of As (V) from aqueous solutions. Food chemistry. 138(1), 133-138.
Pehlivan, E., Tran, T., Ouédraogo, W., Schmidt, C., Zachmann, D. and Bahadir, M. 2013b. Removal of As (V) from aqueous solutions by iron coated rice husk. Fuel Processing Technology. 106, 511-517.
Pena, M.E., Korfiatis, G.P., Patel, M., Lippincott, L. and Meng, X. 2005. Adsorption of As (V) and As (III) by nanocrystalline titanium dioxide. Water Research. 39(11), 2327-2337.
Penke, Y.K., Yadav, A.K., Malik, I., Tyagi, A., Ramkumar, J. and Kar, K.K. 2021. Insights of arsenic (III/V) adsorption and electrosorption mechanism onto multi synergistic (redox-photoelectrochemical-ROS) aluminum substituted copper ferrite impregnated rGO. Chemosphere. 267, 129246.
Pereira, R.C., Anizelli, P.R., Di Mauro, E., Valezi, D.F., da Costa, A.C.S., Zaia, C.T.B. and Zaia, D.A. 2019. The effect of pH and ionic strength on the adsorption of glyphosate onto ferrihydrite. Geochemical Transactions. 20(1), 1-14.

Pierce, M.L. and Moore, C.B. 1982. Adsorption of arsenite and arsenate on amorphous iron hydroxide. Water Research. 16(7), 1247-1253.
Pintor, A.M., Vieira, B.R., Santos, S.C., Boaventura, R.A. and Botelho, C.M. 2018. Arsenate and arsenite adsorption onto iron-coated cork granulates. Science of the Total Environment. 642, 1075-1089.
Pizarro, C., Escudey, M., Caroca, E., Pavez, C. and Zúñiga, G.E. 2021. Evaluation of zeolite, nanomagnetite, and nanomagnetite-zeolite composite materials as arsenic (V) adsorbents in hydroponic tomato cultures. Science of The Total Environment. 751, 141623.
Pozdnyakov, I.P., Ding, W., Xu, J., Chen, L., Wu, F., Grivin, V.P. and Plyusnin, V.F. 2016. Photochemical transformation of an iron(iii)–arsenite complex in acidic aqueous solution. Photochemical & Photobiological Sciences. 15(3), 431-439.
Prabhu, S.M., Park, C.M., Shahzad, A. and Lee, D.S. 2019. Designed synthesis of sulfide-rich bimetallic-assembled graphene oxide sheets as flexible materials and self-tuning adsorption cum oxidation mechanisms of arsenic from water. Journal of Materials Chemistry A. 7(19), 12253-12265.
Putnis, A. 1992. An Introduction to Mineral Sciences. Putnis, A. (ed), pp. 309-332, Cambridge University Press, Cambridge.
Rahman, M.T., Kameda, T., Kumagai, S. and Yoshioka, T. 2017. Adsorption isotherms and kinetics of arsenic removal from aqueous solution by Mg–Al layered double hydroxide intercalated with nitrate ions. Reaction Kinetics, Mechanisms and Catalysis. 120(2), 703-714.
Ramirez-Muñiz, K., Perez-Rodriguez, F., and Rangel-Mendez, R. 2018. Adsorption of arsenic onto an environmental friendly goethite-polyacrylamide composite. Journal of Molecular Liquids. 264, 253-260.
Ranjan, D., Talat, M. and Hasan, S. 2009. Rice polish: an alternative to conventional adsorbents for treating arsenic bearing water by up-flow column method. Industrial Engineering Chemistry Research. 48(23), 10180-10185.
Raul, P.K., Devi, R.R., Umlong, I.M., Thakur, A.J., Banerjee, S. and Veer, V. 2014. Iron oxide hydroxide nanoflower assisted removal of arsenic from water. Materials Research Bulletin. 49, 360-368.
Redlich, O. and Peterson, D.L. 1959. A useful adsorption isotherm. Journal of Physical Chemistry. 63(6), 1024-1024.
Reyes, I.C., Salmones, J., Zeifert, B., Contreras, J. and Rojas, F. 2014. Transesterification of canola oil catalized by calcined Mg–Al hydrotalcite doped with nitratine. Chemical Engineering Science. 119, 174-181.
Rosanoff, A. 2013. The high heart health value of drinking-water magnesium. Medical Hypotheses. 81(6), 1063-1065.
Rott, U., Meyer, C. and Friedle, M. 2002. Residue-free removal of arsenic, iron, manganese and ammonia from groundwater. Water Supply. 2(1), 17-24.
Rout, P. R., Bhunia, P., and Dash, R. R. 2015. A mechanistic approach to evaluate the effectiveness of red soil as a natural adsorbent for phosphate removal from wastewater. Desalination and Water Treatment. 54(2), 358-373.
Roy, P., Mondal, N. K., Bhattacharya, S., Das, B., and Das, K. 2013. Removal of arsenic (III) and arsenic (V) on chemically modified low-cost adsorbent: batch and column operations. Applied Water Science. 3(1), 293-309.

Ryu, S.R., Jeon, E.K., Yang, J.S. and Baek, K. 2017. Adsorption of As(III) and As(V) in groundwater by Fe–Mn binary oxide-impregnated granular activated carbon (IMIGAC). Journal of the Taiwan Institute of Chemical Engineers. 72, 62-69.

Saikaew, W., Kaewsarn, P. and Saikaew, W. 2009. Pomelo peel: agricultural waste for biosorption of cadmium ions from aqueous solutions. World Acad. Sci. Eng. Technol. 56, 287-291.

Samad, A., Furukawa, M., Katsumata, H., Suzuki, T. and Kaneco, S. 2016. Photocatalytic oxidation and simultaneous removal of arsenite with CuO/ZnO photocatalyst. Journal of Photochemistry and Photobiology A: Chemistry. 325, 97-103.

Samsuri, A.W., Sadegh-Zadeh, F. and Seh-Bardan, B.J. 2013. Adsorption of As(III) and As(V) by Fe coated biochars and biochars produced from empty fruit bunch and rice husk. Journal of Environmental Chemical Engineering. 1(4), 981-988.

Sawood, G.M. and Gupta, S. 2020. Arsenate adsorption from aqueous solution using iron-loaded Azadirachta indica roots: batch and fixed-bed column study. Desalination Water Treatment. 203, 292-308.

Schmidt, S. A., Gukelberger, E., Hermann, M., Fiedler, F., Großmann, B., Hoinkis, J., and Bundschuh, J. 2016. Pilot study on arsenic removal from groundwater using a small-scale reverse osmosis system—Towards sustainable drinking water production. Journal of Hazardous Materials. 318, 671-678.

Silva, L. C., Neves, V. A., Ramos, V. S., Silva, R. S., Campos, J. B. D., Silva, A. A. D., Malta, L.F.B., Senra, and J. D. 2019. Layered double hydroxides as bifunctional catalysts for the aryl borylation under ligand-free conditions. Catalysts, 9(4), 302.

Shaji, E., Santosh, M., Sarath, K., Prakash, P., Deepchand, V. and Divya, B. 2020. Arsenic contamination of groundwater: A global synopsis with focus on the Indian Peninsula. Geoscience Frontiers.

Sharma, V.K. and Sohn, M. 2009. Aquatic arsenic: Toxicity, speciation, transformations, and remediation. Environment International. 35(4), 743-759.

Shen, L., Jiang, X., Chen, Z., Fu, D., Li, Q., Ouyang, T. and Wang, Y. 2017. Chemical reactive features of novel amino acids intercalated layered double hydroxides in As (III) and As (V) adsorption. Chemosphere. 176, 57-66.

Sheng, T., Baig, S.A., Hu, Y., Xue, X. and Xu, X. 2014. Development, characterization and evaluation of iron-coated honeycomb briquette cinders for the removal of As(V) from aqueous solutions. Arabian Journal of Chemistry. 7(1), 27-36.

Siddiqui, S.I. and Chaudhry, S.A. 2017. Iron oxide and its modified forms as an adsorbent for arsenic removal: A comprehensive recent advancement. Process Safety and Environmental Protection. 111, 592-626.

Simeonidis, K., Mourdikoudis, S., Kaprara, E., Mitrakas, M. and Polavarapu, L. 2016. Inorganic engineered nanoparticles in drinking water treatment: a critical review. Environmental Science: Water Research & Technology. 2(1), 43-70.

Singh, D., Prasad, G. and Rupainwar, D. 1996. Adsorption technique for the treatment of As (V)-rich effluents. Colloids and Surfaces A: Physicochemical and engineering aspects. 111(1-2), 49-56.

Singh, P., Borthakur, A., Singh, R., Bhadouria, R., Singh, V.K. and Devi, P. 2021. A critical review on the research trends and emerging technologies for arsenic decontamination from water. Groundwater for Sustainable Development. 100607.

Singh, T.S. and Pant, K.K. 2006. Solidification/stabilization of arsenic containing solid wastes using portland cement, fly ash and polymeric materials. Journal of Hazardous Materials. 131(1), 29-36.
Smedley, P.L. and Kinniburgh, D.G. 2002. A review of the source, behaviour and distribution of arsenic in natural waters. Applied Geochemistry. 17(5), 517-568.
Soma, M., Tanaka, A., Seyama, H. and Satake, K. 1994. Characterization of arsenic in lake sediments by X-ray photoelectron spectroscopy. Geochimica et cosmochimica acta. 58(12), 2743-2745.
Sorlini, S. and Gialdini, F. 2010. Conventional oxidation treatments for the removal of arsenic with chlorine dioxide, hypochlorite, potassium permanganate and monochloramine. Water Research. 44(19), 5653-5659.
Sullivan, C., Tyrer, M., Cheeseman, C. R., and Graham, N. J. 2010. Disposal of water treatment wastes containing arsenic—a review. Science of the Total Environment. 408(8), 1770-1778.
Sun, T., Zhao, Z., Liang, Z., Liu, J., Shi, W. and Cui, F. 2017. Efficient As (III) removal by magnetic CuO-Fe_3O_4 nanoparticles through photo-oxidation and adsorption under light irradiation. Journal of Colloid and Interface Science. 495, 168-177.
SunBaek, B. and XiaoGuang, M. 2004. A review of arsenic interactions with anions and iron hydroxides. Environmental Engineering Research. 9(4), 184-192.
Tasaso, P. 2014. Adsorption of copper using pomelo peel and depectinated pomelo peel. Journal of Clean Energy Technologies. 2(2), 154-157.
Taylor, M. and Fuessle, R. 1994. Stabilization of arsenic wastes, DIANE Publishing.
Te, B., Wichitsathian, B., Yossapol, C., and Wonglertarak, W. 2018. Investigation of arsenic removal from water by iron-mixed mesoporous pellet in a continuous fixed-bed column. Water, Air, & Soil Pollution. 229(9), 1-15.
Thirunavukkarasu, O., Viraraghavan, T. and Subramanian, K. 2003. Arsenic removal from drinking water using iron oxide-coated sand. Water, Air, and Soil Pollution. 142(1), 95-111.
Thomas, H. C. 1944. Heterogeneous ion exchange in a flowing system. Journal of the American Chemical Society. 66(10), 1664-1666.
Thommes, M., Kaneko, K., Neimark, A.V., Olivier, J.P., Rodriguez-Reinoso, F., Rouquerol, J. and Sing, K.S. 2015. Physisorption of gases, with special reference to the evaluation of surface area and pore size distribution (IUPAC Technical Report). Pure Applied Chemistry. 87(9-10), 1051-1069.
Tian, Y., Wu, M., Lin, X., Huang, P. and Huang, Y. 2011. Synthesis of magnetic wheat straw for arsenic adsorption. Journal of Hazardous Materials. 193, 10-16.
Tian, Z., Feng, Y., Guan, Y., Shao, B., Zhang, Y. and Wu, D. 2017. Opposite effects of dissolved oxygen on the removal of As (III) and As (V) by carbonate structural Fe (II). Scientific Reports. 7(1), 1-11.
Tocmo, R., Pena-Fronteras, J., Calumba, K.F., Mendoza, M. and Johnson, J.J. 2020. Valorization of pomelo (*Citrus grandis Osbeck*) peel: A review of current utilization, phytochemistry, bioactivities, and mechanisms of action. Comprehensive Reviews in Food Science and Food Safety. 19(4), 1969-2012.
Tomul, F., Arslan, Y., Kabak, B., Trak, D., Kendüzler, E., Lima, E.C. and Tran, H.N. 2020. Peanut shells-derived biochars prepared from different carbonization processes: Comparison of characterization and mechanism of naproxen adsorption in water. Science of the Total Environment. 726, 137828.

Tournassat, C., Charlet, L., Bosbach, D. and Manceau, A. 2002. Arsenic (III) oxidation by birnessite and precipitation of manganese (II) arsenate. Environmental Science & Technology. 36(3), 493-500.

Tran, H.N., Nguyen, D.T., Le, G.T., Tomul, F., Lima, E.C., Woo, S.H., Sarmah, A.K., Nguyen, H.Q., Nguyen, P.T. and Nguyen, D.D. 2019. Adsorption mechanism of hexavalent chromium onto layered double hydroxides-based adsorbents: A systematic in-depth review. Journal of Hazardous Materials. 373, 258-270.

Tran, H.N., Wang, Y.F., You, S.J. and Chao, H.P. 2017a. Insights into the mechanism of cationic dye adsorption on activated charcoal: The importance of π–π interactions. Process Safety and Environmental Protection. 107, 168-180.

Tran, H.N., You, S.J. and Chao, H.P. 2017b. Fast and efficient adsorption of methylene green 5 on activated carbon prepared from new chemical activation method. Journal of Environmental Management. 188, 322-336.

Tran, H.N., You, S.J. and Chao, H.P. 2016. Effect of pyrolysis temperatures and times on the adsorption of cadmium onto orange peel derived biochar. Waste Management & Research. 34(2), 129-138.

Triviño, M.L.T., Hiremath, V. and Seo, J.G. 2018. Stabilization of $NaNO_3$-promoted magnesium oxide for high-temperature CO_2 capture. Environmental Science & Technology. 52(20), 11952-11959.

Tuna, A.Ö.A., Özdemir, E., Şimşek, E.B. and Beker, U. 2013. Removal of As(V) from aqueous solution by activated carbon-based hybrid adsorbents: Impact of experimental conditions. Chemical Engineering Journal. 223, 116-128.

Vandecasteele, C., Dutré, V., Geysen, D. and Wauters, G. 2002. Solidification/stabilisation of arsenic bearing fly ash from the metallurgical industry. Immobilisation mechanism of arsenic. Waste Management. 22(2), 143-146.

Varga, G., Somosi, Z., Kónya, Z., Kukovecz, Á., Pálinkó, I. and Szilagyi, I. 2021. A colloid chemistry route for the preparation of hierarchically ordered mesoporous layered double hydroxides using surfactants as sacrificial templates. Journal of Colloid and Interface Science. 581, 928-938.

Verma, L. and Singh, J. 2019. Synthesis of novel biochar from waste plant litter biomass for the removal of Arsenic (III and V) from aqueous solution: A mechanism characterization, kinetics and thermodynamics. Journal of Environmental Management. 248, 109235.

Vieira, B.R., Pintor, A.M., Boaventura, R.A., Botelho, C.M. and Santos, S.C. 2017. Arsenic removal from water using iron-coated seaweeds. Journal of Environmental Management. 192, 224-233.

Vitela-Rodriguez, A.V. and Rangel-Mendez, J.R. 2013. Arsenic removal by modified activated carbons with iron hydro(oxide) nanoparticles. Journal of Environmental Management. 114, 225-231.

Vithanage, M., Herath, I., Joseph, S., Bundschuh, J., Bolan, N., Ok, Y.S., Kirkham, M.B. and Rinklebe, J. 2017. Interaction of arsenic with biochar in soil and water: A critical review. Carbon. 113, 219-230.

Vu, M.T., Chao, H.P., Van Trinh, T., Le, T.T., Lin, C.C. and Tran, H.N. 2018. Removal of ammonium from groundwater using NaOH-treated activated carbon derived from corncob wastes: Batch and column experiments. Journal of Cleaner Production. 180, 560-570.

Vucelic, M., Jones, W. and Moggridge, G.D. 1997. Cation ordering in synthetic layered double hydroxides. Clays and Clay Minerals. 45(6), 803-813.
Wang, K., Liu, Y., Ding, Z., Chen, Z., Xu, X., Wang, M., Lu, T. and Pan, L. 2021a. Chloride pre-intercalated CoFe-layered double hydroxide as chloride ion capturing electrode for capacitive deionization. Chemical Engineering Journal.
Wang, J., Zhang, T., Li, M., Yang, Y., Lu, P., Ning, P. and Wang, Q. 2018. Arsenic removal from water/wastewater using layered double hydroxide derived adsorbents, a critical review. RSC Advances. 8(40), 22694-22709.
Wang, S. and Mulligan, C.N. 2008. Speciation and surface structure of inorganic arsenic in solid phases: A review. Environment International. 34(6), 867-879.
Wang, S. and Mulligan, C. N. 2006. Occurrence of arsenic contamination in Canada: sources, behavior and distribution. Science of The Total Environment, 366(2-3), 701-721.
Wang, Y., Gao, Y., Zhu, Z., Zhang, L., Zhao, N., Fang, Y., Zhu, Y. and Liu, G. 2021b. Enhanced arsenic removal from aqueous solution by Fe/Mn-C layered double hydroxide composite. Adsorption Science & Technology. 2021, 8891643.
Wang, S., Gao, B., Li, Y., Creamer, A. E., and He, F. 2017. Adsorptive removal of arsenate from aqueous solutions by biochar supported zero-valent iron nanocomposite: batch and continuous flow tests. Journal of Hazardous Materials, 322, 172-181.
Wang, S.L., Liu, C.H., Wang, M.K., Chuang, Y.H. and Chiang, P.N. 2009. Arsenate adsorption by Mg/Al-NO_3 layered double hydroxides with varying the Mg/Al ratio. Applied Clay Science. 43(1), 79-85.
Weerasundara, L., Ok, Y.S. and Bundschuh, J. 2021. Selective removal of arsenic in water: A critical review. Environmental Pollution. 268, 115668.
Wen, Z., Ke, J., Xu, J., Guo, S., Zhang, Y. and Chen, R. 2018. One-step facile hydrothermal synthesis of flowerlike Ce/Fe bimetallic oxides for efficient As (V) and Cr (VI) remediation: Performance and mechanism. Chemical Engineering Journal. 343, 416-426.
WHO 1993. Guidelines for Drinking-water Quality.
WHO 2017. Annual report drinking water.
Winkel, L.H., Trang, P.T.K., Lan, V.M., Stengel, C., Amini, M., Ha, N.T., Viet, P.H. and Berg, M. 2011. Arsenic pollution of groundwater in Vietnam exacerbated by deep aquifer exploitation for more than a century. Proceedings of the National Academy of Sciences.
Wu, P. Y., Jia, Y., Jiang, Y. P., Zhang, Q. Y., Zhou, S. S., Fang, F., and Peng, D. Y. 2014. Enhanced arsenate removal performance of nanostructured goethite with high content of surface hydroxyl groups. Journal of Environmental Chemical Engineering. 2(4), 2312-2320.
Wu, X., Tan, X., Yang, S., Wen, T., Guo, H., Wang, X. and Xu, A. 2013. Coexistence of adsorption and coagulation processes of both arsenate and NOM from contaminated groundwater by nanocrystallined Mg/Al layered double hydroxides. Water Research. 47(12), 4159-4168.
Wu, Y., Cha, L., Fan, Y., Fang, P., Ming, Z. and Sha, H. 2017. Activated biochar prepared by pomelo peel using H_3PO_4 for the adsorption of hexavalent chromium: performance and mechanism. Water, Air, Soil Pollution. 228(10), 1-13.

Xiong, Y., Tong, Q., Shan, W., Xing, Z., Wang, Y., Wen, S. and Lou, Z. 2017. Arsenic transformation and adsorption by iron hydroxide/manganese dioxide doped straw activated carbon. Applied Surface Science. 416, 618-627.

Yan, J., Xue, Y., Long, L., Zeng, Y. and Hu, X. 2018. Adsorptive removal of As (V) by crawfish shell biochar: batch and column tests. Environmental Science Pollution Research. 25(34), 34674-34683.

Yang, J.S., Kim, Y.S., Park, S.M. and Baek, K. 2014. Removal of As (III) and As (V) using iron-rich sludge produced from coal mine drainage treatment plant. Environmental Science and Pollution Research. 21(18), 10878-10889.

Yang, L., Shahrivari, Z., Liu, P.K., Sahimi, M. and Tsotsis, T.T. 2005. Removal of trace levels of arsenic and selenium from aqueous solutions by calcined and uncalcined layered double hydroxides (LDH). Industrial & Engineering Chemistry Research. 44(17), 6804-6815.

Yao, S., Liu, Z. and Shi, Z. 2014. Arsenic removal from aqueous solutions by adsorption onto iron oxide/activated carbon magnetic composite. Journal of Environmental Health Science Engineering. 12(1), 1-8.

Yee, J.J., Arida, C.V.J., Futalan, C.M., de Luna, M.D.G. and Wan, M.W. 2019. Treatment of contaminated groundwater via arsenate removal using chitosan-coated bentonite. Molecules. 24(13), 2464.

Yu, X.Y., Luo, T., Jia, Y., Xu, R.X., Gao, C., Zhang, Y.X., Liu, J.H. and Huang, X.J. 2012. Three-dimensional hierarchical flower-like Mg–Al-layered double hydroxides: highly efficient adsorbents for As (V) and Cr (VI) removal. Nanoscale. 4(11), 3466-3474.

Zhang, B., Wu, Y. and Cha, L. 2019. Removal of methyl orange dye using activated biochar derived from pomelo peel wastes: performance, isotherm, and kinetic studies. Journal of Dispersion Science Technology. 41, 1-12.

Zhang, F.S. and Itoh, H. 2005. Iron oxide-loaded slag for arsenic removal from aqueous system. Chemosphere. 60(3), 319-325.

Zhang, M., Gao, B., Varnoosfaderani, S., Hebard, A., Yao, Y. and Inyang, M. 2013. Preparation and characterization of a novel magnetic biochar for arsenic removal. Bioresource Technology. 130, 457-462.

Zhang, Y., Cao, J., Li, J., Yuan, Z., Li, D., Wang, L. and Han, W. 2022. Self-assembled Cobalt-doped NiMn-layered double hydroxide (LDH)/V2CTx MXene hybrids for advanced aqueous electrochemical energy storage properties. Chemical Engineering Journal. 430.

Zhao, Z., Guan, M., Zeng, H. and Chen, P. 2018. Adsorption and Oxidation of As(III) on Iron (Hydro)Oxides. Water Environment Research. 90(6), 483-489.

Zhou, W., Kong, Z., Wu, Z., Yang, S., Wang, Y. and Liu, Y. 2021. Efficient oxidation of biomass derived 5-hydroxymethylfurfural into 2,5-diformylfuran catalyzed by NiMn layered double hydroxide. Catalysis Communications. 151.

Zhu, H., Jia, Y., Wu, X. and Wang, H. 2009. Removal of arsenic from water by supported nano zero-valent iron on activated carbon. Journal of Hazardous Materials. 172(2), 1591-1596.

Zhu, J., Zhu, Z., Zhang, H., Lu, H., Zhang, W., Qiu, Y., Zhu, L. and Küppers, S. 2018. Calcined layered double hydroxides/reduced graphene oxide composites with improved photocatalytic degradation of paracetamol and efficient oxidation-adsorption of As (III). Applied Catalysis B: Environmental. 225, 550-562.